Examining the metabolic, physiologic and chronobiologic effects of Western diet-induced obesity in a mouse model.

by

Lauren Nicole Woodie

A dissertation submitted to the Graduate Faculty of
Auburn University
in partial fulfillment of the
requirements for the Degree of
Doctor of Philosophy

Auburn, Alabama
December 14, 2019

Keywords: Hippocampus, chronobiology, Western diet, metabolism, obesity, circadian rhythms

Approved by

Michael Greene, Chair, Associate Professor of Nutrition
Vishnu Suppiramaniam, Professor of Drug Discovery and Development
Kevin Huggins, Associate Professor of Nutrition
Ya-Xiong Tao, Professor of Anatomy, Physiology and Pharmacology

Abstract

Obesity is a major public health concern that can result from consuming a Western diet (WD), characterized by a diet high in fat and sugar, including sugar sweetened beverages. A proposed treatment for WD-induced obesity is time-restricted feeding (TRF), which restricts consumption of food to specific times of the 24-hour cycle. TRF improves metabolic health by aligning the timing of food intake with the circadian rhythms of nutrient metabolism. Circadian rhythms are behavioral and physiological patterns that occur every 24 hours. In mammals, circadian rhythms are entrained to light:dark cycles by photic input to the master circadian regulator, the suprachiasmatic nucleus (SCN). Every cell in the body, however, possesses a set of core clock genes and in tissues such as the liver and adipose, rhythmic expression of these genes may be desynchronized from the SCN by fed/fasting cycles. WD feeding, in particular, has been shown to result in significant desynchronization of peripheral clocks from the SCN. TRF shows great promise to prevent obesity and the development of chronic disease by resynchronizing the periphery with the SCN. However, the ability of TRF to reverse metabolic changes in animal models of WD-induced obesity is not known. Moreover, the exact role of timing liquid sugar intake, independent of timing solid food intake, on the development of WD-induced obesity remains to be determined.

The liver is not only one of the most sensitive organs to WD-induced dysfunction, but it is particularly responsive to metabolic improvements after TRF. The hippocampus is also incredibly sensitive to the metabolic disruptions resulting from WD feeding. Until now, the impact of WD feeding and obesity on hippocampal rhythmicity has yet to be examined. Thus, the overarching objective of the presented works was to determine the

role of chronobiology in the metabolic, physiologic and behavioral effects of WD-induced obesity. First, we found that TRF of a WD consisting of a 45% kcal/g high-fat diet supplemented with a 4% fructose/sucrose solution as drinking water did not result in significant weight loss. However, markers of non-alcoholic fatty liver disease (NAFLD) and glucose and insulin intolerance were improved by TRF in the WD group. Next, we examined metabolic and physiologic parameters in mice given liquid sugar at various intervals over 24-hours. The control (Con) group received tap water, the *ad* libitum fructose-glucose (ALFG) group received *ad libitum* access to a 12% fructose/glucose solution (FGS) and the early fructose-glucose (EFG) and late fructose-glucose (LFG) groups received the FGS during the first and last six hours of the active period, respectively. Each group was given free access to chow. The ALFG group exhibited elevated body weight, adipose tissue weight and increased markers of NAFLD. The ALFG group consumed more calories than the other groups during zeitgeber time (ZT) 6-11, indicating that this window may be critical in the promotion of weight gain from liquid sugar consumption. Interestingly, the EFG group exhibited improved metabolic flexibility and insulin tolerance. Finally, WD-induced obesity induced significant alterations in the rhythmicity of hippocampal core clock genes. Furthermore, the expression pattern of genes implicated in Alzheimer's disease (AD) risk and synaptic function were significantly altered in the WD group and *in vivo* hippocampal memory was disrupted in a task- and time-dependent manner.

Overall, the works herein implicate rhythm disruptions as a common link among the metabolic, physiologic and behavioral effects of WD-induced obesity.

Acknowledgments

I would like to express my deepest gratitude to my advisor, Dr. Michael W. Greene, for his excellent mentorship throughout my course of study. I appreciate his encouragement, freedom to explore and his insightful interpretations, which inspired me to ask meaningful research questions and motivated me to perform at my best. His patience and support have been an immense help in completing this dissertation. I would also like to thank Dr. Vishnu Suppiramaniam, Dr. Kevin Huggins, Dr. Ya-Xiong Tao and Dr. Miranda Reed for serving on my dissertation committee and guiding my research. I acknowledge and extend gratitude for the financial support received from the Auburn University Center for Neuroscience Initiative, the Alabama Agricultural Experiment Station, the NDHM Graduate Research Award and the Auburn University Honors College.

I would like to express the utmost gratefulness to my mother, Ms. Patricia Danek, my father, Mr. Marvin Woodie, and my sister, Ms. Jessica Woodie, for their constant inspiration and motivation, for their unwavering love and moral support. I want to specially mention Ms. Olivia Altonji, Mr. Robert Johnson, Mr. Peyton Kuhlers, Mr. William Haynes, Ms. Savanah Fowler, Mr. Bulbul Ahmed, Ms. Beatriz Carmona and the 2017-2019 Honors Research students for their contributions. I'd also like to thank my colleagues Dr. Ann Marie O'Neill, Dr. Yuwen Luo, Ms. Marina Sycheva, Dr. Annie Kirby, Dr. Emily Graff, Dr. Ahmed Alhowail, Dr. Jenna Bloemer and Ms. Priyanka Das Pinky. It was a great pleasure to study and work with you all. I express my sincere gratitude to all faculty members in the Department of Nutrition, Dietetics and Hospitality Management, the College of Veterinary Medicine as well as the Auburn University

Graduate School for giving me the valuable opportunity and excellent atmosphere to not only grow as a scientist, but as an individual.

Finally, I need to thank my dear cat, Mudflap, for her love, companionship and snuggles through every step of my doctoral study.

Reference Style

This document is referenced using the citation style of *Cell Metabolism*.

Table of Contents

Abstract 2

Acknowledgments 4

Reference Style 6

Table of Contents 7

List of Tables 14

List of Figures 15

List of Abbreviations 17

Chapter 1: Introduction 22

Chapter 2: Review of Literature 27

2.1 Western Diet-Induced Obesity 27

2.1.1 Introduction and Definitions 27

2.1.2 Prevalence of Adult Obesity in the United States 28

2.1.3 History 29

2.1.4 Proposed Causes of Obesity 30

2.1.4.1 The Western Diet 30

2.1.4.1.1 Refined Sugar 30

2.1.4.1.1.1 Glucose 32

2.1.4.1.1.2 Fructose 33

2.1.4.1.2 Refined Fats 36

2.1.4.1.2.1 Saturated Fatty Acids 37

2.1.4.1.2.2 *Trans* Unsaturated Fatty Acids 40

2.1.4.2 Evolutionary Influences 41

2.1.4.2.1 The Thrifty Gene Hypothesis....42
2.1.4.2.2 Food Addiction....43
2.2 Pathogenesis of Western Diet-Induced Obesity....45
2.2.1 Pathogenic Adipose Tissue Expansion....45
2.2.2 Insulin Resistance....47
2.2.3 Ectopic Fat Deposition....48
2.3 The Impact of the Western Diet on the Brain....48
2.3.1 The Hypothalamus....49
2.3.1.1 Effects of the Western Diet on the Hypothalamus....50
2.3.2 The Hippocampus....54
2.3.2.1 Anatomy....54
2.3.2.2 Synaptic Plasticity....54
2.3.2.3 The Effects of the WD on the Hippocampus....56
2.4 Circadian Biology....58
2.4.1 Introduction and Definitions....59
2.4.2 The Molecular Mechanisms of Circadian Rhythmicity....61
2.4.2.1 Brain and Muscle Aryl Hydrocarbon-like Protein 1....61
2.4.2.2 Circadian Locomotor Output Cycles Kaput....62
2.4.2.3 Neuronal Per-Arnt-Sim Domain Protein 2....62
2.4.2.4 Period....63
2.4.2.5 Cryptochrome....65
2.4.2.6 REV-ERBs....66
2.4.3 The Suprachiasmatic Nucleus....68

2.4.3.1 Mechanisms of SCN Entrainment 69
2.4.3.2 Melatonin 70
2.4.4 Rhythmicity Beyond the SCN 71
2.4.4.1 The Circadian Rhythms of Metabolism 72
2.4.4.1.1 The Core Clock and the Cellular Redox State 73
2.4.4.1.2 Cryptochromes and Adenosine Monophosphate-Activated Protein Kinase 74
2.4.4.1.3 REV-ERBs and Heme 74
2.4.4.2 The Circadian Rhythms of Memory 75
2.4.4.2.1 Time-of-Day-Dependent Hippocampal Memory 75
2.4.4.2.2 Sleep and Hippocampal Memory 78
2.4.4.2.3 The Core Clock and Hippocampal Memory 83
2.5 Circadian Disruptions 84
2.5.1 Alzheimer's Disease 85
2.5.2 Circadian Disruption by Diet 86
2.5.2.1 Circadian Disruption by the Western Diet 86
2.5.3 Food-Entrainable Oscillators 88
2.5.4 Time-Restricted Feeding 88
2.5.4.1 Rodent Studies of Time-Restricted Feeding 89
2.5.4.2 Human Studies of Time-Restricted Feeding 90
Figures and Figure Legends 92
Chapter 3: Restricted Feeding for Nine Hours in the Active Period Partially Abrogates the Detrimental Metabolic Effects of a Western Diet with Liquid Sugar Consumption in Mice 102
3.1 Abstract 102

3.2 Introduction 103

3.3 Materials and Methods 105

3.3.1 Experimental Approach 105

3.3.1.1 Animals and Diets 105

3.3.1.2 Metabolic Cages 106

3.3.1.3 Tissue Collection and Analysis 106

3.3.1.4 RNA Extraction and Reverse Transcriptase-Quantitative Polymerase Chain Reaction (RT-qPCR) 107

3.3.2 Experiment 1 108

3.3.2.1 Dietary Exposure 108

3.3.2.2 Metabolic Cages 108

3.3.2.3 Liver Histopathologic Analysis 108

3.3.2.4 Adipose Histopathologic Analysis 109

3.3.3 Experiment 2 110

3.3.3.1 Dietary Exposure 110

3.3.3.2 Metabolic Cages 110

3.3.3.3 Glucose Tolerance Test (GTT) 110

3.3.4 Statistics 111

3.4 Results 111

3.4.1 Body Weight 112

3.4.2 Reference Metabolic Phenotype 112

3.4.3 Post-Intervention Metabolic Phenotype 112

3.4.4 Glucose Tolerance Test and Serum Factors 115

3.4.5 Liver Pathophysiology 116

3.4.6 Adipose Tissue Dynamics 118

3.5 Discussion 119

Figures and Figure Legends 124

Chapter 4: The Physio-Metabolic Effects of Time-Restricting Liquid Sugar Intake to Six-Hour Windows during the Mouse Active Phase 139

4.1 Abstract 139

4.2 Introduction 140

4.3 Materials and Methods 143

4.3.1 Animals and Diets.....143

4.3.2 Metabolic Phenotyping 144

4.3.3 Glucose and Insulin Tolerance Tests 145

4.3.4 Tissue Collection and Analysis 146

4.3.5 Liver Histopathology 147

4.4 Results 147

4.4.1 Body Weight 147

4.4.2 Energy Expenditure 148

4.4.3 Macronutrient Utilization 150

4.4.4 Glucose and Insulin Tolerance Tests 151

4.4.5 Food and Water Consumption 152

4.4.6 End-Point Analyses 154

4.5 Discussion 155

Tables 163

Figures and Figure Legends 164

Chapter 5: Evidence for Hippocampal Core Clock Disruptions in a Murine Model of

Western Diet-Induced Obesity 179

5.1 Abstract 179

5.2 Introduction 180

5.3 Materials and Methods 182

5.3.1 Animals and Diets 182

5.3.2 End-Point Procedures 183

5.3.3 Metabolic Phenotyping 184

5.3.4 Glucose and Insulin Tolerance Tests 184

5.3.5 Behavioral Assessments 185

5.3.6 RNA Extraction and RT-qPCR 188

5.3.7 Serum Insulin, Corticosterone, CRP and IL-6 Determination 188

5.3.8 Quantification and Statistical Analysis 188

5.4 Results and Discussion 189

5.4.1 Western Diet Consumption Results in an Obese Phenotype and Disrupts Peripheral Rhythmicity 189

5.4.2 Western Diet-Induced Obesity Disrupts the Diurnal Rhythmicity of Core Clock Gene Expression in the Hippocampus 190

5.4.3 Diurnal Rhythmicity of Genes Associated with Alzheimer's Disease and Synaptic Plasticity are Disrupted in Western Diet-Fed Mice 192

5.4.4 Western Diet-Induced Disruptions in the Hippocampal Clock are Associated with Time- and Task-Dependent Cognitive Deficits 194

5.4.5 Study Limitations 196

Figures and Figure Legends 197

Chapter 6: Summary and Conclusion 207

References 208

Appendix 1: Behavioral Apparatuses 250

Appendix 2: R Code and Example Output for Analysis of Rhythmicity 254

List of Tables

Table 1 163

List of Figures

Figure 1: Pathogenic Adipose Tissue Expansion 92

Figure 2: Insulin Resistance Stemming from Pathogenic Adipose Tissue Expansion 94

Figure 3: The Effects of a WD on the Hypothalamus 96

Figure 4: The Effects of a WD on the Hippocampus 98

Figure 5: The Core Circadian TTFL 99

Figure 6: Photic Entrainment of the SCN 101

Figure 7: WD TRF Body Weight 124

Figure 8: Pre-TRF Metabolic Phenotype 126

Figure 9: EE After TRF 128

Figure 10: RER After TRF 130

Figure 11: Food and Water Uptake and Activity After TRF 131

Figure 12: Glucose Tolerance and Plasma and Serum Parameters After TRF 133

Figure 13: NAFLD Parameters After TRF 135

Figure 14: Adipose Tissue Parameters After TRF 137

Figure 15: Body Weight During Liquid Sugar Restriction 164

Figure 16: EE During Liquid Sugar Restriction 166

Figure 17: 24-hour Activity and 24-hour V_{O2} During Liquid Sugar Restriction 168

Figure 18: RER During Liquid Sugar Restriction 170

Figure 19: GTT and ITT During Liquid Sugar Restriction 172

Figure 20: Diurnal Food and Water Consumption During Week 9 of Liquid Sugar Restriction 173

Figure 21: Time-Dependent Analysis of Food and Water Consumption 175

Figure 22: Liver Histopathology After Liquid Sugar Restriction.....177

Figure 23: WD-Induced Obesity Pathophysiology and Peripheral Rhythm Disruption..197

Figure 24: Metabolic Phenotype.....199

Figure 25: The Effect of WD-Induced Obesity on Core Clock Gene Expression in the Liver, Hypothalamus and Hippocampus.....201

Figure 26: Diurnal Expression of *Reverba* and *Dbp*.....203

Figure 27: The WD Alters Diurnal Expression Patterns of Genes Associated with AD Risk and Synapse Function.....204

Figure 28: WD Feeding Attenuates Memory in a Time- and Task-Dependent Manner .206

List of Abbreviations

AD	Alzheimer's Disease
AgRP	Agouti-Related Protein
ALAS2	5-Aminolevulinic Acid Synthase 1
α-MSH	Alpha Melanocyte-Stimulating Hormone
AMPK	Adenosine Monophosphate-Activated Protein Kinase
ApoC-III	Apolipoprotein C-III
Arc	Arcuate Nucleus (hypothalamic structure)
ARNT	Aryl-Hydrocarbon Receptor Nuclear Translocator
ATP	Adenosine Triphosphate
AUC	Area Under the Curve
AVP	Argenine Vasopressin
BBB	Blood Brain Barrier
bHLH	Basic Helix-Loop-Helix
BMAL1	Brain and Muscle Aryl Hydrocarbon-Like Protein 1
BMI	Body Mass Index
CA	Cornu Ammonis
cAMP	Cyclic Adenosine Monophosphate
CCG	Clock-Controlled Genes
CLOCK	Circadian Locomotor Output Cycles Kaput
CLS	Crown-Like Structures
CR	Chylomicron Remnant
CREB	cAMP Response Element Binding Protein
CRP	C-Reactive Protein
CRY	Cryptochrome
CSF	Cerebrospinal Fluid
CT	Circadian Time
cTPL	Circadian Time-Place Learning

CVD	Cardiovascular Disease
CXCL5	C-X-C Motif Ligand 5
DA	Dopamine
DAG	Diacylglycerol
DBP	D-Box Binding Protein
DG	Dentate Gyrus
DHAP	Dihydroxyacetone Phosphate
DKO	Double Knockout
EE	Energy Expenditure
EEG	Electroencephalogram
ELISA	Enzyme-Linked Immunosorbant Assay
eTRF	Early TRF
eWAT	Epididymal White Adipose Tissue
F1P	Fructose 1-Phosphate
F6P	Fructose 6-Phosphate
FA	Fatty Acid
FEO	Food-Entrainable Oscillator
FFA	Free Fatty Acid
G3P	Glucose 3-Phosphate
G6P	Glucose 6-Phosphate
GABA	Gamma Aminobutyric Acid
GFP	Green Fluorescent Protein
GLUT2	Facilitated Transporter Type 2
GLUT5	Facilitated Transporter Type 5
GR	Glucocorticoid Receptor
GTT	Glucose Tolerance Test
HDL	High-Density Lipoproteins
HDLc	High-Density Lipoprotein Cholesterol
HFCS	High-Fructose Corn Syrup
HOMA-IR	Homeostatic Model Assessment of Insulin Resistance
Iba1	Ionized Calcium-Binding Adaptor Molecule 1

IFN-γ	Interferon-Gamma
IL-1β	Interleukin-1 Beta
IL-6	Interleukin-6
IRS	Insulin Receptor Substrate
ITT	Insulin Tolerance Test
iWAT	Inguinal WAT
KHK	Ketohexokinase
KO	Knockout
LDL	Low-Density Lipoproteins
LDLc	Low-Density Lipoprotein Cholesterol
LTD	Long-Term Depression
LTP	Long-Term Potentiation
lTRF	Late TRF
MAG	Monoacylglycerol
MAPK	Mitogen-Activated Protein Kinase
MCP-1	Monocyte Chemoattractant Protein-1
MEF	Mouse Embryonic Fibroblasts
MF	Mossy Fiber
mTRF	Midday TRF
MUFA	Monounsaturated Fatty Acid
NAc	Nucleus Accumbens
NAD^+	Nicotinamide Adenine Dinucleotide
NAFLD	Non-Alcoholic Fatty Liver Disease
NAM	Nicotinamide
NAMPT	Nicotinamide Phosphoribosyltransferase
NcoR	Nuclear Receptor Corepressor
NF-κB	Nuclear Factor-Kappa B
NMDA	N-Methyl-D-Aspartate
NMN	Nicotinamide Mononucleitide
NOR	Novel Object Recognition
NPAS2	Neuronal PAS Protein 2

NPSC	Neural Progenitor/Stem Cell
NPY	Neuropeptide Y
PAC1	PACAP Type 1 Receptor
PACAP	Pituitary Adenylate Cyclase-Activating Polypeptide
PAS	Per-Arnt-Sim Domain
PBF	Percent Body Fat
PBN	Parabrachial Nucleus
PER	Period (protein)
PFK	Phosphofructokinase
PGC-1	Perioxisome Proliferator-Activating Receptor Transcription Coactivator 1
PK	Pyruvate Kinase
POMC	Preopiomelanocortin
PP	Perforant Path
PPARγ	Perioxisome Proliferator Activating Receptor Gamma
PUFA	Polyunsaturated Fatty Acid
PVN	Paraventricular Nucleus
RE	Reconstitution
RER	Respiratory Exchange Ratio
RGC	Retinal Ganglion Cells
RHT	Retinohypothalamic Tract
ROR	Retinoic Acid-Related Orphan Receptor
RORE	Retinoic Acid-Related Orphan Receptor Binding Element
RT-qPCR	Reverse Transcriptase-Quantitative Polymerase Chain Reaction
rWAT	Retroperitoneal WAT
SC	Schaffer Collateral
SCN	Suprachiasmatic Nucleus
SEM	Standard Error Measurement
SFA	Saturated Fatty Acid
SGLT1	Sodium-Glucose Transporter 1
SIRT1	Sirtuin 1
SO	Slow Oscillation

SubQ	Subcutaneous
T2DM	Type-II Diabetes Mellitus
TAG	Triacylglycerols
TCA	Tricarboxylic Acid
TLR4	Toll-Like Receptor 4
TNF-α	Tumor Necrosis Factor Alpha
TRF	Time-Restricted Feeding
TTFL	Transcription/Translation Feedback Loop
VLDL	Very Low-Density Lipoproteins
VIP	Vasoactive Intestinal Polypeptide
VTA	Ventral Tegmenal Area
WAT	White Adipose Tissue
WD	Western Diet
ZT	Zeitgeber Time

Chapter 1: Introduction

In most cases, obesity is considered to be a pathogenic condition referring to a state of increased adiposity concomitant with metabolic disturbances including hyperlipidemia, hyperinsulinemia, and hyperglycemia which increase the risk of cardiovascular disease, diabetes, certain forms of cancer, and other chronic diseases. The prevalence of obesity in the United States has been steadily rising since the late 1990s. In adults the obesity prevalence increased from 30.5% of the population in 1999-2000 to almost 40% in 2015-2016 (Hales et al., 2015, 2018). As of September 2018, 36 states reported an obesity rate greater than 30% with seven of those states having rates close to 35%. Obesity-related diseases have also risen dramatically within this time frame (The State of Obesity, 2018b, 2018a).

There are many proposed causes for this epidemic, but dietary patterns are perhaps the most culpable. A Western diet (WD) is commonly consumed in areas where obesity is the most prevalent and is characterized by energy-dense foods that are high in refined sugars and fats (Carrera-Bastos et al., 2011; Cordain et al., 2005; Myers and Allen, 2012). The level of sugars and fats available in these foods are in quantities and mixtures that have just recently been available for human consumption (Cordain et al., 2005; Ross et al., 2009). The resulting excess of energy consumed on this diet is stored in adipose tissue. This in and of itself is not detrimental. However, excess energy stored in peripheral tissues beyond the adipose tissue is thought to be detrimental. Further, a sedentary lifestyle and consumption of a calorie-dense WD leads to pathogenic expansion of adipose tissue and subsequent metabolic disease (Sinasac et al., 2016; Sun et al., 2011)

Adipose tissue expansion becomes pathogenic when adipocyte hypertrophy and adipocyte progenitor hyperplasia occur faster than the surrounding vasculature (Figure 1). Adipocytes in these pathogenic conditions become hypoxic and begin to produce hypoxia-inducible factors (Sun et al., 2011). Macrophages resident to healthy adipose tissue will polarizes under hypoxic conditions to the more pro-inflammatory M1 state (Figure 1). A chronic state of low-grade inflammation is propagated by the production of pro-inflammatory cytokines and is thought to lie at the center of most WD-induced diseases, such as Type-II Diabetes Mellitus (T2DM), which is characterized by insulin resistance (Centers for Disease Control and Prevention, 2018). In extreme and prolonged cases of pathogenic adipose tissue expansion, ectopic fat deposition will occur mainly through the disruption of insulin signaling (Shulman, 2014). Impaired insulin signaling in adipocytes will promote lipolysis and encourage the re-esterification of lipids in other tissues such as skeletal muscle and the liver (Figure 2).

Although the semipermeable blood-brain barrier (BBB) is designed to tightly regulate the passage of ions, molecules and cells from the peripheral blood into the brain, it does not render the brain immune to the effects of WD-induced inflammation (Daneman and Prat, 2015). In fact, changes in brain chemistry and function commonly occur with diet-induced metabolic disruptions (André et al., 2014; Hryhorczuk et al., 2017; Kanoski and Davidson, 2011; Kien et al., 2014; Marwitz et al., 2015; Sarfert et al., 2019; Woodie and Blythe, 2017). The hippocampus is a curled ridge of gray matter in the medial temporal lobe that is crucial for memory formation and recall and is particularly sensitive to WD-induced changes in peripheral inflammation and metabolism. The BBB surrounding hippocampal vasculature becomes increasingly permeable as WD

consumption and inflammation progress (Davidson et al., 2013; Hargrave et al., 2016; Mimee et al., 2013).

The WD has also been shown to negatively impact the circadian rhythmicity of whole-body metabolism as well as key genes involved in tissue-specific rhythmicity (Asher and Sassone-Corsi, 2015). The rhythm of all mammals living on the Earth's surface is dictated by the rotation of the Earth around the Sun. These photic signals are transmitted from retinal ganglia to the hypothalamic 24hosphor24t24atic nucleus (SCN). The presence of daylight entrains the rhythms of SCN neurons to a 24 hour cycle by initiating the transcription and translation of core clock genes in a transcription/translation feedback loop (TTFL) (Welsh et al., 2010). The circadian TTFL is comprised of brain and muscle aryl hydrocarbon receptor nuclear translocator-like protein 1 (BMAL1), circadian locomotor output cycles kaput (CLOCK)/neuronal Per-Arnt-Sim (PAS) domain protein 2 (NPAS2), period 1-3 (PER), cryptochrome 1 and 2 (CRY) and REV-ERBα and β (Figure 5). BMAL1 and CLOCK/NPAS2 form the positive arm of the loop, while PER, CRY and REV-ERBs make up the inhibitory or negative arm (Figure 5) (Dibner et al., 2010; Mohawk et al., 2012; Stratmann and Schibler, 2012). The downstream impacts of core clock genes on clock-controlled genes (CCGs) allow the SCN to set the rhythm for the majority of physiological, metabolic and behavioral processes (Mohawk et al., 2012). Indeed, almost half of the mammalian genome exhibits circadian rhythmicity in its pattern of expression (Yan et al., 2008). The core clock genes, however, are ubiquitous and oscillate within the TTFL throughout the body (Dibner et al., 2010). Furthermore, the set of CCGs expressed in each tissue are highly specific and tailored to the function of the tissue in question.

Circadian clocks are now understood to function in a hierarchy, with the SCN at the top of light-entrained rhythms. However, specific tissues possess cell autonomy in other physiological processes. When considering the circadian system and its function in processes other rhythmicity, a defined hierarchy of circadian control becomes difficult to establish. Indeed, peripheral tissues, in particular the liver, may depose the SCN in the rhythm hierarchy when the fed/fasting cycle is disrupted. Several components of the core clock TTFL are found at the intersection of rhythmicity and metabolism. The effects of core clock proteins on metabolism are presumed to dictate where exactly in the hierarchy of rhythmicity a peripheral tissue will fall in relation to the SCN.

What is more, memory has been observed as a time-of-day dependent behavior in species from *Drosophila* to humans. Proteins in the mitogen-activated protein kinase (MAPK) cascade oscillated in the hippocampus in a non-cell-autonomous manner, as SCN lesioning ablated rhythmicity within the pathway (Phan et al., 2011). However, hippocampal long-term potentiation (LTP) has been shown to be a truly circadian, cell-autonomous phenomenon (Cauller et al., 1985; Chaudhury et al., 2005). Therefore, the hippocampus is cell-autonomous and possesses a mechanism through which memories may be formed without input from the SCN. MAPK may act as a non-cell-autonomous pathway and more research needs to be done to identify the cell-autonomous pathways behind hippocampal memory.

Constant access to food and entertainment and shift-work careers and trans-time zone flights push the limits of human circadian physiology. The circadian system evolved to temporally separate cellular states (e.g. the fed and the fasting state) in order to decrease the chance of futile cycling. When endogenous circadian pacing is at odds with

the light:dark cycle, myriad health issues, collectively known as circadian-time sickness, can occur (van Ee et al., 2016). In fact, circadian disruption is classified as both a cause and a symptom of Alzheimer's disease (AD), which is characterized by severe amnesia and forgetfulness caused by cellular changes largely in the hippocampus. Research on shift workers has shown that chronic circadian disruptions can *cause* AD-like impairments in attention and cognitive function (Alhola and Polo-Kantola, 2007; Foster and Wulff, 2005; LeGates et al., 2014). What is more, AD-like disruptions in hippocampal function have been observed after WD feeding. In fact, Type-III Diabetes is now used to describe such WD-induced impairments (de la Monte and Wands, 2008).

Time-restricted feeding (TRF) has been shown to have positive impacts on metabolic health in both animal models and humans. TRF works to synchronize the timing of food intake with the circadian rhythms of nutrient metabolism. Studies utilizing TRF find that restricting food consumption to ~9 hour windows during the active phase can improve glucose metabolism, insulin signaling and markers of non-alcoholic fatty liver disease (NAFLD). These studies indicate the presence of one or more food-entrainable oscillators (FEO) outside of the SCN. Thus far, the liver represents the most viable location for a FEO, as even under dark:dark conditions, 15% of hepatic transcripts retain circadian oscillation (Vollmers et al., 2009). However, given the degree to which the hippocampus is impacted by WD feeding and obesity, it stands to reason that hippocampal core clock rhythmicity may also be impacted to the timing of nutrient availability. The studies presented here in delve into the impacts of nutrient availability on peripheral metabolism and hippocampal chronobiology.

Chapter 2: Review of Literature

2.1 Western Diet-Induced Obesity

2.1.1 Introduction and Definitions

Obesity is one of the greatest and most neglected public health issues of the 21st century. Most commonly defined as an individual with a body mass index (BMI; body weight in kilograms / (height in meters)^2) greater than or equal to 30kg/m^2, obesity is a metabolic disorder comorbid with a number of diseases such as T2DM, NAFLD, hypertension, dyslipidemia and cardiovascular diseases (CVD) as well as certain types of cancers, (e.g. colorectal cancer), and mental illnesses (e.g. major depressive disorder) (Angulo, 2006; Centers for Disease Control and Prevention, 2018; Després et al., 2008; Hales et al., 2018; Luppino et al., 2010; Pi-Sunyer, 2002; World Health Organization, 2018). In some cases, however, BMI fails to fully capture obesity as a pathophysiologic state. In fact, many professional athletes and individuals with low body fat mass, but increased muscle mass will have a BMI placing them in the obese category (ACE, 2018; Harvard Health, 2016).

Obesity, therefore, may be better described by an elevated percent body fat mass (PBF). The typical cut off for an "obese" individual is ≥ 25 PBF for males and ≥ 30 PBF for females (National Institutes of Health, 2000). Indeed, the risk of developing the above-mentioned diseases and disorders comorbid with obesity increases proportionally with the degree of PBF (Després et al., 2008). Yet once again, this definition includes a subset of individuals who are resistant to obesity-related metabolic disturbances. Metabolically-healthy obese individuals have elevated BMI and PBF, but do not present

with insulin insensitivity, unfavorable liver profiles, hypertension or dyslipidemia (Primeau et al., 2011).

While there is yet to be a clear and all-inclusive definition of obesity, for the purposes of this text, obesity will be considered a pathogenic condition referring to a state of increased adiposity concomitant with metabolic disturbances such as hyperlipidemia, hyperinsulinemia, hyperglycemia, etc. Specifically, obesity induced by the overconsumption of high-fat and high-sugar foods will be discussed in the following sections.

2.1.2 Prevalence of Adult Obesity in the United States

The prevalence of obesity in the United States has been steadily rising since the late 1990s. In adults the obesity prevalence increased from 30.5% of the population in 1999-2000 to almost 40% in 2015-2016 (Hales et al., 2015, 2018). As of September 2018, 36 states reported an obesity rate greater than 30% with seven of those states having rates of approximately 35%. Obesity related diseases have also risen dramatically within this time frame. West Virginia, the state with the highest obesity rate in 2017, also had the highest rate of diabetes (15.2%) and the highest rate of hypertension (43.5%) in the country (The State of Obesity, 2018b, 2018a). Obesity also has significant direct and indirect economic impacts on the individual, their family and the US health system. In 2008, the medical costs of obesity were estimated to be $147 billion (Finkelstein et al., 2009). Direct costs include preventative, palliative and treatment services, while indirect costs apply to treatment of comorbid diseases and premature disability as well as

absences and decreased productivity due to obesity-related health issues (Hammond and Levine, 2010; Tremmel et al., 2017; Trogdon et al., 2008; Wolf, 1998).

2.1.3 History

Obesity and its associated pathophysiologies were first clinically described in the Graeco-Roman era with Hippocrates observing that sudden death was more common in overweight individuals than lean (Bray, 2009). Although not associated at the time, it is now hypothesized that these deaths were due to obesity-related CVD. Early Hindu physicians recognized that the sugary taste of diabetic urine was commonly observed in overweight, hyperphagic patients (Bray, 2009). After these observations were made, there were numerous attempts to quantify and define degrees of obesity. It wasn't until the Flemish statistician, Adolphe Quételet, used an individual's weight divided by the square of their height that an index for "fatness" was accepted (Nuttall, 2015; Williams and Frühbeck, 2009). The Quételet Index is now more commonly referred to as BMI.

Thus, obesity became quantifiable, and in the early 1900s it was widely considered a major medical issue. Life insurance companies began publishing data on the average BMI by gender and age (Nuttall, 2015; Williams and Frühbeck, 2009). These reports also included data on the disease and mortality rates associated with elevated BMI (Nuttall, 2015). With the development of sensitive densitometry, PBF began to be used as a metric of obesity. The widespread use of computerized body scanning techniques then refined obesity and its related health issues into categories based on where on the body the excess adipose tissue accumulated (Bray, 2009). Abdominal obesity, as opposed to

gluteofemoral adiposity, is now recognized as conferring the greatest risk of morbidity and mortality (Bray, 2009; Primeau et al., 2011).

Interestingly, the increase in obesity awareness was concurrent with the epidemic-like increase in the prevalence and incidence of obesity and obesity-related diseases. In order to better understand this phenomenon, two of the leading proposed causes of the obesity epidemic will be explored.

2.1.4 Proposed Causes of Obesity

2.1.4.1 The Western Diet

The WD is characterized by energy-dense foods that are high in refined sugars and fats (Cordain et al., 2005; Myers and Allen, 2012). The WD became popular with the rapid advance of food processing technology after the Industrial Revolution (Cordain et al., 2005). Energy-dense foods could now be produced at a low cost and distributed to the ever-growing population. The level of sugars and fats in these foods, however, were in quantities and mixtures that had never before been available for human consumption (Cordain et al., 2005; Ross et al., 2009). How the resulting excess of energy consumed on this diet negatively impacts metabolic health will be discussed in the next few sections.

2.1.4.1.1 Refined Sugar

From 1970 to 2000 refined sugar consumption steadily increased from 54 kg to an alarming 69 kg per capita (United States Department of Agriculture, 2019). Crystalline sucrose was the first refined sugar to gain popularity after the seasonal availability of honey limited its industrial use (Cordain et al., 2005; Ziegler, 1967). Sucrose is a

disaccharide composed of the monosaccharides glucose and fructose in a 50/50 distribution (Macdonald, 2016). Although sucrose occurs naturally in a number of fruits and vegetables, it is added in excess amounts to WD staples such as candies, granola bars, canned foods and beverages (Wiebe et al., 2011). When consumed, sucrose remains intact until it arrives at the upper small intestine where it is hydrolyzed into one glucose and one fructose by sucrase (Gropper and Smith, 2013).

In the late 1970s the chromatographic enrichment of fructose made the manufacture of high-fructose corn syrup (HFCS) from surplus corn much more cost-effective (32 cents/lb HFCS vs. 52 center/lb sucrose) (Cordain et al., 2005; Parker et al., 2010). HFCS is similar in composition to sucrose in that it is made of fructose and glucose molecules, but the most commonly consumed HFCS is HFCS-55, which is 55% fructose and 45% glucose. A study done in 2014, however, determined through metabolomic-type methods that the actual free fructose-to-glucose ratio in popular HFCS sweetened beverages was closer to a 60:40 ratio (Walker et al., 2014).

Since 1970, sucrose consumption per capita has remained between 1.8 and 1.4 kg, while HFCS taken over as the more popular corn-based sweetener (18 kg per capita HFCS vs 1.4 kg per capita sucrose in 2017) (Macdonald, 2016; United States Departmen tof Agriculture, 2019). In the years since 2000, refined sugar consumption has actually decreased to 58 kg per capita in 2017, while HFCS remains the highest added sugar (United States Departmen tof Agriculture, 2019). Glucose and fructose, the two components of sucrose and HFCS, will be discussed in the subsequent sections with detail on their metabolism and their role in the obesity epidemic.

2.1.4.1.1.1 Glucose

Glucose is taken into the enterocyte either by active transport via sodium-glucose transporter 1 (SGLT1) or by facilitated transport by facilitated transporter type 2 (GLUT2) (Gropper and Smith, 2013). SGLT1 binds one molecule of Na^+ and one molecule of glucose to symport the two molecules down a concentration gradient across the apical cell membrane. To maintain a lower Na^+ concentration within the cell, a Na^+/K^+ - ATPase pump moves Na^+ across the basal cell membrane into the bloodstream in exchange for K^+. This maintains the affinity of SGLT1 for glucose to continue transport from the intestinal lumen. Once inside the enterocyte, glucose is released into the bloodstream via GLUT2 and carried through the portal vein to the liver (Gropper and Smith, 2013).

Here, glucose is shuttled into the hepatocyte by GLUT2 and initially phosphorylated by hexokinase to form glucose-6-phosphate (G6P). Depending on the organism's energy needs, G6P may be shuttled into the pentose phosphate pathway during nonoxidative metabolism, be converted to glucose-1-phosphate for glycogen synthesis or enter glycolysis. Glycolysis converts glucose into pyruvate though a series of enzymatic steps, three of which are rate-limiting. The conversion of glucose to G6P is the first rate-limiting step of glycolysis and will be inhibited if there is already a surplus of G6P within the hepatocyte. G6P is then converted to fructose-6-phosphate (F6P), leading to the second rate-limiting step where F6P is converted to fructose-1,6-bisphosphate by phosphofructokinase (PFK). This step is inhibited by signals of energy excess such as adenosine triphosphate (ATP) and the tricarboxylic acid (TCA) cycle intermediate citrate. Phosphoenolpyruvate, made from fructose-1,6-bisphosphate, is converted to pyruvate by

pyruvate kinase (PK) in the final rate-limiting step of glycolysis. PK is also inhibited by molecular signals of energy excess like ATP and acetyl-CoA (Gropper and Smith, 2013).

After a high carbohydrate meal, intestinal glucose concentrations will exceed the transport capacity of SGLT1. Under these conditions, apical GLUT2 will transport glucose into the cell and across the basal membrane into the blood stream. An elevation in blood insulin (in response to increased glucose uptake) will decrease the number of GLUT2 transporters on the apical membrane to maintain glucose homeostasis (Gropper and Smith, 2013).

2.1.4.1.1.2 Fructose

Fructose is absorbed from the intestinal lumen via facilitated transporter type 5 (GLUT5) transporters. Although the rate of fructose absorption is slower than glucose, GLUT5 has a high affinity for fructose and will increase absorption rates when GLUT2 is present on the apical enterocyte membrane (Flegal et al., 2010; Gropper and Smith, 2013). Upon entry into the cell, fructose is phosphorylated to fructose-1-phosphate (F1P) by ketohexokinase (KHK) (Heinz et al., 1968). In the liver, F1P is shuttled into glycolysis in the place of fructose-1,6-bisphosphate, effectively bypassing the PFK rate-limiting step. This essential difference in fructose metabolism compared to glucose metabolism, makes fructose the more lipogenic monosaccharide. Without PFK regulation, fructose is an unregulated source of three-carbon sugars. Aldolase B converts F1P to either dihydroxyacetone phosphate (DHAP) or glyceraldehyde, both of which may be isomerized into glyceraldehyde 3-phosphate (G3P). G3P is shuttled down the glycolytic pathway into acetyl-CoA where it can either enter the TCA cycle or be committed to fatty

acid synthesis. Furthermore, DHAP and glyceraldehyde may also be form glycerol 3-phosphate, which serves as the backbone for triglycerides (Samuel, 2011).

For many years, the fructose was thought to pass through the enterocyte and be released intact into the portal vein. Following this assumption and based on the myriad of rodent studies corroborating hepatosteatosis in sucrose-fed animals, the liver was considered to be the main site of fructose metabolism (Caliceti et al., 2017; Ishimoto et al., 2013; Jegatheesan and De Bandt, 2017; Kim et al., 2017; Lanaspa et al., 2013). A mouse study by Jang *et al* early in 2018 found that when consumed in small doses fructose is primarily metabolized in the small intestine (Jang et al., 2018). While the liver expresses the highest level of KHK, it is also expressed in the kidney, pancreas and small intestine (Ishimoto et al., 2012). They used a dose of 0.5g/kg/day of fructose, which converts to 3g/kg/day fructose in humans (roughly equivalent to eating one orange or 2oz of soda per day) (Jang et al., 2018). An oral dose of 0.5g/kg/day of fructose elicited very little F1P in hepatic samples, but an increased accumulation of F1P in the small intestine. Furthermore, Jang *et al.* found increased levels of glucose, lactate, glycerate, TCA intermediates and amino acids in the portal vein of animals administered fructose (Jang et al., 2018). This suggests that at low doses, the small intestine metabolizes the majority of fructose, effectively shielding the liver from intact fructose metabolism.

This begs the question: Why has fructose been shown to cause hepatosteatosis on multiple accounts? To answer this, it is important to keep in mind that the majority of animal studies administer sugar treatment either in the drinking water or solid food at percentages ranging from 10-60% (Ishimoto et al., 2013; Jegatheesan and De Bandt, 2017; Kim et al., 2017; Stanhope et al., 2009; Woodie and Blythe, 2017). A main take

away from the Jang *et al.* paper is that small intestine fructose metabolism is easily saturated. At 1.0g/kg/day of fructose, the amount of intestinal F1P peaked and the amount of liver F1P rose. At 2.0g/kg/day of fructose the amount of intestinal F1P actually decreased, while liver F1P continued to rise (Jang et al., 2018). Therefore, when fructose is regularly consumed at high concentrations, more intact fructose is metabolized by the liver thereby promoting fructose-induced hepatosteatosis. Indeed, studies observing the most severe hepatosteatosis generally provided their animals with a higher amount of fructose (Jegatheesan and De Bandt, 2017).

What does this mean in terms of human sugar consumption? The initial murine dose of 0.5g/kg/day fructose is equivalent to a human consuming 3g/kg/day fructose. This is roughly comparable to eating one orange or 2oz of soda per day. Not only is a single can of soda 12oz (6x the low dose, 2x the high dose), but according to the Beverage Marketing Corporation, the average American drinks 1.3 cans of soda per day (Zmuda, 2011). In addition to liquid fructose, HFCS is added to a large number of solid foods and condiments to increase palatability (White, 2008). Thus, it stands to reason that WD-consuming humans regularly saturate the fructose metabolizing capabilities of the small intestine, causing increased fructose metabolism in the liver. Consistent with this hypothesis, meta-analyses and primary human research have demonstrated a strong association between the amount of fructose consumed and the development of obesity, NAFLD, and metabolic disease (Hu and Malik, 2010; Ludwig et al., 2001; Malik et al., 2010b, 2010a; Ouyang et al., 2008; Schulze et al., 2004).

With the previous paragraphs in mind, one can begin to see why the increased addition of sucrose to WD foods is detrimental to human health. Large amounts of

dietary sucrose are metabolized into large amounts of glucose and fructose in the small intestine. Under these conditions, GLUT2-facilitated transport becomes the main mode of glucose uptake, which increases GLUT5 absorption of fructose. Furthermore, in insulin resistant individuals, such as in obese and T2DM patients, the homeostatic mechanism of insulin sequestering GLUT2 is lost, continuing elevated glucose and fructose absorption (Gaby, 2005; Ruxton et al., 2009). The rate-limiting steps of glycolysis will halt glucose breakdown and the amount of circulating glucose will increase as well as the amount of glucose stored as glycogen in the liver and skeletal muscle (DeFronzo et al., 1981; Jegatheesan and De Bandt, 2017; Nilsson and Hultman, 1974). Higher consumption and absorption of fructose will cause more fructose to be metabolized by the liver. Eventual glycogen saturation within the liver and muscle as well as accumulation of hepatic trioses will instigate de novo lipogenesis (Acheson et al., 1988; Jegatheesan and De Bandt, 2017; Rippe and Angelopoulos, 2013; Samuel, 2011; Stanhope and Havel, 2008). It is this homeostatic breakdown that is in part behind the phenotypes of hyperglycemia, hyperinsulinemia, and ectopic fat deposition in obese and type-II diabetic individuals.

2.1.4.1.2 Refined Fats

Fatty acids (FA) are a vital energy source in the human diet as they confer the most calories per gram of any macronutrient. Fas have a hydrophilic carboxylic acid head and a hydrophobic chain of hydrogen bound carbons ending in a methyl group. They are most commonly consumed and stored as triacylglycerols (TAG) where three Fas are bound to one glycerol molecule by their hydrophilic head. Singularly, Fas fall into three categories: saturated (SFA), monounsaturated (MUFA) and polyunsaturated (PUFA) fatty acids

(Cordain et al., 2005; Gropper and Smith, 2013). SFAs consists of single bound carbons while MUFAs and PUFAs contain one or more double bound carbons, respectively. SFAs are considered "unhealthy" fats, while MUFAs and PUFAs are traditionally thought of as "healthy" fats. PUFAs, however, may also occur in an n-3 or an n-6 conformation, with a double bond located either three or six carbons from the methyl end. A diet containing a more balanced ratio of n-6:n-3 is beneficial in regard to risk of CVD and metabolic disease (Cordain et al., 2005; Kris-Etherton et al., 2002; Nelson et al., 1995; Simopoulos, 2002). Furthermore, unsaturated fatty acids may assume either a *cis* or *trans* geometric conformation. The *cis* formation creates a kink in the hydrophobic chain that limits the ability of *cis* unsaturated Fas to be tightly packed into TAGs and allowing them to remain liquid at room temperature (Hernandez, 2016; Lopez et al., 2010). For example, increased consumption of olive oil, which is primarily composed of the *cis* MUFA, oleic acid, is associated with decreased CVD risk (Lopez et al., 2010). *Trans* unsaturated Fas, on the other hand, assume a conformation that makes them similar to SFAs and more easily packed and stored as TAGs. As such, *trans* unsaturated Fas are heavily associated with heart and metabolic disease (Cordain et al., 2005).

Thus, it is the type of fat consumed rather than the absolute amount of dietary fat that is important in the risk and development of obesity and its comorbidities. For the purposes of this text, the two types of fatty acid most linked to obesity and metabolic disease will be discussed: SFAs and *trans* unsaturated Fas.

2.1.4.1.2.1 Saturated Fatty Acids

The current recommendation from the American Heart Association is for saturated fat to make up 5-6% of daily calories of a 2,000 calorie/day diet (American Heart Association, 2015). However, 80% of Americans exceed this limitation with 10% being the average percentage of daily calories obtained from SFAs (de Souza et al., 2015; US Department of Health and Human Services, 2015). SFAs are commonly consumed in foods like fatty meat, butter, bovine milk and milk products and plant oils such as coconut and palm oil (Cordain et al., 2005; de Souza et al., 2015). Meta-analyses report a significantly increased risk of developing CVD proportional to the amount of SFA consumed (Mozaffarian et al., 2010; Siri-Tarino et al., 2010). Furthermore, intervention studies found that replacing SFAs with PUFAs in participants' diets resulted in improved cardiometabolic outcomes (Hooper et al., 2015).

The mechanism behind the pathogenesis of dietary SFAs may be attributed to the unique qualities of SFA metabolism. Upon absorption in the small intestine, long-chain SFAs specifically are reformed into TAGs and, due to the hydrophobic nature of their tails, must be packaged in lipoprotein vessels known as chylomicrons. Short and medium chain SFAs travel unpackaged to the liver through the portal vein (Pelley, 2007). A 1999 study in rabbits found that a diet high in SFAs significantly increased chylomicron secretion in isolated enterocytes when compared to diets high in n-3 PUFAs or n-6 PUFAs (Cartwright and Higgins, 1999). Chylomicrons deliver dietary fats primarily to the adipose tissue where lipoprotein lipase solubilizes the chylomicron outer layer to release TAGs for absorption into the adipocyte. TAGs are then broken down into glycerol, free fatty acids (FFA), diacylglycerols (DAG) or monoacylglycerols (MAG), all of which stimulate lipogenesis in the adipocyte (Gropper and Smith, 2013). Thus,

increased SFA consumption will yield increased chylomicron formation and delivery to the adipose with subsequent increased lipogenesis in the adipocyte.

After transport to the adipose tissue, what remains of the chylomicron is known as a chylomicron remnant (CR). The CR goes to the liver where the remainder of its contents (FFAs, DAGs, MAGs, phospholipids and cholesterols) are released into the hepatocyte. Hepatocytes use these remaining contents to make very low-density lipoproteins (VLDL), low-density lipoproteins (LDL), and high-density lipoproteins (HDL) (Gropper and Smith, 2013). SFAs once again exacerbate this process by increasing the number of chylomicrons and CRs present. Furthermore, increased FFAs, DAGs, and MAGs present in the hepatocyte will contribute to the hepatic TAG and fatty acid pools, thereby contributing to the development of NAFLD (Nakamura and Terauchi, 2013).

SFAs have also been shown to stimulate cholesterol biosynthesis and inhibit tissue uptake of LDL. An elevated LDL cholesterol (LDLc) to HDL cholesterol (HDLc) ratio is clinically considered as a risk for CVD. LDLs, which are derived from VLDLs, transport TAGs and cholesterol throughout the body, while HDLs remove lipids from the cell and transport them to the liver for elimination in bile (Gropper and Smith, 2013). A high dietary intake of SFAs has been shown to induce the expression and activation of peroxisome proliferator activating receptor transcription coactivator 1 (PGC-1) and simultaneously upregulate cholesterol biosynthesis and reduce cell surface expression of LDL receptors, thereby significantly increasing circulating lipids (German and Dillard, 2010; Lin et al., 2005). It is important to note, however, that while SFAs increase circulating LDLc, they do not decrease circulating HDLc (Mensink and Katan, 1992).

2.1.4.1.2.2 *Trans* Unsaturated Fatty Acids

Trans unsaturated Fas contribute to ~2-5% of consumed energy in North America and were not common in the human diet until 1897 (Cordain et al., 2005; de Souza et al., 2015). Prior to that time, *trans* fats were only found in ruminant meat and milk in very small percentages (4-8% of total fat) (Cordain et al., 2005; Gropper and Smith, 2013; de Souza et al., 2015). Industrial hydrogenation technology was optimized in 1897 allowing for vegetable oil to become solidified and opened up a vast market for spreadable, shelf-stable shortening and margarine (Cordain et al., 2005; Emken, 1984).

In 2003 the Food and Drug Administration amended its regulations to require that *trans* fats be reported on the nutrition label of all foods and supplements. This amendment also declared that foods containing 0.5g of *trans* fats could legally be considered a *trans* fat "free" food (Food and Drug Administration, HHS, 2003). However, due to the extreme and unequivocal evidence that *trans* fats are detrimental to human health, the FDA banned its use for general consumption in 2015 (Food and Drug Administration, 2015). Numerous reports found that *trans* fat consumption in any amount greater than 1% of total daily energy not only increased LDLc, but lowered HDLc (Katan et al.; Liu et al., 2017). Furthermore, *trans* fat consumption increases inflammatory markers such as tumor necrosis factor alpha (TNF-α), interleukin-6 (IL-6) and C-reactive protein (CRP) (Gropper and Smith, 2013; Liu et al., 2017). The combination of LDLc:HDLc imbalance with an increase in inflammation makes *trans* fat consumption particularly dangerous for the formation of atherosclerotic plaques and CVD risk (Ascherio et al., 1994; Cordain et al., 2005).

2.1.4.2 Evolutionary Influences

The current obesity pandemic is caused largely by the combination of years of evolutionary pressures on metabolic efficiency and the widely available, highly palatable, calorie-dense foods in the modern world (Bellisari, 2008; Samuel et al., 2010). Healthy humans are able to cope and respond to fluctuating energy supplies by storing excess energy as triglyceride in adipose tissue. While this response was useful in pre-Industrial time periods when food rich in calories was hard to come by, it now predisposes persistently over-nourished individuals to weight gain and ultimately to obesity (Bellisari, 2008; Savage et al., 2007). In Western society today, energy dense foods are easily accessible and plentiful in grocery stores and restaurants. The WD is a prime example of foods high in calories from refined sugars and fats. All of these are added to a base ingredient, such as soy, dairy or corn, to make high energy, highly palatable meals. Additionally, fiber, vitamins, and minerals in the original base ingredient are extracted in processing (Cordain et al., 2005). The end product is packaged and sold conveniently and inexpensively to quickly deliver high levels of sugar and fat.

Evolutionarily, foods high in calories, sugar, and fat were sought after not only to provide quick energy for immediate needs, but also to enable storage of energy for times of famine (Bellisari, 2008; Ghasemi et al., 2013). Today, however, energy dense foods are hypothesized to be a main player in the obesity epidemic because they are easily accessible and processed to enhance flavor, color, texture and other features to increase palatable attributes (Cordain et al., 2005). As an example, fruits, by nature, are some of the most sugar dense foods, but they are very low in fats. In contrast, the WD combines

sugar and fats in combinations and concentrations that are detrimental for metabolic health.

2.1.4.2.1 The Thrifty Gene Hypothesis

In 1982 James Neel proposed the thrifty gene hypothesis to explain the significant uptick in obesity observed after the Second World War. He reasoned that humans evolved to resist famine by developing mechanisms of quick insulin release, efficient glucose conversion to energy and storage of extra energy as fat (Neel, 2013). He proposed that the energy conserving function of these genes that once served a very important purpose, were now a burden in a world with constant food availability (Bellisari, 2008).

While there is a considerable amount of evidence to support the heritability of adiposity and obesity, details concerning their combinations and interactions with the external environment are forthcoming. Genes such as *LEP*, *LEPR,* and *MC4R* are known to disrupt the hypothalamic control of satiety and food intake behavior (Bellisari, 2008; O'Rahilly and Farooqi, 2006). Other genes are known to be involved in physical activity and athletic performance and influence the propensity for an individual to be more inactive than another (Chakravarthy and Booth, 2004; Rankinen et al., 2006; Simonen et al., 2003). Genetic factors involving metabolic rate, food preference and increased satiety have been identified as well (Bulik and Allison, 2001). Although the thrifty gene hypothesis is an attractive idea, it is too simplistic to fully explain the obesity epidemic. Indeed, if thrifty genotypes conferred significant reproductive success, they would have been fixed within the modern population and obesity would be even more prevalent.

Gene pleiotropy, epigenetics, and environmental factors are all likely to add to the complexity of obesity (Reddon et al., 2018).

2.1.4.2.2 Food Addiction

The neural processes involved in food seeking and intake behaviors are evolutionarily selected, redundant and conserved due to their necessity for survival (Bellisari, 2008; DiLeone et al., 2012; Zheng and Berthoud, 2008). The foods of the WD, containing unprecedented mixtures and amounts of sugars and fats, have been shown to stimulate hyperphagia and induce obesity (Li et al., 2018). Due to the similarity of these behavioral patterns and neural pathways to abusive drug addiction, food addiction has been posited as a potential driving factor behind WD-induced obesity (DiLeone et al., 2012; Zheng and Berthoud, 2008). Dopamine (DA) is one of the most heavily researched and well-characterized neurotransmitters involved the perception of reward. The ventral tegmental area (VTA) and its dopaminergic efferents to the nucleus accumbens (Nac) are generally agreed upon as the center for DA-mediated reward (Haber and Knutson, 2010). The primary site of DA output from the VTA is the Nac, but VTA efferents also project to the cerebral cortex, the hypothalamus, the amygdala and the hippocampus. Upon the receipt of a pleasurable stimulus, DA will be released from the VTA to the Nac and elsewhere for consolidation into reward-related behaviors such as reinforcement, motivation, prediction, and salience processing (DiLeone et al., 2012).

The DA system, however, is highly susceptible to peripheral inflammation, which is increased in association with pathogenic adipose tissue expansion (this will be discussed in more detail in a subsequent section). Human and animal studies have shown

that increased circulation of inflammatory factors such as pro-inflammatory cytokines and acute phase proteins decrease DA signaling in reward circuitry (Brydon et al., 2008; Burger and Stice, 2011; Felger and Treadway, 2017; Felger et al., 2013; Harrison et al., 2016; van Heesch et al., 2013; Kitagami et al., 2003; Nunes et al., 2014). Furthermore, obese individuals are more susceptible to the increased palatability of WD foods, as evidenced by enhanced activity in the somatosensory cortex in anticipation of a reward (e.g. a chocolate milkshake) (Stice et al., 2008a, 2008b). Thus, WD consumption may lead to a "reward deficiency syndrome" where an increased perception of food palatability in conjunction with a hypoactive DA system could elicit compensatory behaviors where food is overconsumed to meet its perceived value (Blum et al., 2014; Das, 2001; Volkow et al., 2011).

Drug addiction is simply described as a pharmacological seizure of the neural systems designed to process rewarding and salient stimuli; systems that did not evolve in the presence of drugs of abuse (DiLeone et al., 2012). By the same token, the neural mechanisms responsible for hunger and satiety did not evolve in the presence of processed foods with enhanced palatability. Furthermore, the neural systems of food intake have significant rewarding and emotional components in addition to the energy-sensing circuits necessary for survival. Despite these similarities, it is not entirely appropriate to compare WD-induced food addiction to abusive drug addiction. First, the metabolic centers for feeding homeostasis integrate central and peripheral signals, such as leptin and insulin, to ultimately determine food intake, while the DA system is proposed to modulate food intake behaviors. Where the dopamine system is indispensable for abusive drug reward, direct stimulation of key areas involved satiety and food intake will

alter food-seeking behaviors independent of the dopamine system (Aponte et al., 2011; DiLeone et al., 2012; Schwartz, 2000). Furthermore, leptin and insulin act directly on dopamine neurons to modulate the perception of a food stimulus (aversive vs attractive) depending on metabolic state (Tiedemann et al., 2017; Zheng and Berthoud, 2008). This particularly distinguishes food addiction from drug addiction.

2.2 Pathogenesis of Western Diet-Induced Obesity

While the majority of consumed calories are used to meet an individual's basal energy needs, excess calories are sequestered away as glycogen for short-term storage and in adipose tissue for short- and long-term storage. This in and of itself is not detrimental to metabolic health. In fact, this is exactly how the body is supposed to function; storing away energy for times when calories are scarce (Sarjeant and Stephens, 2012; Wang et al., 2013). However, most of the Westernized world does not have to worry about a calorie shortage, and times of famine are few and far between. Therefore, the excess energy stored in adipose tissue will continue to accumulate as a sedentary lifestyle and consumption of a calorie-dense diet proceed. It is this consistent and continued positive energy balance that results in the pathogenic expansion of adipose tissue and subsequent metabolic disease (Sinasac et al., 2016; Sun et al., 2011). There are several proposed mechanisms linking pathogenic adipose expansion to deteriorations in metabolic health, but a process that is commonly agreed upon is that of inflammation (Furukawa et al., 2004; Sun et al., 2011).

2.2.1 Pathogenic Adipose Tissue Expansion

As adipose tissue expands, sufficient vasculature and extracellular support cells must also increase. Adipogenesis allows for the proliferation of adipocytes in a well-supported, oxygen-rich environment (Sarjeant and Stephens, 2012; Wang et al., 2013). Adipose tissue becomes unhealthy when adipocyte hypertrophy and adipocyte progenitor hyperplasia occur faster than the surrounding vasculature (Figure 1). Adipocytes in these pathogenic conditions become hypoxic and begin to produce hypoxia-inducible factors (Sun et al., 2011). Macrophages resident to healthy adipose tissue are predominantly of the anti-inflammatory M2 phenotype, but hypoxia polarizes adipose-resident macrophages to the more pro-inflammatory M1 state (Figure 1). Subsequently, inflammatory conditions are propagated by the production of pro-inflammatory cytokines namely TNF-α, interleukin-1 beta (IL-1β) and interferon-gamma (IFN-γ) (Sarjeant and Stephens, 2012; Sun et al., 2011). Furthermore, chemokines such as monocyte chemoattractant protein-1 (MCP-1) and C-X-C motif ligand 5 (CXCL5) secreted from adipocytes will exacerbate macrophage recruitment leading to eventual adipocyte necrosis and the release FFAs, which exacerbate the inflammatory state by activating nuclear factor-kappa B (NF-κB) transcription of inflammatory genes via toll-like receptor 4 (TLR4) (Sun et al., 2011).

Pathogenic adipose tissue expansion and inflammation also results in the overproduction of and eventual resistance to the adipokine leptin (Dandona et al., 2004). Leptin and insulin function as two of the most important peripherally produced mediators of satiety. In a metabolically healthy state, leptin and insulin signal the body's nutritional status to suppress hunger and food seeking behaviors (Dandona et al., 2004). As WD-

induced inflammation progresses, however, these regulatory mechanisms become disrupted and energy balance can no longer be maintained.

2.2.2 Insulin Resistance

The chronic state of low-grade inflammation brought on by WD feeding and pathogenic adipose tissue expansion is thought to lie at the center of most WD-induced diseases. T2DM, for example, is characterized by insulin resistance (Figure 2) (Centers for Disease Control and Prevention, 2018). Insulin is released from pancreatic β-cells in anticipation of and response to consumption of glucose and amino acids. The insulin receptor is made up of two extracellular α subunits and two intracellular β subunits. Insulin binds to the α subunit to initiate conformational changes that activate the β subunits via a series of intracellular transphosphorylation reactions in which one β subunit phosphorylates the adjacent β subunit on specific tyrosine residues (Pessin and Saltiel, 2000). Activated insulin receptors then phosphorylate tyrosine residues on a number of proximal substrates, in particular, members of the insulin receptor substrate (IRS) family, which interact with other downstream targets to potentiate insulin cell signaling and action (Pessin and Saltiel, 2000).

Activating and inactivating phosphorylation of IRS-1 and IRS-2, specifically, has been extensively studied to understand the role of these substrates in insulin resistance (Greene and Garofalo, 2002; Greene et al., 2003; Saltiel and Kahn, 2001). While tyrosine phosphorylation activates IRS-1 and -2, phosphorylation of these substrates at serine residues has been found to have inactivating effects on insulin signaling (Greene et al., 2003; Hotamisligil, 2003; Hotamisligil et al., 1996). In the obese state, tyrosine

phosphorylation of IRS-1 and -2 is decreased, while serine phosphorylation is increased. This is in part due to inflammatory cytokines and FFAs activating cell signaling pathways resulting in the serine phosphorylation of IRSs at inactivating residues, effectively blocking insulin-dependent glucose uptake and action (Copps and White, 2012; Hotamisligil, 2003; Tanti and Jager, 2009).

2.2.3 Ectopic Fat Deposition

In WD-induced obesity, ectopic fat deposition occurs when energy intake exceeds energy expenditure. In extreme and prolonged cases of excess energy intake, ectopic fat deposition will become pathogenic mainly through the disruption of insulin signaling (Shulman, 2014). Impaired insulin signaling in adipocytes will promote lipolysis and encourage the re-esterification of lipids in other tissues such as skeletal muscle and the liver (Figure 2). In skeletal muscle, intramyocellular lipid accumulation will reduce the amount of insulin-mediated glucose uptake (Samuel and Shulman, 2012). The resulting hyperglycemia will be managed by hepatic insulin-independent glucose absorption. However, hepatic lipid accumulation will disrupt the regulation of gluconeogenesis and activate glycogen synthesis. Furthermore, hepatic lipogenesis will not be affected, thereby promoting energy excess in the liver and worsening NAFLD (Samuel and Shulman, 2012).

2.3 The Impact of the Western Diet on the Brain

Although the semipermeable blood-brain barrier (BBB) is designed to tightly regulate the passage of ions, molecules and cells from the peripheral blood into the brain, it does not

render the brain immune to the effects of WD-induced inflammation (Daneman and Prat, 2015). In fact, changes in brain chemistry and function commonly occur with diet-induced metabolic disruptions (André et al., 2014; Hryhorczuk et al., 2017; Kanoski and Davidson, 2011; Kien et al., 2014; Marwitz et al., 2015; Sarfert et al., 2019; Woodie and Blythe, 2017). Insulin and leptin signaling are essential for neuron growth and maintenance as well as protection against neuronal apoptosis (Plum et al., 2005). Portions of the hypothalamus essential to feeding and metabolism are circumventricular organs that lack the protective BBB. The BBB of other brain regions, such as the hippocampus, also becomes increasingly permeable as WD consumption and inflammation progress (Davidson et al., 2013; Hargrave et al., 2016; Mimee et al., 2013).

2.3.1 The Hypothalamus

Located on ventromedial aspect of the brain, the hypothalamus consists of several nuclei each with unique clusters of neurons that boast high levels of connectivity. This allows for the hypothalamic nuclei to carry out distinct functions while permitting the hypothalamus as a whole to act as a central site of integration of homeostatic cues. A hypothalamic nucleus of particular interest to this review is the arcuate nucleus (Arc), which harbors several populations of neurons with differing impacts on satiety, namely agouti-related protein (AgRP) / neuropeptide Y (NPY) and pro-opiomelanocortin (POMC) expressing neurons (Figure 3a). AgRP/NPY neurons co-express AgRP and NPY to promote appetite while POMC neuron activity has the opposite affect by expressing α-melanocyte-stimulating hormone (α-MSH) to induce satiety (Heisler and Lam, 2017; Xu and Xie, 2016).

Both AgRP/NPY and POMC neurons project from the Arc to the paraventricular nucleus (PVN) where their excitatory or inhibitory signals are integrated and relayed to the parabrachial nucleus (PBN, Figure 3a) (Heisler and Lam, 2017; Xu and Xie, 2016). AgRP/NPY signaling potentiates inhibitory efferents to the PBN, which allows for the execution of food seeking behaviors and the release or preparatory mechanisms for nutrient digestion (Aponte et al., 2011; Gropp et al., 2005; Krashes et al., 2011). POMC neurons, on the other hand, produce α-MSH to potentiate excitatory efferents from the PVN to the PBN, subsequently inducing satiety (Fenselau et al., 2017; Garfield et al., 2015). Interestingly, AgRP/NPY neurons possess the ability to inhibit POMC neurons from producing α-MSH with no compensatory mechanism for the inhibition of AgRP/NPY expression (D'Agostino and Diano, 2010; Essner et al., 2017). Although this mechanism may have been evolutionarily useful to override satiety when food was scarce, it is now working to the detriment of human health by potentiating WD consumption in the face of satiety.

2.3.1.1 Effects of the WD on the Hypothalamus

The intricate workings of feeding signals from the Arc are further complicated by afferent signals from the periphery. Insulin and leptin are of particular importance in the context of WD feeding because their production and potency are significantly altered by pathogenic weight gain (Xu and Xie, 2016). Changes in the peripheral signals of nutrient availability alter the delicate signaling balance in the hypothalamus. This is in addition to WD-induced inflammation that not only disrupts peripheral insulin and leptin signaling

but can induce hypothalamic inflammation early after dietary exposure (Dalvi et al., 2017; Waise et al., 2015).

In the periphery, macrophages mediate a large portion of WD-induced inflammation. Behind the BBB, neuroglia, such as astrocytes, and the brain's resident macrophages, microglia, provide support and protection to the central nervous system (Jeong et al., 2013; Sofroniew, 2015). Astrocytic foot processes interact with brain microvessels and capillaries to maintain the BBB and regulate the passage of ions, water and nutrients into the brain. Astrocytes are also superbly sensitive to circulating cytokines and are known to mount a pro-inflammatory response to peripheral injury (Hamby et al., 2012; John et al., 2005; Zamanian et al., 2012). Microglia work to survey the brain for abnormalities or damage. They can rapidly respond to injury to aid in the recovery of a healthy brain but can also become over-active and detrimental to the brain during WD-induced inflammation (Figure 3b) (Kim and Joh, 2006; Valdearcos et al., 2014).

Indeed, hypothalamic inflammation is commonly observed in the hypothalamus of both rodents and humans after consumption of a WD (Baufeld et al., 2016; Dalvi et al., 2017; De Souza et al., 2005; Waise et al., 2015). However, it is unclear whether this activation is caused by the infiltration of peripheral macrophages, due to proliferating neuroglia, or by a combination of both. In 2016 Baufeld *et al.* developed a mouse line with green fluorescent protein (GFP) expressing myeloid cells to answer this question. They found that while the WD did not increase the number of GFP expressing cells in the hypothalamus, the diet did increase the number microglia as assessed by staining with ionized calcium-binding adaptor molecule 1 (Iba1+), suggesting the increase in these

Iba1+ cells was due to WD-induced proliferation of resident microglia (Baufeld et al., 2016).

Another noteworthy point examined by Baufeld *et al*. was the time course of hypothalamic inflammation after WD feeding. In their study, hypothalamic inflammation was only present after eight weeks of WD with no apparent microglial activation after three days or four weeks (Baufeld et al., 2016). Furthermore, a 2017 study by Dalvi *et al*. found that while astrocytic activity in the Arc increased after eight weeks of WD feeding, inflammatory cytokines such as TNF-α did not significantly differ from chow fed animals until the twentieth week of WD exposure (Dalvi et al.). In contrast, other studies have observed increases in hypothalamic microglial activation after just one to three days of WD feeding (Thaler et al., 2012; Waise et al., 2015). These differences may be attributed to methodological differences among these studies such as percentage and source of saturated fat in the WD.

Interestingly, the source of TNF-α observed by Dalvi and colleagues was not from neuroglia, but from AgRP expressing neurons (Dalvi et al.). In fact, several studies have observed that consumption of a WD not only induces pro-inflammatory cytokine production in the hypothalamic neuroglia, but that saturated fats also induce apoptosis and upregulate markers of endoplasmic reticulum stress in the neurons themselves (Dalvi et al.; Hryhorczuk et al., 2017; Mayer and Belsham, 2010; Milanski et al., 2009; Moraes et al., 2009; Won et al., 2009). This effect of saturated fat is mediated through TLR4 as WD-induced pathogenic adipose expansion results in the necrosis of adipocytes and the release of FFAs into circulation. Adipocyte-derived FFAs, including the saturated fatty acid palmitate, readily cross the BBB and interact with TLR4-expression neuroglia to

upregulate central inflammatory signaling (Hamilton and Brunaldi, 2007). Neurons and neuroglia over-express TLR4 after WD feeding and subsequently increase pro-inflammatory cytokine production via IKKβ/NF-κB signaling (Akira and Takeda, 2004; Dalvi et al.; Hayden and Ghosh, 2008; Moraes et al., 2009).

The susceptibility of hypothalamic neurons to the effects of WD-induced inflammation and FFA release, however, seems to depend on the neuronal subpopulation. Palmitate treatment to hypothalalmic neurons both *in vivo* and *in vitro* upregulates the expression of NPY mRNA via IKKβ signaling (Dalvi et al.; Posey et al., 2009). Furthermore, genetic manipulations to induce IKKβ signaling in the hypothalamus have been shown to increase feeding while manipulations to reduce its signaling promote anorexic behaviors (Zhang et al., 2008). POMC neurons, on the other hand, particularly in mice with genetic propensities to develop diabetes, were substantially more susceptible to WD-induced inflammation and apoptosis (De Souza et al., 2005, 2007; West et al., 1994). Mechanistic studies directly examining these selective effects are sure to be forthcoming. Nevertheless, selective WD-induced changes in hypothalamic neural subpopulations likely play a key role in the homeostasis of body adiposity and the balance between appetite and satiety (Figure 3b).

The balance between appetitive and satiated signals will, for the foreseeable future, always be tipped in favor of feeding. Evolutionary pressures have resulted in the capacity of humans to gain weight when energy is plentiful and to maintain body weight at all costs. The current availability of energy dense foods plays into this tipped scale and has promoted the obesity epidemic that Western society struggles with today. However, the WD effects on the brain do not stop at the hypothalamus and weight homeostasis.

Along with obesity and metabolic diseases, the Western world is dealing with an uptick in diet-induced dementias. Type-III Diabetes has been continually used to refer to Alzheimer's disease-like dementias that are comorbid with WD-induced metabolic diseases (de la Monte and Wands, 2008). Thus, the next section will discuss how WD feeding disrupts the chemistry and function of the hippocampus, the mammalian center for learning and memory.

2.3.2 The Hippocampus

2.3.2.1 Anatomy

The hippocampus is a curled ridge of gray matter in the medial temporal lobe that is crucial for memory formation and recall and plays a key regulatory role in the limbic system, particularly concerning fear, anxiety, and stress. Structurally, the hippocampus consists of the dentate gyrus (DG), the subiculum and the main body, or cornu ammonis (CA), which is divided into subfields CA1-CA4 (Figure 4a). The DG receives information from the entorhinal cortex which is relayed to the CA3 via the mossy fiber circuit (Bartsch and Wulff, 2015). After processing by the DG and CA3, information passes through the Schaffer collateral pathway to the CA1 then to the entorhinal cortex via the 54hosphor54t pathway (Figure 4a) (Aksoy-Aksel and Manahan-Vaughan, 2015).

2.3.2.2 Synaptic Plasticity

The main excitatory neurotransmitter within the hippocampus is glutamate, which is essential for hippocampal plasticity (Nakanishi, 1992). LTP and long-term depression (LTD) are the electrochemical events through which glutamate maintains plasticity. LTP

describes the excitatory events that underlie memory formation by eliciting long-term structural and chemical changes to strengthen synaptic pathways (Collingridge and Bliss, 1995). LTD, on the other hand, actively weakens synaptic pathways that are no longer needed (Ito, 1989). Hippocampal synaptic efficiency is upheld by the interplay between LTP and LTD and is fundamental for information processing and storage within the brain.

Glutamate receptors are categorized into two groups: ionotropic and metabotropic (Nakanishi, 1992). For the purposes of this discussion, the ionotropic N-methyl-D-aspartate (NMDA) receptor will be the point of focus. When a neuron is in a resting, depolarized state, NMDA receptors are blocked by a magnesium ion. Upon glutamate binding, magnesium is released and the inward flow of calcium hyperpolarizes the neuron (Paoletti et al., 2013). A proposed mechanism for the conversion between LTP and LTD is an alteration in the polarity of hippocampal neurons brought on by changes in NMDA receptor subunit composition. NMDA receptors are tetramers made up of di- and tri-heteromeric combination of GluN1, GluN2A-D and GluN3A-B (Paoletti et al., 2013). GluN2A and GluN2B have been the subject of much debate in the context of LTP-LTD switching. Various genetic and pharmacological studies suggest that GluN2A subunits are a driver for LTP while GluN2B subunits are more involved in LTD. Brigman *et al.* performed electrophysiological experiments on brain slices from mice lacking GluN2B in CA1 pyramidal cells. The mutant slices exhibited an intact response to a LTP protocol, but an abolished response to an NMDA receptor-dependent LTD protocol (Brigman et al., 2010). Furthermore, the selective inhibition of GluN2A-containing receptors with zinc specifically inhibited LTP and not LTD (Papouin et al., 2012). GluN2A-GluN2B

subunit switching does not appear to be a general or the only mechanism through which LTP-LTD alteration occurs. A myriad of studies suggest alternate and conjunctive mechanisms (e.g. extrasynaptic NMDA receptor composition, subunit interaction with CaMKII, expanded role of the GluN1/GluN2A/GluN2B tri-heteromer, etc.) (Barria and Malinow, 2005; Harney et al., 2008; Paoletti et al., 2013).

2.3.2.3 The Effects of the WD on the Hippocampus

The signaling and passage of peripheral cytokines across the BBB serves an adaptive purpose by alerting the brain to illness or injury and mainly works to the benefit of an organism by initiating the expression of sickness behavior (Dantzer and Kelley, 2007). Chronic passage of peripheral factors across the BBB, however, becomes detrimental to brain health when the BBB becomes "leaky" in response to WD feeding (Figure 4b). This WD-induced effect is in part due to the reduced expression of BBB tight junction proteins along the hippocampal vasculature (Freeman and Granholm, 2012). Indeed, exogenously administered dye was found exclusively in the hippocampus and not in the amygdala or other limbic structures of WD-fed rats (Davidson et al., 2012). Increased permeability may also result from WD-induced hypertriglyceridemia and hyperinsulinemia that disrupts homeostatic signaling across the BBB. Several studies have found increased peripheral triglycerides and insulin to correlate with impairments in hippocampal neuronal signal transmission, transduction, and function (Almeida-Suhett et al., 2017; Arnold et al., 2014; Farr et al., 2008; Ho et al., 2015). Additionally, neurotoxic agents and other peripheral cytokines are able to pass through the permeable BBB, causing hippocampal neurodegeneration and neuroinflammation (Hargrave et al., 2016).

In particular, a WD-induced increase in hippocampal IL-1β has been associated with impaired hippocampal function. Mice fed a WD had poorer spatial memory abilities as measured by performance on a Y-maze task, which was correlated with increased IL-1β levels in the hippocampus (Almeida-Suhett et al., 2017). Spatial memory in the Morris Water Maze task was also impaired after WD and was once again accompanied by elevated hippocampal IL-1β (Boitard et al., 2014). Additionally, increased IL-1β expression has been observed in the hippocampi of WD-fed rats following a foot-shock. This increase was found to lead to impaired fear conditioning and blocking IL-1β signaling with an IL-1 receptor antagonist ameliorated memory disruption even after WD feeding (Sobesky et al., 2014).

It is widely known that diets high in saturated fat lead to peripheral insulin resistance, but the effect of the WD on brain insulin resistance has more recently been investigated. Insulin is a regulator of hippocampal neuroplasticity, and its action is critical to normal cognitive function (Fadel and Reagan, 2016). Arnold and colleagues found that a WD caused hippocampal insulin resistance, synaptodendritic abnormalities, and impaired spatial working memory (Arnold et al., 2014). Their results pointed to serine phosphorylation of IRS-1 as a potential mechanism for these impairments as it was increased in the WD fed group. Indeed, this inactivating phosphorylation was associated with neuronal abnormalities and cognitive impairment. Arnold *et al.* found that animals with increased hippocampal IRS-1 serine phosphorylation also exhibited impaired LTP and structural abnormalities in the CA3 as demonstrated by decreased postsynaptic density marker PSD-95 and dendritic spine markers like spinophilin. Interestingly, these adverse effects were more severe after short-term, 60% kcal from fat WD exposure than

after a chronic, moderate (45% kcal from fat) WD feeding (Arnold et al., 2014). Furthermore, another study found that reverting to a chow diet after WD feeding not only rescued hippocampal insulin sensitivity and IRS-1 tyrosine phosphorylation, but also restored short-term memory capability (Sims-Robinson et al., 2016).

The WD impacts hippocampus-dependent memory and cognition through several distinct mechanisms, including insulin resistance, inflammation, and BBB disturbances. Insulin resistance is characterized by phosphorylation of IRS-1 and -2 at inactivating serine residues and interferes with LTP. The inflammatory cytokine IL-1β causes memory disruption, particularly in contextual fear conditioning (Sobesky et al., 2014). Leakiness in the BBB caused by WD can contribute to inflammation and disruption to hippocampal homeostasis (Figure 4b). Fortunately, WD-induced memory impairment may be recovered with dietary intervention, due in part to the neuroplasticity of the hippocampus.

2.4 Circadian Biology

The 2017 Nobel Prize in Physiology or Medicine was awarded to Michael Young, Michael Rosbash, and Jeffrey Hall for their pioneering work in chronobiology. Since their influential studies using *Drosophila* in the late 1980s to early 1990s, their careers have continued to center around identifying core clock genes and understanding how they function with in the circadian machinery. In past years, the field of chronobiology has exploded and inspired manifold works on rhythmicity around the world.

It is important to note that a "true" circadian rhythm is defined by any rhythm that, 1) oscillates within a 24 hour period in the absence of an external cue (e.g. light or

food), 2) is entrainable to an external cue (e.g. light or food) and 3) persists across a variety physiological temperatures (Takahashi et al., 2008). Therefore, studies performed under 12:12 light:dark conditions are not measuring circadian rhythmicity. Light:dark studies are actually measuring diurnal rhythmicity since light is acting as a zeitgeber, or as an entraining factor on all behavioral and molecular rhythms. In true circadian studies, animals are kept under dark:dark conditions and experimental timing is referred to as "subjective day" or "subjective night" and denoted by circadian time (CT). The timing of diurnal experiments is set to the presence of light and denoted by zeitgeber time (ZT), with the time of lights on indicating ZT 0 and lights off as ZT 12.

2.4.1 Introduction and Definitions

The rhythm of all mammals living on the Earth's surface is dictated by the rotation of the Earth around the Sun. These photic signals are transmitted from retinal ganglia to the hypothalamic SCN. The presence of daylight entrains the rhythms of SCN neurons to a 24 hour cycle by initiating the transcription and translation of core clock genes in a TTFL (Welsh et al., 2010). These genes exhibit specific times of heightened expression (phase or acrophase), times of lowered expression (nadir) and a tempo of acrophase and nadir (period). The difference in expression values between acrophase and nadir is known as the amplitude of a gene. Although the circadian TTFL contains several redundant genes, circadian rhythms can still be disrupted by a number of external and internal factors. Disruptions result in phase advances or delays within a 24-hour cycle and cause periods to be shortened to occur more than once in 24 hours (ultradian) or elongated to occur over 24 hours (infradian). Finally, circadian disruptions can cause the difference between

acrophase and nadir to either be increased (enhanced amplitude) or decreased (dampened amplitude).

The circadian TTFL is comprised of BMAL1, CLOCK/NPAS2, PER1-3, CRY1 and 2 and REV-ERBα and β (Figure 5). BMAL1 and CLOCK/NPAS2 form the positive arm of the loop, while PER, CRY and REV-ERB make up the inhibitory or negative arm (Figure 5) (Dibner et al., 2010; Mohawk et al., 2012; Stratmann and Schibler, 2012). BMAL1 and CLOCK/NPAS2 form a heterodimer in the cytoplasm and, upon translocation to the nucleus, activate gene expression of *Per, Cry* and *Rev-erb*s (Figure 5a). PER and CRY complex in the cytoplasm and return to the nucleus to inhibit the transcriptional activity of BMAL1:CLOCK/NPAS2. REV-ERB inhibits *Bmal1* by actively repressing gene transcription at the negative response element (Mohawk et al., 2012). Therefore, accumulation of the PER:CRY complex and REV-ERB decreases the levels of, BMAL, CLOCK and NPAS2 (Figure 5b). Reduced abundance and activity of the positive arm will decrease transcription of the negative arm components thereby releasing expression of the positive arm to begin the loop again. Furthermore, PER out of complex with CRY will inhibit REV-ERB repression of *Bmal1* (Schmutz et al., 2010). This series of interlocking regulatory loops creates the stable and precise oscillatory pattern of core clock gene expression.

The downstream impacts of core clock genes on CCGs allow the SCN to set the rhythm for the majority physiological, metabolic and behavioral processes (Mohawk et al., 2012). Indeed, almost half of the mammalian genome exhibits circadian rhythmicity in its pattern of expression (Yan et al., 2008). The core clock genes, however, are ubiquitous and oscillate within the TTFL throughout the body with the exception of

embryonic stem cells (Dibner et al., 2010; Dierickx et al., 2017, 2018). Furthermore, the set of CCGs expressed in each tissue are highly specific and tailored to the function of the tissue in question.

2.4.2 The Molecular Mechanisms of Circadian Rhythmicity

2.4.2.1 Brain and Muscle Aryl Hydrocarbon-like Protein 1

BMAL1 is a basic helix-loop-helix (bHLH)-PAS transcription factor that forms a complex with CLOCK and NPAS2 to form the positive arm of the circadian TTFL (DeBruyne et al., 2007; Lowrey and Takahashi, 2004). BMAL1 and CLOCK/NPAS2 heterodimerize in the cytoplasm and then translocate to the nucleus to activate transcription at E-box enhancer sequences. Specifically, the BMAL1:CLOCK/NPAS2 complex binds to the M34 *cis* element that contains a core E-box element and the BMAL1:CLOCK/NPAS2 consensus sequence 5'-G/TGA/GACACGTGACCC-3' (Haque et al., 2019; Hogenesch et al., 1998). BMAL1:CLOCK/NPAS2 activates transcription of its own repressors, *Per*, *Cry* and *Rev-erbα*, as well as a host of CCGs (Haque et al., 2019; Lowrey and Takahashi, 2004). Transcript and protein levels of BMAL1 exhibit acrophases in the middle of the dark phase with peaks in BMAL1:CLOCK/NPAS2 DNA binding events occurring during the light phase (Maywood et al., 2003; Menet et al., 2014; Tamaru et al., 2000).

Whole-body knockout experiments found *Bmal1* to be the only non-redundant core clock gene. Indeed, animals with single gene knockouts for every other core clock gene were able to generate circadian rhythms (Liu et al., 2007; Lowrey and Takahashi, 2004). A whole-body *Bmal1* knockout (*Bmal1*-KO), on the other hand, completely

eliminates central and peripheral rhythmicity and results in a myriad of other health issues (e.g. low body weight, reduced lifespan and low activity) (Bunger et al., 2000; Kondratov et al., 2006; Sun et al., 2006). Recent work using a *Bmal1*-KO with liver-only *Bmal1* reconstitution (Liver-RE) found that the rhythmicity of the hepatic core clock and carbohydrate metabolism genes were restored in Liver-RE mice. Body weight, lifespan, and hepatic lipid metabolism, however, were not rescued by the liver-specific *Bmal1* reconstitution, indicating the importance of *Bmal1* in the full circadian system (Koronowski et al., 2019).

2.4.2.2 Circadian Locomotor Output Cycles Kaput

The mRNA and protein levels of CLOCK are constitutively expressed in most tissues and considered to be dispensable for circadian rhythmicity (DeBruyne et al., 2006; Maywood et al., 2003). CLOCK-deficient mice maintain robust rhythms in locomotion and CLOCK may be functionally replaced by NPAS2 in the positive arm heterodimer to maintain the circadian transcriptional program (DeBruyne et al., 2007; Mohawk et al., 2012). Without CLOCK, animals do exhibit a shortened circadian period and slight alterations in rhythmic patterns, but overall retain circadian rhythmicity (DeBruyne et al., 2006, 2007). The main role of CLOCK within the core clock, therefore, is modulatory. CLOCK-deficient mice exhibit rhythmic, but significantly dampened expression of core clock genes and CCGs (DeBruyne et al., 2006).

2.4.2.3 Neuronal Per-Arnt-Sim Domain Protein 2

NPAS proteins were first identified by two separate labs in 1997. In January of that year, NPAS1 and 2 were described as bHLH-PAS transcription factors selectively expressed in the brain (Zhou et al., 1997). Then in March, they were found to interact with aryl-hydrocarbon receptor nuclear translocator (ARNT; the protein from which BMAL1 gets its name) (Hogenesch et al., 1997). Joseph Takahashi's lab then detected a striking similarity between the *CLOCK* gene sequence and the *NPAS2* gene sequence, and in 2001, NPAS2 was found to participate in the forebrain circadian clock (King et al., 1997; Reick et al., 2001). Finally, in 2007, NPAS2 was characterized as a functional substitute for CLOCK in the SCN (DeBruyne et al., 2007).

Continuing with its similarity to CLOCK, NPAS2 is also dispensable for circadian rhythmicity. Since NPAS2 is only expressed in a subset of tissues, whole-body knockouts produce a mild phenotype. *Npas2*$^{-/-}$ and wild type animals developed similar free-running behavioral patterns under dark:dark conditions. The amplitude of *Bmal1* expression was dampened in the SCN of *Npas2*$^{-/-}$ mice, but rhythmic expression of *Rev-erb* and *Per1* and *2* were maintained (DeBruyne et al., 2007).

2.4.2.4 Period

Period was the gene of interest for Young, Rosbash, and Hall in their initial *Drosophila* studies. Not only did they observe that a loss of *Per* gene expression and protein function resulted in arrhythmic behaviors, but they identified other core clock genes through their interactions with *Per* (e.g. *timeless* and *double-time*) (Liu et al., 1992; Price et al., 1998; Vosshall et al., 1994; Zehring et al., 1984). The PER protein is a part of the negative arm

of the circadian TTFL and works in conjunction with CRY to inhibit the actions of BMAL1:CLOCK/NPAS2.

Per is now known to exist in three mammalian paralogs: *Per1* (the first identified mouse ortholog), *Per2* and *Per3* (Kim et al., 2019). PER1 and PER2 differ by a single amino acid and exhibit oscillatory expression patterns in the SCN. *Per1* and *Per2* transcription is also acutely activated by a light flash. However, *Per1* transcription is activated by light throughout the subjective night, while *Per2* expression may only be induced during the beginning of the subjective night (Albrecht et al., 2001; Zylka et al., 1998). The biological significance of this distinction was probed by Albrecht *et al*. in 2001 by exposing *Per1* and *Per2* mutant mice to flashes of light during the subjective night. *Per1* mutant and wild type animals exhibited behavioral phase delays when exposed to an early night light pulse, but this response was lost in the *Per2* mutant animals. Furthermore, a late night light pulse elicited significantly phase advanced behaviors in *Per2* mutant mice. The *Per1* and wild type animals did not respond to a late night photic stimulus (Albrecht et al., 2001). *Per2* works to regulate the degree of phase advancement elicited by *Per1* in response to an aberrant pulse of light during the late night. *Per2* is also integral for setting phase delays in response to extended light cues. Therefore, *Per1* and *Per2* work in conjunction to modulate light-induced phase resetting.

PER3 shares gene sequence and protein structural similarities to PER1 and PER2, and *Per3* expression closely resembles the circadian pattern of *Per1* and *Per2* in the SCN. However, *Per3* transcription is not light inducible during the subjective night (Zylka et al., 1998).

The PER2 paralog is set apart from its family members by its distinct ability to interact with nuclear receptors. Of particular importance to this discussion, is the ability of PER2 to bind to REV-ERBα and modulate the repression of *Bmal1*. *Per2* appears to regulate the phase in which REV-ERBα represses *Bmal1* transcription. In a 2010 study by Schmutz *et al*., *Per2* mutant animals exhibited phase advanced repression of *Bmal1* that retained normal amplitude when compared to wild type. The *Rev-erba*-/- mice, however, had significantly de-repressed *Bmal1* expression (repression was not completely abolished; most likely owing to the repressor activity of REV-ERBβ, which will be discussed in a subsequent section). Further confirming the PER2's role in regulating REV-ERBα repression, *Bmal1* repression and rhythm of expression were completely lost in *Rev-erba-/-/Per2* mutants (Schmutz et al., 2010).

2.4.2.5 Cryptochrome

The initial function of Cryptochromes was elusive and inspired the crypto- prefix to their name. However, they were identified as blue light photoreceptors that regulated seedling growth and circadian rhythmicity in plants (Devlin and Kay, 1999). The role of CRYs in plant rhythmicity spurred an investigation in to whether they were present in *Drosophila* and mammals. Indeed, CRY1 and CRY2 homologues were identified in flies and mice in the late 1990s (Emery et al., 1998; Miyamoto and Sancar, 1998; Stanewsky et al., 1998). *Cry*s were found to have a similar oscillatory expression profile to *Per* with acrophase occurring at the transition from day to night (Lee et al., 2001). Then CRYs were identified as essential partners for PER-mediated inhibition of BMAL1:CLOCK/NPAS2. The PER:CRY complex maintains PER stability and allows for more efficient nuclear

translocation, but CRY1 and CRY2 may be functionally interchanged (Lee et al., 2001). In the absence of both CRY1 and CRY2, however, circadian rhythms are lost due to decreased PER-mediated BMAL:CLOCK/NPAS2 inhibition (Horst et al., 1999; Kume et al., 1999).

CRYs have recently been found to interact with nuclear receptors (NR) to repress transcription. Work from the labs of Katja Lamia and Ronald Evans found that CRYs impose circadian rhythmicity on the activity NRs (Kriebs et al., 2017). In a study examining glucocorticoid receptor (GR) activity, Lamia *et al.* found that CRYs interact with the GR in an inhibitory fashion as CRY deficiency resulted in glucose intolerance and constitutively high levels of corticosterone (Lamia et al., 2011). CRY1 and 2 also interact with peroxisome proliferator-activated receptor delta to modulate lipid metabolism and exercise capacity (Jordan et al., 2017).

2.4.2.6 REV-ERBs

REV-ERBα (*NR1D1*) and the highly related REV-ERBβ (*NR1D2*) were discovered in 1989 and 1994, respectively (Lazar et al., 1989; Miyajima et al., 1989; Yin et al., 2010). REV-ERBα was then identified as a potent transcriptional repressor. REV-ERBα monomers bind to the canonical nuclear receptor "AGGTCA" half-site to repress genes throughout the genome (Harding and Lazar, 1995). For circadian control, REV-ERBα binds within elements for the constitutively active orphan receptor, retinoid acid-related orphan receptor (ROR; ROREs), to repress *Bmal1*, *Clock,* and *Npas2* expression (Giguère et al., 1995; Preitner et al., 2002; Yin et al., 2010; Zhang et al., 2015). Although monomeric REV-ERBα cannot actively repress transcription, it can prevent transcription

at specific binding elements by preventing activator binding (Harding and Lazar, 1995). Active transcriptional repression is achieved by two REV-ERBα monomers binding to their response elements (Zamir et al., 1997). This initiates recruitment of histone deacetylase and nuclear receptor corepressor (NcoR) to the transcription site (Guenther et al., 2000; Ishizuka and Lazar, 2003, 2005; Yin and Lazar, 2005; Zamir et al., 1996; Zhang et al., 2002). Furthermore, REV-ERBα and β have nearly identical cistromes and can bind noncompetitively to collaborate and form a functional repressor unit (Bugge et al., 2012).

REV-ERBα and β are able to compensate for each other in circadian clock regulation, but REV-ERBα appears to be the more dominant isoform in metabolic regulation. REV-ERBα and β peak in mRNA expression during the late light phase with the strongest DNA binding occurring at the end of the light phase (Bugge et al., 2012). A loss of only REV-ERBα or REV-ERBβ results in mild de-repression of *Bmal1* (Bugge et al., 2012). A knockdown of REV-ERBβ in REV-ERBα–null mice, however, dramatically de-represses *Bmal1* and *Npas2* (Bugge et al., 2012). There is no metabolic phenotype observed in *Rev-erbb* knockout animals, but a *Rev-erba* knockout results in mild hepatosteatosis (Bugge et al., 2012). Deficiency of both isoforms causes a severe disruption in liver lipid metabolism, extreme hepatosteatosis and significant dampening of metabolic rhythms (Bugge et al., 2012; Chaix et al., 2019). Furthermore, REV-ERBα has been shown to repress a number of genes involved in metabolic homeostasis. A lack of REV-ERBα results in unregulated gluconeogenesis via the de-repression of glucose 6-phosphatase (Yin et al., 2007). REV-ERBα is also known to repress apolipoprotein C-III (apoC-III) and animals lacking REV-ERBα exhibit elevated serum

levels of apoC-III, triglycerides and VLDLs (Raspé et al., 2002). The impacts of REV-ERB on both *Bmal1* and metabolic homeostasis, it is considered to be a key regulator at the intersection of circadian rhythmicity and metabolism.

2.4.3 The Suprachiasmatic Nucleus

The SCN is a bilateral structure located just above the optic chiasm on the anteroventral aspect of the hypothalamus (Welsh et al., 2010). The SCN is arranged by neurochemical content into two regions: the dorsal shell and the ventral core. The shell is mostly comprised of arginine vasopressin (AVP) containing cells while the core is made mostly of neurons that contain vasoactive intestinal polypeptide (VIP) (Welsh et al., 2010). AVPergic and VIPergic neurons, however, make up the minority of cells in the SCN as the major neurotransmitter is the inhibitory gamma aminobutyric acid (GABA) (Moore and Speh, 1993; Strecker et al., 1997).

Both sides of the SCN contain approximately 10,000 neurons, each of which is cell-autonomous. This means that their circadian TTFL oscillates independent of rhythmic input from other cells. In the core, autonomous rhythms are entrained to photic signals originating from retinal ganglion cells (RGC). RGC axons project along the retinohypothalamic tract (RHT) and synapse within the SCN (Figure 6). A subset of axons synapse on VIP neurons within the SCN core (Yan et al., 2007). The rhythm of cells within the core are synchronized with one another by the light-induced activity of VIPergic neurons (Figure 6) (Aton et al., 2005; Jones et al., 2018; Maywood et al., 2006). Core neurons also synchronize and maintain the rhythm of the shell through the rhythmic release of VIP (Figure 6) (Yamaguchi et al., 2003).

2.4.3.1 Mechanisms of SCN Entrainment

RGC axons project along the RHT to release glutamate and pituitary adenylate cyclase-activating polypeptide (PACAP) at synapses with SCN neurons (Figure 6). NMDA receptor-mediated glutamate signaling depolarizes the cell membrane resulting in calcium influx and activation of several kinase pathways. Glutamate-induced phosphorylation of cyclic adenosine monophosphate (cAMP) response element binding protein (CREB) initiates transcription of the core clock genes *Per1* and *Per2*. Responsiveness of the SCN to both glutamate is highly dependent on the time of day. Experiments performed on animals maintained under dark:dark conditions found that glutamate release, NMDA receptor-mediated CREB phosphorylation, and *Per* transcription occur within minutes of a light flash, but only during the subjective night (Akiyama et al., 1999; Colwell, 2001; Gau et al., 2002; Ginty et al., 1993; Pennartz et al., 2001; Shigeyoshi et al., 1997; Tischkau et al., 2003).

There are two theories to explain the time-of-day differences in SCN glutamate response. PACAP is released with glutamate at the RHT synapses in the SCN and works primarily though the G-protein-coupled receptor, PACAP type 1 receptor (PAC1) (Michel et al., 2006). During the subjective night, PACAP activity enhances the effect of glutamate on by inducing phase delays in neuronal firing and behavior. During the day, however, PACAP was found to inhibit phase advances (Chen et al., 1999). This seemingly contradictory role of PACAP may be governed by the presentation of particular PAC1 splice variants on the neuron membrane. PAC1-null for example is primarily coupled with $G\alpha_s$, while PAC1-hip-hop couples with $G\alpha_q$ and PAC1-hop1 will

couple with both $G\alpha_s$ and $G\alpha_q$ (Blechman and Levkowitz, 2013). It is tempting to postulate that the core clock TTFL has a hand in PAC1 splice variation, but this has yet to be determined.

The second theory involves time-of-day-dependent NMDA receptor subunit variability. NMDA receptors are known to be less responsive to RHT signaling during the day and more responsive at night. Furthermore, NMDA receptors exhibited a tonic level of activity only during the night, suggesting a potential priming mechanism to increase light sensitivity at night (Pennartz et al., 2001). Studies utilizing NR2A and NR2C deficient mice found that the A and C receptor subtypes played a minimal role in the SCN (Moriya et al., 2000). NR2B, however, seems to have a significant impact on SCN glutamate sensitivity. In a joint mouse and hamster study by Wang *et al*. in 2008, *Grin2b* (NR2B) mRNA expression was found to peak during the late light to early dark phase, while the NR2A 70hosphor-protein peaked during the dark phase. Blocking the activity of NR2B not only attenuated the light-induced delay in dark phase activity, but it reduced the magnitude of NMDA-mediated hyperpolarization in SCN neurons (Wang et al., 2008). Despite the above studies outlining an association between certain NMDA receptor subunits and light sensitivity, whether NMDA receptor subunit composition shifts in a circadian manner has yet to be examined. Due to the astonishing variability of NMDA receptor subunit composition within a single membrane, a clear, time-of-day shift may not even exist.

2.4.3.2 Melatonin

No discussion of circadian rhythms would be complete without the mention of melatonin. Melatonin is primarily produced from the pineal gland. Cells within the pineal gland are not cell-autonomous and the rhythmic production of melatonin is dictated by the SCN (Arendt, 2019). The concentration of melatonin in the cerebrospinal fluid (CSF) and plasma increases significantly with the induction of darkness and remains elevated until a sharp reduction to negligible levels during the light phase (Tan et al., 2016). This is brought on by the decrease of excitatory input from the RHT to the SCN in fading light and the subsequent release of melatonin production (Tan et al., 2018). Melatonin, therefore, acts as a feedback signal upon the SCN to ensure proper photoperiod or daylight length. Without melatonin signaling, mammals exhibit a free-running rhythm in which the onset of endogenous rhythms progressively shift out of phase (Tan et al., 2018).

Melatonin is often wrongly thought of as a sleep-inducing hormone primarily due to the fact that individuals sleep better when in phase with melatonin production (and the circadian system as a whole). In a small, but elegant and impressive study on pinealectomized humans, sleep efficiency and onset were not impaired in individuals missing a pineal gland (Slawik et al., 2016). Thus, melatonin is better thought of as a darkness hormone that feeds back on the SCN at the end of a photoperiod to “set” the biological clock.

2.4.4 Rhythmicity Beyond the SCN

As previously outlined, the SCN is regarded as the master circadian clock. Why it initially earned that distinction was due to the observations that; 1. SCN ablation resulted

in loss of behavioral rhythmicity; and 2. SCN transplant caused the recipient to adopt the circadian patters of the donor (Ralph et al., 1990; Sujino et al., 2003). Circadian clocks are now understood to function in a hierarchy, with the SCN at the top of light-entrained rhythms. However, specific tissues possess cell autonomy in other physiological processes. When considering the circadian system and its function in processes other rhythmicity, a defined hierarchy of circadian control becomes difficult to establish. In the next few sections, peripheral clocks and their distinct rhythmicity will be discussed.

2.4.4.1 The Circadian Rhythms of Metabolism

The rhythms of carbohydrate, lipid, and protein metabolism have been outlined at the macronutrient level in humans and mice. During the active phase (light cycle for humans, dark cycle for rodents), blood glucose rises to elicit an increase in glucose absorption and glycogen synthesis in the skeletal muscle and liver. Lipids are also absorbed more readily and lipoprotein lipase activity increases. Protein absorption and skeletal muscular and hepatic protein synthesis also increase during the active phase. During the inactive phase (dark cycle for humans; light cycle for rodents), more catabolic processes take place. Glycogenolysis is upregulated in the skeletal muscle and liver and lipolysis is increased in the adipose tissue. The activity of glutamine synthase and autophagy pathways are upregulated in the skeletal muscle, cardiac muscle, and liver during inactivity. Further breakdown of macronutrient metabolism during the active phase reveals that carbohydrates are preferred and more easily metabolized during the early active phase, where lipids and proteins are preferred and metabolized during the late active phase.

The rhythms of metabolism at the macronutrient level track closely with the fed/fasting cycle. Indeed, upon a continuous 24-hour fast, approximately 80% of oscillating transcripts lose their rhythmicity in the mouse liver. Interestingly, this is due to a dampening in oscillation amplitude with the peak level decreasing. Thus, peripheral tissues, in particular the liver, may depose the SCN in the rhythm hierarchy when the fed/fasting cycle is disrupted. Indeed, several components of the core clock TTFL are found at the intersection of rhythmicity and metabolism and the effects of core clock proteins on metabolism are presumed to dictate where in the rhythm hierarchy a peripheral tissue will fall in relation to the SCN. The discussion below will highlight several key proteins that couple the circadian clock to metabolism.

2.4.4.1.1 The Core Clock and Cellular Redox State

The cellular redox state and nicotinamide adenine dinucleotide (NAD^+) pathways are also used as markers for cellular metabolism and have been heavily researched in the context of circadian metabolism. For the purposes of this discussion, the NAD^+ salvage pathway will be the area of focus. NAD^+ may be salvaged through the conversion of nicotinamide (NAM) to nicotinamide mononucleotide (NMN) and NMN conversion to NAD^+. The NAM to NMN step is catalyzed via nicotinamide phosphoribosyltransferase (NAMPT). The *NAMPT* gene contains the consensus binding side for BMAL1:CLOCK/NPAS2 and chromatin immunoprecipitation results from two separate labs confirmed BMAL1:CLOCK/NPAS2 binding to the *NAMPT* regulatory elements (Nakahata et al., 2009; Ramsey et al., 2009). Ramsey *et al*. found that *Bmal*$^{-/-}$ mice exhibited a significant reduction in *Nampt* expression, while animals with a *Cry1/Cry2* double KO had elevated

Nampt expression (Ramsey et al., 2009). Work from Nakahata *et al.* and Ramsey *et al*. also found that NAD^+ will feedback on BMAL1:CLOCK/NPAS2 to reduce its synthesis via sirtuin deacetylases (SIRT). SIRT1, specifically, downregulates the transcriptional activity of BMAL1:CLOCK/NPAS2 (Nakahata et al., 2009; Ramsey et al., 2009). NAD^+, therefore, not only functions as an important metabolic output of the circadian clock, but also as an additional negative regulator of the positive arm through SIRT1 activity.

2.4.4.1.2 Cryptochromes and Adenosine Monophosphate-Activated Protein Kinase

Rhythmic degradation of CRY1 is mediated by the AMP/ATP sensor adenosine monophosphate-activated protein kinase (AMPK). In experiments using mouse embryonic fibroblasts (MEF), Lamia *et al*. identified two serine sites on CRY1 that, upon AMPK phosphorylation, were necessary and sufficient for interaction with ubiquitin ligases and proteasomal degradation. Furthermore, they found that the amplitude of circadian clock gene expression in MEFs was modulated by glucose concentration and that this response was lost in cells lacking AMPK. Finally, they observed an accumulation of AMPK and AMPK phosphorylation targets in the mouse liver that oscillated in a circadian manner (Lamia et al., 2009). These findings marked AMPK and CRY1 as key proteins in the link between nutrient availability and the circadian clock.

2.4.4.1.3 REV-ERBs and Heme

For many years after their discovery, REV-ERBα/β were considered to be orphan nuclear receptors. In 2007, however, two labs independently identified heme as the endogenous ligand for REV-ERBs (Raghuram et al., 2007; Yin et al., 2007). Heme is an iron-

containing porphyrin that participates as a prosthetic group in a series of oxidative metabolic processes. Heme binding to REV-ERB stabilizes the REV-ERB/NCoR repressor complex to increase REV-ERB-mediated repression. As previously mentioned, REV-ERBs repress *Npas2* expression. They also repress the expression of peroxisome proliferator-activated receptor gamma coactivator 1-alpha (*Pgc1a)*. The rate-limiting enzyme for heme synthesis is 5-aminolevulinic acid synthase 1 (ALAS1), the transcription of which can be activated by either NPAS2 or PGC-1a (Yin et al., 2010). Therefore, REV-ERBs function in a metabolic feedback loop to control the production of heme. High levels of heme increase REV-ERB-mediated repression to decrease *Alas1* transcription and subsequently decrease heme production. Low levels of heme will destabilize the REV-ERB/NCoR repressor complex to release the production of heme.

2.4.4.2 The Circadian Rhythms of Memory

Memory has been observed as a time-of-day dependent behavior in species from *Drosophila* to humans. One of the earliest studies to describe a time-of-day dependent behavior was in bees offered sugar water. In 1927, a German scientist by the name of Ingeborg Beling observed bees not only anticipating the reward, but returning to the feeder at the same time of day even when sugar was removed from the water (Beling, 1929). Since then, species ranging from other insects to mammals have displayed time-of-day dependent behaviors that suggest the existence of time-stamped memories.

However, since the molecular circadian clock was not entirely understood until the 1990s, how it functions in processes such as memory has yet to be fully established.

This section will review the studies that have pioneered the area of circadian neuroscience with a particular focus on hippocampus-dependent memory.

2.4.4.2.1 Time-of-Day-Dependent Hippocampal Memory

Studies utilizing hippocampus-dependent memory tasks have observed performance to differ depending on time-of-day in a wide variety of model organisms. Passive tasks, such as an open field task or maze tasks, are better acquired and performed during the active phase (Hauber and Bareiß, 2001; de Oliveira et al., 2014). Fear tasks, however, are better acquired during the inactive phase. In a study testing fear-conditioning in mice at different times of day, Chaudhury and Colwell speculate that improved inactive phase acquisition was due to the fact that day time is a "fearful time" for nocturnal animals (Chaudhury and Colwell, 2002). Furthermore, in tasks that require training, animals perform better in the probe trial when it is run at increments of 24-hours after the last training (Chaudhury et al., 2008; Eckel-Mahan et al., 2008; Holloway and Wansley, 1973).

A proposed reason for this 24-hour recall is "time-stamping" of events within hippocampal memory (Mulder et al., 2013). This notion is corroborated by the presence of time cells within the hippocampus and it is postulated that these cells place time as a contextual facet of a memory (Eichenbaum, 2014; Ekstrom and Ranganath, 2018; MacDonald et al., 2011, 2013; Sakon et al., 2014; Salz et al., 2016). These time-cells, however, do not represent the only way memory behaviors are circadian. The cellular machinery of memory has been found to oscillate in expression level throughout the day. The MAPK cascade is one of the many pathways involved in hippocampal long-term

memory formation and one of the best studied in the context of circadian rhythmicity. Work by Kristin Eckel-Mahan *et al.* found that MAPK and cAMP oscillate within the hippocampus in a circadian manner. In mice, both MAPK isoforms (Erk1 and Erk2) as well as the upstream MAPK kinase (MEK) exhibited an acrophase in phosphorylation during the light phase and nadir during the dark. Interfering with MAPK activity either by maintaining animals in light:light conditions or by pharmacological inhibition of MEK, impaired long-term memory in their animals. Interestingly, total protein levels of Erk1/2 and MEK did not oscillate over time, indicating that the circadian control of this pathway is dictated by phosphorylation events. Furthermore, cAMP levels within the hippocampus also peaked during the light phase and the light phase peak of both cAMP and MAPK were due to calcium-stimulated adenylyl cyclase activity. The findings from this study are interesting in that they suggest the molecular machinery of memory is upregulated during the inactive phase rather than the active phase. Indeed, in this particular work, Eckel-Mahan *et al.* utilized a fear conditioning task and found that animals performed better during the light phase when the MAPK pathway was active. However, taking these results along with those from Chaudhury and Colwell in 2002, suggest that fear conditioning is a stressful task better acquired during the inactive period. Furthermore, these results highlight an important aspect of memory that will be further discussed in a subsequent section: reconsolidation during sleep.

Work by Phan *et al.* suggests that oscillations in the hippocampal MAPK cascade are non-cell-autonomous as SCN lesioning ablates rhythmicity within the pathway (Phan et al., 2011). However, hippocampal LTP has been shown to be a truly circadian, cell-autonomous phenomenon (Cauller et al., 1985; Chaudhury et al., 2005). In a 2005 study

by Chaudhury *et al.*, animals kept in dark:dark conditions exhibited improved LTP maintenance when slices were collected during the subjective night as opposed to collection during the subjective day. They also found that under 12:12 light:dark conditions, slices taken during the day, but incubated until recording during the night, maintained LTP just as well as slices taken and recorded during the night (Chaudhury et al., 2005). Therefore, the hippocampus is cell-autonomous and possesses a mechanism through which memories may be formed without input from the SCN. MAPK may act as a non-cell-autonomous pathway and more research needs to be done to identify the cell-autonomous pathways behind hippocampal memory.

2.4.4.2.2 Sleep and Hippocampal Memory

Memory consolidation is the process through which newly collected experiences are established into an enduring memory. Human and rodent studies alike have indicated that reactivation or replaying memories during sleep is essential for consolidation (Buzsáki, 1998; Oudiette and Paller, 2013). Memories, however, are complex and continually being formed in the conscious animal with a multitude of associated information. A large amount of these associations are repetitive and share overlapping features with one another (Bekinschtein et al., 2014). Therefore, memory consolidation must not only function to strengthen a memory for storage, but it must also streamline the associated details to include the most relevant information. What remains to be determined is exactly how certain memories are selected and intensified while others are weakened. Without this unknown mechanism of selective intensification, long-term memory

representations would be convoluted with extraneous and possibly conflicting associations.

A human study by Oyarzún *et al*. in 2017 developed an overlapping memory paradigm to determine the impact of sleep on delayed memory reactivation (Oyarzún et al., 2017). Two sets of card pairs were shown to participants with the X1 card remaining constant and the X2 or X3 card differing in location. The X1-X2 card pair was presented without a sound cue, while the X1-X3 card pair was presented with a tone. A contiguous group learned the X1-X2 pair immediately before learning the X1-X3 pair, while a delayed group learned the X1-X3 pair after a three-hour delay. In the first experiment, recall for X2 was tested immediately after X1-X3 training. Here, they confirmed their initial hypothesis that making memories continuously increases the associative strength of separate items (X2 or X3) with an overlapping item (X1). Indeed, the delay group had a more difficult time recalling the location of X2 than the contiguous group. For the second set of experiments, both groups slept for approximately 48 minutes after learning X1-X3. While the participants were sleeping, electroencephalogram (EEG) data was collected and the same sound cue presented during X1-X3 training was played to facilitate memory reactivation. Upon waking, participants were asked to recall and recognize the location of X2 based on X1. Reactivating memories during sleep improved X2 association in the contiguous group, but decreased associative recall for X2 in the delay group. Their results indicate that associations made closer in time to the reactivated memory may be coded as “more important” to the main memory and are therefore remembered better than associations made farther apart.

A possible explanation for decreased recall in the delay group could be that reactivation "deletes" the less associated memory. Just considering recall of the memory, however, does not tell the whole story. Participants in the delay group were able to recognize that they had seen X2 presented with X1, but they were not able to accurately recall the location of X2 based on X1. Additionally, EEG data collected during nap-time reactivation revealed that the sound cue elicited theta wave responses, which indicate memory reactivation, in both the contiguous and delay groups. Theta wave presentation along with intact X2 recognition in the delay group signifies that the memory was sufficiently reactivated and persisted after waking. Interestingly, however, a beta response was also observed upon reactivation in the delay group. In contrast to theta wave, beta waves are associated with network scaling and indicate that while delayed memories were reactivated, they were also weakened (Hanslmayr et al., 2012). Therefore, memory reactivation during sleep may function as a way to call up collected memories for further processing into which associative networks are strengthened and which ones are weakened.

Key areas involved in this network level processing are the cerebral cortex, thalamus, and hippocampus. Coordinated activity among these three areas has been extensively researched as a mechanism of memory consolidation during sleep (Clemens et al., 2007; Dudai et al., 2015; Siapas and Wilson, 1998). In a recent paper by Latchoumane *et al.*, hippocampal ripples were found to nest within the trough of thalamic spindles that were in-phase with cortical slow oscillations (SO). The establishment of this "triple phase-lock" allowed for memories to be transmitted across neural networks to promote consolidation and long-term storage (Latchoumane et al., 2017). Whether the

strengthening or weakening of associated memories addressed by Oyarzún *et al.* is resolved before, after, or during the formation of the triple phase-lock in Latchoumane *et al.* is unclear. Since the reactivation of delayed memories in this study functioned to weaken the association (as determined by beta bands in the delay group), it can be postulated that memories would be streamlined early in the consolidation process, prior to being communicated to the cortex. Cortical SOs are also known to regulate hippocampal ripples and memory reactivation (Ngo et al., 2013; Sirota et al., 2003; Staresina et al., 2015). Furthermore, Oyarzún *et al.* hypothesize that the appearance of beta band activity is indicative of several brain regions being recruited to process the importance of an associated memory. Therefore, memories could be pruned of their unnecessary associations by regulatory regions during the initial rounds of cortical SO-induced ripple reactivation and become increasingly salient up to the instance of triple phase-lock.

Another lingering question is exactly how an associated memory is identified as unnecessary. What aspect of the delay in Oyarzún *et al.* changed the X2 association for it to be weakened? Introducing a delay between the reactivated memory and an associated memory presents a new accessory factor: time. Neuronal time keeping is a complex topic and time-memory specifically is the subject of many research efforts. Time cells in the CA1 region of the hippocampus encode the temporal structure of a memory through a sequence of firing patters specific to each memory (Gill et al., 2011; Manns et al., 2007). There is sufficient evidence to indicate when a delay is introduced to memories with overlapping features, the time cell firing pattern reduced (Eichenbaum, 2014). Indeed, MacDonald *et al.* found that when a training paradigm was elongated by a delay,

hippocampal time cells did not simply encode a delay into their firing pattern. Instead, they formed a new pattern that was distinct from the firing pattern associated with the non-delayed memory (MacDonald et al., 2011). Additionally, a human study found that the sequence of time cell firing that occurred during exposure to an event was recapitulated when asked to recall the event (Gelbard-Sagiv et al., 2008). Thus, delayed and contiguous memories have completely different associated time cell firing patterns and it may be this aspect of the delayed memory that, upon reactivation, targets it for weakening.

Oyarzún *et al.* also found that employing the same reactivation paradigm while the participants were awake did not improve recall. This indicates that the success of sound cue stimulated memory reactivation is state dependent. That is, it is not sound cue-induced reactivation itself that initiates memory strengthening or weakening, it is the brain state during which the sound cue occurs that determines modifications in associative strength (Frank and Cantera, 2014). This is important, as the sleep state is associated with an increase in mRNA and proteins involved in the synthesis of new and maintenance of existing synapses (Seibt and Frank, 2012; Seibt et al., 2012; Vecsey et al., 2012). Therefore, a circuit may be "primed" to handle reactivated memories when it is in a particular molecular state. In the aforementioned Eckel-Mahan *et al.* study from 2008, the MAPK signaling cascade is upregulated in the hippocampus of mice during their inactive period (Eckel-Mahan et al., 2008). This inactive phase activation may act as a sort of molecular replay mechanism and suggests that a specific brain state is required for replay and consolidation of a memory with its relevant associations.

2.4.4.2.3 The Core Clock and Hippocampal Memory

Studies utilizing core clock knockouts and mutants have begun to identify specific ways that the circadian clock affects memory. BMAL1, for example, is important for cell proliferation and pruning with in the dentate gyrus. Bouchard-Cannon *et al.* found that cell proliferation within the DG has an acrophase during the active phase and a nadir during the inactive phase. They also found that PER2 restricted the entry of neural progenitor/stem cells (NPSC) into the cell cycle, while BMAL1 was involved in the determination of how many cell cycles NPSCs were able to go through before entering quiescence. Furthermore, their *Bmal1*$^{-/-}$ animals had impaired pattern separation memory (Bouchard-Cannon et al., 2013). A separate study found that a *Bmal1* knockout increases the number of mature neurons within the DG due to a decrease in cell death (Rakai et al., 2014). Although they did not test memory behaviors to identify the implications, interpreting these results with those of Bouchard-Cannon *et al.* indicates that BMAL1 controls healthy cell cycling, and without it, there may be a buildup of unnecessary cells.

Hippocampal CRY and REV-ERB may be essential for time-place learning and food-anticipatory behaviors. Van der Zee *et al*. developed a circadian time-place learning (cTPL) paradigm where one of three arms was food baited at either 9am, 12pm, or 3pm. When not baited, the arms were rigged to provide a foot shock (Van der Zee et al., 2008). This mimics the natural scenario in which animals must remember where is safe to search for food at specific times of day. In their cTPL paradigm, they found that *Cry1/2* double knockout (*Cry* DKO) animals were unable to employ a circadian strategy in solving the maze and instead randomly searched the arms at all tested time points. This was not due to general cognitive deficits in the *Cry* DKO animals as they performed comparable to

wild type in both fear conditioning and spatial memory tasks (Van der Zee et al., 2008). Therefore, CRYs appear to be essential for time-of-day dependent learning and circadian memory. Finally, mice with a brain specific knockout of *Rev-erba* displayed de-repression of hippocampal *Bmal1* gene expression and a loss of food-anticipatory behaviors (Delezie et al., 2016).

2.5 Circadian Disruptions

The modern world is active for all 24 hours of the day. Constant access to food and entertainment and shift-work careers and trans-time zone flights push the limits of human circadian physiology. The circadian system evolved to temporally separate cellular states (e.g. the fed and the fasting state) in order to decrease the chance of futile cycling. When endogenous circadian pacing is at odds with the light:dark cycle, myriad health issues, collectively known as circadian-time sickness, can occur (van Ee et al., 2016).

Disrupted sleep is a major contributor to circadian-time sickness. Indeed, just one night of sleep disturbance impairs glucose metabolism in humans (van den Berg et al., 2016; Cedernaes et al., 2016; Nedeltcheva et al., 2009). Decreased sleep quality and quantity also increase the risk of developing T2DM (Li et al., 2016; Tsuneki et al., 2016). Melatonin production was observed to be low in a rat model of T2DM as well as human patients and exogenous melatonin administration prevents weight gain, hyperglycemia, hyperinsulinemia, and hyperlipidemia (Agil et al., 2012; Nduhirabandi et al., 2010; Peschke et al., 2006; Ríos-Lugo et al., 2010). Finally, sleep disturbances elevate orexin-mediated sympathetic nervous system activity, which causes elevated gluconeogenesis and can lead to glucose intolerance and insulin resistance (Li et al., 2013).

Circadian disruptions without significant alterations in sleep quantity or quality can still have a negative impact on mood, cognition, and general health (LeGates et al., 2014; Logan and McClung, 2019). Mice exposed to aberrant light:dark cycles exhibited elevated anxiety- and depression-like behaviors (LeGates et al., 2012). Furthermore, night shift-workers exhibited decreased performance and clear-headedness no matter if they were assessed on the first night shift or subsequent night shifts (McHill and Wright, 2019). Finally, a 2015 study found that sustained exposure to variability in light-dark cycles and constant alteration in behaviors to accommodate said variability (e.g. consistently traveling to and working in different time zones), but without changing sleep duration or sleep onset latency, predicted mortality in older people (Zuurbier et al., 2015).

2.5.1 Alzheimer's Disease

Building off of the discussion on circadian disruptions and decreased cognitive health, circadian disruption is classified as both a cause and a symptom of memory impairments (Alhola and Polo-Kantola, 2007; Foster and Wulff, 2005; LeGates et al., 2014). Dementias, including AD, are projected to become one of the most prevalent and costly diseases of the modern world. AD is characterized by severe amnesia and forgetfulness caused by cellular changes largely in the hippocampus. Research on shift workers has shown that chronic circadian disruptions can *cause* impairments in attention and cognitive function (Alhola and Polo-Kantola, 2007; Foster and Wulff, 2005; LeGates et al., 2014). In mice, constant circadian misalignment results in a phase advance in hippocampal *Per2* expression, decreased object memory, and impaired LTP maintenance (Loh et al., 2015). On the other hand, changes in the daily patterns of activity and

feeding as well as a decrease in the amplitude of core clock gene expression are known to appear early in AD progression, indicating that rhythm disruptions manifest as a *result* of AD development (Musiek et al., 2015).

2.5.2 Circadian Disruption by Diet

The majority of animals alternate between periods of feeding and periods of fasting. One of the major evolutionary theories for circadian rhythmicity is to establish temporal separation of feeding and fasting (Panda, 2016). This theory is supported by the breakdown of rhythmicity and decline in overall health that results when fed/fasting rhythms are not maintained.

In chow-fed mice, TRF to the inactive phase resulted in elevated triglycerides, altered glucose metabolism, and weight gain when compared to active fed mice. This phenotype was exacerbated when an inactive phase shift-work paradigm was added to inactive phase TRF. Active phase TRF, however, was able to correct inactive phase shift-work. Inactive workers on active TRF had corrected rhythms in activity, blood glucose, and triglycerides and had significantly reduced body weight an body fat (Salgado-Delgado et al., 2010). A 2016 study by Yasumoto *et al.* found that inactive TRF also increased plasma corticosterone, insulin and leptin. Core clock genes were also phase delayed or shifted in liver, white adipose tissue (WAT) and skeletal muscle in inactive fed mice (Yasumoto et al., 2016). Uncoupling feeding from the internal clock, therefore, is detrimental to overall health.

2.5.2.1 Circadian Disruption by the Western Diet

The above studies utilized a standard rodent chow diet and observed circadian disruptions induced by inactive phase feeding. Studies utilizing the rodent equivalent of a WD show that dietary content can exacerbate diet-induced circadian disruption. Among the seminal studies exploring this connection was a 2007 paper from Joseph Bass's lab. In it, Kohsaka *et al*. found that wild type mice fed an *ad lib* 60% fat/kcal diet exhibited disrupted rhythms in feeding and locomotion. Upon switch to the experimental diet, the animals spread their activity and food consumption out over the day and night cycle. Animals maintained on the *ad lib* normal chow diet self-restricted their feeding and activity to the night phase. Furthermore, they found that the rhythmicity of *Clock*, *Bmal1* and *Per2* gene expression was significantly dampened in the liver and epididymal WAT (eWAT) of high-fat fed mice (Kohsaka et al., 2007). In 2005, work by Joseph Bass and Joseph Takahashi also highlighted the synergistic effects core clock disruptions and high-fat feeding can have on metabolism health. *Clock* mutant mice were more sensitive to weight gain on a 60% fat/kcal diet than wild type mice maintained on the same diet (Turek et al., 2005).

Along with her work in the circadian rhythmicity of memory, Kristin Eckel-Mahan also published a study diving deeper into the mechanism through which the WD induces circadian disruptions. Her work with Paolo Sassone-Corsi and others found that a 60% fat/kcal inhibited BMAL1:CLOCK chromatin recruitment thereby decreasing a number of oscillatory CCGs. Unexpectedly, they also observed a number of genes gain oscillatory rhythm. They found that this was due to a diet-induced upregulation in peroxisome proliferator activating receptor gamma (PPARγ) chromatin recruitment and

transcription events, thereby reprogramming the circadian clock (Eckel-Mahan et al., 2013).

2.5.3 Food-Entrainable Oscillators

Interestingly, Kohsaka *et al.* found hypothalamic *Clock, Bmal1* and *Per2* were resistant to diet-induced changes and maintained similar rhythmicity in chow- and WD-fed groups (Kohsaka et al., 2007). Other studies have observed a similar resistance to dietary intervention in the hypothalamic clock. TRF to the inactive cycle phase shifts *Per1/2* expression from low in the day and high at night to high in the day and low at night. This occurs in a variety of brain regions, but not in the SCN (Wakamatsu et al., 2001). Food-anticipatory behaviors also remain intact in SCN-lesioned animals (Hara et al., 2001). These findings indicate that the SCN is resistant to nutritional challenge. Therefore, one or more FEO must exist outside of the master clock. Thus far, the liver represents the most viable location for a FEO as even under dark:dark conditions, 15% of hepatic transcripts retain circadian oscillation. When food is removed as a zeitgeber, however, only a small subset of transcripts retained rhythmic expression (Vollmers et al., 2009).

2.5.4 Time-Restricted Feeding

Since the presence of FEOs were suggested by the above studies, multitudes of research efforts have been launched to locate and better understand them. TRF studies have been the most popular way to examine cell-autonomous FEOs. Moreover, TRF has been thoroughly examined as an alternative to traditional, restrictive dieting for improving

metabolic health. In the following sections, rodent and human studies utilizing TRF will be discussed.

2.5.4.1 Rodent Studies of Time-Restricted Feeding

Hatori *et al*. published one of the first large-scale physiologic and metabolomic TRF studies. Mice were given either standard rodent chow or a 60% fat/kcal diet and were allowed only eight hours of food access during the active period. The restricted animals consumed an equivalent amount of calories as their *ad lib* counterparts, but restricted high-fat fed animals were protected against of the metabolic impacts of the diet. TRF preserved the rhythmic transcription of *Per2, Bmal1, Rev-erba,* and *Cry1* in the liver of high-fat fed mice while protecting against diet-induced impairments in glucose and lipid homeostasis (Hatori et al., 2012).

A subsequent study from the same lab examined several different feeding paradigms and TRF schedules varying from 8 to 12 hours of restriction. They found that a TRF schedule less than 12 hours was the most effective at protecting against weight gain and metabolic disruption. An 8-9 hour TRF schedule was effective for both high fat and high fructose fed mice in protecting against weight gain, inflammation, hyperglycemia, and hyperinsulinemia. Furthermore, TRF improved the high-fat and high-fructose fed metabolic profile with clear circadian separation of transcripts and metabolites involved in fed and fasting states. The legacy effect of TRF was only observed to last two days as the metabolic "imprint" was lost and animals adopted the ad lib gene signature and subsequently lost the protective benefits of TRF (Chaix et al., 2014).

Other labs have corroborated these findings either using a similar 60% fat/kcal diet or utilizing a 45% fat/kcal diet. A 2010 study compared a 12-hour TRF to an 8-hour TRF and found that giving a high fat diet for 12 hours during active or inactive phase did not significantly improve metabolic parameters compared to *ad lib*. Similar to the above mentioned papers, animals on the 8-hour TRF during the dark phase were metabolically healthier. In contrast to the findings from Hatori *et al*. and Chaix *et al.*, the 8-hour TRF group did not have decreased body weight and body fat. To examine this further, they restricted the high-fat diet to the early or late active period. When the diet was restricted to the late active period, animals gained more weight and were more metabolically unhealthy than the early active-fed animals (Bray et al., 2010). Finally, on a 45% fat/kcal diet, both a 12- and 8- hour active phase TRF decreased weight gain and body fat compared to the *ad lib* group. TRF animals also had improved metabolic rhythms, decreased serum insulin and leptin as well as increased ghrelin and adiponectin. (Sundaram and Yan, 2016).

2.5.4.2 Human Studies of Time-Restricted Feeding

TRF studies have just recently moved out of the rodent model and into the human. Before TRF was explored in a therapeutic context in humans, a 2017 study examined the ability of food to shift metabolic rhythms in humans. A 5.5-hour shift in meal time was found to result in a significant phase delay in circulating glucose in healthy young men. Meal shifting did not alter circulating insulin or triglycerides, but it did cause a phase delay in WAT *Per2* acrophase. All participants retained normal sleep patterns indicating that, like in rodents, the human SCN resistant to meal timing (Wehrens et al., 2017). This study set

the stage for human TRF work by showing that the human peripheral clock was sensitive to nutrient timing.

Courtney Peterson's lab then applied an early TRF paradigm to pre-diabetic men to explore TRF as a clinical approach for improving metabolic health. They found that individuals consuming all of their meals before 3pm (early TRF; eTRF) had significantly improved insulin sensitivity, pancreatic β cell responsivity, blood pressure and markers of oxidative stress. The eTRF group did not lose weight when compared to individuals allowed to eat for a full 12 hours; therefore, the improvements in metabolic health were independent of body weight (Sutton et al., 2018). In a subsequent study with healthy subjects, they found that eTRF improved glucose handling, but increased both LDL and HDL cholesterol (Jamshed et al., 2019). eTRF may, therefore, be better suited as a therapeutic intervention for unhealthy adults rather than a lifestyle for healthy individuals.

Figures and Figure Legends

Figure 1

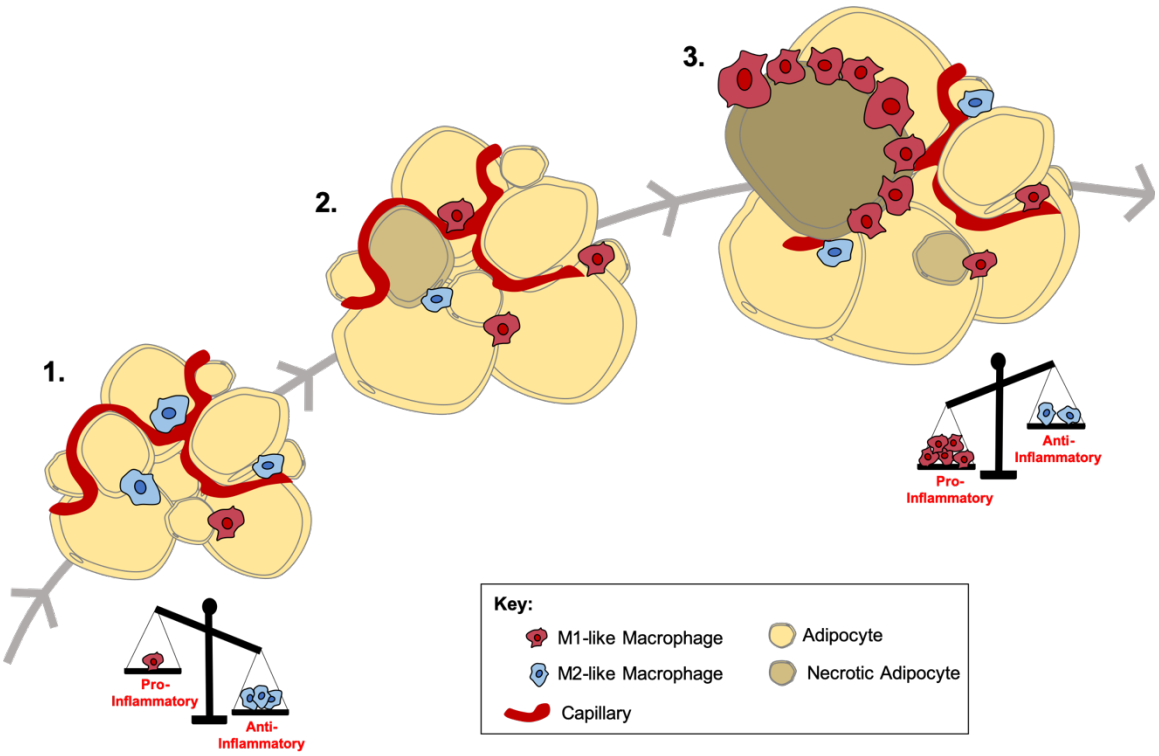

Figure 1: Pathogenic Adipose Tissue Expansion. Adipose tissue functions to expand during times of energy surplus and act as an energy sink to support an organism during times of famine. (1) During healthy adipose tissue expansion, sufficient vasculature and extracellular support cells must also increase. Adipogenesis allows for the proliferation of adipocytes in a well-supported, oxygen-rich, largely anti-inflammatory environment. (2) Adipose tissue becomes unhealthy when adipocyte hypertrophy and adipocyte progenitor

hyperplasia occur faster than the surrounding vasculature. Adipocytes in these pathogenic conditions become hypoxic and begin to produce hypoxia-inducible factors that polarize adipose-resident macrophages to the more pro-inflammatory M1 state. Subsequently, inflammatory conditions are propagated by the production of pro-inflammatory cytokines and chemokines which exacerbate macrophage recruitment leading to eventual adipocyte necrosis and the release FFAs. (3) Adipocytes will become hypertrophic and M2 macrophages will surround necrotic adipocytes to form crown-like structures.

Figure 2

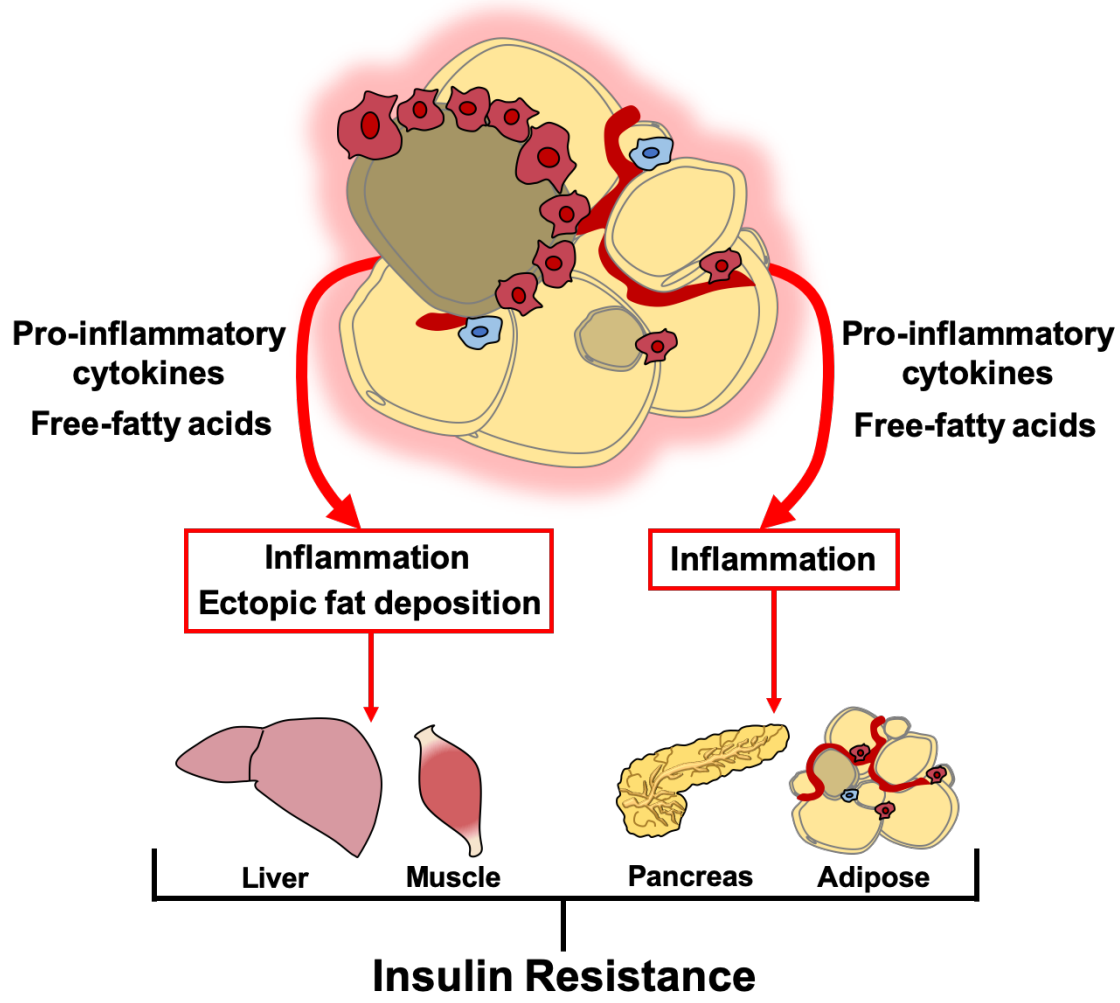

Figure 2: Insulin Resistance Stemming from Pathogenic Adipose Tissue Expansion. The chronic state of low-grade inflammation brought on by WD feeding and pathogenic adipose tissue expansion is thought to lie at the center of most WD-induced diseases.

In extreme and prolonged cases of excess energy intake, ectopic fat deposition will become pathogenic mainly through the disruption of insulin signaling in the pancreas and adipose. Impaired insulin signaling in adipocytes will promote lipolysis and encourage the re-esterification of lipids in other tissues such as skeletal muscle and the liver. In skeletal muscle, intramyocellular lipid accumulation will reduce the amount of insulin-mediated glucose uptake.

Figure 3

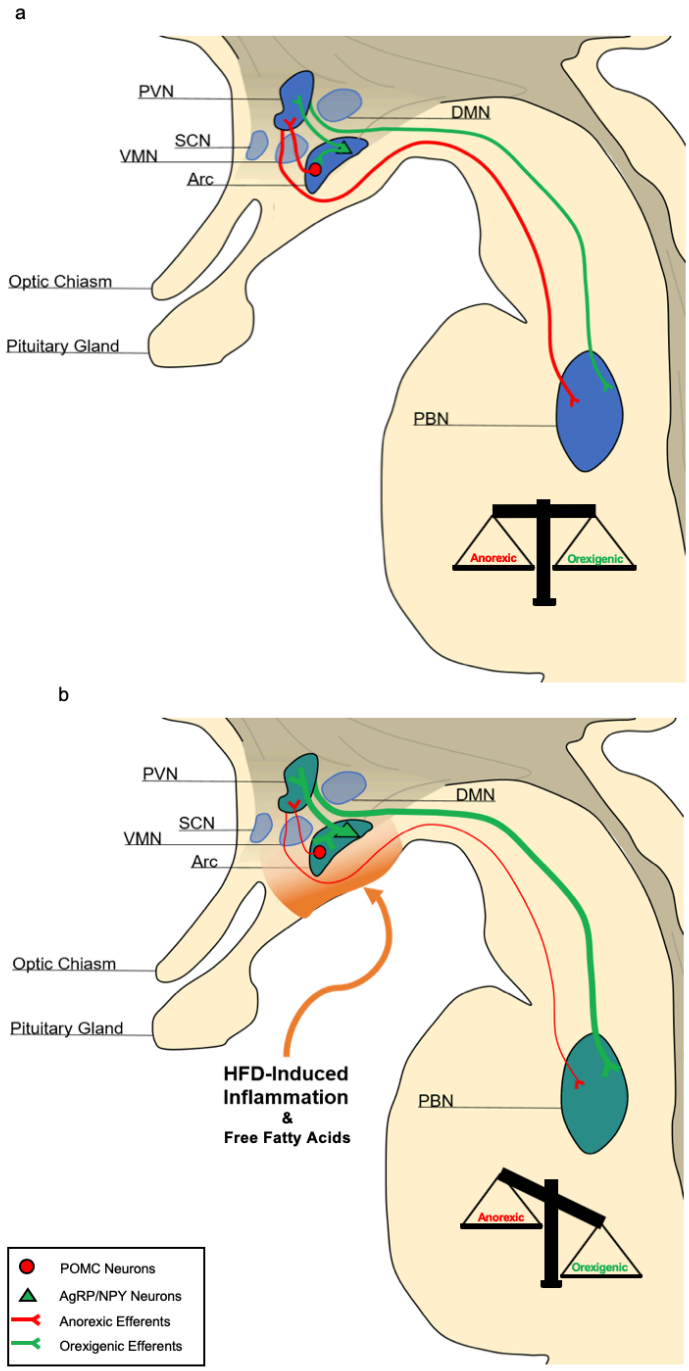

Figure 3: The Effects of a WD on the Hypothalamus. a) Orexigenic AgRP/NPY expressing neurons and anorexic POMC expressing neurons are located in the Arc. They project to the PVN where their signals are integrated and relayed to the PBN to promote or inhibit feeding. Under metabolically healthy conditions, the anorexic and orexigenic

signals from these neurons are balanced to maintain body weight. b) POMC expressing neurons are highly sensitive to WD-induced inflammation and free fatty acid release (orange shaded area) and will decrease their activity under these conditions. AgRP/NPY neurons continue to express appetitive signals effectively tipping the scales to promote feeding behaviors.

Figure 4

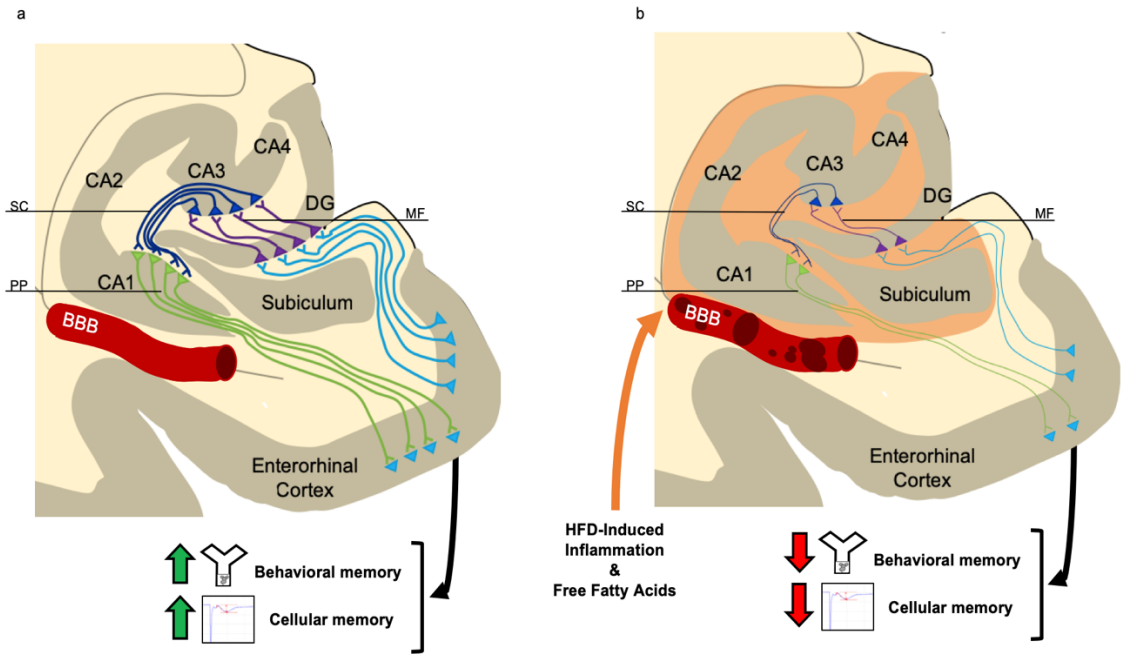

Figure 4: The Effects of a WD on the Hippocampus. a) The hippocampal tri-synaptic circuit begins with information entering the DG from the entorhinal cortex. DG neurons synapse with the CA3 via the MF circuit, which relays the signal through the SC to the CA1. Information from the CA1 travels to the entorhinal cortex for long-term storage through the PP. b) The BBB surrounding the hippocampus becomes progressively leaky as WD-induced inflammation and FFA release increases (orange shaded area). The resulting structural and functional deficits in the hippocampal circuitry cause deficits in behavioral and cellular measures of memory.

Figure 5

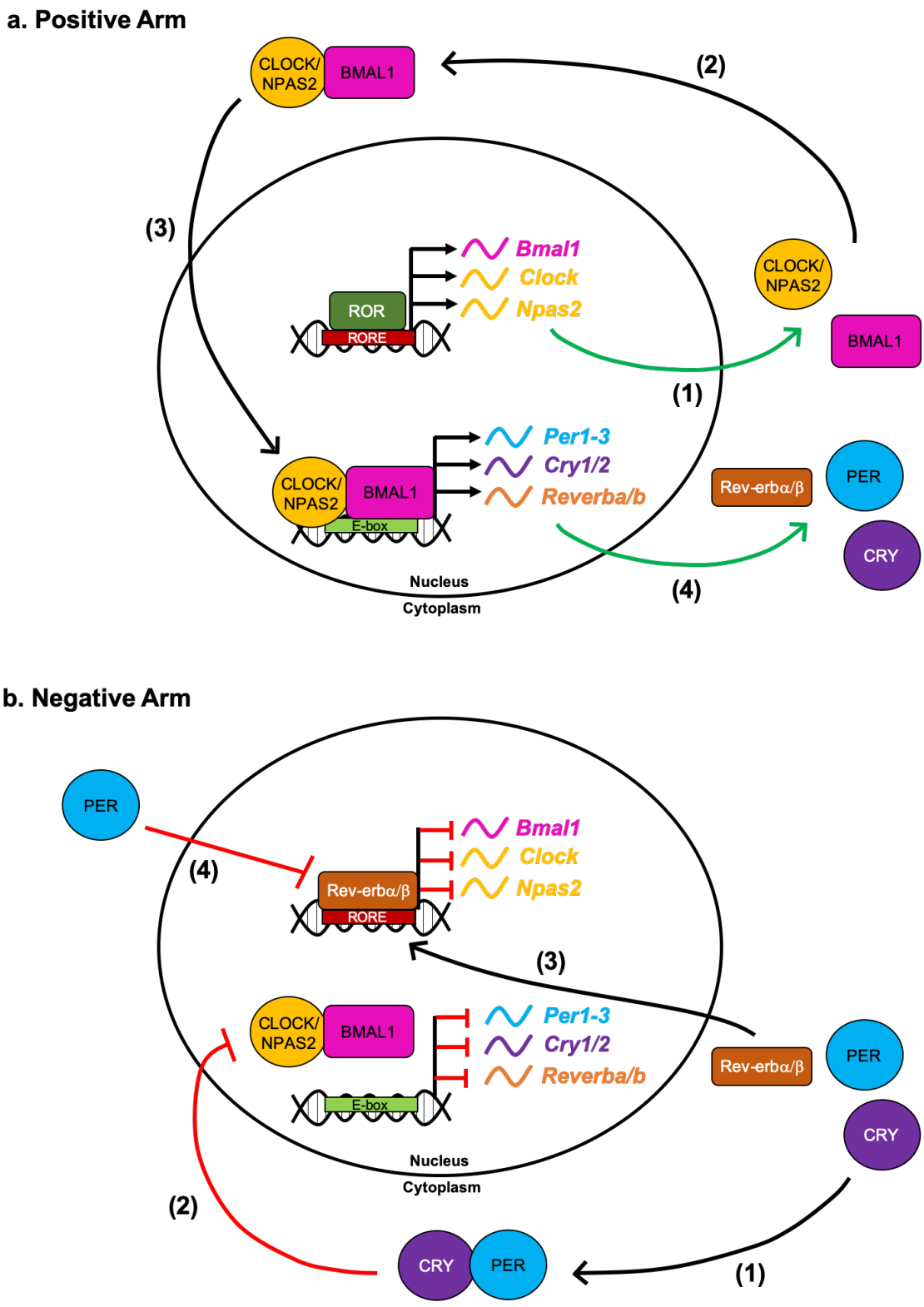

Figure 5: The Core Circadian TTFL. a) (1) ROR binding to the RORE initiates transcription of *Bmal1*, *Clock* and *Npas2*., which are shuttled to the cytoplasm for

translation. (2) BMAL1 and CLOCK/NPAS2 form a complex in the cytoplasm. (3) The BMAL1:CLOCK/NPAS2 complex translocates to the nucleus where it binds to an E-box element to (4) upregulate transcription of *Per, Cry* and *Reverba/b* and other core clock genes. b) (1) PER and CRY form a complex that (2) translocates to the nucleus and inhibits the transcriptional activity of BMAL1:CLOCK/NPAS2. REV-ERBα/β translocates to the nucleus and represses transcription of *Bmal1, Clock* and *Npas2*. (4) PER monomers inhibit REV-ERBa/β repression.

Figure 6

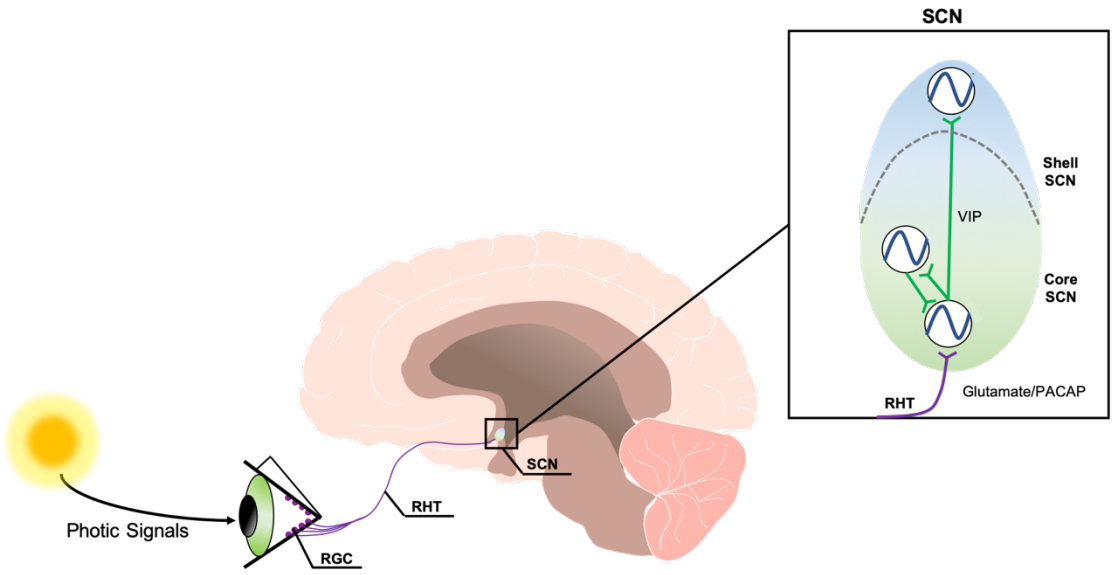

Figure 6: Photic Entrainment of the SCN. RGC axons project along the RHT to release glutamate and PACAP at synapses with SCN neurons. In the core, autonomous rhythms are entrained to photic signals originating from RGCs. A subset of axons synapse on VIP neurons within the SCN core to synchronize other neurons with in the core and also set and maintain the rhythm of the shell.

Chapter 3: Restricted Feeding for Nine Hours in the Active Period Partially Abrogates the Detrimental Metabolic Effects of a Western Diet with Liquid Sugar Consumption in Mice

3.1 Abstract

Obesity is a major public health concern that can result from diets high in fat and sugar, including sugar sweetened beverages. A proposed treatment for dietary-induced obesity is TRF, which restricts consumption of food to specific times of the 24-hour cycle. Although TRF shows great promise to prevent obesity and the development of chronic disease, the effects of TRF to reverse metabolic changes and the development of NAFLD in animal models of a Western diet with sugary water consumption is not known. The objective of the current study was to evaluate the role of TRF in the treatment of obesity and NAFLD through examination of changes in metabolic and histopathologic parameters. To better understand the role of TRF in the treatment of obesity and NAFLD, we investigated the metabolic phenotype and NAFLD parameters in a mouse model of NAFLD in which obesity and liver steatosis is induced by a WD: a high fat diet of lard, milkfat and Crisco with sugary drinking water. Mice were subjected to a short-term (4-weeks) and long-term (10-weeks) TRF in which food was restricted to 9 hours at night. Prior to TRF treatment, the WD mice had increased body mass, and exhibited less activity, and higher average daytime energy expenditure (EE) than chow fed mice. Approximately 4- and 10-weeks following TRF treatment, WD-TRF had moderate but not statistically significant weight loss compared to WD-*ad libitum* (WD-AL) mice. There was a modest but significant reduction in the inguinal adipose tissue weight in both

WD-TRF groups compared to the WD-AL groups; however, there was no difference in epididymal and retroperitineal adipose tissue mass or adipocyte size distribution. In contrast, the diet-induced increase in normalized liver tissue weight, hepatic triglyceride, and NAFLD score were partially abrogated in the 4-week WD-TRF mice, while systemic insulin resistance was partially abrogated and glucose intolerance was completely abrogated in the 10-week WD-TRF mice. Importantly, WD-induced metabolic dysfunction (substrate utilization, energy expenditure, and activity) were partially abrogated by 4- and 10-week TRF. Our results support the hypothesis that TRF aids in reducing the detrimental metabolic effects of consuming a WD with sugary drinking water but does not ameliorate obesity.

3.2 Introduction

Approximately one-third of the world's population is either obese or overweight (World Health Organization, 2018). Obesity is a complex condition largely defined by the accumulation of excess adipose tissue within the body. As a strong predictor of overall mortality (Adams et al., 2006) and an established risk factor for ischemic heart disease, stroke, diabetes, and certain forms of cancer (Danaei et al., 2009; World Health Organization, 2009), obesity is also strongly associated with NAFLD which is thought to be a clinical manifestation of the metabolic syndrome and a risk factor for CVD (Ballestri et al., 2014; Than and Newsome, 2015). Currently, lifestyle modification for weight loss is the basis of NAFLD management (Chalasani et al., 2012; Lonardo et al., 2015). Major changes in diet and physical activity patterns across the world have been contributing to the obesity epidemic. In particular, shifts in fat, caloric sweeteners (including sugar

sweetened beverages), and animal source foods has led to "Western" dietary pattern (Popkin and Gordon-Larsen, 2004).

To model obesity and its associated condition of NAFLD in rodents, high-fat diets providing 45-60% of the energy in the form of fat have been commonly employed (Hariri and Thibault, 2010). To better model the human condition, experimental Western diets have been used. These diets are characterized by a high-fat content combined with a high sugar content which is accomplished by replacing polysaccharides with simple sugars including fructose in the diet, or in the drinking water to model the consumption of sugar sweetened beverages (Longato, 2013). Consumption of a high fat diet disrupts the normal circadian rhythm of energy intake in rodents by shifting food consumption from primarily the active phase (night) to the inactive phase (day) (Kohsaka et al., 2007; Pendergast et al., 2013) and leads to the development of obesity, glucose intolerance, insulin resistance, and NAFLD (den Boer et al., 2004; Hariri and Thibault, 2010; Nakamura and Terauchi, 2013). Consumption of sugar-sweetened drinking water in combination with a high fat Western diet exacerbates disruption of the normal circadian rhythm of energy intake, obesity, and NAFLD progression in mice (Luo et al., 2016). Food consumption restricted to the inactive phase has inconsistently resulted in obesity and metabolic dysfunction in mice (Sherman et al., 2012; Yasumoto et al., 2016). In contrast, TRF of a high-fat diet during the active phase has consistently been shown to reduce weight gain, attenuate metabolic disease development in rodents (Bray et al., 2010; Chaix et al., 2014; Duncan et al., 2016; Hatori et al., 2012; Sundaram and Yan, 2016), and reverse the progression of metabolic disease in male mice (Hatori et al., 2012) and postmenopausal female mice (Chung et al., 2016) with preexisting obesity. TRF in

humans largely confirms the animal study findings of improved metabolic homeostasis including lipid factors and blood glucose and significant reductions in body weight, albeit only a 1 – 2% reduction is observed over a typical 4-week period (Rothschild et al., 2014).

Taken together, these results suggest that TRF may be an innovative strategy for prevention and treatment of obesity and obesity-related metabolic diseases, including NAFLD. However, the effects of TRF to reverse metabolic changes and the development of NAFLD in models of Western diet fed mice consuming sugary drinking water is not known. Therefore, the objective of the current study was to examine the metabolic phenotype, serum parameters, and adipose and hepatic histopathologic features of obese mice subjected to TRF using a Western food and drink consumption mouse model of NAFLD. Two TRF experiments were performed to assess the effects of short-term TRF (4-weeks) and long-term (10-weeks) on the pathophysiology of obesity in the Western food and drink consumption mouse model of NAFLD.

3.3 Materials and Methods

3.3.1 Experimental Approach

3.3.1.1 Animals and Diets

Five to six-week–old male C57BL/6NHsd mice from Harlan Laboratories (Somerville, NJ) were singly housed in standard microisolator cages within the Greene Hall Annex of the Veterinary Research Building, College of Veterinary Medicine, Auburn University. All experimental procedures were approved by the Auburn University Animal Care and Use Committee. Animals were fed standard rodent chow for 1-week during acclimation

to the facility. After this, animals were split into groups receiving diets previously used in our lab (Luo et al., 2016): a standard chow diet (Chow, Teklad Global Rodent Diet 2018) or a 45% fat Western Diet with 42 g/L fructose/sucrose (55%/45%) in the drinking water (WD, TestDiet 5TJN). Under dim red light, food was provided to the TRF animals from ZT 13 to ZT 22, but access to sugary water was not restricted. Non-TRF animals had continuous access to food and water throughout the studies.

3.3.1.2 Metabolic Cages

Promethion Mouse Cages (Sable Systems, Las Vegas, NV) were utilized for metabolic phenotyping as described previously (Luo et al., 2016). Briefly, animal activity, food uptake, water uptake, and body weight were measured along with ambient water vapor, CO_2, and O_2. EE was calculated in kcal by utilizing the Weir equation: $60*(0.003941*VO_2\ (n) +0.001106*VCO_2\ (n))$. RER was determined by the ratio of CO_2 produced to the volume of O_2 consumed ($RER = VCO_2 / VO_2$) where a RER ~ 0.7 indicates lipid utilization and a RER ~ 1.0 indicates carbohydrate utilization. During TRF, readings from food uptake monitors were briefly suspended and the entire food hopper was removed while its accompanying sensor was detached from the food hopper and returned to the metabolic cage. Animals that were not subjected to TRF did not have their food uptake readings suspended at any time. All metabolic phenotyping data were analyzed using ExpeData software (version 1.8.2 Sable Systems) with Universal Macro Collection (version 10.1.3; Sable Systems).

3.3.1.3 Tissue Collection and Analysis

Upon completion of dietary exposure, all animals were fasted and then sacrificed via CO_2 asphyxiation and quickly decapitated by guillotine. Trunk blood was collected and WAT was collected from the eWAT, retroperitoneal (rWAT) and inguinal (iWAT) depots, and livers were excised and weighed. Final blood glucose was measured by a Contour One blood glucose meter. Serum insulin levels were determined by an insulin enzyme-linked immunosorbent assay (ELISA) (Crystal Chem,, Inc., Downers Grove, IL) and data were analyzed for insulin resistance using the homeostatic model assessment of insulin resistance (HOMA-IR) score (HOMA-IR = (26 * fasting serum insulin * fasting blood glucose)/405).

3.3.1.4 RNA Extraction and Reverse Transcriptase-Quantitative Polymerase Chain Reaction (RT-qPCR)

TRI Reagent (Millipore Sigma, Billerica, MA) was used to isolate total RNA from frozen liver following the manufacturer's protocol. RNA quantity and quality were assessed using a NanoDrop (Thermo Scientific). Reverse transcription was performed on mRNA extracted from the liver using a QuantiTect Reverse Transcription Kit (Qiagen, Valencia, CA). qPCR was performed using the RT^2 SYBR Green qPCR Mastermix (Qiagen) and gene-specific primers (Millipore Sigma) using a MyIQ Real-Time PCR system (Bio-Rad, Hercules, CA). After amplification, melt curve analyses were performed on each reaction to confirm specificity. *gapdh* and *gusb* were used as reference genes to normalize gene expression. The $2^{-\Delta\Delta CT}$ method was used to analyze the qPCR data and measure relative expression.

3.3.2 Experiment 1

3.3.2.1 Dietary Exposure

In Experiment 1, animals were split into two groups receiving either a standard chow diet (Chow-AL, n = 5) or the WD (n = 16). At 8-weeks, half of the WD-fed animals (n = 8) were maintained on the WD *ad libitum* (WD-AL) while other half on WD diet were selected for TRF (WD-TRF). Food and water in the AL and TRF groups was provided as outlined in 2.1.1. Approximately 4-weeks after initiation of the TRF treatment and 12-weeks from initiation of the WD feeding, the animals were fasted for 5 h and then sacrificed between ZT 7 and ZT 10. Fasting blood glucose, triglyceride, and cholesterol content were measured with a Lipid Panel test strip using a Cardio check PA analyzer. Fasting blood glucose was collected by a Contour One blood glucose meter.

3.3.2.2 Metabolic Cages

Animals from each group were placed in the metabolic cages at two time points from the initiation of WD feeding: 7- and 12-weeks.

3.3.2.3 Liver Histolopathologic Analysis

Hepatic triglycerides were assayed using the Infinity Triglycerides Liquid Stable Reagent (Thermo Scientific, Rockford, IL) and normalized to the protein content measured using the BCA protein assay reagent (Thermo Scientific).

Paraffin-embedded sections were stained with hematoxylin and eosin examined in a blinded fashion by a board-certified veterinary pathologist. A component based and general NAFLD score was assigned based on a previously published criteria (Liang et al.,

2014). Briefly, micro- and macro-vesicular steatosis were separately scored and the severity was graded, based on the percentage of the total area affected, into the following categories: 0 (<5%), 1 (5–33%), 2 (34–66%) and 3 (>66%). The level of hepatocellular hypertrophy, defined as cellular enlargement more than 1.5 times the normal hepatocyte diameter, was scored, based on the percentage of the total area affected, into the following categories: 0 (<5%), 1 (5–33%), 2 (34–66%) and 3 (>66%) [Liang 2014]. Hepatic inflammation was determined by counting the number of inflammatory foci per field at × 100 magnification (view size 3.1 mm^2) in five different fields per specimen. A cumulative NAFLD score for each liver biopsy was calculated based on the sum of scores for steatosis, hypertrophy and inflammation.

3.3.2.4 Adipose Histopathologic Analysis

Paraffin-embedded sections from all animals in each group were stained with hematoxylin and eosin and examined in a blinded fashion by a board certified veterinary pathologist. Crown-like structures (CLS) were defined as shrunken adipocytes completely surrounded by morphologically identified macrophages and were counted on hematoxylin and eosin stained slides (Cinti et al., 2005). The entire surface area of each fat pad was counted to provide a total number of CLS per fat pad. Adipocyte area was determined by scanning the slides using an Aperio ScanScope scanner (Vista, CA) and evaluated on VisioPharm software (Hoersholm, Denmark). Briefly, the entire adipocyte section was evaluated at 20X increments using the following rules, to identify and measure adipocyte area. Objects were identified and counted as adipocytes if, (1) the area was between 500 and 20,000 μm; (2) it had a shape factor of 0-0.7, where a shape

factor of 1 indicated a straight line and 0 indicates a perfect circle. Approximately 80-90% of the adipocytes were counted for each section.

3.3.3 Experiment 2

3.3.3.1 Dietary Exposure

In order to observe the effects of TRF on the Chow fed animals and to examine the impact of longer term WD-TRF, Experiment 2 was performed. The animals were split into two groups receiving either the Chow diet (n = 31) or the WD (n = 27). At 6-weeks, a subset of the Chow-fed (n = 15) and WD-fed animals (n = 13) were maintained on their diets *ad libitum* (Chow-AL and WD-AL, respectively) while the rest of the Chow (n = 16) and WD (n = 14) animals were selected for TRF (Chow-TRF, WD-TRF). Food and water in the AL and TRF groups was provided as outlined in 2.1.1. Approximately 16-weeks from the initiation of WD feeding and 10-weeks after initiation of the TRF treatment, the animals were fasted for 6 hours and then sacrificed between ZT 5 and ZT 8.

3.3.3.2 Metabolic Cages

Animals from each group were placed in the metabolic cages 10-weeks after initiation of the TRF treatment.

3.3.3.3 Glucose Tolerance Test (GTT)

After 8-weeks of TRF, the treatment groups (n = 8) were fasted for 11 hours (from ZT 22 to ZT 9) prior to the beginning of the GTT. Animals in the WD group also had their

sugary drinking water replaced with tap water for the duration of the fast. The GTT was performed as previously described (Greene et al., 2014; Luo et al., 2016). Briefly, blood was collected from the dorsal vein on a Contour One blood glucose meter strip at baseline, then 15, 30, 60, and 120 min after a 25% intraperitoneal glucose injection (2g/kg body weight). The area under the curve (AUC) was obtained by calculating the Riemann sum for each group.

3.3.4 Statistics

A Student's t-test was performed on pre-TRF food uptake and metabolic phenotyping data. Data collected after TRF began was analyzed using an ANOVA with a Newman-Keuls *post-hoc* test. The 24-hour cycle data was assessed by a repeated measures ANOVA so that animals in one diet group could be compared with animals in another diet group at corresponding time points within the 24-hour cycle. The above statistical analyses were performed using SigmaPlot with significance determined at $p < 0.05$. Multiple linear regression analysis (ANCOVA) was employed to assess the impact of body mass on metabolic cage parameters. Utilization of the National Mouse Metabolic Phenotyping Centers Energy Expenditure analysis page (https://www.mmpc.org/shared/regression.aspx) allowed for the assessment of body weight as a covariate on energy expenditure with significance determined at $p < 0.05$. All data are presented as group mean + standard error measurement (SEM) unless stated otherwise.

3.4 Results

3.4.1 Body Weight

Body weight was tracked over the entire course of both TRF experiments (Figure 7). WD-AL fed mice had significantly greater percent body mass change than Chow fed mice after 12 weeks of diet exposure ($p < 0.05$). Weekly body weight in the WD-AL and WD-TRF groups was nearly identical until week 8 when TRF was implemented, however, statistical significance was not observed between the two groups (Figure 7A). We observed similar results after 16-weeks on the diets. WD fed animals gained significantly more weight than both of the Chow groups beginning at week 4 and persisting until the final week (Figure 7B; $p < 0.01$). Additionally, TRF had no observable effect on the weight gain trajectory of WD or Chow fed animals when compared to their *ad libitum* fed counterparts.

3.4.2 Reference Metabolic Phenotype

To define the metabolic condition prior to starting the TRF intervention, we determined food, kilocalorie and water uptake, total EE, substrate utilization, and total activity of the mice fed chow or WD diets (Figure 8 and data not shown). Compared to Chow fed, WD fed mice consumed less food during the night ($p < 0.001$), but more kilocalories during the day and in total ($p < 0.05$; Figure 8A, 8B, and 8C). Before TRF implementation, total EE in WD-fed mice during the day and night phase was significantly greater than that in the Chow group (Figure 8D). Average RER and night phase activity were lower in the WD fed animals ($p < 0.001$; Figure 8E and 8F).

3.4.3 Post-intervention Metabolic Phenotype

To define the metabolic condition after 4- or 10-weeks of TRF intervention, we analyzed energy expenditure and substrate utilization prior to sacrifice (Figure 9 and Figure 10). In the 4-week TRF experiment, average EE was significantly elevated only in the WD-AL group during the light phase from ZT 1-ZT 4 (Figure 9A, $p < 0.01$). There was a significant reduction in average EE for the WD-TRF group when compared to the WD-AL group during at ZT 4, ZT 7-ZT 8, ZT 10-ZT 12 and ZT 13-ZT 15 (Figure 9A, $p < 0.05$). Without adjusting for body weight as a covariate, both the WD-AL and WD-TRF groups had significantly higher resting EE than Chow animals during both the day and light phases ($p < 0.001$), but the WD-TRF group had a significantly lower resting EE when compared to WD-AL (Figure 9B, *top panel*, $p < 0.05$). Adjusting for body weight as a covariate removed the differences during the light phase, but during the night phase the WD-TRF group had a significantly lower resting EE than both the Chow and the WD-AL groups (Figure 9B, *bottom panel,* $p < 0.05$). Additionally, quiet resting EE analysis before body weight adjustment revealed that during the day and night phases the WD-TRF group had a quiet resting EE that was significantly lower than the WD-AL group ($p<0.05$), but not different from the Chow-AL group (Figure 9C, *top panel*). When adjusted for body weight as a covariate; however, the WD-TRF group was only significantly different than the WD-AL group during the light phase (Figure 9C, *bottom panel,* $p < 0.05$).

Similar results in circadian EE were observed after 10-weeks of TRF (Figure 9D). The WD-AL group expended significantly more energy than the Chow groups during the day. Specifically, EE was elevated compared to Chow-AL at ZT 1, ZT 4-5 and ZT 9-11 and compared to Chow-TRF at ZT 1, ZT 3-6 and ZT 8-12 (Figure 9D, $p < 0.05$). WD-

TRF treated mice had significantly elevated EE at ZT 2 and ZT 9 compared to Chow-AL and ZT 4, ZT 6, ZT 9 and ZT 11 compared to Chow-TRF ($p < 0.05$). Although WD-AL and WD-TRF groups were only significantly different from each other at ZT 1 ($p < 0.01$), the WD-TRF group exhibited a phenotype intermediate to the WD-AL and Chow groups. TRF of the Chow diet had minimal impact on circadian EE with the only significant time point being an increase at ZT 21 ($p < 0.01$).

After 4-weeks of TRF, Chow fed mice exhibited a diurnal rhythm in RER with a greater lipid metabolism during the day and more carbohydrate utilization during the night (Figure 10A). This rhythm was significantly blunted in the WD-AL group during the entirety of the dark phase, but also at ZT 4, ZT 6-ZT9, and ZT 12 during the light phase ($p < 0.05$). RER was significantly increased in the WD-TRF group compared to the WD-AL group from ZT 15 to ZT 24 during the dark phase ($p < 0.01$), yet was less than the Chow group during the same time point throughout the dark phase. Interestingly, 2 hours prior (ZT 12-ZT 13) and 1 hour (ZT 14) within the introduction of food to the mice in the WD-TRF group, the RER was significantly reduced ($p < 0.01$) compared to the WD-AL group, indicating greater reliance on lipid as a substrate. Taken together, these data suggest that the metabolic flexibility apparent in the Chow group is partially rescued in the WD-TRF group.

After 10-weeks of TRF, both Chow groups had a diurnal rhythm in RER (Figure 10B). An interesting spike in RER is observed in the Chow-TRF group from ZT 13-18. Although this was not significantly different from Chow-AL, it suggests a potential enhancing effect of TRF on Chow substrate utilization rhythmicity. The WD-AL animals had a similar daytime RER to the Chow groups, but exhibited a significantly lower RER

at ZT 17, ZT 19-20 compared to Chow-AL and from ZT 14-21 compared to Chow-TRF. WD-TRF treated animals were not significantly different from the Chow groups at any point in the 24-hour analysis. However, WD-TRF was only significantly different from WD-AL at ZT 19 and ZT 20 (Figure 10B, $p < 0.05$). These data recapitulate the results of the 4-week TRF experiment in that the WD-AL group has significantly reduced metabolic flexibility that may be partially abrogated by 10 weeks of TRF.

The WD-AL group consumed a significantly smaller amount of food during the night when compared to Chow (Figure 11A, *left panel,* $p < 0.01$). Despite restricted time to access food, the WD-TRF group did not consume a significantly different amount of total food than Chow or WD-AL. No significant differences were observed in total water consumption among the three groups (Figure 11B, *left panel*).

Mice in both experiments were more active during the dark phase than the light phase indicating that dietary treatments did not alter normal rodent sleep-wake behavior (Figure 11C and 11D). When food was introduced to the 4-week TRF WD-TRF group at ZT 14, meters traveled in the WD-TRF group was significantly increased compared to the WD-AL group (Figure 11C, $p < 0.05$). In the 10-week TRF experiment, the WD-AL and WD-TRF animals had periods of significantly lower activity during the night phase compared to Chow-AL and Chow-TRF (Figure 11D, $p < 0.05$).

3.4.4 Glucose Tolerance Test and Serum Factors

After 8-weeks of TRF, the WD-AL group had significantly elevated blood glucose compared to chow-AL, Chow-TRF, and WD-TRF groups at 60 and 120 minutes after glucose injection (Figure 12A, *left panel*, 30: $p < 0.05$, 60: $p < 0.05$, 120: $p < 0.05$). AUC

calculations revealed that the WD-AL group had significantly elevated blood glucose across the GTT time points (Figure 12A, *right panel*, $p < 0.05$).

Trunk blood was collected during sacrifice in both experiments to analyze fasting blood glucose and serum insulin. After 4-weeks of TRF, fasting serum hyperinsulinemia was observed in the WD-AL and WD-TRF groups (Figure 12B, *left panel,* $p < 0.01$), but there was not a difference in fasting insulin levels between the two groups. No differences were observed in fasting serum glucose levels among the three groups (Figure 12C, *left panel*). Consistent with these results, HOMA-IR was significantly elevated in the WD-AL and WD-TRF groups compared to the Chow-AL group (Figure 12D, *left panel,* $p < 0.01$) with no observable difference between the WD fed groups. Ten-weeks of TRF produced similar results in that the WD groups had significantly elevated fasting serum insulin compared to both of the Chow groups (Figure 12B, *right panel,* $p < 0.001$). However, 10-weeks of TRF was sufficient to significantly lower insulin in the WD-TRF group compared to the WD-AL group ($p < 0.001$). Once again, we did not observe significant differences in fasting blood glucose. WD exposure caused significant insulin resistance in both the AL and TRF group (Figure 12D, *right panel,* $p < 0.01$), but TRF of the diet significantly improved this phenotype ($p < 0.001$).

3.4.5 Liver Pathophysiology

Next, we sought to determine the impact of TRF on diet-induced liver pathophysiology. Twelve weeks of WD feeding significantly increased normalized liver weight regardless of TRF treatment when compared to Chow fed animals (Figure 13A, *left panel,* $p < 0.05$). However, 4-weeks of TRF significantly decreased normalized liver weight when

comparing the WD-AL and WD-TRF groups ($p < 0.05$). Consistent with this latter result, a significant reduction in hepatic triglyceride levels was observed in the WD-TRF group compared to the WD-AL group (Figure 13B, *left panel,* $p < 0.05$). Interestingly, 16 weeks of WD diet exposure did not induce a dietary effect on normalized liver weight (Figure 13A, *right panel*). Liver triglycerides were significantly elevated in both WD groups with no apparent effect of TRF (Figure 13B, *right panel*).

In the 4-week TRF experiment, there was no histopathologic evidence of NAFLD in Chow fed mice (Figure 13C and 13D). In contrast, micro- and macro-vesicular steatosis and hypertrophy, but not inflammation was observed in the WD-AL and WD-TRF groups (Figure 13C and 13D). Although not significant, a strong trend in lower NAFLD presentation was observed in the WD-TRF group compared to the WD-AL group ($p = 0.059$).

Relative gene expression was determined for fat oxidation and lipogenic genes in livers from both the 4-week and 10-week TRF experiments (Figure 13E). After 4-weeks of TRF, there was a decrease in three of the four fat oxidation genes in the WD-TRF group compared to control (Figure 13E a-d, *ppara*: $p < 0.001$, *bdh1*: $p < 0.001$, *cpt1a*: $p < 0.05$). Compared to the WD-AL group, WD-TRF treated animals had decreased *ppara* and *cpt1a* hepatic gene expression (Figure 13Ea-d, *ppara*: $p < 0.001$, *cpt1a*: $p < 0.01$). Additionally, three of the four lipogenesis genes were also down regulated in the WD-TRF group compared to Chow (Figure 13E e-h, *elovl6*: $p < 0.001$, *pparg*: $p < 0.01$, *srebf*: $p < 0.05$) while *elovl6*, *pparg* and *srebf* exhibited lower expression in WD-TRF compared to WD-AL (Figure 13E *elovl6*: $p < 0.001$, *pprg*: $p < 0.01$, *srebf*: $p < 0.05$). On the other

hand, *scd1* had elevated expression in both of the WD fed groups with no difference between A and R (Figure 13E f, $p < 0.001$).

Ten-weeks of TRF caused an increase in the expression of three fat oxidation genes in the WD-AL group compared to Chow-TRF and one gene when compared to Chow-AL (Figure 13E a-d, Chow-TRF- *ppara*: $p < 0.05$, *cpt1a*: $p < 0.05$, *fgf21*: $p < 0.05$; Chow-AL- *fgf21*: $p < 0.05$). Expression of two fat oxidation genes in the WD-TRF group were decreased compared to the WD-AL group (Figure 13E a-d, *ppara*: $p < 0.05$, *cpt1a*: $p < 0.05$). Lipogenesis genes *scd1* and *srebf* were significantly upregulated in the WD-AL treated animals compared to both Chow groups while *elovl6* was elevated in WD-AL just compared to Chow-AL (Figure 13E e-h, Chow-TRF- *scd1*: $p < 0.01$, *srebf*: $p < 0.001$; Chow-AL- *elovl6*: $p < 0.05$, *scd1*: 0.001, *srebf*: $p < 0.001$). The WD-TRF group had increased expression of *scd1* compared to both chow groups, decreased expression of *pparg* compared to Chow-TRF and significantly down regulated expression of *srebf* compared to WD-AL (Chow-TRF- *scd1*: $p < 0.05$, *pparg*: $p < 0.05$; Chow-AL- *scd1*: $p < 0.05$; WD-AL- *srebf*: $p < 0.001$).

3.4.6 Adipose Tissue Dynamics

To assess changes in adipose tissue, eWAT, rWAT, and iWAT tissues were harvested and weighted during sacrifice in both experiments. We found that normalized eWAT and rWAT weights were markedly higher in the WD-AL and WD-TRF groups compared to the Chow-fed animals after 4- and 10-weeks of TRF (Figure 14A and E, *right* and *middle panels*, 4-week TRF: $p < 0.01$; 10-week TRF: $p < 0.001$). We also observed the same effect of TRF on the iWAT fat depot. While the WD caused a significant increase in

iWAT weight compared to Chow (Figure 14A, *left panel,* 4-week TRF: $p < 0.01$; 10-week TRF: $p < 0.001$) the WD-TRF group in both experiments had significantly lighter iWAT fat pads (Figure 14E, *left panel*, 4-week TRF: $p < 0.05$; 10-week TRF: $p < 0.05$).

When depot sections from the 4-week TRF experiment were analyzed for adipocyte size, the Chow fed group had significantly smaller adipocytes and fewer large adipocytes in the eWAT and iWAT depots (Figure 14B, $p < 0.05$). In contrast, there was no difference in the size distributions between the WD-AL and WD-TRF groups in any of the adipose tissue depots. Overall, the iWAT depot had the fewest total number of crown-like structures, however, there were no significant group differences observed in this depot (Figure 14C). On the other hand, the WD-AL group had significantly more crown-like structures in the rWAT depot than the Chow and WD-TRF groups (Figure 14C, *middle panel*, Chow-AL $p < 0.05$, WD-TRF- $p < 0.05$). There was a positive association between crown-like structure number and adipocyte size in the eWAT and iWAT (Figure 14D, *left* and *right panel*, eWAT: $p < 0.05$, iWAT: $p < 0.05$), but no such relationship was observed in rWAT.

3.5 Discussion

The objective of the current study was to examine the metabolic phenotype, serum parameters, and histopathologic features of adipose and hepatic tissue in obese mice subjected to short-term and long-term TRF in a Western food and drink consumption mouse model of NAFLD. We sought to determine whether TRF would improve metabolic and NAFLD parameters. By allowing *ad libitum* access to the sugary drinking water in the restricted fed mice, we also assessed whether consumption of liquid sugar

would compensate for the absence of food. We found that WD-fed mice subjected to TRF did not consume more sugary water than the mice allowed *ad libitum* access to the WD. This result is not surprising given the observation that food and water consumption is tightly linked (Ellacott et al., 2010; Jensen et al., 2013). There was no evidence of gorging behavior on sugary water consumption in our study (data not shown), which is consistent with findings that only intermittent access to sugar (Avena et al., 2009) and restricted daytime feeding (Kliewer et al., 2015) are associated with gorging behavior.

In contrast to previous rodent TRF studies that have observed significant weight loss (Chaix and Zarrinpar, 2015; Hatori et al., 2012), a non-significant reduction in weight was observed in the WD-TRF groups in both 4-week and 10-week TRF experiments. This result indicates that TRF is not an effective strategy for weight reduction with a Western diet that also models consumption of sugar sweetened beverages and suggests that the beneficial metabolic effects of TRF can be independent of significant weight loss

A key finding in our study was observed in the RER data: mice in the 4-week WD-TRF group were able to use more lipid as a fuel source during the last two hours of the day phase than mice in the Chow and WD-AL groups and then more carbohydrate as a fuel source during the night phase than mice in the 4- and 10-week WD-AL groups. Thus, metabolic flexibility was restored to mice in the WD-TRF groups which is in agreement with previous studies in which TRF treatment resulted in significant weight loss in high fat diet fed mice (Chung et al., 2016; Sundaram and Yan, 2016) The capacity of TRF to increase metabolic flexibility is also observed when mice are restricted to feeding during the inactive phase and in *Cry* deficient mice which lack a functional

circadian oscillator (Vollmers et al., 2009). Metabolic substrate usage reflects the composition of diet and feeding pattern (Hoevenaars et al., 2013; Joo et al., 2016) ; however, TRF has the ability to supersede the composition of diet.

Changes in resting and total EE in response to weight gain and loss function as a compensatory mechanism to maintain body weight (Keesey and Hirvonen, 1997; Leibel et al., 1995). Our observations that total EE was greatest in the 4- and 10-week WD-AL groups and that TRF reduced total EE even after adjusting for body weight as a cofactor are consistent with a compensatory EE mechanism to maintain body weight. The 4-week WD-AL-induced significant increases in resting EE were not retained when adjusted for changes in body weight. However, a significant reduction in resting EE in the WD-TRF group compared to the WD-AL group was retained when adjusted for changes in body weight. This data suggests that adaptation to the TRF treatment was partially independent from body weight.

In the current study, we did not observe significant weight loss in the 4- and 10-week WD-TRF groups compared to the WD-AL groups. However, a modest but significant reduction in the iWAT but not eWAT or rWAT adipose depots was detected. Yet, no difference in adipocyte volume was observed in any of the measured adipose tissue depots between the 4-week WD-TRF and WD-AL groups, nor did we observe significant differences in CLS. Taken together, TRF appeared to minimally affect adipose tissue dynamics. Consistent with these results plasma glucose, serum insulin, and HOMA-IR were not significantly different between the 4-week WD-TRF and WD-AL groups, which suggests that systemic changes to insulin sensitivity were not achieved in the short term TRF treatment. In contrast, a significant reduction in serum insulin levels,

HOMA-IR score, and blood glucose levels in the GTT were observed between the 10-week WD-TRF and WD-AL groups, suggesting longer-term TRF is required to observe systemic changes to insulin sensitivity and glucose tolerance.

In our assessment of NAFLD, we observed a significant reduction in liver weight normalized to body weight and hepatic triglyceride levels in the 4-week TRF experiment but not the 10-week TRF experiment, and a strong trend towards a lower NAFLD score in the 4-week WD-TRF group compared to the WD-AL group, which is consistent with previous studies that have examined hepatic triglyceride levels and/or lipid droplet staining in TRF studies (Chung et al., 2016; Sundaram and Yan, 2016). To further examine the hepatic effect of TRF, we assessed the expression of genes regulating hepatic fat oxidation and lipogenesis. Our results indicate that 4- and 10-week TRF resulted in significantly reduced hepatic expression of *pparg* and *srebf*, key lipogenic genes, compared to the WD-AL groups, suggesting a down regulation of lipid synthesis which has been observed in previous rodent TRF studies (Chaix et al., 2014; Chung et al., 2016; Hatori et al., 2012). Differential regulation of lipid oxidation genes was observed in the TRF groups in our studies which is similar to a previous TRF study with modest but significant body weight loss (Chung et al., 2016) but in contrast to studies with highly significant body weight loss (Chaix et al., 2014; Hatori et al., 2012).

There were several limitations with the current study. First, whole body fat and lean mass were not determined. Second, more sensitive measures of insulin sensitivity were not performed. Third, our animal study relied on mice, which unlike humans are nocturnal. A potential limitation is that we did not restrict access to the sugary drinking water during the food restriction, which could possibly have led to caloric intake during

the food restriction. However, the average consumption of sugary water in the WD-TRF groups was less than 0.5 g of liquids during the day, which equates to less than 0.08 kcal of sugar consumed. Thus, although caloric intake from sugar consumed during the day was marginal, it may have had a non-caloric effect.

Obesity is an important risk factor for the development of chronic diseases. Thus, weight loss is a well-accepted strategy to reduce the development of chronic disease, such as type 2 diabetes, cardiovascular disease, fatty liver disease, and cancer in obese individuals (Goodwin and Stambolic, 2015; Klein et al., 2004). Indeed, even modest weight loss can reduce risk factors and clinical parameters associated with chronic diseases (Gaziano et al., 2007; Mason et al., 2011; Vilar-Gomez et al., 2015; Zomer et al., 2016). TRF has been proposed as an innovative strategy to reduce body weight (Chaix and Zarrinpar, 2015; Sofer et al., 2015). In conclusion, our results suggest that metabolic improvement can occur by TRF. However, our results do not support TRF as a strategy to ameliorate obesity when consumption of a WD is accompanied by drinking sugary water.

Figures and Figure Legends

Figure 7

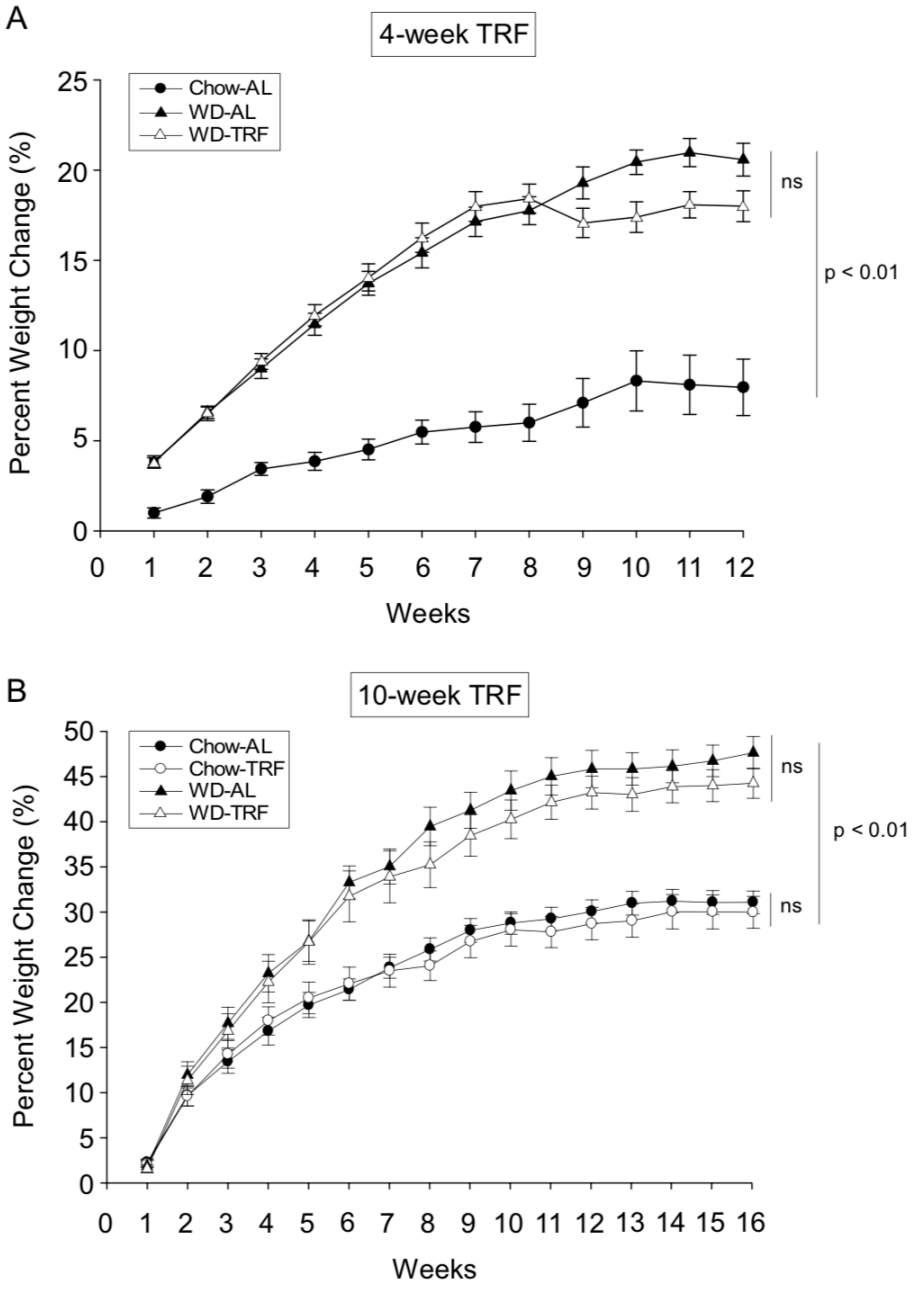

Figure 7: WD TRF Body Weight. Weekly percent body weight change (± SEM) over time is shown for the (A) Chow-AL, WD-AL, and WD-TRF groups and (B) Chow-AL, Chow-TRF, WD-AL, and WD-TRF groups. A. TRF was started after 8 weeks of WD-

feeding. B. TRF was started after 6 weeks of WD-feeding. Group differences over the course of the TRF treatment were analyzed by ANOVA with a Newman-Keuls *post-hoc* test.

Figure 8

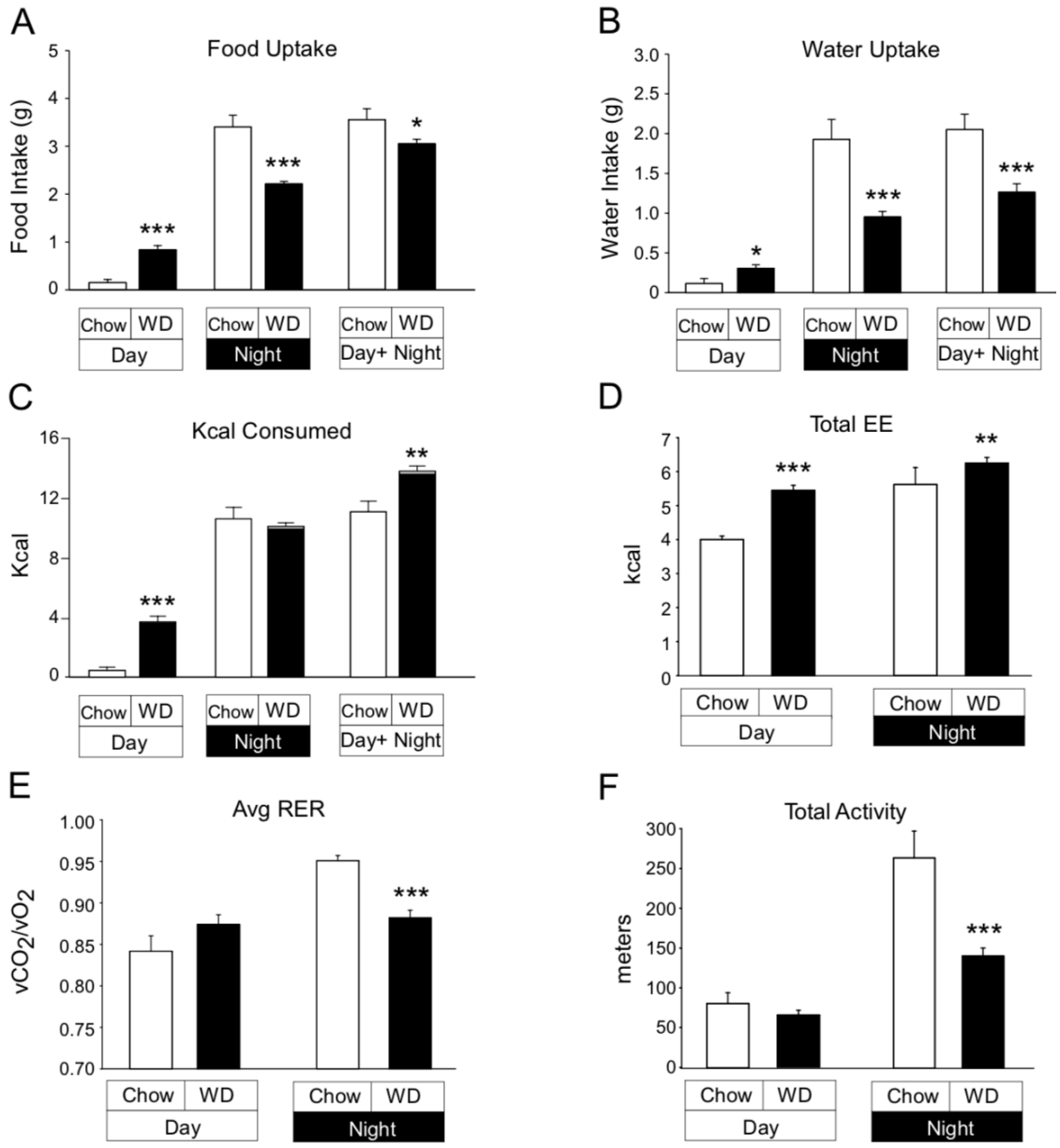

Figure 8: Pre-TRF Metabolic Phenotype. Circadian analysis of food uptake (A), water uptake (B), and kcal consumed (C) for the day and night phases and total amount over a 24 period in the chow and WD groups are shown as the Mean + SEM. Circadian analysis of total energy expenditure (Tot_EE) (D) and average respiratory exchange ratio (Avg_RER) (E) are shown as the Mean + SE for the chow and WD groups. F. Circadian

analysis of total activity is shown as the Mean + SE for the chow and WD groups. (*, $p < 0.05$; **, $p < 0.01$; ***, $p < 0.001$ compared to chow)

Figure 9

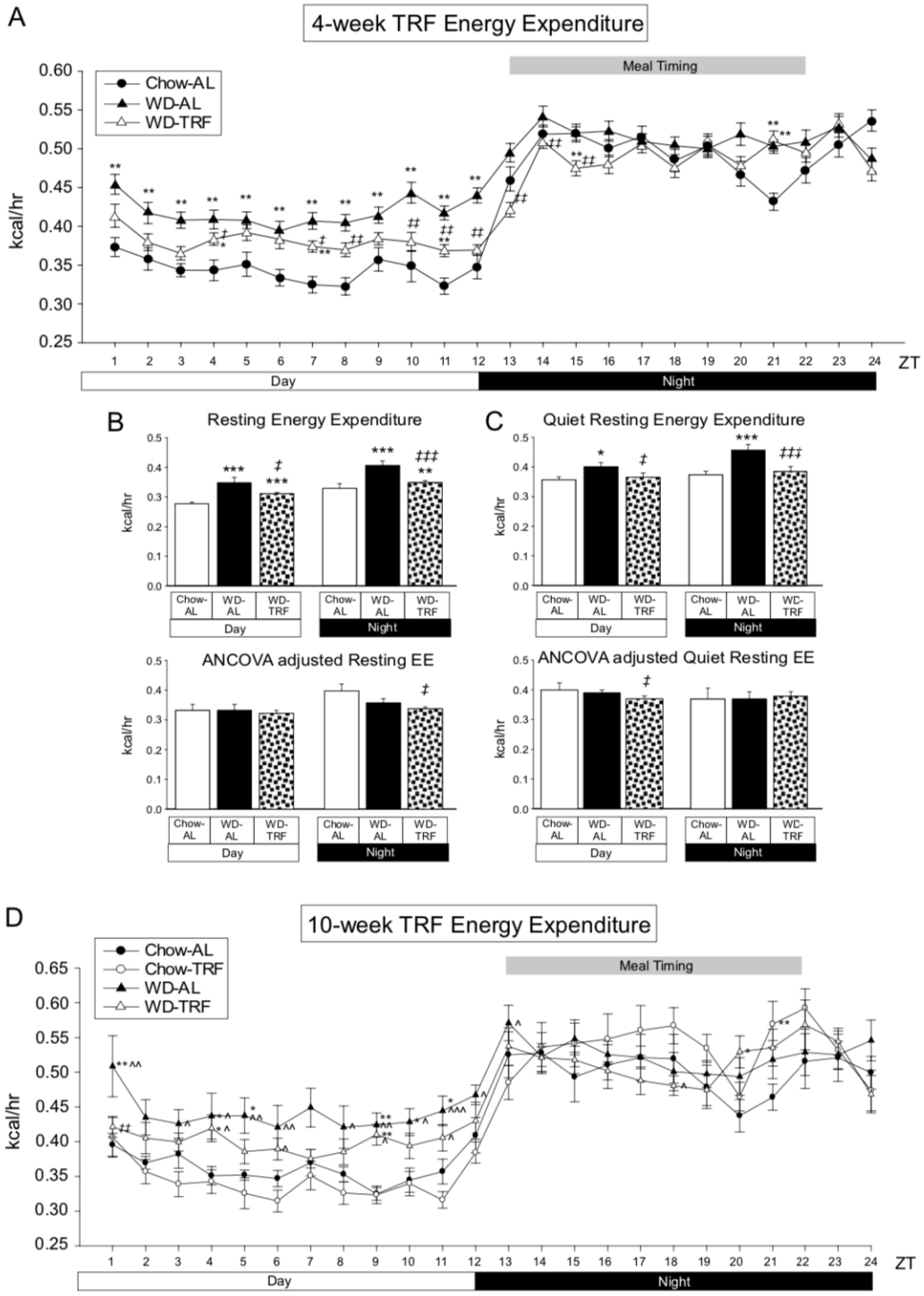

Figure 9: EE After TRF. A-C. Energy expenditure data from the 4-week TRF experiment. A. Mean (± SEM) circadian analysis of total energy expenditure (Tot_EE) at each hour in the 24 hour cycle in the Chow-AL, WD-AL, and WD-TRF groups are

shown. B. Mean (+ SEM) circadian analysis of resting energy expenditure (R_EE) measured as the mean value for the 30 minute period with the lowest EE (*upper panel*) and ANCOVA adjusted R_EE (*lower panel*) is shown. C. Mean (+ SEM) circadian analysis of resting energy expenditure (QR_EE) measured as the mean value from the isolated 30 minute period in which the activity score was lowest (*upper panel*) and ANCOVA adjusted R_EE (*lower panel*) is shown. D. Energy expenditure data from the 10-week TRF experiment. Mean (± SE) circadian analysis of total energy expenditure (Tot_EE) at each hour in the 24 hour cycle in the Chow-AL, Chow-TRF, WD-AL, and WD-TRF groups are shown. (*, $p < 0.05$; **, $p < 0.01$; ***, $p < 0.001$ compared to Chow-AL; ^, $p < 0.05$; ^^, $p < 0.01$; ^^^, $p < 0.001$ compared to Chow-TRF; ‡, $p < 0.05$; ‡‡, $p < 0.01$; ‡‡‡, $p < 0.001$ compared to WD-AL)

Figure 10

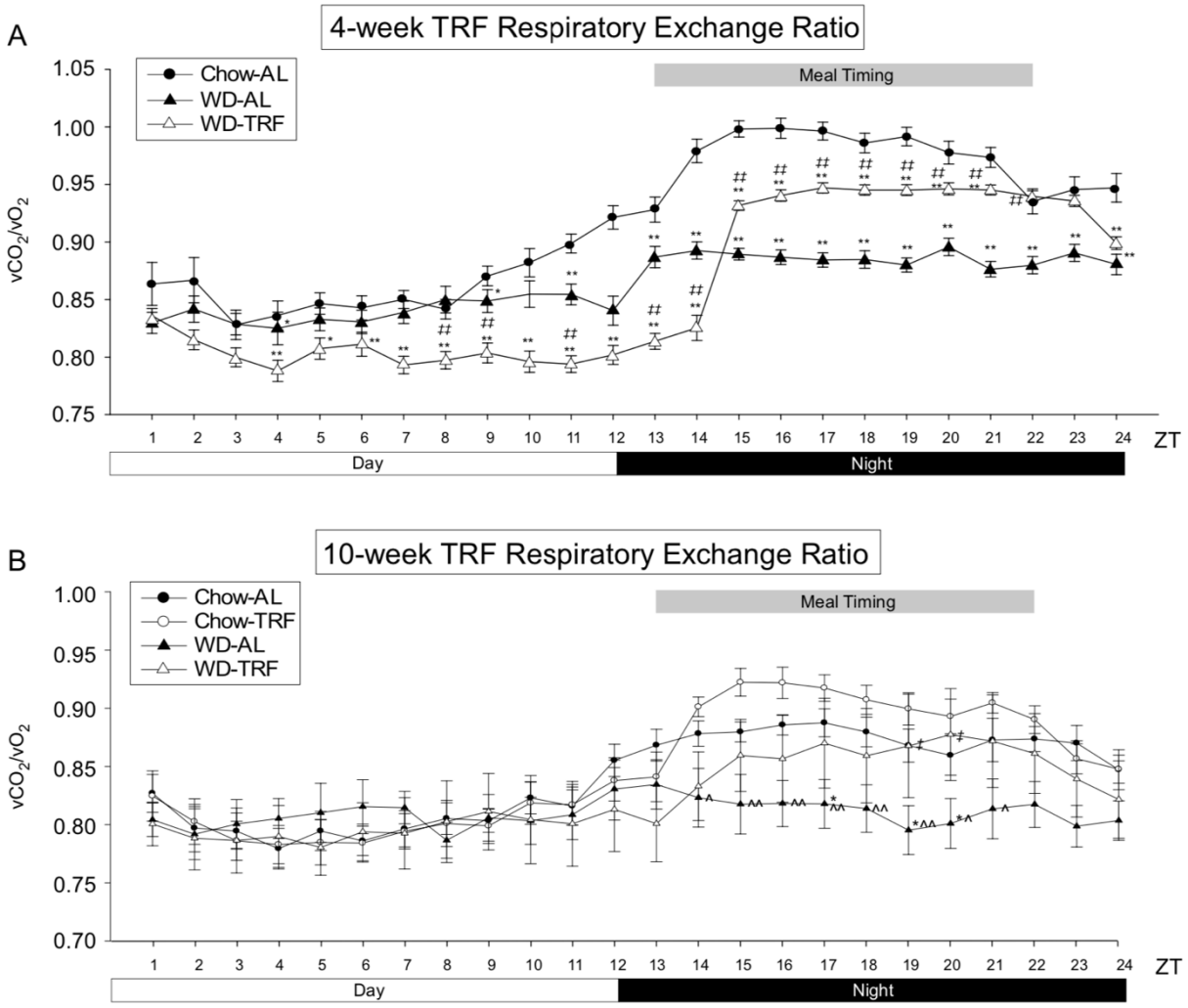

Figure 10: RER After TRF. Mean (± SEM) circadian analysis of respiratory exchange ratio at each hour in the 24 hour cycle in the 4-week TRF experiment is shown for the Chow-AL, WD-AL, and WD-TRF groups (A) and in the 10-week TRF experiment is shown for the Chow-AL, Chow-TRF, WD-AL, and WD-TRF groups (B). (*, $p < 0.05$; **, $p < 0.01$; ***, $p < 0.001$ compared to Chow-AL; ^, $p < 0.05$; ^^, $p < 0.01$; ^^^, $p < 0.001$ compared to Chow-TRF; ‡, $p < 0.05$; ‡‡, $p < 0.01$; ‡‡‡, $p < 0.001$ compared to WD-AL)

Figure 11

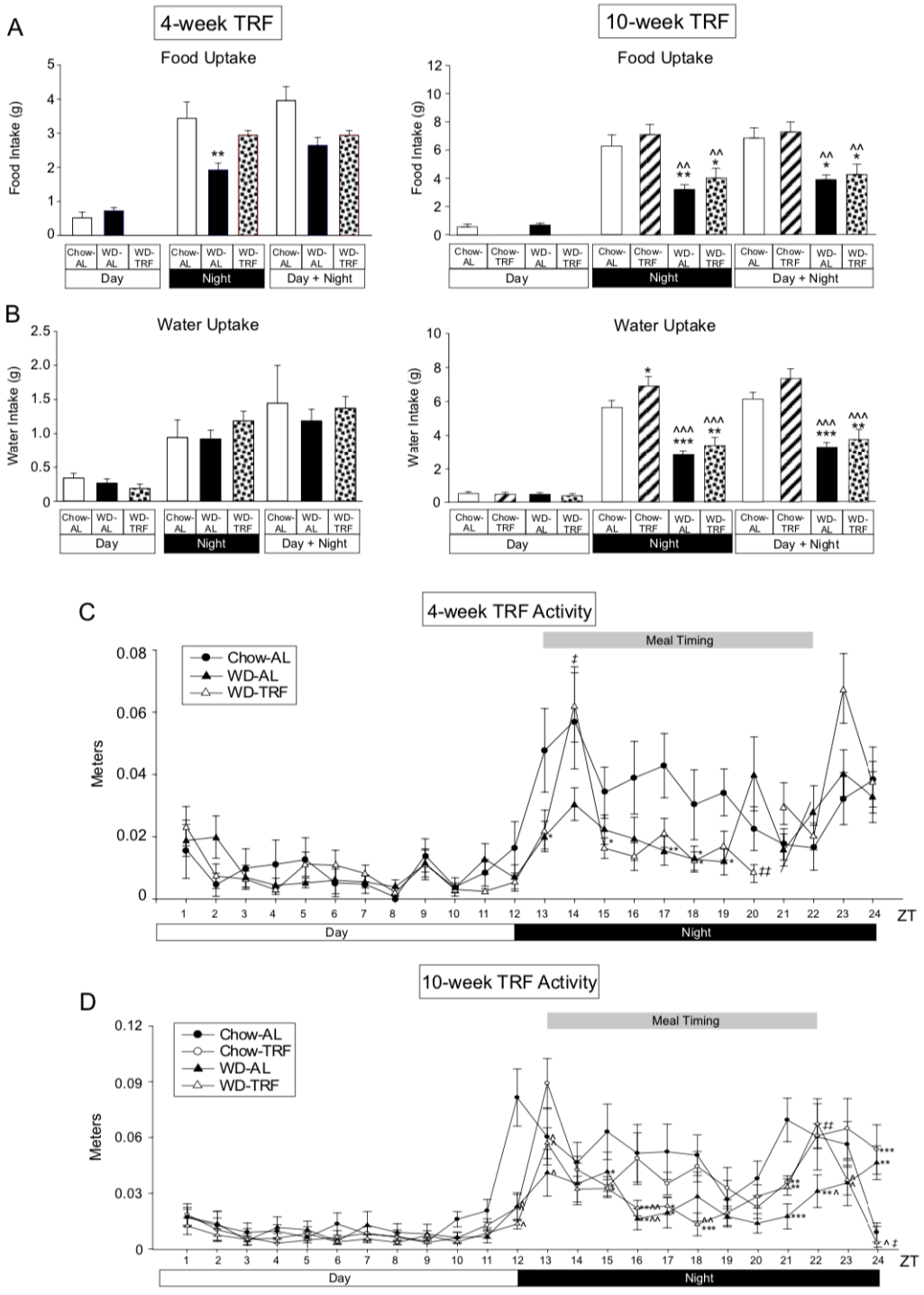

Figure 11: Food and Water Uptake and Activity After TRF. A-B. Mean (+ SEM) circadian analysis of food uptake (A) and water uptake (B) in the 4-week TRF experiment (*left panels*) and 10-week TRF experiment (*right panels*) for the day and

night phases and total amount over a 24 period is shown. C-D. Circadian analysis of total meters traveled at each hour (± SE) in the 24 hour cycle in the 4-week TRF experiment (C) and 10-week TRF experiment (D) are shown. (*, $p < 0.05$; **, $p < 0.01$; ***, $p < 0.001$ compared to chow-AL; ^, $p < 0.05$; ^^, $p < 0.01$; ^^^, $p < 0.001$ compared to chow-TRF; ‡, $p < 0.05$; ‡‡, $p < 0.01$; ‡‡‡, $p < 0.001$ compared to WD-AL)

Figure 12

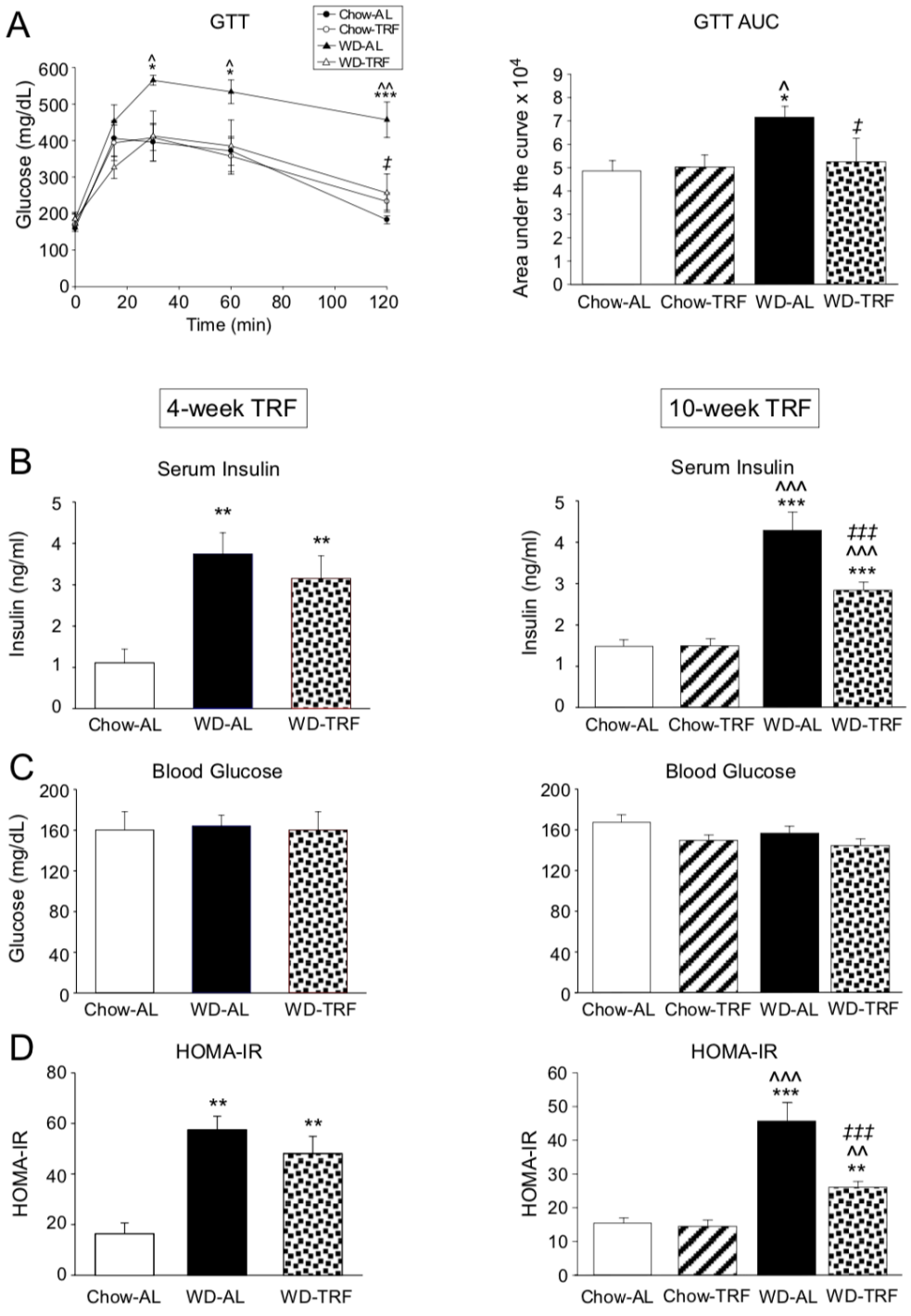

Figure 12: Glucose Tolerance and Plasma and Serum Parameters After TRF. A. The mean glucose concentration ± SE in GTT curves from the 10-week TRF experiment (*left panel),* and the means + SEM of the Area Under the Curve calculated for each GTT

curve (*right panel)*. B-D. Serum insulin (B), plasma glucose (C), and HOMA-IR score (D) from the 4-week (*left panels*) and 10-week (*right panels*) TRF experiments. (*, $p < 0.05$; **, $p < 0.01$; ***, $p < 0.001$ compared to Chow-AL; ^, $p < 0.05$; ^^, $p < 0.01$; ^^^, $p < 0.001$ compared to Chow-TRF; ‡, $p < 0.05$; ‡‡, $p < 0.01$; ‡‡‡, $p < 0.001$ compared to WD-AL)

Figure 13

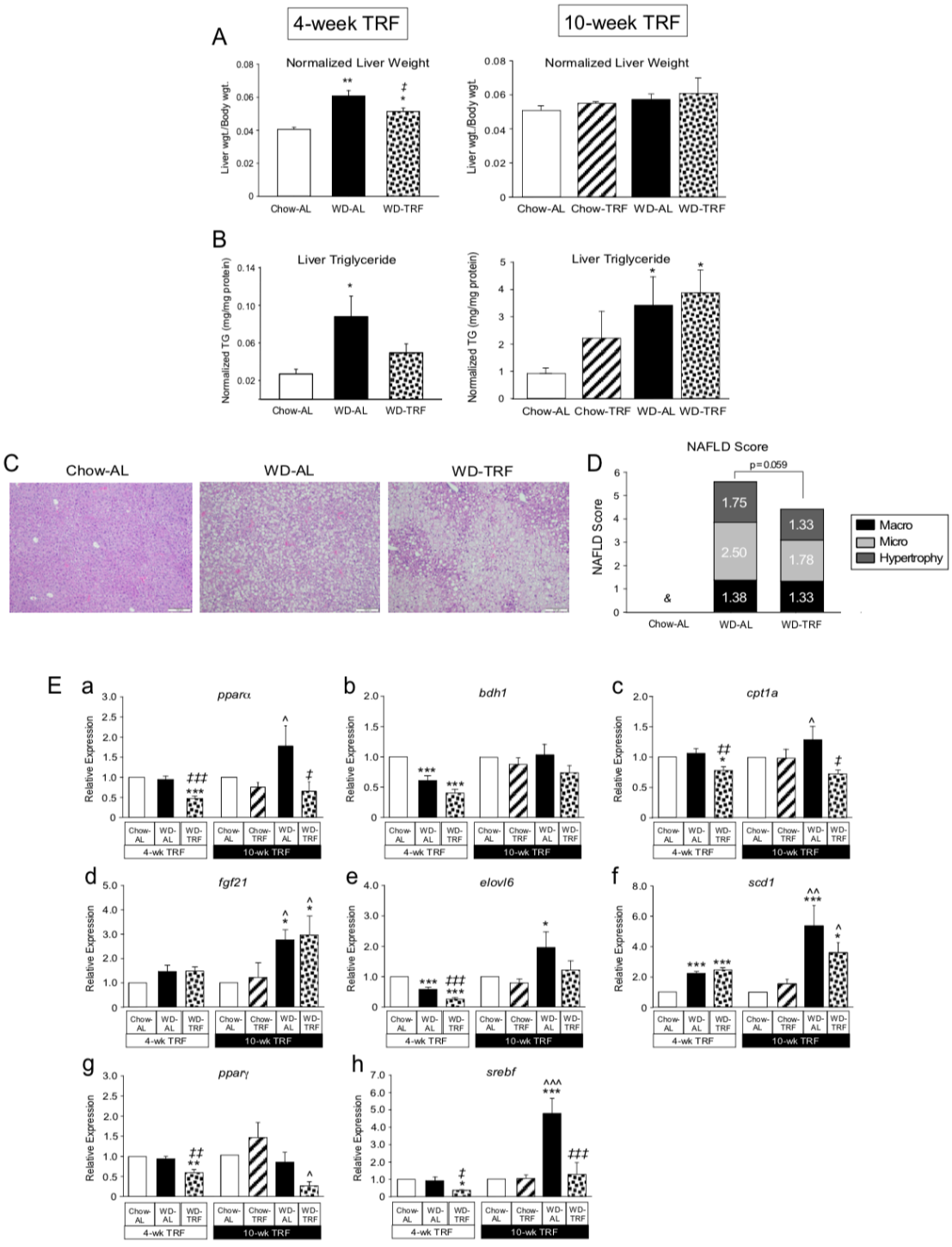

Figure 13: NAFLD Parameters After TRF. A-B. Liver weight normalized to body weight (A) and liver triglyceride content (B) for the 4-week TRF experiment (*left panels*) and 10-week TRF experiment (*right panels*) are shown as the Mean + SEM. C.

Representative hematoxylin and eosin (H&E) stained liver sections are shown for the 4-week TRF experiment. D. NAFLD scoring of H&E stained liver sections for micro- and macro-vesicular steatosis, hypertrophy, and inflammation as described in the Materials and Methods section for the 4-week TRF experiment (the NAFLD score was zero in the Chow-AL-fed mice). E. Relative mRNA expression of *pparα* (a), *bdh1* (b), *cpt1a* (c), *fgf21* (d), *elovl6* (e), *scd1* (f), *pparγ* (g) and *srebf* (h) in liver samples from the 4-week and 10-week TRF experiments. (*, $p < 0.05$; **, $p < 0.01$; ***, $p < 0.001$ compared to Chow-AL; ^, $p < 0.05$; ^^, $p < 0.01$; ^^^, $p < 0.001$ compared to Chow-TRF; ♯, $p < 0.05$; ♯♯, $p < 0.01$; ♯♯♯, $p < 0.001$ compared to WD-AL)

Figure 14

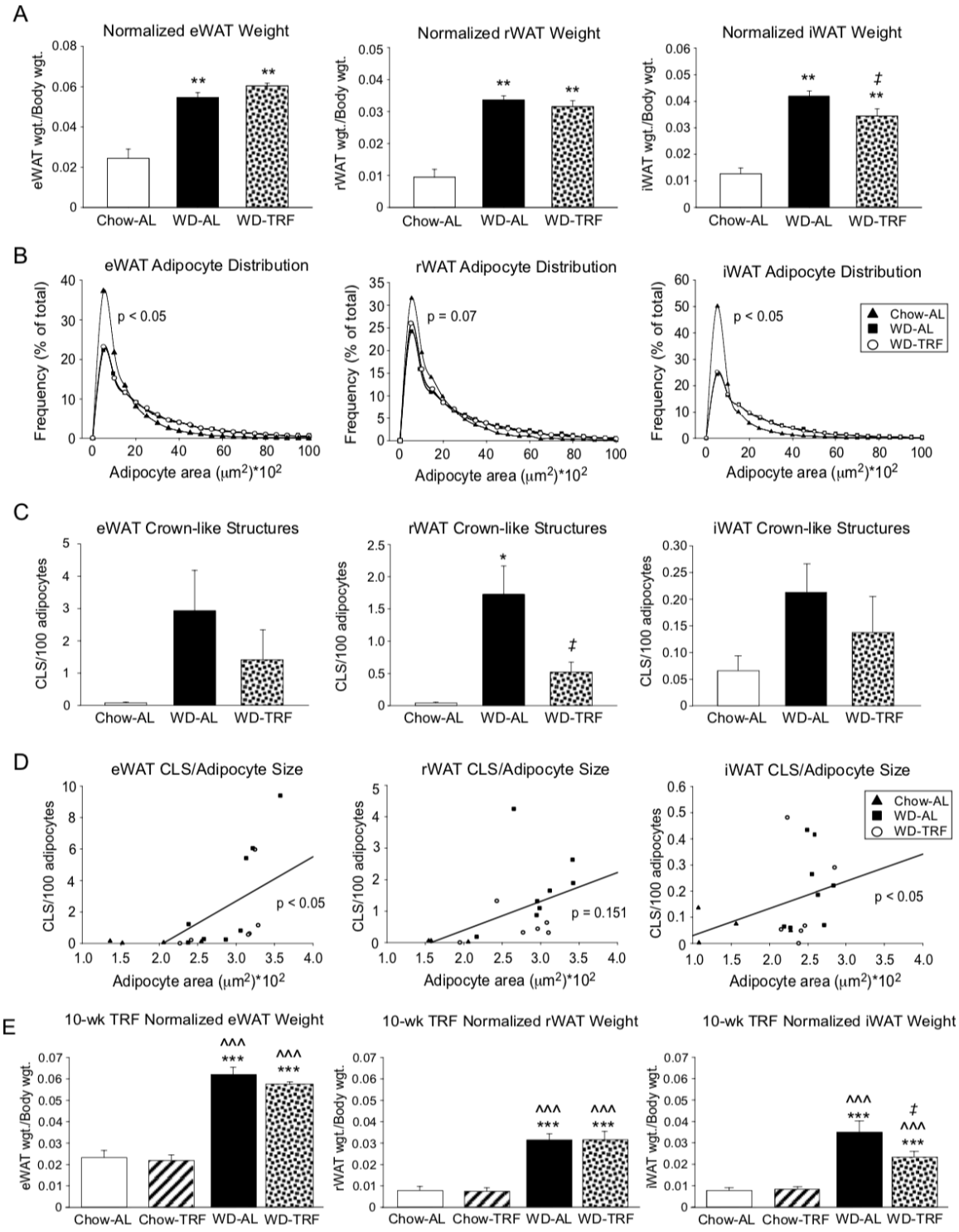

Figure 14: Adipose Tissue Parameters After TRF. A. Adipose weight normalized to body weight for the eWAT (*left panel*), rWAT and (*middle panel*), and iWAT (*right panel*) are

shown as the Mean + SEM in the Chow-AL, WD-AL, and WD-TRF groups from the 4-week TRF experiment. B. Frequency of adipocyte area from 0 to 1500 μm^2 in increments of 500 μm^2 is shown for the eWAT (*left panel*), rWAT and (*middle panel*), and iWAT (*right panel*). P-values for the Kolmogorov-Smirnov test for sample distribution compared the chow group are shown from the 4-week TRF experiment. C. Quantitation of CLS for the eWAT (*left panel*), rWAT and (*middle panel*), and iWAT (*right panel*) are shown as the mean + SEM from the 4-week TRF experiment. D. Relationship between mean adipocyte area and CLS in the eWAT (*left panel*), rWAT and (*middle panel*), and iWAT (*right panel*) is shown from the 4-week TRF experiment. Linear regression was performed and P-values are shown. E. Adipose weight normalized to body weight for the eWAT (*left panel*), rWAT and (*middle panel*), and iWAT (*right panel*) are shown as the Mean + SE in the Chow-AL, Chow-TRF, WD-AL, and WD-TRF groups from the 10-week TRF experiment. (*, $p < 0.05$; **, $p < 0.01$; ***, $p < 0.001$ compared to chow-AL; ^, $p < 0.05$; ^^, $p < 0.01$; ^^^, $p < 0.001$ compared to chow-TRF; ‡, $p < 0.05$; ‡‡, $p < 0.01$; ‡‡‡, $p < 0.001$ compared to WD-AL)

Chapter 4: The Physio-Metabolic Effects of Time-Restricting Liquid Sugar Intake to Six-Hour Windows During the Mouse Active Phase

4.1 Abstract

Obesity is a major public health concern and overconsumption of unhealthy fats and sugary beverages are contributing factors. TRF can reduce obesity-associated pathophysiological parameters by limiting food consumption to specific times of day; however, the effects of time-restricted sugary water consumption are unknown. To examine whether liquid calorie restriction impacts metabolic health, we measured metabolic parameters in mice given liquid sugar at various intervals over 24-hours. The control (Con) group received tap water, the *ad* libitum fructose-glucose (ALFG) group received *ad libitum* sugar water and the early fructose-glucose (EFG) and late fructose-glucose (LFG) groups received liquid sugar during the first and last six hours of the active period, respectively. Each group was given free access to chow. The ALFG group exhibited elevated body and adipose tissue weights compared to the other groups and increased hepatic steatosis compared to Con. The ALFG group consumed more calories than the other groups during ZT 6-11, indicating that this window may be critical in the promotion of weight gain from liquid sugar consumption. The EFG group exhibited higher levels of energy expenditure than the Con and LFG groups during the first half of the active period (ZT 12-17); however, there was no difference among the groups during the second half of activity (ZT 18-23). In contrast, the EFG group exhibited lower reparatory exchange ratio than other groups during the inactive period as well as the second half of the active period, indicating that the EFG group had greater metabolic

flexibility and utilized lipids when carbohydrates from liquid sugar were not available. Additionally, the EFG group was more insulin tolerant than the ALFG and Con groups. Our results support the hypothesis that time-restricted liquid calorie restriction aids in reducing the detrimental metabolic effects of sugary drink consumption.

4.2 Introduction

In 1997 the World Health Organization recognized obesity as "…one of the greatest neglected public health issues of our time…" (McDowell, 2002). Although awareness of the obesity epidemic has increased over the past two decades, adult obesity rates continue to rise in the twenty-first century (Institute for Health Metrics and Evaluation, 2014; World Health Organization, 2018). The United States has been particularly afflicted by this epidemic and in 2017 prevalence estimates indicate that over half of all states have greater than 30% of their adult population qualified as obese (Hales et al., 2015). This current epidemic is hypothesized to be caused largely by the intersection of centuries of evolutionary pressures placed on humans to maximize metabolic efficiency with the prevalence of highly palatable, calorie-dense diets popular in the modern world (Popkin et al., 2012).

The WD, which consists of foods high in saturated fats and refined sugars, is commonly associated with increased weight gain and markers of metabolic disease (Kanoski and Davidson, 2011; Luo et al., 2016; Marwitz et al., 2015; Molteni et al., 2002; Myers and Allen, 2012; Woodie et al., 2018). In recent years, there has been increased focus on how the refined sugar component of this diet can affect human health. Sweetened food and beverage intake, mostly in the form of soft drinks sweetened with

HFCS, has increased markedly over the past three decades (Bray et al., 2004). HFCS was first introduced to the United States as a sweetener in the 1960's and has since experienced incredible growth in its popularity and uses (Bleich et al., 2018). Although HFCS is similar to sucrose in composition, HFCS contains a higher percentage of fructose. The most common form of HFCS, HFCS-55, is 55% fructose and 42% glucose and is sweeter per gram than either crystalline sucrose, glucose or fructose alone (Tappy et al., 2014). This means that less HFCS is needed to obtain the same amount of sweetness in food and beverages and has allowed HFCS to become the most cost-effective sweetener on the market (Duffey and Popkin, 2008; White, 2008). For many years, dietary fructose was considered a benign and common ingredient in most foods and beverages (Glinsmann and Bowman, 1993). However, recent human and animal studies have found that HFCS-sweetened beverage consumption is actually detrimental to metabolic health and increases the risk of developing obesity and metabolic diseases (Bocarsly et al., 2010; Bray et al., 2013; Jürgens et al., 2005; Mock et al., 2017; Stanhope et al., 2009; Teff et al., 2004).

While the complete elimination of HFCS-sweetened foods and beverages has been proposed as an effective intervention for ameliorating diet-induced weight gain and metabolic dysfunction, restrictive dietary interventions have a notoriously low adherence rate (Grief and Miranda, 2010; Wadden, 1993). Additionally, most individuals regain the weight they lost while adhering to the restrictive diet less than a year after they return to their previous habits (Curioni and Lourenço, 2005). Given this, research efforts have begun to explore other dietary patterns that restrict the time during which calories are consumed rather than the type of calories consumed. TRF, which is defined as limiting

food access to 8-9 hours during the active phase, is one such method that has produced promising results in both animal models and human intervention studies (Chaix et al., 2014; Chung et al., 2016; Gabel et al., 2018; Hatori et al., 2012; Longo and Panda, 2016; Rothschild et al., 2014; Sutton et al., 2018; Woodie et al., 2018). TRF is different than other fasting regimens in that it works to align the timing of caloric consumption to the body's natural rhythms of feeding and fasting (Chaix et al., 2014). In rodent models, TRF of high-fat diets supplemented with sugary water has been found to restore metabolic circadian rhythms, improve metabolic function and, in some cases, it has even been shown halt the progression of pre-existing metabolic diseases without altering total caloric intake (Chaix et al., 2014; Chung et al., 2016; Gabel et al., 2018; Longo and Panda, 2016; Woodie et al., 2018).

These TRF studies focused more on time-restricting solid calorie consumption, but there have been a few previous works examining the effect of time-restricting liquid calories (Faria et al., 2017; Morris et al., 2012; Oosterman et al., 2015; Senador et al., 2012); de Senador *et al*., 2012; Oosterman *et al*., 2014; Almeida Faria *et al*., 2017). However, these studies restricted liquid calorie consumption to 12-hour light or dark phases and provided solutions containing only fructose. Other works have observed that solid calorie TRF is actually more effective in improving metabolic health when the food is restricted to specific windows of the active period, with calorie consumption restricted to early-active period having the most beneficial effect on metabolic health (Gill and Panda, 2015; Moro et al., 2016; Stote et al., 2007; Sutton et al., 2018; Tinsley et al., 2017). However, the metabolic effects of restricting liquid calorie consumption to the early-active or late-active period is not known. Therefore, we sought to determine the

best time of the day for liquid calorie consumption by limiting sugary water availability either an early-active or late-active period. Over the course of nine weeks, metabolic parameters and rhythms as well as food and water behaviors were measured in mice with *ad libitum* access to a standard chow diet and provided with a fructose/glucose solution under time-restricted paradigms.

4.3 Materials and Methods

4.3.1 Animals and Diets

Male C57Bl/6N mice, aged 5-6 weeks, were obtained from Envigo and housed in triplet in standard microisolator cages in an AAALAC accredited animal facility at the Auburn University College of Veterinary Medicine. All experimental procedures were approved by the Auburn University Animal Care and Use Committee. The animals were maintained in a temperature and humidity-controlled room on a 12:12 light cycle with lights on as ZY 0 and lights off as ZT 12. Mice were allowed to acclimate to the facility for one week with standard chow diet and tap water. After this time, animals were randomly assigned to one of four groups: a negative control group that received *ad libitum* tap water (Con; n=9), a positive control group that received *ad libitum* fructose/glucose solution (FG) access (ALFG; n=8), an early-access group that received FG only during the first six hours of the active period from ZT 12-ZT 18 (EFG; n=9), or a late-access group that had their FGS access restricted to the last six hours of the active period from ZT 18-ZT 0 (LFG; n=9). To allow the time-restricted animals access to the 12% solution during the dark period, water bottles containing tap water were switched to FG in the EFG and LFG cages under dim red light. To control for manipulation of the

cages in the EFG and LFG, water bottles were also changed in the Con group (tap water to tap water) and ALFG group (FG to FG). We chose to maintain all groups on their respective water regimen for nine weeks to compare with the 8-10 week liquid sugar exposure periods commonly observed in rodent studies examining similar physio-metabolic parameters (Bocarsly et al., 2010; Bursać et al., 2013; Faria et al., 2017; Jürgens et al., 2005; Light et al., 2009; Mock et al., 2017; Senador et al., 2012).

To recapitulate the composition of the HFCS commonly consumed as an added sweetener, a 12% 55%/45% FG was prepared by dissolving 66 g/L of fructose (Alfa Aesar, Haverhill, MA) and 54 g/L of glucose (Alfa Aesar, Haverhill, MA) in Milli-Q purified water (MilliporeSigma, Burlington, MA). Standard rodent chow diet was provided *ad libitum* to all groups (24.5% kcal/g protein, 13.1% kcal/g fat, 62.3% kcal/g carbohydrate; PicoLab Rodent Diet 20 #5053, LabDiet, St. Louis, MO).

4.3.2 Metabolic Phenotyping

Promethion metabolic cages (Sable Systems, Las Vegas, NV) were utilized for metabolic screening and phenotyping as previously described (Luo et al., 2016; Woodie et al., 2018). Mice were transferred from their home cages and singly housed in the metabolic cages during the ninth experimental week prior to sacrifice. Activity by Promethion XYZ Beambreak Activity Monitors calibrated to each cage. Food, water and body weight were measured by Promethion MM-1 Load Cell sensors. The amount in grams, frequency, duration, and rate at which food and water were withdrawn from the hoppers were measured and analyzed. During sugar water restriction, readings from the water uptake monitors were briefly suspended and waters were switched accordingly then

returned to the cages to resume monitoring. Animals that were not subjected to sugar water restriction (the Con and ALFG groups) did not have their food uptake readings suspended at any time. The body mass monitors were plastic tubes that also functioned as in-cage enrichment and nesting devices.

A Promethion GA-3 gas-analyzer measured water vapor, CO_2 and O_2 in mL/min to provide detailed respirometry data. EE was calculated in kcal by utilizing the Weir equation: $60*(0.003941*VO_2\ (n) +0.001106*VCO_2\ (n))$. RER was determined by the ratio of CO_2 produced to the volume of O_2 consumed ($RER = VCO_2 / VO_2$) where a RER ~ 0.7 indicates lipid utilization and a RER ~ 1.0 indicates carbohydrate utilization. Metabolic phenotyping data was analyzed using ExpeData software package (version 1.8.2, Sable Systems, Las Vegas, NV) the Universal Macro Collection (version 10.1.3, Sable Systems, Las Vegas, NV). The total EE, RER and activity were averaged over an entire day or night cycle to assess whole cycle differences among the groups as well as during the most active (active EE, active RER) and most inactive (resting EE, resting RER) periods measured during each cycle. EE and RER were also analyzed every hour over a 24-hour period to assess the pattern of rhythmicity in these parameters.

4.3.3 Glucose and Insulin Tolerance Tests

After seven weeks on the restricted liquid sugar schedule, all groups were fasted for fifteen hours (ZT 12-ZT 3), and the ALFG, EFG, and LFG groups were only given access to tap water during this time. The GTT was performed as previously described at the beginning of ZT 3 (Luo et al., 2016; Woodie et al., 2018). Briefly, the dorsal vein of the tail was superficially nicked 1.5 cm near the distal end with a sterile razor.

Approximately 5 μL of blood was collected on a Contour One blood glucose meter strip to obtain a baseline blood glucose measure for each mouse. An intraperitoneal (i.p.) injection of a sterile 25% glucose solution (2g/kg body weight) was then administered to each animal. Blood was collected from the tail nick at 15, 30, 60 and 120 min after injection. The area under the curve (AUC) was obtained by calculating the Riemann sum for each group.

One week after the GTT, animals were fasted and provided with only tap water for six hours (ZT 3-ZT 9) before performing an ITT. Beginning at ZT 9, blood was sampled from a nick in the dorsal tail vein to obtain a baseline blood glucose measurement as described for the GTT. Then an i.p. injection of Humulin R (Eli Lilly, Indianapolis, IN) was administered at a dose of 0.9 U/kg body weight and blood glucose was tested at 15, 30, 60 and 90 min after injection. The rate constant for glucose disappearance (K_{ITT}) was calculated from the ITT time course data as previously described (Luo et al., 2016).

Fasting durations for the GTT and ITT were chosen based on guidelines from the Mouse Metabolic Phenotyping Center (Ayala et al., 2010). The GTT fast at ZT 12 and the ITT fast at ZT 3 were performed to avoid inferring with the liquid sugar restriction paradigm in the EFG and LFG groups.

4.3.4 Tissue Collection and Analysis

At the end of the ninth week, animals were euthanized via CO_2 asphyxiation followed by decapitation. Trunk blood was used to obtain a final blood glucose measurement and was collected and centrifuged at 12,000 rpm to draw off serum, which was then stored at -

80°C. Livers, eWAT, rWAT and iWAT were excised on ice and weighed. eWAT and rWAT weights were summed to calculate visceral adipose tissue mass and iWAT was used as a measure for subcutaneous (SubQ) fat mass. All tissue weights were normalized to final body weight. Serum insulin levels were determined by an insulin ELISA assay (Crystal Chem, Inc., Downers Grove, IL) and data were analyzed for insulin resistance using the HOMA-IR score (HOMA-IR = (26 * fasting serum insulin * fasting blood glucose)/405).

4.3.5 Liver histopathology

Liver histopathology was carried out as previously described (Woodie et al., 2018). Briefly, a 1-3 cm^3 piece of tissue from the left lobe of each liver was immediately fixed in 10% buffered formalin during sacrifice. The fixed tissue was paraffin embedded, and then sections were stained with hematoxylin and eosin. The stained sections were examined in a blinded fashion by a board-certified veterinary pathology and assigned a steatosis score based on previously published criterion (Liang et al., 2014). A cumulative steatosis score was calculated for each section based on the sum of scores for microsteatosis, macrosteatosis and hypertrophy.

4.4 Results

4.4.1 Body Weight

For the first seven weeks of exposure, there was no significant effect of liquid sugar consumption on absolute body weight (Figure 15A). However, the animals provided with *ad libitum* access to the 12% 55%/45% FG (ALFG) weighed significantly more than the

other three groups after eight and nine weeks of liquid sugar exposure ($F(36,270) = 3.93$, $p<0.05$; Figure 15A). Furthermore, the ALFG group exhibited a significantly elevated percent change in body weight ($F(36,270) = 3.93$, $p <0.05$; Figure 15B). After nine weeks, the ALFG group had a 41% increase in body weight when compared to initial body weight. The percent change was significantly higher when comparing the ALFG treatment group to the Con group during week 1 and weeks 3-10 ($p<0.05$; Figure 15B). Additionally, the ALFG group had a significantly elevated percent body weight change compared to the EFG group during weeks 1-10 ($p<0.05$) and to the LFG group during week 1 and weeks 3-10 ($p<0.05$; Figure 15B). Con, EFG, and LFG groups did not exhibit significantly different percent body weight changes when compared to each other and each group ended the study with a body weight percent increase close to 27%.

4.4.2 Energy Expenditure

All groups exhibited the natural diurnal rhythm of mouse EE with low EE during the day and elevated EE during the night cycle (Figure 16). During the day, groups ALFG and LFG had significantly higher total EE when compared to the Con group ($F(3,31) = 6.14$, ALFG v Con: $p<0.001$, LFG v Con: $p<0.05$; Figure 16A). During the night the Con group continued to have significantly lower EE than the ALFG group ($F(3,31) = 8.41$, $p<0.05$), but was not significantly different from the LFG group. The EFG treatment group, however, exhibited significantly higher EE than both the Con and the LFG treatment groups ($F(3,31) = 8.41$, EFG v Con: $p<0.001$; EFG v LFG: $p<0.05$; Figure 16A). During each day and night cycle, the average EE for each mouse was collected at their most active and resting point (Figure 16B and 16C). Active and resting EE were

significantly lower for the Con group during the day than all treatment groups (Active: $F(3,31) = 40.9$, $p<0.001$; Resting: $F(3,31) = 460.6$, $p<0.001$; Figure 16B and C). During the night, the Con group showed significantly lower average active and resting EE than ALFG or EFG treatment groups (Active: $F(3,31) = 6.51$ $p<0.05$; Resting: $F(3,31) = 6.91$, $p<0.01$) Figure 16B and C). The EFG and LFG groups only had different resting EEs during the night cycle, where LFG exhibited significantly lower resting EE ($F(3,31) = 6.91$, $p<0.05$; Figure 16C). Therefore, liquid sugar consumption induces an upward shift in average mouse EE at both the most active and inactive points of the day and night cycles. However, when EE was assessed every hour over a 24-hour period, the most significant changes were observed during the first six hours of the dark period (Figure 16D). During this time, the EFG group EE was significantly elevated from the Con and LFG groups from ZT 13-ZT 15 ($F(69,744) = 1.85$, $p<0.05$) and elevated compared to all of the other groups at ZT 17 ($p<0.05$). Additionally, the LFG group demonstrated significantly lower values than ALFG treatment group during ZT15 and ZT16 ($F(69,744) = 1.85$, $p<0.01$; Figure 16D). No significant differences were seen between the LFG treatment group and the other groups during their period of FG access.

Two major components of EE are metabolic rate measured by VO_2 and activity (Even and Nadkarni, 2012). As an animal becomes more active, they will consume more oxygen and expel more CO_2 thereby increasing measured EE during that time. On the other hand, changes in VO_2 measurements would represent treatment-induced alterations in metabolic rate. To determine whether the animals were simply altering their activity around sugar water availability the diurnal nature of these two parameters were assessed (Figure 17). Interestingly, we did not observe significant differences in the diurnal

rhythm of activity with the animals in the EFG and LFG groups, indicating that the EFG and LFG animals did not increase activity before or during FG availability (Figure 17A). Although the ALFG group increased their activity at ZT 0, ZT 5, ZT 13 and ZT 16, this did not contribute to a difference in EE at those times (Figure 17A). The rhythms of VO_2, a measure for metabolic rate, however, followed the same pattern of those found in EE (Figure 17B). Thus, timing liquid sugar consumption significantly affects the natural rhythms of murine metabolic rate, which alters overall energy expenditure.

4.4.3 Macronutrient Utilization

RER values, which are a measure of macronutrient utilization, were averaged over the day and night cycle as well as at the most active and resting points during each cycle (Figure 18A-C). On average, each group exhibited the normal rodent rhythm in RER with more lipids being utilized during the fasting, day cycle and more carbohydrates being used during the feeding, night cycle (Figure 18A). However, the Con group had significantly higher average RER in the daytime than all other groups indicating greater lipid utilization in the groups exposed to liquid sugar during the resting cycle ($F(3,31) = 185$, $p<0.001$; Figure 18A). There were very few variations among groups during the night cycle for average and active RER with each group utilizing more carbohydrates at night (Figure 18A and 18B). Interestingly, the EFG treatment group had significantly lower active RER than the other groups during the day ($F(3,31) = 313$, $p<0.001$; Figure 18B). This suggests that the EFG group had greater metabolic flexibility during daytime bouts of activity compared to the other three groups and utilized lipids when liquid carbohydrates were not available.

Average resting RER demonstrated marked differences among the groups during the daytime (Figure 18C). Animals in the Con group showed a significantly higher resting RER than all of the treatment groups, while the LFG group had the lowest resting RER when compared to Con, ALFG, and EFG ($F(3,31) = 35.3$, $p<0.05$). During the night period, the EFG group once again displayed a significantly lower resting RER than either the Con or ALFG groups ($F(3,31) = 6.91$, $p<0.01$; Figure 18C).

When RER was measured over a 24-hour period, the most remarkable changes were once again observed during the night cycle. The LFG group maintained lipid utilization with a significantly lower RER for the first six hours of the active period and did not exhibit an RER similar to the Con and ALFG groups until FG was available at ZT18 ($F(69,744) = 5.37$, $p<0.05$). The EFG group, on the other hand, began the night cycle with FG access and exhibited increased carbohydrate utilization similar to the Con and ALFG groups from ZT 12-18. Once the FG was taken from the EFG group, they began utilizing more lipids for energy than all other groups from ZT1 9-23 ($F(69,744) = 5.37$, $p<0.001$; EFG versus ALFG at ZT 20, $p<0.05$; Figure 18D). Overall, the RER results showcase robust changes in macronutrient utilization and alterations in natural, rodent metabolic flexibility driven by six-hour windows of sugar availability.

4.4.4 Glucose and Insulin Tolerance Tests

The ALFG treatment group demonstrated significantly higher blood glucose levels than the other three groups at 15-min post-injection and from the EFG group at 30-min post-injection during the GTT ($F(16,150) = 1.44$, $p<0.05$; Figure 19A). At 30 minutes post-injection, the EFG group also had lower blood glucose levels than the LFG treatment

group ($F(16,150) = 1.44$, $p<0.05$). Despite these differences observed over the time course of GTT testing, we did not observe significant differences among the groups when the data was assessed as AUC (Figure 19B).

The ITT results showed no significant differences among the groups at 15- or 30-minutes post-injection. However, after 60 minutes, the EFG treatment group had significantly lower blood glucose than the Con group ($F(16,140) = 1.11$, $p<0.01$; Figure 19C). At the 90-minute post-injection time point, the EFG treatment group exhibited significantly lower blood glucose than both the Con and ALFG groups ($F(16,140) = 1.11$, $p<0.05$). The LFG treatment group was also significantly lower at the 90-min time point when compared to the Con group ($F(16,140) = 1.11$, $p<0.05$; Figure 19B).

Plasma glucose disappearance rates (K_{ITT}) were calculated from the ITT data. The EFG treatment group exhibited significantly lower rates of glucose disappearance than Con and ALFG groups indicating quicker blood glucose uptake after an insulin injection ($F(3,28) = 4.25$, $p<0.05$; Figure 19D). No significant variation was found in blood glucose clearance among Con, ALFG, and LFG groups.

4.4.5 Food and Water Consumption

No significant differences were found in total food uptake when averaged over the day or night cycle (Figure 20A). There were, however, several differences in cycle water uptake. During the day and night cycles, the ALFG group consumed significantly more grams of water than the control group (Day: $F(3,30) = 33.5$, $p<0.05$; Night: $F(3,30) = 20.5$, $p<0.05$; Figure 20B). The EFG group consumed the least amount of water during the day cycle even compared to control ($F(3,30) = 33.5$, $p<0.05$). Interestingly, LFG consumed an

amount of water comparable to the ALFG group and significantly higher than groups Con and EFG ($F(3,30) = 33.5$, LFG v Con: $p<0.05$, LFG v EFG: $p<0.001$; Figure 20B).

Food kilocalories consumed by the animals were higher at night and lower during the day period, as is to be expected due to the animals' active period being the night cycle. However, there were no significant differences in food kilocalorie consumption among the groups for either cycle (Figure 20C).

Water kilocalorie consumption varied widely between groups, although this can partly be contributed to the amount of time the groups had access to FG. Due to the 24 group being the only group with access to FG during the daytime, they consumed significantly more liquid calories than the other groups during the daytime ($p<0.001$; Figure 20D). The ALFG group also had significantly higher water kilocalorie consumption during the night period, which is again expected due to their consistent access to caloric water throughout the entire cycle ($F(3,31) = 73.0$, $p<0.001$; Figure 20D). Interestingly, the EFG group did not vary significantly from the ALFG group when liquid kilocalorie consumption was averaged over the night cycle, despite EFG animals only having access to FG for half of this period. When both food and water kilocalories were summed for day and night cycles, however, there were no significant differences among the groups (Figure 20E). Likewise, when total kilocalorie consumption was assessed in relation to final body weight there were no significant differences among the groups (Figure 20F).

Food kilocalories, water grams, and total kilocalorie consumption were further examined as percentages binned in six-hour windows over 24 hours (Figure 21). The percentage of food kilocalorie consumption within each six-hour bin was not altered by

liquid sugar availability with each group consuming roughly 24% of their daily solid calories from ZT 0-5, 8% from ZT 6-11, 36% from ZT 12-17 and 33% from ZT 18-23 (Figure 21A). Since the tap water available to the Con group *ad libitum* and to groups EFG and LFG during restriction had no calories, water kilocalorie consumption could not be assessed over 24 hours. However, we were able to assess the amount of water consumed in grams within the same six-hour bins to reach similar conclusions. The EFG and LFG groups consumed the majority of their water when the FG was available. The EFG group consumed 59% of their daily water from ZT 12-17, and the LFG consumed 59% of their daily water from ZT 18-23; both of which were nearly double the amount of water consumed by the Con group during the same bins (Figure 21B). This did not cause changes in the distribution of total kilocalorie consumption in the EFG and LFG groups compared to Con (Figure 21C). The ALFG group, however, did have altered total kilocalorie consumption, specifically in the ZT 6-11 bin. The Con, EFG and LFG groups consumed approximately 7% of their daily calories from ZT 6-11, while the ALFG group doubled that amount with 14% of their kilocalorie consumption occurring during that time (Figure 21C). Together, these data indicate that the physio-metabolic changes observed in our study were not caused by an overall increase in calorie consumption, but instead due to the impact of liquid sugar access on diurnal metabolism and feeding behaviors.

4.4.6 End-point Analyses

At sacrifice, whole livers and adipose tissue pads were collected and weighed. Although there was no significant difference in liver weights among the groups (Table 1),

the ALFG group had more hepatic fat deposition and an increased steatosis score than the other three groups ($F(3,27) = 3.43$, $p<0.05$; Figure 22). The ALFG group also had more visceral fat than the Con group and significantly more SubQ adipose tissue than the other three groups (Visceral: $F(3,29) = 4.01$, $p<0.05$, SubQ: $F(3,29) = 5.43$, $p<0.05$; Table 1). There were no observable differences among the groups in fasting blood glucose, fasting serum insulin, or insulin resistance measures (Table 1).

4.5 Discussion

Sugar sweetened foods and beverages constitute a large portion of the diet in the Western world, and HFCS is the most common substance used to sweeten them (Bleich et al., 2018; Bray et al., 2004). A common complication resulting from overconsumption of HFCS sweetened products is obesity, which continues to be a problem throughout the world (Bocarsly et al., 2010; Bray et al., 2013; Jürgens et al., 2005; Mock et al., 2017; Stanhope et al., 2009; Teff et al., 2004). Numerous approaches have been proposed to combat obesity and its associated metabolic diseases (Jakicic et al., 2001; Sacks et al., 2009).

Restrictive diets are one such approach commonly used by individuals seeking to lose weight and improve overall health (MacLean et al., 2015). However, these diets focus mainly on changes in solid calorie consumption. Liquid calories, on the other hand, have proven to be more difficult to track than solid calories as their consumption does not induce satiety as effectively as solid calories (Almiron-Roig et al., 2013; Chambers et al., 2015). Rodents and humans alike gain weight when administered caloric beverages and are not able to reduce the amount of solid calories consumed to compensate for liquid

calories (Light et al., 2009; Malik et al., 2006; Swithers and Davidson, 2008; Vartanian et al., 2007). Furthermore, restrictive diets, although effective in the short-term, are rarely sustainable for long periods of time and weight regain is quite common (Kayman et al., 1990; MacLean et al., 2015; Wu et al., 2009). Time-restricted feeding of solid calories has been suggested as an alternative and more manageable approach for improving metabolic health (Gabel et al., 2018; Rothschild et al., 2014; Sutton et al., 2018). In fact, the American Heart Association suggests that meal timing interventions, instead of changing the types or amounts of foods consumed, may be a more effective way to promote metabolic health (St-Onge et al., 2017). Therefore, we sought to apply the idea behind TRF to liquid calorie consumption. Specifically, we restricted the consumption of a 12% 55%/45% FG to the early and late murine active periods and compared their physio-metabolic outcomes to groups receiving either *ad libitum* tap water or *ad libitum* FG.

Body weight and fat mass were significantly increased only in the group with 24-hour access to the FG, as animals in both the EFG and LFG groups exhibited body and fat weights comparable to the Con group. This type of weight gain is commonly observed in animal and human studies allowing *ad libitum* access to sugar sweetened beverages and is normally attributed to increased calorie consumption (Malik et al., 2010a; Swithers and Davidson, 2008). Interestingly, however, the increase in body weight and body fat in the ALFG group was not due to an overall increase in calorie consumption. All four of the groups consumed similar amounts of kilocalories during the day and night period. However, when the percentage of daily calorie consumption was observed in six-hour windows, it was only during the ZT 6-11 window that the ALFG group consumed more

kilocalories. Thus, an alteration in the daily distribution of kilocalorie consumption and not an overall increase in daily kilocalorie consumption may drive the ALFG phenotype.

Other than the changes in body and fat weights, we did not observe differences in other tissue weights among the groups. However, we did find that the ALFG animals had significantly more hepatic fat deposition. Previous studies have found that fructose consumption elicits significant elevation in normalized liver weights and liver fat content (Schwarz et al., 2015, 2017; Sellmann et al., 2015; Stanhope et al., 2009). The association between fructose consumption and increased liver size and/or fat deposition lead to the belief that the majority of intact dietary fructose was metabolized by the liver, which made the similarity in liver size observed in the present study quite perplexing (Thornley et al., 2012). However, a recent publication by Jang *et al.* found that the majority of fructose metabolism actually occurs in the small intestine. In fact, very little intact fructose was found in the livers of animals given less than 0.5 g/kg of fructose or given fructose after feeding. It was observed that only when the small intestine is saturated after a fructose gavage greater than 0.5 g/kg or fructose is consumed under fasting conditions that intact fructose is metabolized by the liver (Jang et al., 2018). Synthesizing our endpoint and histology data with these findings suggest that the 12% FG may in fact saturate the small intestine's capacity for fructose metabolism. However, due to either the length of our study or the percentage of sugar water used, our treatment did not impact overall liver weight.

Findings of particular interest in the present study are the robust differences in the diurnal patterns of EE and RER that were observed in the time-restricted FG groups. 24-hour access to the FG did not significantly alter these metabolic patterns with the ALFG

group, which exhibited similar diurnal EE and RER rhythmicity to the Con group. Interestingly, the LFG group exhibited a reduction in EE during the first six hours of activity. A calorie restriction-induced dampening of EE has been observed previously when total calorie consumption was shifted to the inactive phase (Bray et al., 2013). This supports the hypothesis that EE amplitude can be altered by calorie availability. However, the diurnal rhythm of rodent EE was maintained in our sugar restriction paradigm: the LFG animals still exhibited an increase in EE when moving from day to night; however, it was blunted during the first six hours. It was not until we provided sugar water to the LFG group that they exhibited an EE similar to the Con group.

Additionally, recent human studies have found that eTRF and midday TRF (mTRF) are more beneficial for metabolic outcomes than lTRF. eTRF can increase insulin sensitivity and improve β cell function in men with prediabetes as well as decrease glycemic excursions in overweight individuals (Jamshed et al., 2019; Sutton et al., 2018). Likewise, mTRF studies observed reduced hyperglycemia, hyperinsulinemia, insulin resistance, and inflammation in their participants (Gill and Panda, 2015; Moro et al., 2016). However, lTRF either does not induce any metabolic benefits or is detrimental to metabolic health (Carlson et al., 2007; Tinsley et al., 2017). Our LFG paradigm dampens the diurnal rhythms of EE during the first six hours of activity, while our EFG paradigm amplifies the rhythm of EE during this time. Although diurnal EE was not measured in the human studies, our data suggests that the dampening of EE during the early feeding window may diminish the efficacy of sugar restriction on protecting against the negative impacts of sugar water consumption (i.e. decreased glucose and insulin tolerance).

The EFG group, on the other hand, preferentially utilized lipids during daytime activity. Neither the EFG nor LFG group had access to the FG during the daytime, which suggests that restricting liquid sugar consumption to the earliest six hours of the active period, but not the last six hours, limits the use of carbohydrates exclusively to the period during which they are being consumed. Furthermore, the robust metabolic flexibility observed in the EFG group was not due to significant changes in activity or metabolic rate after FG access. Therefore, the EFG animals maintained activity and metabolic rate (VO_2) comparable to the Con group, but they were using lipids to do so. This begs the question: If the mice are utilizing lipids more often, why did we not observe a decrease in adipose tissue weight in the EFG treatment group? One possibility may be due to the length of our study: nine weeks is a relatively short-term diet study and as such is a limitation to the current study.

A key finding in our study was the impact of liquid calorie restriction on the diurnal patterns of macronutrient utilization. After just nine weeks on the liquid restriction paradigm, the EFG animals exhibited robust diurnal patterns of RER. In the EFG group, carbohydrate utilization was robust only during the first six hours of activity, when sugar water was available, while lipid utilization occurred throughout the rest of the day. This indicates that early-active liquid carbohydrate consumption may increase metabolic flexibility and induce a state of selective carbohydrate utilization that promotes lipid metabolism when liquid carbohydrates are not available. TRF of a solid high-fat diet to the active phase has been shown to increase metabolic flexibility, and this increased flexibility is thought to underlie some of the metabolic benefits of TRF (Chaix et al., 2014; Hatori et al., 2012; Woodie et al., 2018). Therefore, the robust flexibility induced

by early-active sugar water restriction may be involved in the improved insulin tolerance we observed in the EFG group. Furthermore, early-active restriction may play into the diurnal rhythms of mouse metabolism. As mice transition from the inactive, day phase to their active, night phase, they switch from utilizing lipids to utilizing carbohydrates (Panda, 2016; Young and McGinnis, 2016) This is driven by the master clock, the hypothalamic SCN. In mice, SCN output increases the mobilization of glycogen stores from the liver and insulin sensitivity in peripheral tissues from the late inactive to the beginning of the active period, thereby preparing the organism for meal consumption during the active phase (la Fleur et al., 2001; Kim et al., 2017). By providing liquid carbohydrates during this transition, our EFG paradigm facilitated this naturally occurring switch. The LFG group, on the other hand, did not transition to the same degree of carbohydrate usage as the other three groups during the first six hours of activity. Instead, LFG animals did not exhibit elevated RER until later in the active phase when sugar water was provided. Furthermore, the LFG group exhibited a significant dip in EE during the first six hours of activity. This also indicates a delay in diurnal metabolic rhythms induced by our LFG paradigm. The long-term implications of this delayed switch remain to be determined; however, previous studies have shown that murine blood glucose levels and insulin sensitivity decrease as the active period progresses (la Fleur et al., 2001; Kim et al., 2017). The LFG paradigm, therefore, may require alterations in the diurnal rhythm of mouse macronutrient metabolism to accommodate for late-active carbohydrate availability. These results should encourage future mechanistic and long-term studies to further examine the impacts of our liquid calorie restriction paradigm.

Also, of note are our GTT and ITT results. During the GTT, the ALFG group had significantly higher blood glucose readings 15 minutes post-injection, indicating that glucose metabolism in these animals was dysregulated compared to the EFG, LFG or Con groups. After 30 minutes, the EFG group had significantly lower blood glucose levels than any of the other groups, indicating that these animals were more glucose tolerant. In the ITT, the EFG group once again exhibited significantly lower blood glucose readings than other groups 60 minutes post-injection. When looking at the rate of glucose clearance during the ITT *(K_{ITT}),* the values for the EFG animals were significantly lower than LFG, ALFG or Con mice. Together, the GTT and ITT data further supports the notion that restricting liquid carbohydrate calories to the first six hours of activity imparts alterations in rodent metabolism that are not observed when liquid calories are restricted to the last six hours of activity. However, it is important to note that the timing of the GTT and ITT did not take advantage of the natural rhythms of rodent glucose metabolism. Work by la Fleur *et al.* in 2001, found that glucose utilization and insulin sensitivity peaked around ZT 14 in male Wistar rats (la Fleur et al., 2001). However, if we were to have performed our tests at ZT 14, the animals would need to be fasted beginning at ZT 23 for the GTT. This would attenuate the LFG sugar access. For the ITT, the fast would begin at ZT 8 and last until ZT 14, once again disrupting the sugar access to only one treatment group (EFG). Furthermore, if we chose to perform the ITT at ZT 3 or the GTT at ZT 9, we would have again disrupted the daily sugar access to the LFG group. Although we chose the fasting and testing time points to best fit our liquid sugar restriction schedule, this does represent a limitation in the present study.

Human studies have also explored the potential of restricting carbohydrate consumption to improve human health. Consistent with the RER, GTT, and ITT data from the EFG treatment group, a study of human eating habits found that metabolic parameters such as blood glucose and energy intake were regulated more efficiently when individuals confined their carbohydrate-heavy meal consumption to breakfast time, i.e. early in the active phase (Almoosawi et al., 2013). In fact, this feeding pattern may be the most metabolically and behaviorally beneficial. Several sources have recommended decreasing sugary beverage intake to improve health while also warning of withdrawal symptoms when removing these beverages from the diet immediately and completely (Thornley et al., 2012). Therefore, an early-active restriction paradigm may be a way for human subjects to improve their metabolic health while avoiding undesirable withdrawal symptoms.

Overall, these results suggest that limiting liquid calorie consumption to either early or late periods of the active phase is an effective way of combatting the weight gain and fat deposition commonly observed after HFCS exposure. Limiting liquid calories to the first six hours of activity, in particular, may allow for enhanced metabolic flexibility and improved glucose and insulin tolerance. The mechanisms behind these observations as well as the long-term impacts of this liquid calorie access schedule should be examined in future studies. The present study, however, provides an important first examination of the beneficial physio-metabolic effects of time-restricted liquid calorie consumption.

Tables

Table 1: Final measures for normalized liver weight, normalized body fat weights, fasting blood glucose, fasting serum insulin and HOMA-IR score.

	Con	ALFG	EFG	LFG
Normalized Liver Weight (g)	1.36±0.07	1.46±0.09	1.44±0.07	1.34±0.05
Normalized Visceral Fat Weight (g)	1.104±0.101	1.786±0.186*	1.34±0.11	1.26±0.17
Normalized SubQ Fat Weight (g)	0.28±0.04	0.63±0.13**	0.31±0.04#	0.32±0.04#
Fasting Blood Glucose (mg/dL)	173.9±8.4	192.0±14.9	183.8±17.4	193.2±5.0
Fasting Serum Insulin (ng/mL)	0.07±0.02	0.09±0.02	0.08±0.01	0.07±0.02
HOMA-IR	0.74±0.16	1.07±0.20	0.98±0.17	0.82±0.16

Data were analyzed by an ANOVA with Tukey post-hoc test. Data presented as mean ± SEM. * different from Con, # different from ALFG, % different from EFG, ^ different from LFG. *p<0.05, **p<0.01, ***p<0.001.

Figures and Figure Legends

Figure 15

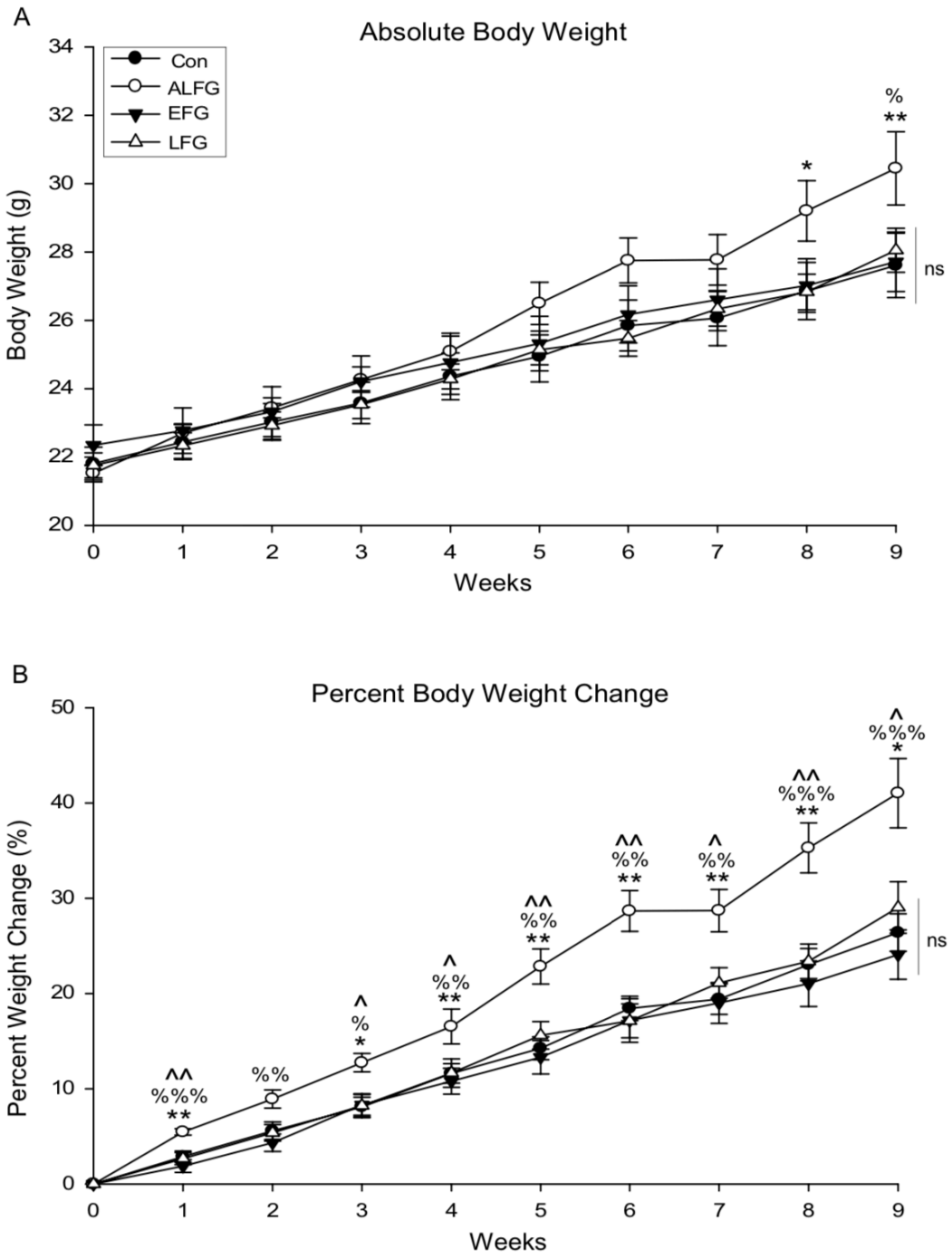

Figure 15: Body Weight During Liquid Sugar Restriction. A) Animals were weighed weekly. There were no differences among the body weights of the four groups until week

seven and eight when the ALFG group began to weigh significantly more than Con and EFG. B) Percent change in body weight was calculated each week from the initial weight. The ALFG group exhibited significantly higher weight gain from the other three groups starting at week 1 and persisting through the study. The Con, EFG and LFG groups maintained consistent weight gain and did not significantly differ from one another. Data presented as mean ± SEM. * different from Con, # different from ALFG, % different from EFG, ^ different from LFG. *p<0.05, **p<0.01, ***p<0.001.

Figure 16

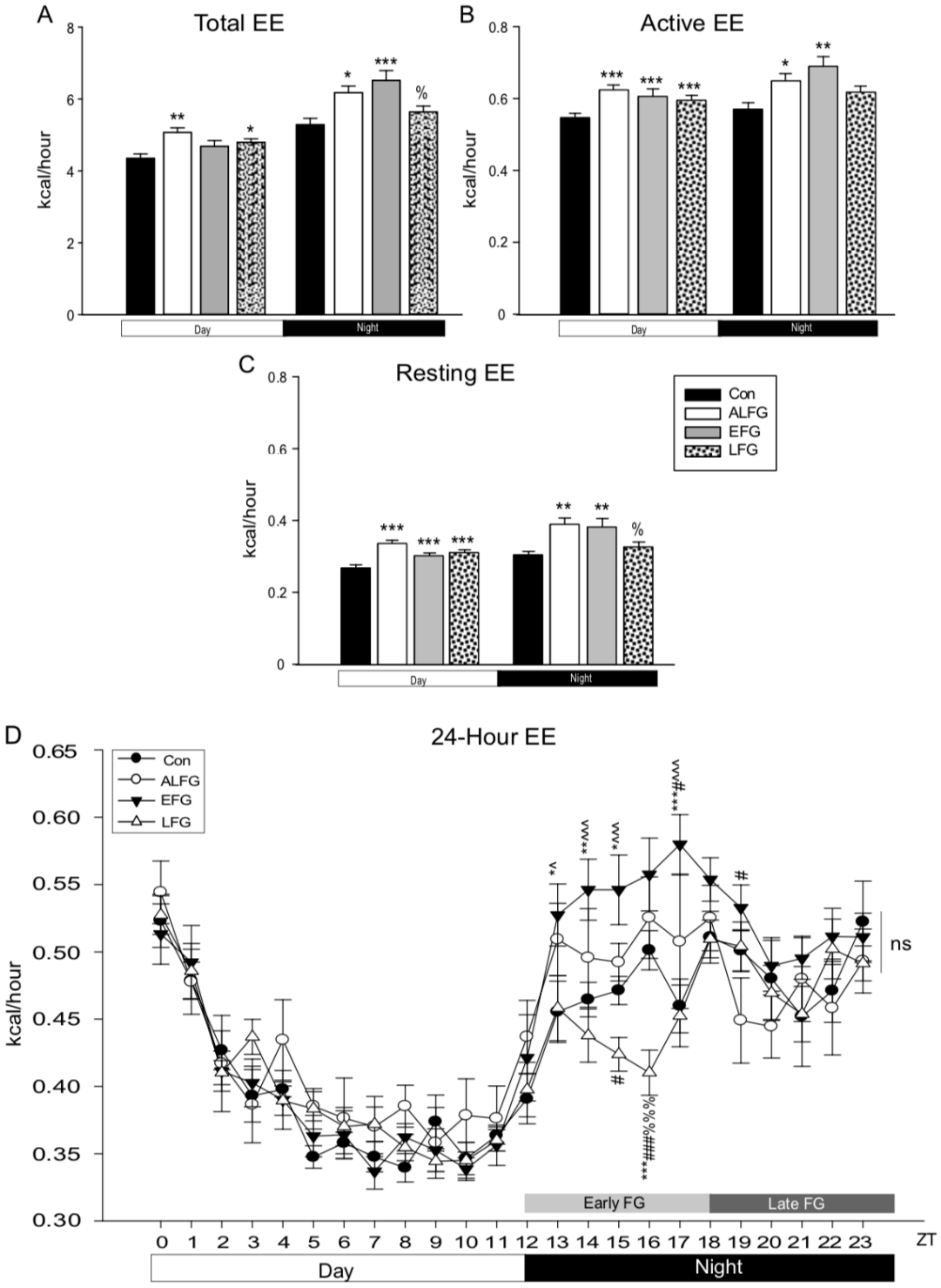

Figure 16: EE During Liquid Sugar Restriction. A) The total amount of energy expended was collected from each animal and averaged within the groups during the day and night

cycles. When analyzed with a one-way ANOVA, the ALFG group expended more total energy than Con during the day and night, while EFG expended more total energy than Con and LFG only during the night. B) EE at the highest level of activity during the day and night cycles was collected from each animal and averaged within the groups. C) EE at the lowest level of activity during the day and night cycles was collected from each animal and averaged within the groups. D) Energy expenditure was measured for each animal every hour for 24 hours and then averaged within the groups. Data presented as mean ± SEM. * different from Con, $^{\#}$ different from ALFG, $^{\%}$ different from EFG, ^ different from LFG. *$p<0.05$, **$p<0.01$, ***$p<0.001$.

Figure 17

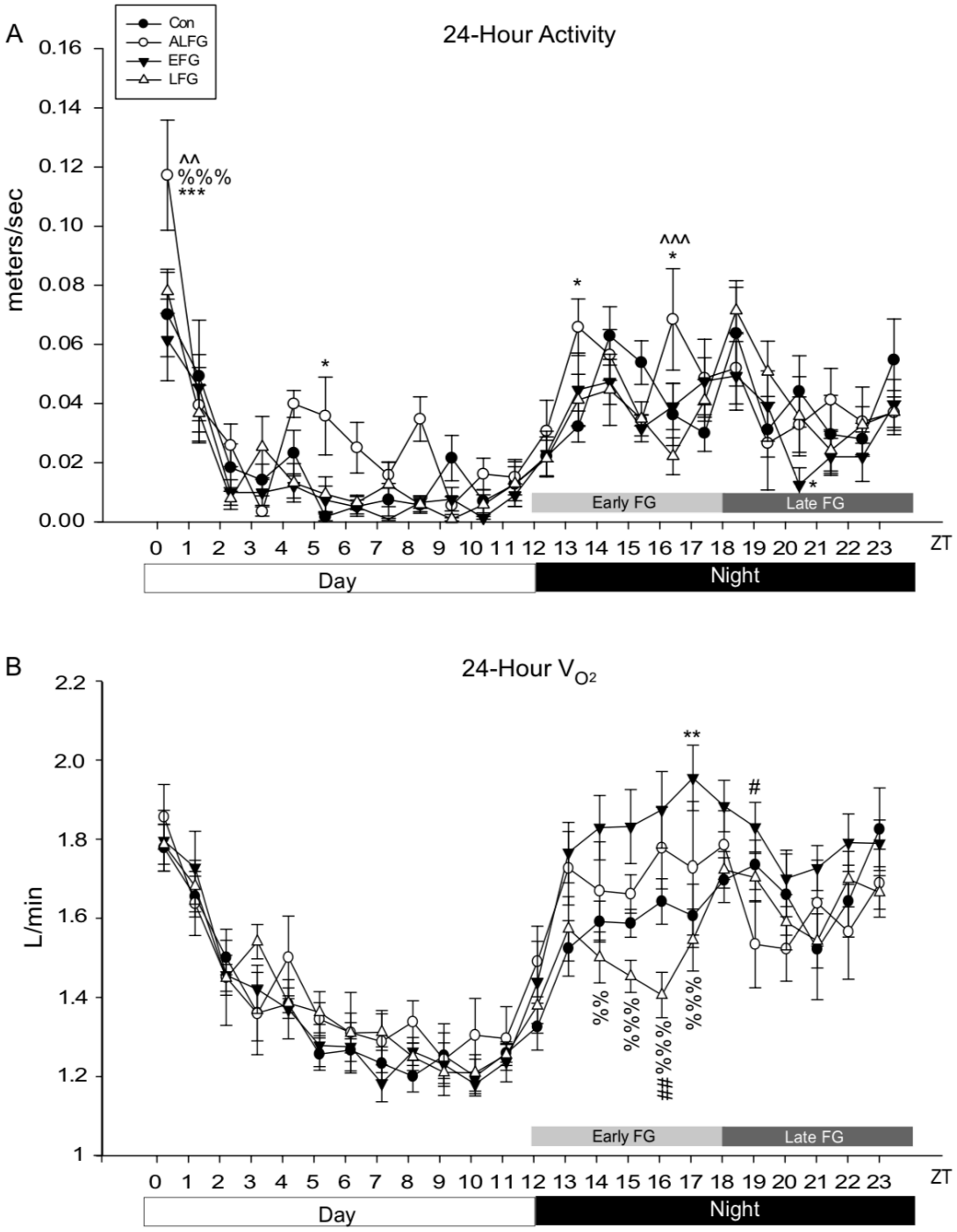

Figure 17: 24-hour Activity and 24-hour V_{O2} During Liquid Sugar Restriction. (A) At a few time points the ALFG group exhibited significant alterations in activity, however, access to FG did not induce large scale alterations in the diurnal rhythm of activity. (B)

Metabolic rate, as measured by V_{O2}, was significantly altered in the LFG group between ZT 14-ZT 17. This indicates that changes in diurnal EE were not due to changes in activity, but FG timing-induced disruptions in diurnal metabolic rate. Data presented as mean ± SEM. * different from Con, $^{\#}$ different from ALFG, $^{\%}$ different from EFG, ^ different from LFG. *p<0.05, **p<0.01, ***p<0.001.

Figure 18

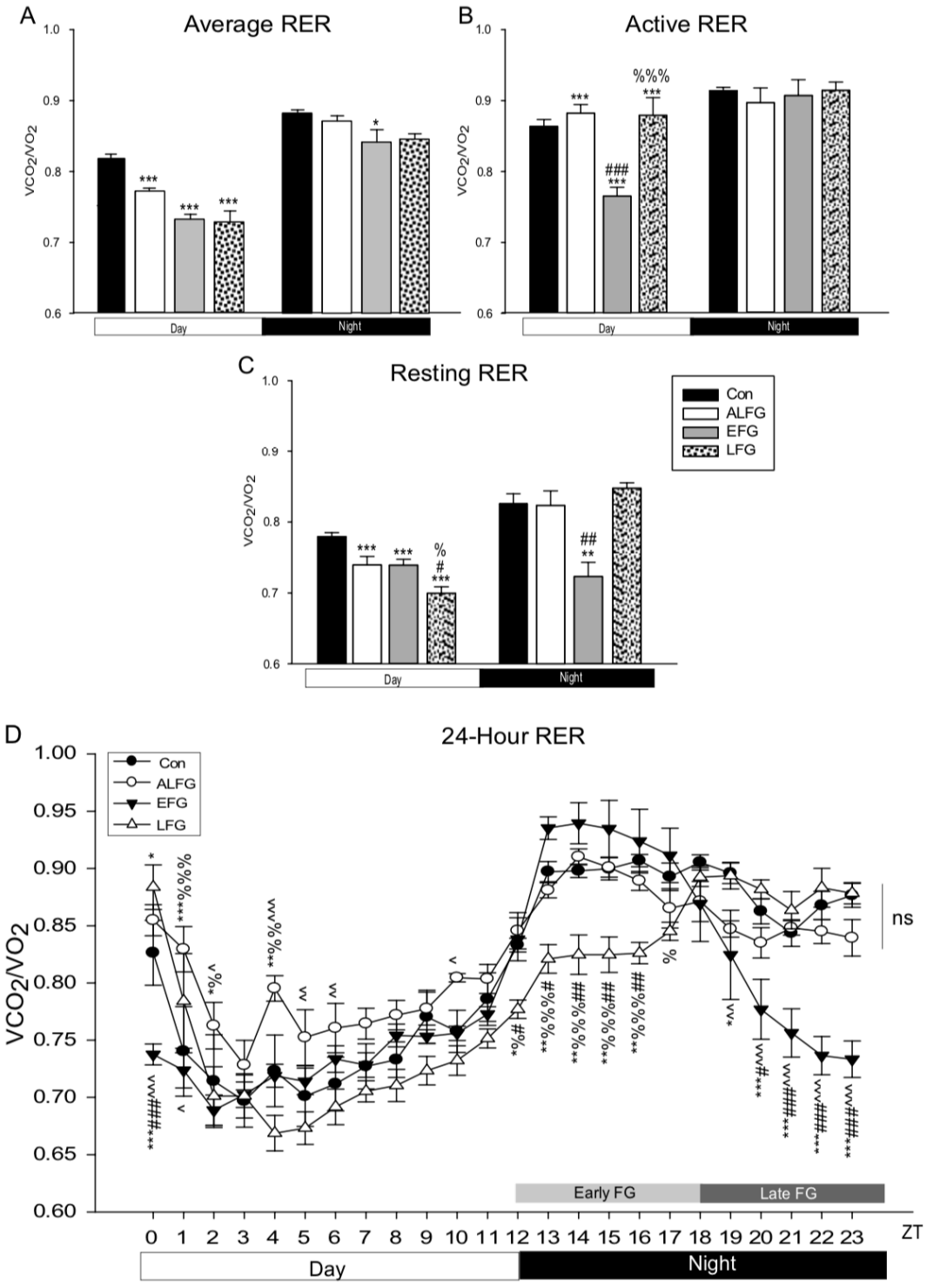

Figure 18: RER During Liquid Sugar Restriction. A) The average RER was collected from each animal and averaged within the groups during the day and night cycles. B)

RER at the highest level of activity during the day and night cycles was collected from each animal and averaged within the groups. C) RER at the lowest level of activity during the day and night cycles was collected from each animal and averaged within the groups. D) RER was measured for each animal every hour for 24 hours and then averaged within the groups. Data presented as mean ± SEM. * different from Con, $^{\#}$ different from ALFG, $^{\%}$ different from EFG, ^ different from LFG. *p<0.05, **p<0.01, ***p<0.001.

Figure 19

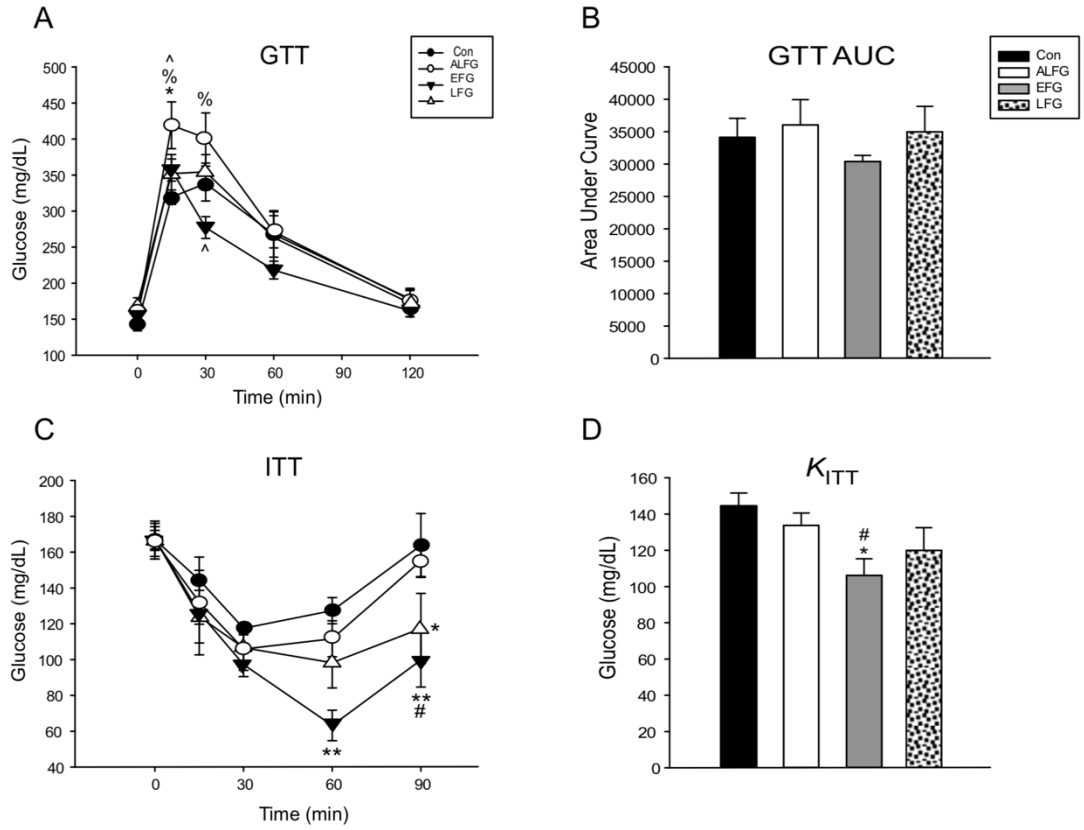

Figure 19: GTT and ITT During Liquid Sugar Restriction. A) The ALFG group exhibited significantly impaired glucose tolerance than the other three groups. B) Despite the significant differences observed in the time course of the GTT, there were no significant differences among the groups when analyzed by AUC. C) The EFG group had improved insulin tolerance compared to the Con at 60 min and compared to Con and ALFG after 90 min. D) This translated into a significantly improved rate of glucose clearance in the EFG group when analyzed as K_{ITT}**.** Data presented as mean ± SEM. * different from Con, $^{\#}$ different from ALFG, $^{\%}$ different from EFG, ^ different from LFG. *p<0.05, **p<0.01, ***p<0.001.

Figure 20

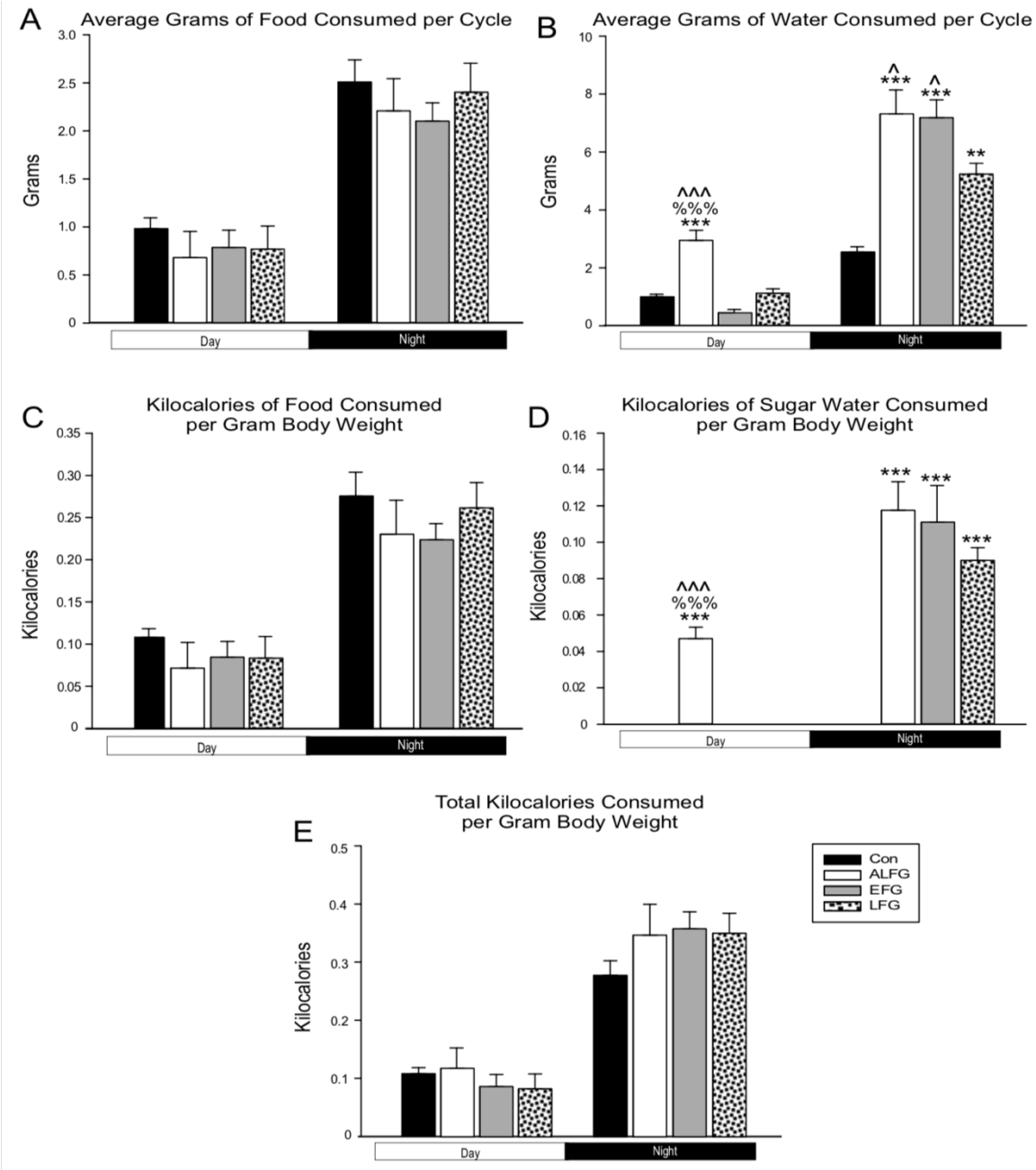

Figure 20: Diurnal Food and Water Consumption During Week 9 of Liquid Sugar Restriction. (A) FG availability did not significantly alter the grams of food animals ate during the day or night. (B) The ALFG and LFG groups consumed significantly more grams of water during the day than Con, while the EFG group consumed significantly less grams of water than the other three groups. During the night, all three FG groups

consumed more water than Con. (C) FG availability did not significantly alter the kcal of food animals ate during the day or night. (D) Since the Con, EFG and LFG groups had calorie-free tap water during the day, the ALFG group consumed significantly more kcal from water during that time. Likewise, ALFG and EFG groups consumed more liquid kcal during the night. (E) FG availability did not significantly alter the total kcal consumed by animals during the day or night. Data presented as mean ± SEM. * different from Con, $^{\#}$ different from ALFG, $^{\%}$ different from EFG, ^ different from LFG. *$p<0.05$, **$p<0.01$, ***$p<0.001$.

Figure 21

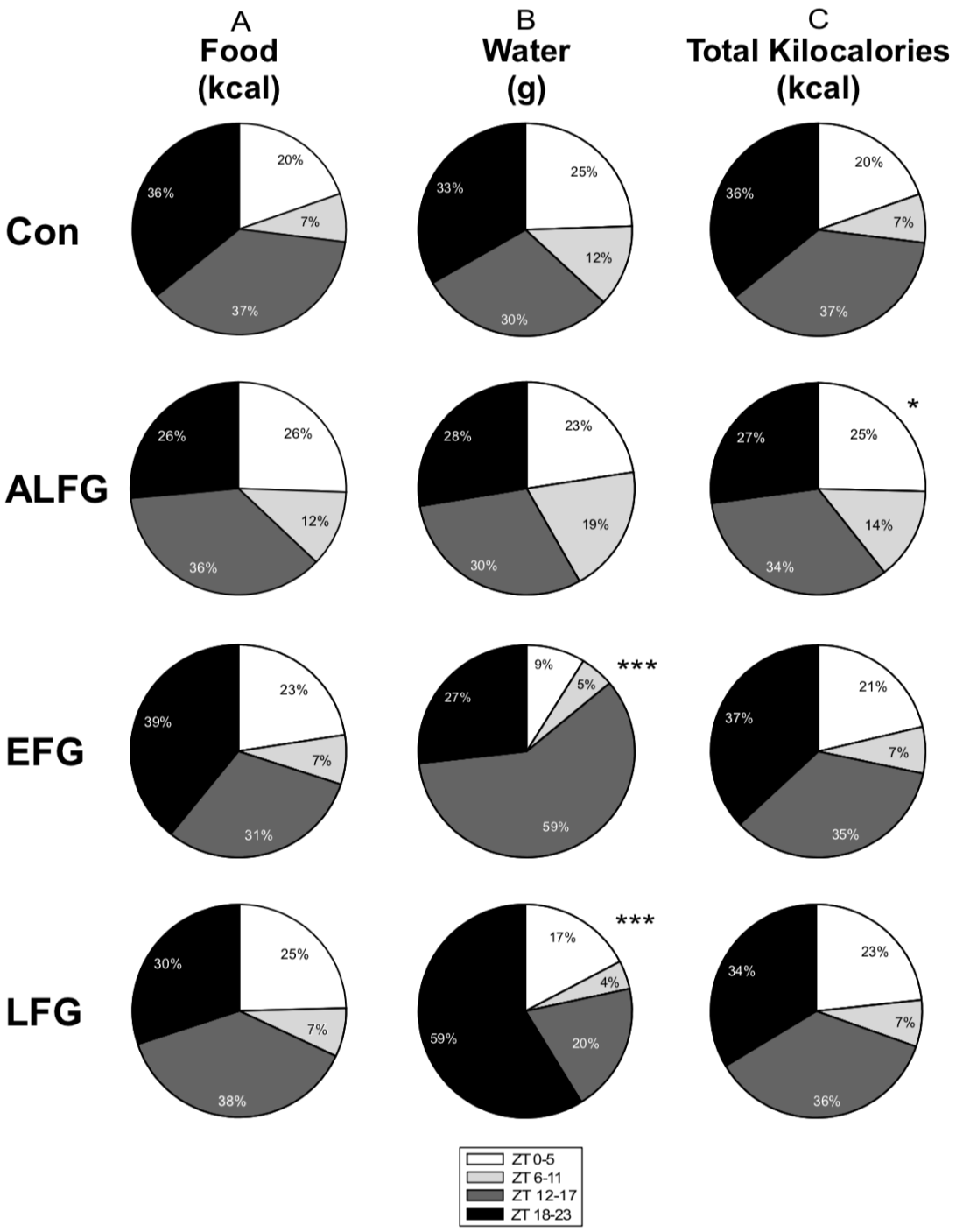

Figure 21: Time-Dependent Analysis of Food and Water Consumption. A) Chi-squared analysis of differences in food kcal consumption distribution from Con. The percentage of food kilocalorie consumption within each six-hour bin was not altered by FG

availability. B) Chi-squared analysis of differences in water gram consumption distribution from Con. The EFG group consumed 59% of their daily water from ZT 12-17, and the LFG consumed 59% of their daily water from ZT 18-0; nearly double the amount of water consumed by the Con group during the same time bins. C) Chi-squared analysis of differences in total kcal consumption distribution from Con. Con, EFG and LFG groups consumed approximately 7% of their daily calories from ZT 6-11 while the ALFG group doubled that amount with 14% of their kilocalorie consumption occurring during that time. * different from Con, $^{\#}$ different from ALFG, $^{\%}$ different from EFG, ^ different from LFG. *$p<0.05$, **$p<0.01$, ***$p<0.001$.

Figure 22

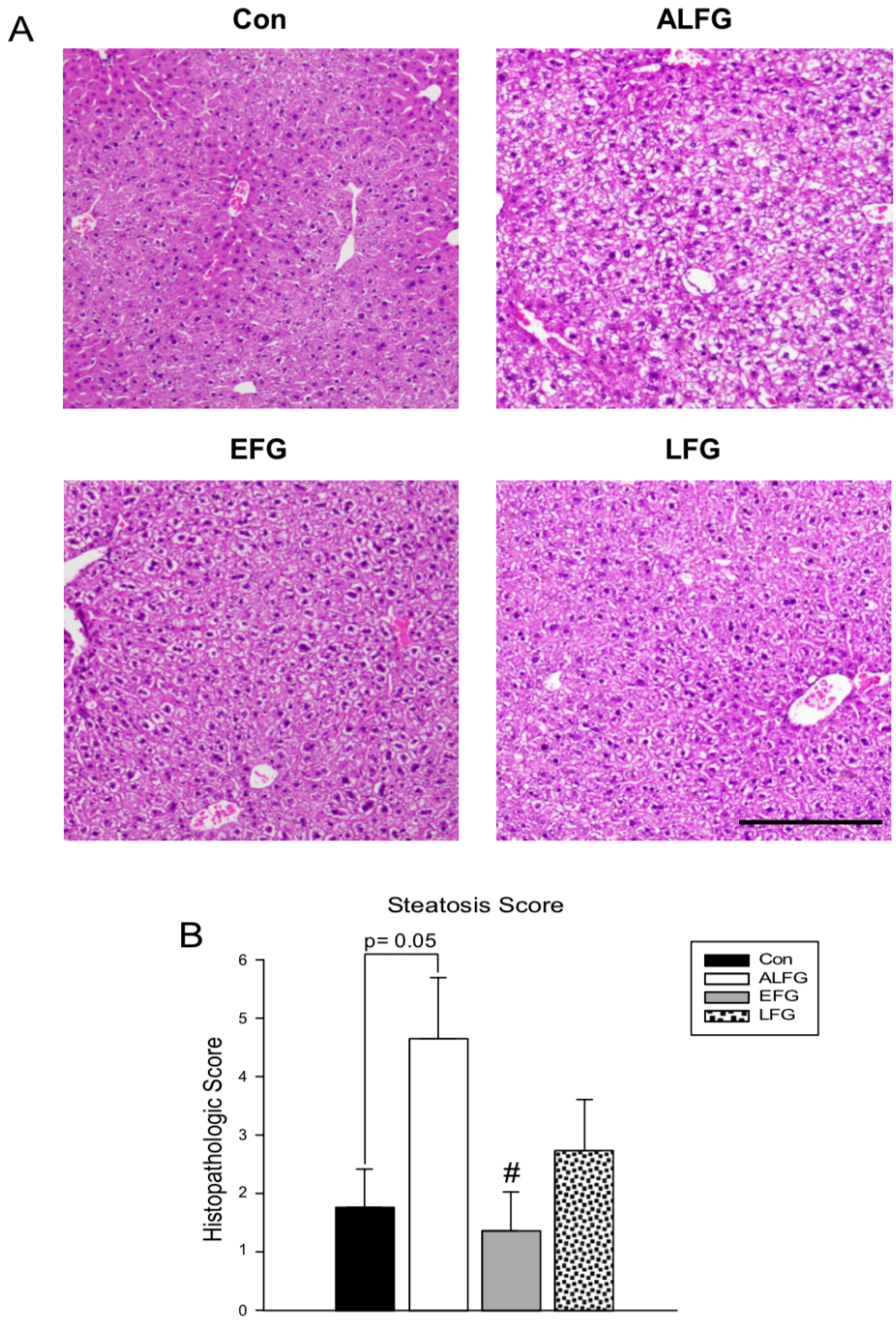

Figure 22: Liver Histopathology After Liquid Sugar Restriction. (A) Images of hematoxylin and eosin (H&E) stained liver sections. Scale bar = 200 μm. (B) Histologic grading for hepatic steatosis. The ALFG group had a significantly elevated hepatic

steatosis score compared to the EFG group. Data presented as mean ± SEM. * different from Con, # different from ALFG, % different from EFG, ^ different from LFG. *p<0.05, **p<0.01, ***p<0.001.

Chapter 5: Evidence for Hippocampal Core Clock Disruptions in a Murine Model of Western Diet-Induced Obesity

5.1 Abstract

Mammalian circadian rhythms are dictated by solar signals transmitted to the hypothalamic SCN. Although the SCN is the central clock for circadian rhythms, molecular clocks are found in every cell and are composed of the core clock proteins BMAL1, CLOCK/NPAS2, PER and CRY. Disruptions in the core clock occur in peripheral tissues after WD feeding and contribute to WD-induced metabolic disease. The mammalian center of memory, the hippocampus, is also sensitive to WD-induced dysfunction, but whether the WD disrupts the hippocampal core clock is not known. The present research explores this gap in our knowledge by examining hippocampal core clock rhythmicity in a mouse model of WD-induced obesity. Male C57Bl/6 mice were maintained on either standard rodent chow with tap water or a 45%/kcal fat WD with a 4% sugar solution (WD). Hippocampal memory was assessed during the 13th and 14th week of dietary exposure while diurnal metabolic rhythms were collected for 24 h in metabolic cages during the 16th week. Livers, hypothalami and hippocampi were then collected at 4-h increments over 24 h. mRNA expression was measured using RT-qPCR and assessed by cosinor-based rhythmometry. WD feeding significantly increased body weight and normalized liver weight ($p<0.001$) and significantly dampened diurnal rhythms of whole-body metabolism ($p<0.05$). As expected, the WD also induced significant alterations in the hepatic rhythmicity of *Bmal1* and *Reverba* expression ($p<0.05$). In line with previous findings, the rhythm of the hypothalamic *Bmal1, Npas2*

and *Per2* did not significantly differ between the dietary groups. All measured core clock genes were significantly disrupted in hippocampus after WD feeding. What is more, the expression pattern of key genes implicated in AD risk and associated with synaptic function were significantly altered in the WD group. Finally, hippocampal memory was disrupted in a task- and time-dependent fashion. Our results indicate that WD feeding significantly alters the rhythmicity of core clock mRNA expression in the hippocampus. These results suggest that WD-induced disruptions of the core clock may have implications in memory diseases with significant circadian etiologies, such as AD.

5.2 Introduction

The rhythm of all mammals living on the Earth's surface is dictated by the rotation of the Earth around the Sun. Photic signals are transmitted from retinal ganglia to the hypothalamic SCN. The presence of daylight entrains the rhythms of SCN neurons to a 24 hour cycle by initiating the transcription and translation of core clock genes in a TTFL (Welsh et al., 2010). The circadian TTFL is comprised of BMAL1, CLOCK/ NPAS2, PER1-3 and CRY1-2. BMAL1 and CLOCK/NPAS2 form the positive arm of the loop, while PER and CRY make up the inhibitory or negative arm (Dibner et al., 2010; Mohawk et al., 2012; Stratmann and Schibler, 2012). The BMAL1:CLOCK/NPAS2 heterodimer activates gene expression of *Per, Cry* and other CCGs while the PER:CRY complex inhibits the transcriptional activity of BMAL1:CLOCK/NPAS2 (Takahashi, 2017). This regulatory loop creates the stable and precise oscillatory patterns of circadian gene expression and molecular rhythmicity.

The SCN is regarded as the master regulator in the circadian hierarchy, but core clock genes are ubiquitous and oscillate within the circadian TTFL in most cells (Guillaumond et al., 2005; Solt et al., 2011). While peripheral tissues may be entrained to light:dark cycles via neural and hormonal signals from the SCN, they also possess cell-autonomous oscillators that are entrained to other exogenous cues. Indeed, the liver and adipose are established FEOs whose molecular and metabolic rhythmicity may be disrupted and/or corrected by nutrient availability (Asher and Sassone-Corsi, 2015). The WD is characterized by high-fat and high-sugar foods and its consumption is associated with obesity and metabolic disease (Carrera-Bastos et al., 2011; Cordain et al., 2005; Malik et al., 2013). Studies utilizing animal models of WD-induced obesity have shown that the WD significantly disrupts metabolic rhythmicity and dampens core clock gene expression in peripheral tissues (Eckel-Mahan et al., 2013; Hatori et al., 2012; Kohsaka et al., 2007). Metabolic rhythm disruption is also a part of the etiology of WD-induced metabolic disease, as realigning food consumption with the rhythms of nutrient metabolism via time-restricted feeding attenuates some of the negative impacts of the WD (Chaix et al., 2019; Eckel-Mahan et al., 2013; Hatori et al., 2012). Remarkably, the SCN is resistant to the WD and remains entrained to light:dark cycles (Hara et al., 2001; Kohsaka et al., 2007).

Outside of the SCN, the WD's impact on rhythmicity in the rest of the brain remains to be fully determined. The hippocampus exhibits distinct time-of-day-dependent rhythms in behavioral function, synaptic plasticity and protein phosphorylation events and is known to be negatively impacted by the WD (Chaudhury and Colwell, 2002; Chaudhury et al., 2005; Eckel-Mahan et al., 2008; Hsu and Kanoski, 2014; Woodie et al.,

2019). Indeed, Type-III Diabetes is now used to describe the AD-like cognitive deficits induced by the WD (de la Monte and Wands, 2008).

Herein, we report substantial WD-induced alterations in hippocampal diurnal gene expression. WD-induced obesity elicited significant changes in core clock gene expression and altered the diurnal landscape of synaptic and AD-associated genes in the mouse hippocampus. Moreover, this is the first study to date to establish a diurnal expression profile for key synaptic integrity and AD-associated genes in the hippocampus of chow-fed mice. Our work identifies disruptions in the circadian TTFL as a potential facet in the etiology of WD-induced cognitive deficits. Importantly, our data recognize the hippocampus as a centrally-located peripheral oscillator that can be disrupted by WD-induced obesity.

5.3 Materials and Methods

5.3.1 Animals and Diets

Male C5Bl/6N mice were obtained from Envigo at six weeks of age. The animals were pair housed in standard microisolator cages within the AAALAC accredited Veterinary Research Building (VRB) at the Auburn University College of Veterinary Medicine. All experimental procedures were approved by the Auburn University Institutional Animal Care and Use Committee in accordance with the NIH guidelines. The animals were maintained in a temperature and humidity-controlled room on a 12:12 light cycle with lights on as ZT 0 and lights off as ZT 12. The mice were allowed to acclimate to the facility for one week with *ad libitum* access to the standard rodent chow and tap water. After this time, animals were divided into two, weight-matched groups: Chow and

Western Diet (WD). The Chow group was given *ad libitum* access to the standard rodent diet (24.5% kcal/g protein, 13.1% kcal/g fat, 62.3% kcal/g carbohydrate; PicoLab Rodent Diet 20 #5053, LabDiet, St. Louis, MO) and tap water. The WD group was given *ad libitum* access to a 40% fat diet based on AIN-93G (16% kcal/g protein, 40% kcal/g fat, 44% kcal/g carbohydrate; Western Diet for Rodents #5TJN, TestDiet, St. Louis, MO). The WD group was also given *ad libitum* access to a 42 g/L 55% fructose/ 45% sucrose solution prepared by dissolving 231 g fructose and 189 g of sucrose in 1 L of Milli-Q purified water (MilliporeSigma, Burlington, MA). The animals were maintained on their respective diets for 16 weeks.

One cohort of animals was euthanized every four hours for 24 hours starting at ZT 1 to assess the effect of diet on diurnal rhythmicity. Two separate cohorts of animals were used to perform behavioral tasks. One of the behavioral cohorts performed tasks during the inactive phase (ZT 3), while the other performed tasks during the active phase (ZT 15). Animal numbers for each cohort may be found in the figure legends.

5.3.2 End-point Procedures

At the end of sixteen weeks, the animals were euthanized *via* CO_2 asphyxiation followed by decapitation. Animals were sacrificed every four hours for 24 hours starting at ZT 1 and were not fasted to preserve diurnal rhythmicity. After decapitation, the brains were quickly removed and weighed prior to dissection of right and left hippocampi and cerebral cortices as well as the hypothalamus. Trunk blood was used to obtain a final blood glucose measurement and was then collected and centrifuged at 12,000 rpm to draw off serum, which was frozen at -80º C until further analysis. Livers, eWAT, WAT

rWAT and iWAT were excised on ice and weighed. eWAT and rWAT weights were summed to calculate visceral adipose tissue mass and iWAT was used as a measure for SubQ fat mass. All tissues were flash frozen in liquid N_2 and stored in -80º C for further analysis.

5.3.3 Metabolic Phenotyping

Promethion metabolic cages (Sable Systems, Las Vegas, NV) were utilized for metabolic screening and phenotyping as previously described (Luo et al., 2016; Woodie et al., 2018). Mice were transferred from their home cages and singly housed in the metabolic cages during the sixteenth experimental week prior to sacrifice. Activity was measured by Promethion XYZ Beambreak Activity Monitors calibrated to each cage. The body mass monitors were plastic tubes that also functioned as in-cage enrichment and nesting devices.

A promethion GA-3 gas analyzer measured water vapor, CO_2 and O_2 in mL/min to provide detailed respirometry data. EE was calculated in kcal by using the Weir equation: $60*(0.003941*VO_2(n) + 0.00106VCO_2(n))$. RER was determined by the ratio of CO_2 produced to the volume of O_2 consumed ($RER = VCO_2/VO_2$) where a RER of ~ 0.7 indicated lipid utilization and a RER of ~ 1.0 indicated carbohydrate utilization. Metabolic phenotyping data was analyzed using ExpeData software with the Universal Macro Collection (Sable Systems, Las Vegas, NV).

5.3.4 Glucose and Insulin Tolerance Tests

After thirteen weeks on the diets, both groups were fasted with tap water for fifteen hours (ZT 12-3) for a GTT. During the fast, the WD group had their sugar water removed and replaced with tap water. The GTT was performed as previous described beginning at ZT 3 (Woodie et al., 2018). Briefly, the dorsal vein of the tail was superficially nicked 1.5 cm near the distal end with a sterile razor. Approximately 5 mL of blood was collected on a Contour One blood glucose meter strip to obtain a baseline blood glucose measure for each mouse. A sterile 25% glucose solution (2 g glucose/ kg body weight) was injected intraperitoneally (i.p.) in each animal. Blood was collected from the tail nick at 15, 30, 60 and 120 min after injection. The AUC was obtained by calculating the Reimann sum for each group.

One week after the GTT, animals were fasted with tap water for six hours (ZT 3-ZT 9) before performing an ITT. Beginning at ZT 9, blood was sampled from a nick in the dorsal tail vein to obtain a baseline glucose measurement as described for the GTT. Then an i.p. injection of Humulin R (Eli Lilly, Indianapolis, IN) was administered at a dose of 0.9U insulin/kg body weight and blood glucose was tested at 15, 30, 60 and 90 min after injection.

Procedure start times and fasting durations and for the GTT and ITT were chosen based on guidelines from the Mouse Metabolic Phenotying Center (Ayala et al., 2010).

5.3.5 Behavioral Assessments

Starting after 12 weeks of dietary exposure, the animals ran a series of behavioral tasks at one-week intervals to assess hippocampal function. In order to minimize stress and extraneous novelty, the inactive phase testing conditions were similar to that of the

normal housing conditions standard to the Auburn University VRB. Therefore, the cohort of animals performing the tasks during the inactive phase (ZT 3) were run under white, fluorescent light. The cohort of animals performing the tasks during the active phase (ZT 15) ran the tests under dim, red light. Both cohorts ran the same tasks in the same order with tasks increasing in complexity.

The first task was the Y-Maze task. The maze consisted of three arms made of opaque, corrugated plastic at 120º angles from each other with each arm measuring approximately 30 cm long and 10 cm wide. Twenty cm high walls lined the entire apparatus (Figure 28A). The arms were randomly labeled as Arm A, B and C and visual cues unique to each arm were affixed to the back wall of the arms. The maze was situated directly under light so that no shadows were formed in the maze. All sessions were recorded using an overhead camera. Each animal went through training and probe sessions. During the training session, one of the arms was closed off with an opaque divider (Novel Arm) so that animals can only explore the arm they started in (Start Arm) and the other open arm (Familiar Arm). The mouse was released into the Start Arm and allowed to explore the Start and Familiar Arm for 15 min. After which, they were removed from the maze and returned to their home cage for 3 hours. Finally, they were returned to the maze with the Novel Arm open and allowed to explore for 5 min. Upon completion of the test period, animals were returned to their home cages. The maze was thoroughly cleaned with 70% EtOH before the start of all sessions and between each animal. First choice, time in Novel Arm and entries into Novel Arm were scored from the recorded probe sessions. A recognition index was calculated by (time in Novel Arm/ total time in maze) * 100. The identity of the Start, Familiar and Novel Arms were randomized

for each animal, but remained constant within each animal for the training and probe sessions. All videos were scored by two individuals who were blind to dietary treatments.

The final task was the novel object recognition (NOR) task. The apparatus was a 40 cm x 40 cm x 40 cm box made of clear Plexiglass. Visual cues unique to each wall were affixed to the inside of the box. The Familiar Object was a 50 mL conical tube, filled with 30 mL of water and affixed by its lid to the bottom of the box with duct tape. The Novel Object consisted of a 5 cm diameter bottle lid affixed with duct tape to the top of a 10 cm diameter bottle lid. Objects were place approximately 5 cm from one of the four walls (Figure 28B). Which wall the objects were placed by and the orientation of the Novel and Familiar Object (to the left or the right of the mouse starting position) were randomized for each animal to control for side preference. The box was situated directly under light so that no shadows were formed. All sessions were recorded using an overhead camera. Each animal went through habituation, training and probe sessions. During the habituation session, the animal was placed in the center of the box facing two Familiar Objects. Animals were allowed to explore the box and the objects for ten minutes. They were then returned to their home cage for 24 hours. The following day, the animals performed the training session. Once again, the animals were placed in the center of the box facing two Familiar Objects. They were allowed to explore the box and the objects for 5 min. After this time, they were returned to their home cage for 1 hour. Then they performed the probe session where one of the Familiar Objects was replaced with the Novel Object. The animals were placed in the center of the box facing the objects and were allowed to explore the box and the objects for 5 min. The box and objects were thoroughly cleaned with 70% EtOH before the start of all sessions and between each

animal. A recognition index was calculated from (time spent exploring Novel Object / total time spent exploring objects) * 100. All videos were scored by two individuals who were blind to dietary treatments.

5.3.6 RNA Extraction and RT-qPCR

RNA was extracted from frozen liver samples using TRIzol following the manufacturer's instructions. RNA was extracted from frozen hippocampus samples using a RNeasy Plus Mini Kit and from frozen hypothalamus samples using a RNeasy Plus Micro Kit both following the manufacturer's instructions. RNA concentration and quality for each sample was determined on a ThermoScientific NanoDrop One^{C} immediately after extraction. cDNA from each tissue was synthesized using the SuperScript IV reverse-transcription system following the manufacturer's instructions. Gene expression was analyzed by qPCR and normalized to tissue specific housekeeping genes (Liver: *Gapdh* and A*ctb*, brain: *Actb* and *Sdha*) and the level of the gene of interest in the Chow samples.

5.3.7 Serum Insulin, Corticosterone, CRP and IL-6 Determination

Serum insulin levels were determined by an insulin ELISA assay. Insulin resistance was assessed by HOMA-IR score (HOMA-IR = (26 * serum insulin (ng/mL) * blood glucose (mg/dL))/405). Serum corticosterone, CRP and IL-6 levels were determined using ELISA assays specific to each protein.

5.3.8 Quantification and Statistical Analysis

Running body weight, GTT, ITT, 24-hour EE, 24-hour RER and 24-hour activity were analyzed using a two-way repeated measures ANOVA with Tukey's post-hoc test. Group differences in diurnal RT-qPCR and serum measures as well as behavioral tests were assessed using two-way ANOVA with a Tukey's post-hoc test. All data are presented as mean ± SEM with a p value ≤ 0.05 considered statistically significant. Statistical parameters (n, mean and SEM) can be found in the figure legends. Statistical tests were run using SPSS Statistics and R. The rhythmicity, amplitude and acrophase for each gene and serum measure were analyzed using the R packages JTK_CYCLE and psych.

5.4 Results and Discussion

5.4.1 WD Consumption Results in an Obese Phenotype and Disrupts Peripheral Rhythmicity

In order to determine the impact of the WD on hippocampal diurnal rhythmicity, we first needed to confirm that WD feeding induced an obese phenotype with markers of metabolic disease and diurnal disruptions in our model. To do so, we followed a 16-week feeding paradigm with behavioral and metabolic tasks occurring from week 12-16 (Figure 23A). WD mice gained significantly more weight than their Chow-fed counterparts beginning at week 2 and continuing to the end of the study (Figure 23B). Results from the GTT and ITT indicated impaired glucose metabolism in the WD group at 13 and 14 weeks of feeding (Figure 23C-D). This phenotype progressed in severity through dietary exposure as the WD group exhibited hyperglycemia, severe hyperinsulinemia and significant insulin resistance at the time of sacrifice (Figure 23E-I). WD feeding also resulted in disrupted metabolic rhythmicity with elevated EE during the inactive phase (Figure 24A), reduced metabolic flexibility as measured by RER (Figure

24B) and decreased activity during the active phase (Figure 24C). Moreover, we observed significant changes in the rhythms of inflammatory markers in our WD-fed animals. Serum corticosterone levels were phase advanced and increased at ZT 1 in the WD group (Figure 23J). The acrophase for both inflammatory markers CRP and IL-6 were phase advanced to the light cycle, despite the lack of significant difference in absolute levels (Figure 23K-L).

At sacrifice, the WD group had significantly heavier livers and SubQ and visceral fat pads (Figure 23M-O). Interestingly, the WD group had significantly reduced brain weight compared to Chow (Figure 23P). Similar to previous works, our WD-fed group had significantly dampened hepatic rhythms of *Bmal1* (Figure 25A *left panel*) and *Nr1d1* (*Reverba*) (Figure 26A *left panel*) (Eckel-Mahan et al., 2013; Hatori et al., 2012; Kohsaka et al., 2007). The WD group also exhibited advanced acrophase for *Bmal1* and *Reverba* (Figure 25E, Figure 26A *left panel).* Although absolute expression hepatic *Clock, Per2* and *Cry1*was not affected by our diet (Figure 25B-C *left panel*), *Cry1* acrophase was advanced in the WD group (Fig 25E). Therefore, we were able to conclude that our 16-week WD feeding paradigm produced a mouse model with metabolic and rhythmic disruptions similar to those previously published (Eckel-Mahan et al., 2013; Hatori et al., 2012; Kohsaka et al., 2007).

5.4.2 WD-induced Obesity Disrupts the Diurnal Rhythmicity of Core Clock Genes in the Hippocampus

Having established WD-induced obesity and disruptions in peripheral rhythmicity, we next sought to examine the diurnal expression of core clock genes in central structures.

First, we found that hypothalamic expression of three out of the four measured core clock genes was unaffected by the WD (Figure 25A-C *middle panel*). The WD also did not alter acrophase for any of the measured core clock genes (Fig. 2F). The hypothalamic SCN is resistant to diet-induced rhythm disruptions, which supports our findings in *Bmal1*, *Npas2* and *Per2* expression (Hara et al., 2001; Kohsaka et al., 2007). *Cry1* expression, however, was significantly amplified at all measured time points in the WD-fed group (Figure 25D *middle panel*). This may be due to the fact that we collected the whole hypothalamus instead of specifically isolating the SCN. Therefore, areas of the hypothalamus that are involved in feeding and satiety (e.g. lateral hypothalamus and arcuate nucleus) may have been altered by the WD. Given our results, the specific role of hypothalamic *Cry1* in the context of diet-induced obesity warrants future study.

In contrast to the hypothalamus, the diurnal expression patterns of all measured core clock genes were significantly disrupted in the hippocampi of WD mice. *Bmal1, Npas2*, *Per2* and *Reverba* were amplified at select timepoints (Figure 25A-C *right panel* and Figure 26A *right panel*) while diurnal *Cry1* expression was dampened compared to Chow (Figure 25D *right panel*). In addition to amplification in the dark phase, *Bmal1* acrophase was delayed in the WD group (Fig. 25G), which may have influenced the stark induction of gene expression for the transcription factor, D-box binding protein (*Dbp*) (Figure 26B). *Dbp* is within the BMAL1:CLOCK/NPAS2 cistrome and DBP moderates the expression of clock-controlled genes (Takahashi, 2017).

Of additional interest is the observation that the core clock co-activator, *Npas2,* was not rhythmically expressed under Chow-fed conditions, but gained rhythmicity in the WD group (Figure 25B *right panel*). The core clock repressors, *Per2* and *Cry1*, on the

other hand, maintained similar expression patterns between Chow and WD, but were elevated and decreased, respectively, in absolute expression (Figure 25C-D *right panel*).

5.4.3 Diurnal Rhythmicity of Genes Associated with Synaptic Plasticity and AD are Disrupted in WD-fed Mice

Circadian disruptions have been recognized to not only influence the development of AD-like memory deficits, but to also be a key symptom of dementias such as AD (Karatsoreos, 2014; Musiek, 2015; Musiek et al., 2015). Additionally, several AD-risk genes have been identified as hippocampal clock-controlled genes that may be regulated at the level of expression by peripheral inputs (Ma et al., 2016). Given the observation that the WD group had smaller brains and the degree to which the WD disrupted hippocampal core clock gene expression in our model, we hypothesized that the hippocampal expression of AD-risk genes would also be disrupted in the WD-fed animals. Thus, we examined the diurnal expression of four genes associated with AD: *Apoe, Casp3* and *Gsk3a* and *Gsk3b*. All four markers exhibited significant WD-induced changes in both their absolute expression levels and temporal expression patterns (Figure 27A-D). All of our tested genes were overexpressed at ZT 9, while *Apoe* and *Gsk3b* exhibited additional overexpression at ZT 17. Furthermore, in the WD group, all four genes exhibited a phase advance in acrophase when compared to Chow (Figure 27E).

What is more, it has been established that the hippocampus functions as a circadian oscillator with time-of-day-dependent changes occurring at the levels of behavior, synaptic plasticity and protein phosphorylation (Chaudhury and Colwell, 2002; Chaudhury et al., 2005; Eckel-Mahan et al., 2008). The hippocampus is also known to be

particularly sensitive to WD-induced damage. Importantly, WD-induced changes in peripheral inflammation and insulin sensitivity have central implications that negatively impact hippocampal structure and function (Hsu and Kanoski, 2014; Kanoski and Davidson, 2011; Woodie et al., 2019). As demonstrated in Figure 23, the WD group exhibited insulin resistance and disrupted rhythmicity in inflammatory markers. These observations in conjunction with the core clock disruptions observed in Figure 25, led us to test whether diurnal expression of genetic markers for hippocampal structure and function were also disrupted by the WD. We first examined the expression of two established markers of synaptic activity, *Arc* and *c-fos*. Both immediate-early genes exhibited time points of elevated expression in the WD group, with *c-fos* displaying overt overexpression at ZT 1 (Figure 27F-G). *Bdnf* and *Dlg4* (PSD95), which are markers of synapse formation and maintenance, were also overexpressed at ZT 9 and ZT 17 (Figure 27H-I). Acrophase for every gene, with the exception of *Arc*, was shifted in the WD group (Figure 27J).

Expression of these markers is traditionally associated the beneficial activation of synaptic activity, plasticity and memory formation (El-Husseini et al., 2000; Guzowski et al., 2001; Vicario-Abejón et al., 2002). However, chronic overexpression can cause neuronal hyperactivity and detrimental excitotoxic events (Cunha et al., 2009; Sommer et al., 2017; Walker and Carlock, 1993). Whether excitotoxicity is occurring in the hippocampi of the WD group requires further work. However, the data herein are supportive of this hypothesis. Of particular interest is our observation that *Dbp* was highly overexpressed in the WD hippocampus. DBP is well known as a modulator of clock-controlled gene expression. However, DBP overexpression can also impair

hippocampal function: in a model of hippocampus-specific DBP overexpression, animals exhibited impaired spatial learning abilities and extreme sensitivity to kainite-induced seizures (Klugmann et al., 2006). These observations were paralleled by chronic activation of the MAPK pathway, which is a key signaling cascade activated during excitatory glutamate neurotransmission (Eckel-Mahan, 2012; Klugmann et al., 2006). What is more, we observed decreased brain weight in the WD group concurrent with overexpression of *Apoe*, which has been shown to be elevated after excitotoxic injury, and overexpression of *Casp3*, which is involved in excitotoxic apoptosis (Brecht et al., 2001; Liao et al., 2017; Tzeng et al., 2013).

5.4.4 WD-Induced Disruptions in the Hippocampal Clock are Associated with Time- and Task-Dependent Cognitive Deficits

Finally, we examined whether the WD-induced changes in diurnal gene expression translated into *in vivo* memory deficits. The hippocampus is heavily involved in the episodic memory processes required for spatial, navigational and object memory tasks (Eichenbaum, 2017; Lisman et al., 2017). Thus, we utilized two passive tasks to avoid the development of stress or fear in our animals, particularly while testing during the inactive phase. The Y Maze was used to assess the spatial and navigational memory capacity of our animals (Figure 28A), while a NOR task was used to assess object memory (Figure 28B). Two cohorts of animals, separate from those used for diurnal tissue collection, were used to assess hippocampal memory. One cohort performed the tasks during the inactive phase starting at ZT 3 and the second cohort performed the tasks during the active phase starting at ZT 15. Memory for the tasks was assessed by a recognition index,

which measures how well an animal can remember familiar spaces and objects (by spending less time exploring them) while recognizing a novel space or a novel object (by spending more time exploring them). The WD significantly impaired performance in the Y Maze during both the inactive and active phases (Figure 28C). Object recognition, on the other hand, was significantly impaired by the WD but only during the active phase (Figure 28D). The difference between our Y Maze and NOR results highlights the intricacies of different types of memory. Indeed, in fear-conditioning tasks, which may be modified to test hippocampal and/or amygdala function, performance is improved during the inactive phase (Chaudhury and Colwell, 2002; Maren et al., 2013). Perhaps this is due to the fact that the light/inactive phase is a hypervigilant, fearful time for nocturnal animals e.g. mice and rats. This could potentially explain the NOR results: mice may be more vigilance of their environment and the items in it and thereby more interested in a novel object during the daytime. Novel spaces may not warrant the same level of consideration. Nevertheless, the behavioral deficits observed at both time points in the Y Maze and during the active phase in the NOR, parallel the significant disruption in diurnal gene expression that we observed in the WD group.

Overall, we provide the first set of data indicating WD-induced diurnal disruptions in hippocampal gene expression. Our findings also highlight that AD-risk and synapse-associated genes become disrupted and amplified in the hippocampus after WD feeding and that these disruptions correspond with deficits in behavioral markers of hippocampal function. Although causational conclusions will require further study, we can draw meaningful associations on the impact of WD-induced obesity and diurnal disruptions on hippocampal rhythmicity and function.

5.4.5 Study Limitations

We collected our diurnal samples at 4-hour intervals over 24 hours. Although 4-hour sampling provided us with compelling evidence for WD-induced hippocampal diurnal disruptions, sampling at 2-hour intervals may provide better resolution in the future. Furthermore, we collected and tested gene expression in the whole hypothalamus. Our data suggests that diurnal *Bmal1*, *Npas2* and *Per2* expression was not altered by the WD in the whole hypothalamus. This fits with previous research on the SCN; these areas remain entrained to light:dark cycles and are resistant to diet-induced changes in rhythmicity. However, our *Cry1* results suggest that there are nuclei within the hypothalamus that are sensitive to WD-induced disruptions. Further studies are needed to examine the dysregulation of expression and function of *Cry1* in hypothalamic nuclei. Finally, the C57Bl/6 mouse model that we used is melatonin-deficient. Rhythmic melatonin is a crucial component of the circadian clock and feeds back upon the SCN to maintain light:dark entrainment. We used the C57Bl/6 mouse to be consistent with the extensive number of previous studies on WD-induced obesity as well as other circadian and diurnal rhythm works. However, subsequent work should be in confirmed in melatonin-proficient models.

Figures and Figure Legends

Figure 23

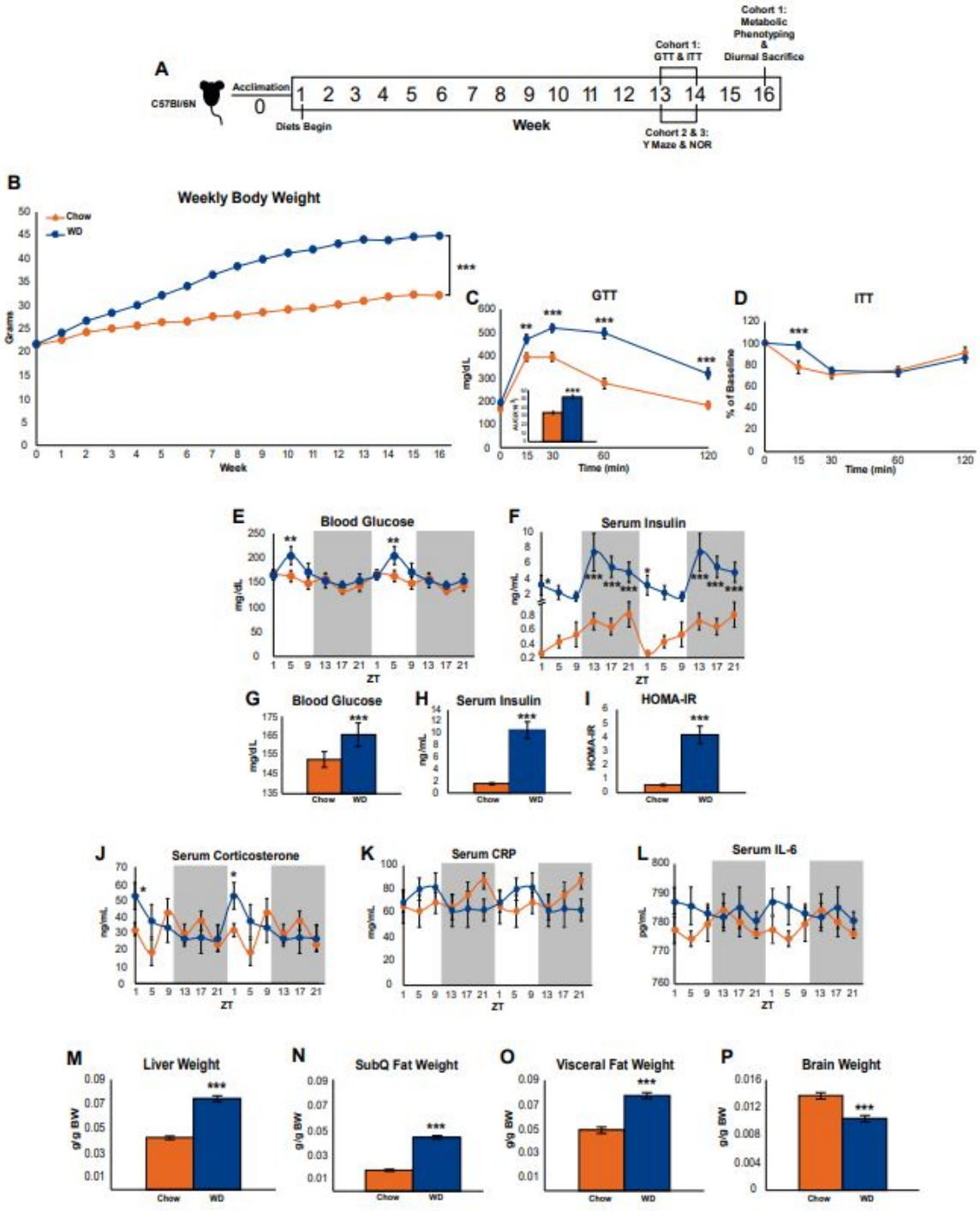

Figure 23. WD-Induced Obesity Pathophysiology and Peripheral Rhythm Disruption

(A) 16-week experimental timeline.

(B) Weekly body weight measurements for Chow and WD groups (n = 41 – 43).

(C – D) GTT (C) and ITT (D) performed after 13 – 14 weeks on experimental diets (n = 20 – 23). (C inset) GTT area under the curve.

(E – F) Diurnal pattern of non-fasted blood glucose (E) and serum insulin (F) from samples collected every 4 hours for 24 hours (n = 3 – 7 per group per time point). Data are double-plotted for visualization.

(G – I) Non-fasted blood glucose (G) serum insulin (H) and HOMA-IR (I) for each group averaged over all collected time points (n = 41 – 43).

(J – L) Diurnal pattern of corticosterone (J) and the inflammatory markers, CRP (K) and IL-6 (L) in serum samples collected from Chow- and WD-fed animals every 4 hours for 24 hours (n = 3 – 7 per group per time point). Data are double-plotted for visualization.

(M – P) Normalized liver weight (M), normalized SubQ fat weight (N), normalized visceral fat (O) and normalized brain (P) weight after 16 weeks of dietary exposure averaged for each group across all collected time points (n = 41 – 43).

Data are presented as mean ± SEM. *$p<0.05$, **$p<0.01$, ***$p<0.001$

Figure 24

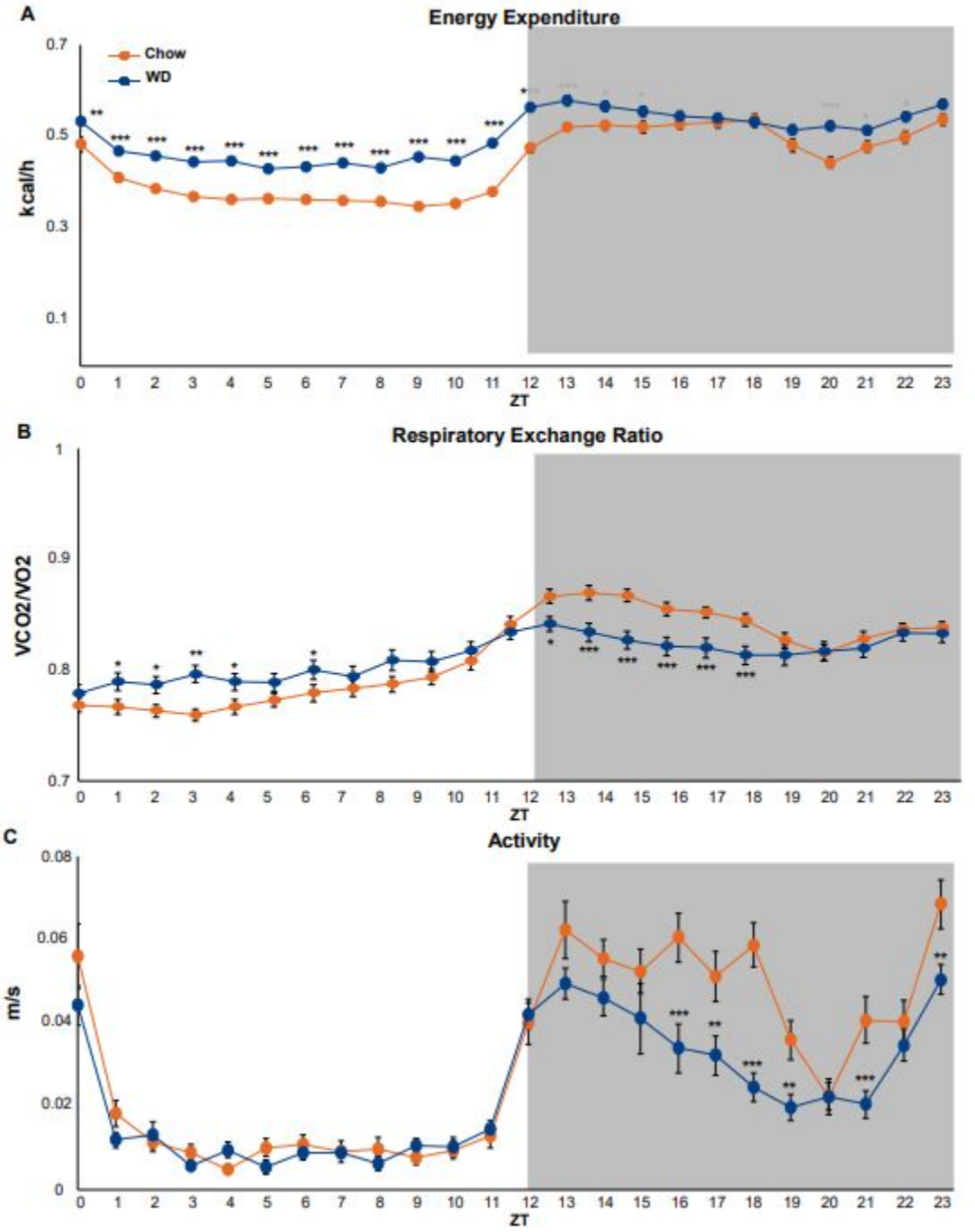

Figure 24. Metabolic Phenotype

(A) EEmeasured every hour over 24 hours during the 16th week of dietary exposure.

(B) Macronutrient utilization as measured by RER collected every hour over 24 hours during the 16th week of dietary exposure.

(C) Activity measured every our over 24 hours during the 16th week of dietary exposure. n = 41 – 43. Data are presented as mean ± SEM. *p<0.05, **p<0.01, ***p<0.001

Figure 25

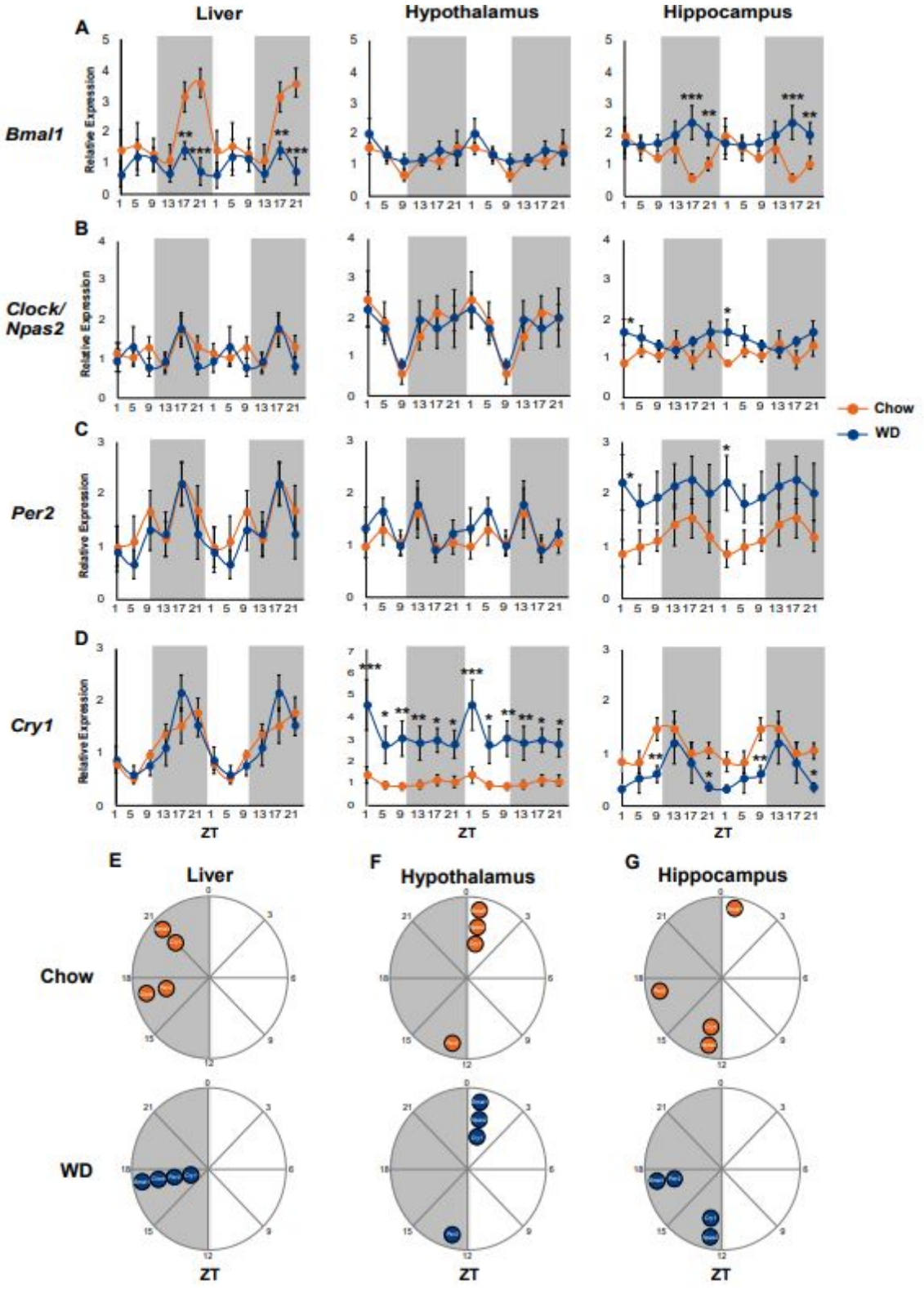
Liver
Hypothalamus
Hippocampus
A
Bmal1
B
Clock/
Npas2
C
Per2
D
Cry1
Relative Expression
ZT
Chow
WD
E
F
G
Liver
Hypothalamus
Hippocampus
Chow
WD
ZT

Figure 25. The Effect of WD-Induced Obesity on Core Clock Gene Expression in the Liver, Hypothalamus and Hippocampus

(A) Diurnal expression of *Bmal1* in the liver (*left panel*), hypothalamus (*middle panel*) and hippocampus (*right panel*) collected after 16 weeks on diets from Chow- and WD-fed animals every 4 hours for 24 hours (n = 3 – 7 per group per time point).

(B) Diurnal expression of *Clock* in the liver (*left panel*) and *Npas2* in the hypothalamus (*middle panel*) and hippocampus (*right panel*) collected after 16 weeks on diets from Chow- and WD-fed animals every 4 hours for 24 hours (n = 3 – 7 per group per time point).

(C) Diurnal expression of *Per2* in the liver (*left panel*), hypothalamus (*middle panel*) and hippocampus (*right panel*) collected after 16 weeks on diets from Chow- and WD-fed animals every 4 hours for 24 hours (n = 3 – 7 per group per time point).

(D) Diurnal expression of *Cry1* in the liver (*left panel*), hypothalamus (*middle panel*) and hippocampus (*right panel*) collected after 16 weeks on diets from Chow- and WD-fed animals every 4 hours for 24 hours (n = 3 – 7 per group per time point).

(E – G) Schematic representation of acrophase for *Bmal1*, *Clock/Npas2, Per2* and *Cry 1* in the liver (E), hypothalamus (F) and hippocampus (G) of Chow- (*top row*) and WD- (*bottom row*) fed mice.

(A – D) Data are double-plotted for visualization. Data are presented as mean ± SEM. *p<0.05, **p<0.01, ***p<0.001

Figure 26

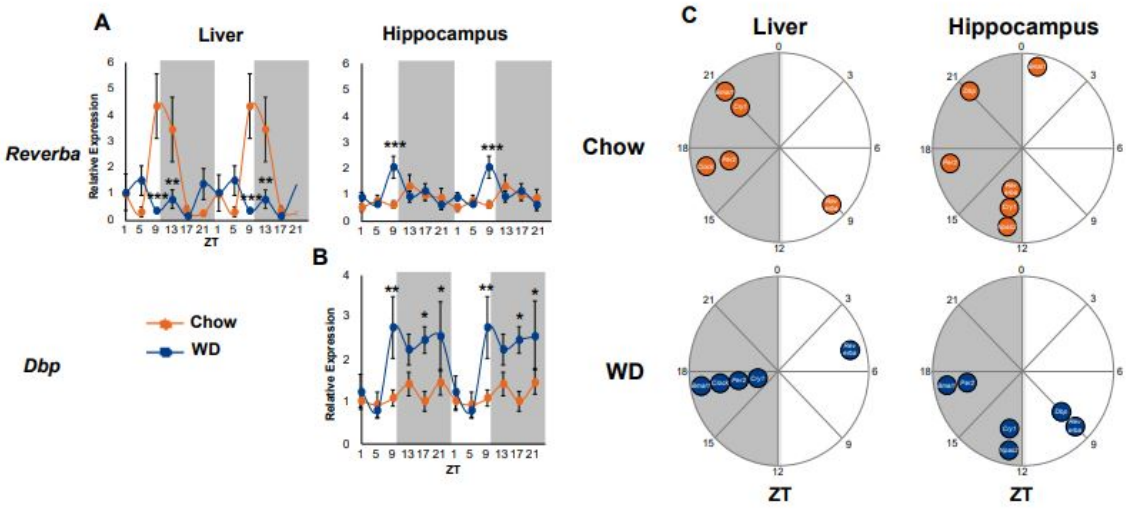

Figure 26. Diurnal Expression of *Reverba* and *Dbp*

(A) Diurnal expression of *Reverba* in the liver (*left panel*) and hippocampus (*right panel*) collected after 16 weeks on diets from Chow- and WD-fed animals every 4 hours for 24 hours (n = 3 – 7 per group per time point).

(B) Diurnal expression of *Dbp* in the hippocampus collected after 16 weeks on diets from Chow- and WD-fed animals every 4 hours for 24 hours (n = 3 – 7 per group per time point).

(C) Schematic representation of acrophase for *Reverba* and *Dbp* in the liver (*left panel*), and hippocampus (*right panel*) of Chow- (*top row*) and WD- (*bottom row*) fed mice. Time of core clock gene acrophase is included for reference.

(A – B) Data are double-plotted for visualization. Data are presented as mean ± SEM. *p<0.05, **p<0.01, ***p<0.001

Figure 27

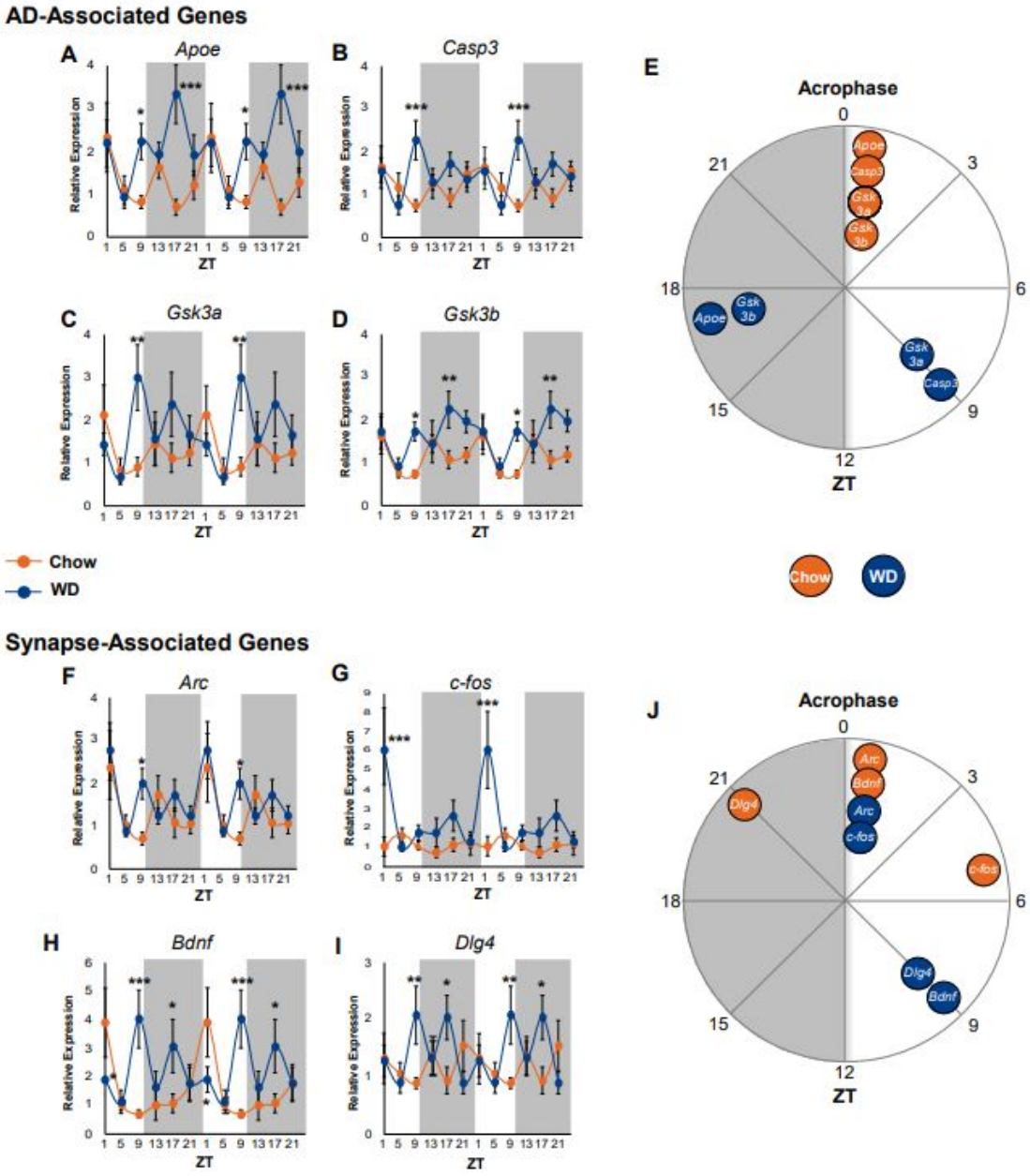

Figure 27. The WD Alters Diurnal Expression Patterns of Genes Associated with AD Risk and Synapse Function

(A – D) Diurnal expression of the AD-associated genes *Apoe* (F), *Casp3* (G), *Gsk3a* (H) and *Gsk3b* (I) in the hippocampus collected every 4 hours for 24 hours after 16 weeks of Chow or WD feeding (n = 3 – 7 per group per time point).

(E) Schematic representation of acrophase for *Apoe, Casp3, Gsk3a* and *Gsk3b* in the hippocampus of Chow- (orange circles) and WD- (blue circles) fed mice.

(F – I) Diurnal expression of the synapse-associated genes *Arc* (A), *c-fos* (B), *Bdnf* (C) and *Dlg4* (D) in the hippocampus collected every 4 hours for 24 hours after 16 weeks of Chow or WD feeding (n = 3 – 7 per group per time point).

(J) Schematic representation of acrophase for *Arc, c-fos, Bdnf* and *Dlg4* in the hippocampus of Chow- (orange circles) and WD- (blue circles) fed mice.

(A – D & F – I) Data are double-plotted for visualization. Data are presented as mean ± SEM. *p<0.05, **p<0.01, ***p<0.001

Figure 28

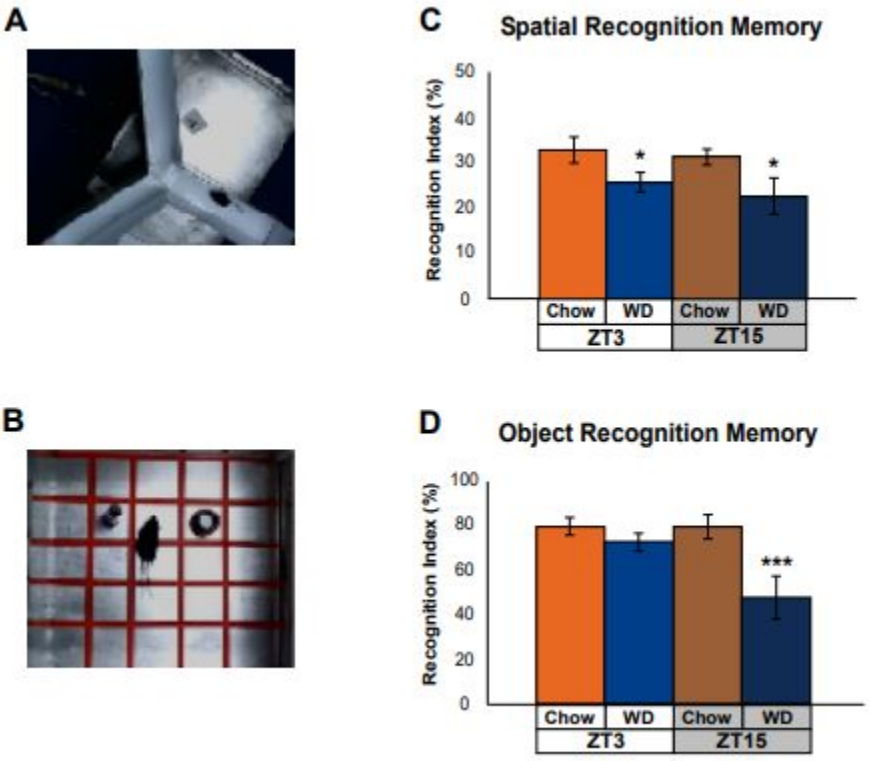

Figure 28. WD Feeding Attenuates Memory in a Time- and Task-Dependent Manner

(A) Image of Y Maze apparatus.

(B) Image of NOR apparatus including the familiar (conical tube) and novel object (bottle caps).

(C) Spatial recognition memory measured by time in novel arm/total time in maze*100 during the inactive (ZT3) and active (ZT15) phase (n = 5 – 10).

(D) Object recognition memory measured by time exploring novel object/total time exploring objects*100 during the inactive (ZT3) and active (ZT15) phase (n = 5 – 10).

Data are presented as mean ± SEM. *p<0.05, **p<0.01, ***p<0.001

Chapter 6: Summary and Conclusion

The works presented herein provide unequivocal evidence for the detrimental impacts of WD consumption on murine metabolic health. In the first study, TRF was examined as a possible method for rescuing WD-induced obesity and metabolic disruption. Under our experimental design, TRF did not ameliorate WD-induced body weight gain, but markers of NAFLD were improved in the WD animals on a TRF schedule. TRF also improved insulin sensitivity and glucose tolerance and restored rhythmicity in whole body metabolism of WD-fed mice. Furthermore, time-restricted liquid sugar consumption was determined to have significant effects on physiology and metabolism, independent of solid calorie consumption. By the end of the study, the group with free, 24 hour access to sugar water had elevated body and adipose tissue weights compared to the other groups and increased hepatic steatosis compared to the control. This group also consumed more calories from ZT 6-11, indicating that this may be a critical window of time in the promotion of weight gain from liquid sugar consumption. Interestingly, the group only allowed early active access to sugar water had greater metabolic flexibility and utilized lipids when carbohydrates from liquid sugar were not available. Additionally, the early access group was more insulin tolerant than even the control group that received tap water. In the final study, the hippocampus was identified as a centrally-located peripheral diurnal oscillator that may be significantly disrupted by WD-induced obesity. Our results indicate that WD feeding significantly alters the rhythmicity of core clock mRNA expression in the hippocampus. What is more, these alterations are paralleled by disruptions in the rhythmic expression of markers for AD risk and synaptic integrity.

Overall, the research outlined herein highlights chronobiologic disturbances as a common factor underpinning WD-induced disruptions in physiology, metabolism and behavior. Peripheral metabolism and tissues may be, in part, rescued by time-restricting WD access or by providing specific macronutrients during certain times of the active phase. Whether the hippocampus may be rescued by TRF or macronutrient timing, remains to be determined. Future work should delve into this possibility, particularly in reference to nutrient timing as a therapeutic intervention for AD-like dementias.

References

Acheson, K.J., Schutz, Y., Bessard, T., Anantharaman, K., Flatt, J.P., and Jéquier, E. (1988). Glycogen storage capacity and de novo lipogenesis during massive carbohydrate overfeeding in man. Am. J. Clin. Nutr. *48*, 240–247.

Adams, K.F., Schatzkin, A., Harris, T.B., Kipnis, V., Mouw, T., Ballard-Barbash, R., Hollenbeck, A., and Leitzmann, M.F. (2006). Overweight, Obesity, and Mortality in a Large Prospective Cohort of Persons 50 to 71 Years Old. N. Engl. J. Med. *355*, 763–778.

Agil, A., Rosado, I., Ruiz, R., Figueroa, A., Zen, N., and Fernández-Vázquez, G. (2012). Melatonin improves glucose homeostasis in young Zucker diabetic fatty rats. J. Pineal Res. *52*, 203–210.

Akira, S., and Takeda, K. (2004). Toll-like receptor signalling. Nat. Rev. Immunol. *4*, 499–511.

Akiyama, M., Kouzu, Y., Takahashi, S., Wakamatsu, H., Moriya, T., Maetani, M., Watanabe, S., Tei, H., Sakaki, Y., and Shibata, S. (1999). Inhibition of light- or glutamate-induced mPer1 expression represses the phase shifts into the mouse circadian locomotor and suprachiasmatic firing rhythms. J. Neurosci. *19*, 1115–1121.

Aksoy-Aksel, A., and Manahan-Vaughan, D. (2015). Synaptic strength at the temporoammonic input to the hippocampal CA1 region in vivo is regulated by NMDA receptors, metabotropic glutamate receptors and voltage-gated calcium channels. Neuroscience *309*, 191–199.

Albrecht, U., Zheng, B., Larkin, D., Sun, Z.S., and Lee, C.C. (2001). *mPer1* and *mPer2* Are Essential for Normal Resetting of the Circadian Clock. J. Biol. Rhythms *16*, 100–104.

Alhola, P., and Polo-Kantola, P. (2007). Sleep deprivation: Impact on cognitive performance. Neuropsychiatr. Dis. Treat. *3*, 553–567.

Almeida-Suhett, C.P., Graham, A., Chen, Y., and Deuster, P. (2017). Behavioral changes in male mice fed a high-fat diet are associated with IL-1β expression in specific brain regions. Physiol. Behav. *169*, 130–140.

Almiron-Roig, E., Palla, L., Guest, K., Ricchiuti, C., Vint, N., Jebb, S.A., and Drewnowski, A. (2013). Factors that determine energy compensation: a systematic review of preload studies. Nutr. Rev. *71*, 458–473.

Almoosawi, S., Prynne, C.J., Hardy, R., and Stephen, A.M. (2013). Time-of-day and nutrient composition of eating occasions: prospective association with the metabolic syndrome in the 1946 British birth cohort. Int. J. Obes. *37*, 725–731.

American Council on Exercise (2018). BMI Calculator with Average BMI Statistics; Tools and Calculators. https://www.acefitness.org/education-and-resources/lifestyle/tools-calculators/bmi-calculator.

American Heart Association (2015). Saturated Fat. https://www.heart.org/en/healthy-living/healthy-eating/eat-smart/fats/saturated-fats.

André, C., Dinel, A.-L., Ferreira, G., Layé, S., and Castanon, N. (2014). Diet-induced obesity progressively alters cognition, anxiety-like behavior and lipopolysaccharide-induced depressive-like behavior: Focus on brain indoleamine 2,3-dioxygenase activation. Brain. Behav. Immun. *41*, 10–21.

Angulo, P. (2006). NAFLD, obesity, and bariatric surgery. Gastroenterology *130*, 1848–1852.

Aponte, Y., Atasoy, D., and Sternson, S.M. (2011). AGRP neurons are sufficient to orchestrate feeding behavior rapidly and without training. Nat. Neurosci. *14*, 351–355.

Arendt, J. (2019). Melatonin: Countering Chaotic Time Cues. Front. Endocrinol. *10*, 391.

Arnold, S.E., Lucki, I., Brookshire, B.R., Carlson, G.C., Browne, C.A., Kazi, H., Bang, S., Choi, B.-R., Chen, Y., McMullen, M.F., et al. (2014). High fat diet produces brain insulin resistance, synaptodendritic abnormalities and altered behavior in mice. Neurobiol. Dis. *67*, 79–87.

Ascherio, A., Hennekens, C.H., Buring, J.E., Master, C., Stampfer, M.J., and Willett, W.C. (1994). Trans-fatty acids intake and risk of myocardial infarction. Circulation *89*, 94–101.

Asher, G., and Sassone-Corsi, P. (2015). Time for Food: The Intimate Interplay between Nutrition, Metabolism, and the Circadian Clock. Cell *161*, 84–92.

Aton, S.J., Colwell, C.S., Harmar, A.J., Waschek, J., and Herzog, E.D. (2005). Vasoactive intestinal polypeptide mediates circadian rhythmicity and synchrony in mammalian clock neurons. Nat. Neurosci. *8*, 476–483.

Avena, N.M., Rada, P., and Hoebel, B.G. (2009). Sugar and fat bingeing have notable differences in addictive-like behavior. J. Nutr. *139*, 623–628.

Ayala, J.E., Samuel, V.T., Morton, G.J., Obici, S., Croniger, C.M., Shulman, G.I., Wasserman, D.H., and McGuinness, O.P. (2010). Standard operating procedures for describing and performing metabolic tests of glucose homeostasis in mice. Dis. Model. Mech. *3*, 525–534.

Ballestri, S., Lonardo, A., Bonapace, S., Byrne, C.D., Loria, P., and Targher, G. (2014).

Risk of cardiovascular, cardiac and arrhythmic complications in patients with non-alcoholic fatty liver disease. World J. Gastroenterol. *20*, 1724.

Barria, A., and Malinow, R. (2005). NMDA Receptor Subunit Composition Controls Synaptic Plasticity by Regulating Binding to CaMKII. Neuron *48*, 289–301.

Bartsch, T., and Wulff, P. (2015). The hippocampus in aging and disease: From plasticity to vulnerability. Neuroscience *309*, 1–16.

Baufeld, C., Osterloh, A., Prokop, S., Miller, K.R., and Heppner, F.L. (2016). High-fat diet-induced brain region-specific phenotypic spectrum of CNS resident microglia. Acta Neuropathol. *132*, 361–375.

Bekinschtein, P., Kent, B.A., Oomen, C.A., Clemenson, G.D., Gage, F.H., Saksida, L.M., and Bussey, T.J. (2014). Brain-derived neurotrophic factor interacts with adult-born immature cells in the dentate gyrus during consolidation of overlapping memories. Hippocampus *24*, 905–911.

Beling, I. (1929). Uber das Zeitgedachtnis der Bienen. Z. Vgl. Physiol. *9*, 259–338.

Bellisari, A. (2008). Evolutionary origins of obesity. Obes. Rev. *9*, 165–180.

van den Berg, R., Mook-Kanamori, D.O., Donga, E., van Dijk, M., van Dijk, J.G., Lammers, G.-J., van Kralingen, K.W., Prehn, C., Romijn, J.A., Willems van Dijk, K., et al. (2016). A single night of sleep curtailment increases plasma acylcarnitines: Novel insights in the relationship between sleep and insulin resistance. Arch. Biochem. Biophys. *589*, 145–151.

Blechman, J., and Levkowitz, G. (2013). Alternative Splicing of the Pituitary Adenylate Cyclase-Activating Polypeptide Receptor PAC1: Mechanisms of Fine Tuning of Brain Activity. Front. Endocrinol. *4*, 55.

Bleich, S.N., Vercammen, K.A., Koma, J.W., and Li, Z. (2018). Trends in Beverage Consumption Among Children and Adults, 2003-2014. Obesity *26*, 432–441.

Blum, K., Thanos, P.K., and Gold, M.S. (2014). Dopamine and glucose, obesity, and reward deficiency syndrome. Front. Psychol. *5*, 919.

Bocarsly, M.E., Powell, E.S., Avena, N.M., and Hoebel, B.G. (2010). High-fructose corn syrup causes characteristics of obesity in rats: increased body weight, body fat and triglyceride levels. Pharmacol. Biochem. Behav. *97*, 101–106.

den Boer, M., Voshol, P.J., Kuipers, F., Havekes, L.M., and Romijn, J.A. (2004). Hepatic Steatosis: A Mediator of the Metabolic Syndrome. Lessons From Animal Models. Arterioscler. Thromb. Vasc. Biol. *24*, 644–649.

Boitard, C., Cavaroc, A., Sauvant, J., Aubert, A.A., Castanon, N., Lay??, S., Ferreira, G., Layé, S., and Ferreira, G. (2014). Impairment of hippocampal-dependent memory induced by juvenile high-fat diet intake is associated with enhanced hippocampal inflammation in rats. Brain. Behav. Immun. *40*, 9–17.

Bouchard-Cannon, P., Mendoza-Viveros, L., Yuen, A., Kærn, M., Cheng, H.-Y.M., Eichele, G., Lee, C.C., Bradley, A., Ge, S., Enikolopov, G., et al. (2013). The Circadian Molecular Clock Regulates Adult Hippocampal Neurogenesis by Controlling the Timing of Cell-Cycle Entry and Exit. Cell Rep. *5*, 961–973.

Bray, G.A. (2009). History of Obesity. In Obesity : science to practice, G. Williams and G. Fruhbeck, ed. (Chichester, UK: John Wiley & Sons), pp. 4-18.

Bray, G.A., Nielsen, S.J., and Popkin, B.M. (2004). Consumption of high-fructose corn syrup in beverages may play a role in the epidemic of obesity. Am. J. Clin. Nutr. *79*, 537–543.

Bray, M.S., Tsai, J.-Y., Villegas-Montoya, C., Boland, B.B., Blasier, Z., Egbejimi, O., Kueht, M., and Young, M.E. (2010). Time-of-day-dependent dietary fat consumption influences multiple cardiometabolic syndrome parameters in mice. Int. J. Obes. *34*, 1589–1598.

Bray, M.S., Ratcliffe, W.F., Grenett, M.H., Brewer, R.A., Gamble, K.L., and Young, M.E. (2013). Quantitative analysis of light-phase restricted feeding reveals metabolic dyssynchrony in mice. Int. J. Obes. *37*, 843–852.

Brecht, S., Gelderblom, M., Srinivasan, A., Mielke, K., Dityateva, G., and Herdegen, T. (2001). Caspase-3 activation and DNA fragmentation in primary hippocampal neurons following glutamate excitotoxicity. Mol. Brain Res. *94*, 25–34.

Brigman, J.L., Wright, T., Talani, G., Prasad-Mulcare, S., Jinde, S., Seabold, G.K., Mathur, P., Davis, M.I., Bock, R., Gustin, R.M., et al. (2010). Loss of GluN2B-Containing NMDA Receptors in CA1 Hippocampus and Cortex Impairs Long-Term Depression, Reduces Dendritic Spine Density, and Disrupts Learning. J. Neurosci. *30*, 4590–4600.

Brydon, L., Harrison, N.A., Walker, C., Steptoe, A., and Critchley, H.D. (2008). Peripheral Inflammation is Associated with Altered Substantia Nigra Activity and Psychomotor Slowing in Humans. Biol. Psychiatry *63*, 1022–1029.

Bugge, A., Feng, D., Everett, L.J., Briggs, E.R., Mullican, S.E., Wang, F., Jager, J., and Lazar, M.A. (2012). Rev-erbα and Rev-erbβ coordinately protect the circadian clock and normal metabolic function. Genes Dev. *26*, 657–667.

Bulik, C.M., and Allison, D.B. (2001). The genetic epidemiology of thinness. Obes. Rev. *2*, 107–115.

Bunger, M.K., Wilsbacher, L.D., Moran, S.M., Clendenin, C., Radcliffe, L.A., Hogenesch, J.B., Simon, M.C., Takahashi, J.S., and Bradfield, C.A. (2000). Mop3 Is an Essential Component of the Master Circadian Pacemaker in Mammals. Cell *103*, 1009–1017.

Burger, K.S., and Stice, E. (2011). Variability in reward responsivity and obesity: evidence from brain imaging studies. Curr. Drug Abuse Rev. *4*, 182–189.

Bursać, B.N., Djordjevic, A.D., Vasiljević, A.D., Milutinović, D.D.V., Veličković, N.A., Nestorović, N.M., and Matić, G.M. (2013). Fructose consumption enhances glucocorticoid action in rat visceral adipose tissue. J. Nutr. Biochem. *24*, 1166–1172.

Buzsáki, G. (1998). Memory consolidation during sleep: a neurophysiological perspective. J. Sleep Res. *1*, 17–23.

Caliceti, C., Calabria, D., Roda, A., and Cicero, A. (2017). Fructose Intake, Serum Uric Acid, and Cardiometabolic Disorders: A Critical Review. Nutrients *9*, 395.

Carlson, O., Martin, B., Stote, K.S., Golden, E., Maudsley, S., Najjar, S.S., Ferrucci, L., Ingram, D.K., Longo, D.L., Rumpler, W. V., et al. (2007). Impact of reduced meal frequency without caloric restriction on glucose regulation in healthy, normal-weight middle-aged men and women. Metabolism *56*, 1729–1734.

Carrera-Bastos, P., Fontes, M., O'Keefe, J.H., Lindeberg, S., and Cordain, L. (2011). The western diet and lifestyle and diseases of civilization. Res. Reports Clin. Cardiol. *2*, 15.

Cartwright, I.J., and Higgins, J.A. (1999). Increased dietary triacylglycerol markedly enhances the ability of isolated rabbit enterocytes to secrete chylomicrons: an effect related to dietary fatty acid composition. J. Lipid Res. *40*, 1858–1866.

Cauller, L.J., Boulos, Z., and Goddard, G. V. (1985). Circadian rhythms in hippocampal responsiveness to perforant path stimulation and their relation to behavioral state. Brain Res. *329*, 117–130.

Cedernaes, J., Lampola, L., Axelsson, E.K., Liethof, L., Hassanzadeh, S., Yeganeh, A., Broman, J.-E., Schiöth, H.B., and Benedict, C. (2016). A single night of partial sleep loss impairs fasting insulin sensitivity but does not affect cephalic phase insulin release in young men. J. Sleep Res. *25*, 5–10.

Centers for Disease Control and Prevention (2018). Type 2 Diabetes. https://www.cdc.gov/diabetes/basics/type2.html.

Chaix, A., and Zarrinpar, A. (2015). The effects of time-restricted feeding on lipid metabolism and adiposity. Adipocyte *4*, 319–324.

Chaix, A., Zarrinpar, A., Miu, P., and Panda, S. (2014). Time-Restricted Feeding Is a Preventative and Therapeutic Intervention against Diverse Nutritional Challenges. Cell Metab. *20*, 991–1005.

Chaix, A., Lin, T., Le, H.D., Chang, M.W., and Panda, S. (2019). Time-Restricted Feeding Prevents Obesity and Metabolic Syndrome in Mice Lacking a Circadian Clock. Cell Metab. *29*, 303-319.

Chakravarthy, M. V., and Booth, F.W. (2004). Eating, exercise, and "thrifty" genotypes: connecting the dots toward an evolutionary understanding of modern chronic diseases. J. Appl. Physiol. *96*, 3–10.

Chalasani, N., Younossi, Z., Lavine, J.E., Diehl, A.M., Brunt, E.M., Cusi, K., Charlton, M., and Sanyal, A.J. (2012). The diagnosis and management of non-alcoholic fatty liver disease: Practice Guideline by the American Association for the Study of Liver Diseases, American College of Gastroenterology, and the American Gastroenterological Association. Hepatology *55*, 2005–2023.

Chambers, L., McCrickerd, K., and Yeomans, M.R. (2015). Optimising foods for satiety. Trends Food Sci. Technol. *41*, 149–160.

Chaudhury, D., and Colwell, C.S. (2002). Circadian modulation of learning and memory in fear-conditioned mice. Behav. Brain Res. *133*, 95–108.

Chaudhury, D., Wang, L.M., and Colwell, C.S. (2005). Circadian Regulation of Hippocampal Long-Term Potentiation. J. Biol. Rhythms *20*, 225–236.

Chaudhury, D., Loh, D.H., Dragich, J.M., Hagopian, A., and Colwell, C.S. (2008). Select cognitive deficits in Vasoactive Intestinal Peptide deficient mice. BMC Neurosci. *9*, 63.

Chen, D., Buchanan, G.F., Ding, J.M., Hannibal, J., and Gillette, M.U. (1999). Pituitary adenylyl cyclase-activating peptide: a pivotal modulator of glutamatergic regulation of the suprachiasmatic circadian clock. Proc. Natl. Acad. Sci. *96*, 13468–13473.

Chung, H., Chou, W., Sears, D.D., Patterson, R.E., Webster, N.J.G., and Ellies, L.G. (2016). Time-restricted feeding improves insulin resistance and hepatic steatosis in a mouse model of postmenopausal obesity. Metabolism *65*, 1743–1754.

Cinti, S., Mitchell, G., Barbatelli, G., Murano, I., Ceresi, E., Faloia, E., Wang, S., Fortier, M., Greenberg, A.S., and Obin, M.S. (2005). Adipocyte death defines macrophage localization and function in adipose tissue of obese mice and humans. J. Lipid Res. *46*, 2347–2355.

Clemens, Z., Molle, M., Eross, L., Barsi, P., Halasz, P., and Born, J. (2007). Temporal coupling of parahippocampal ripples, sleep spindles and slow oscillations in humans. Brain *130*, 2868–2878.

Collingridge, G.L., and Bliss, T. V (1995). Memories of NMDA receptors and LTP. Trends Neurosci. *18*, 54–56.

Colwell, C.S. (2001). NMDA-evoked calcium transients and currents in the suprachiasmatic nucleus: gating by the circadian system. Eur. J. Neurosci. *13*, 1420–1428.

Copps, K.D., and White, M.F. (2012). Regulation of insulin sensitivity by serine/threonine phosphorylation of insulin receptor substrate proteins IRS1 and IRS2. Diabetologia *55*, 2565–2582.

Cordain, L., Eaton, S.B., Sebastian, A., Mann, N., Lindeberg, S., Watkins, B.A., O'Keefe, J.H., and Brand-Miller, J. (2005). Origins and evolution of the Western diet: health implications for the 21st century. Am. J. Clin. Nutr. *81*, 341–354.

Cunha, C., Angelucci, A., D'Antoni, A., Dobrossy, M.D., Dunnett, S.B., Berardi, N., and Brambilla, R. (2009). Brain-derived neurotrophic factor (BDNF) overexpression in the forebrain results in learning and memory impairments. Neurobiol. Dis. *33*, 358–368.

Curioni, C.C., and Lourenço, P.M. (2005). Long-term weight loss after diet and exercise: a systematic review. Int. J. Obes. *29*, 1168–1174.

D'Agostino, G., and Diano, S. (2010). alpha-Melanocyte stimulating hormone: production and degradation. J. Mol. Med. *88*, 1195–1201.

Dalvi, P.S., Chalmers, J.A., Luo, V., Han, D.-Y., Wellhauser, L., Liu, Y., Tran, D.Q., Castel, J., Luquet, S., Wheeler, M.B., et al. High fat induces acute and chronic inflammation in the hypothalamus: effect of high-fat diet, palmitate and TNF-α on appetite-regulating NPY neurons. Int. J. Obes. *41*, 149–158.

Danaei, G., Ding, E.L., Mozaffarian, D., Taylor, B., Rehm, J., Murray, C.J.L., and Ezzati, M. (2009). The Preventable Causes of Death in the United States: Comparative Risk Assessment of Dietary, Lifestyle, and Metabolic Risk Factors. PLoS Med. *6*, e1000058.

Dandona, P., Aljada, A., and Bandyopadhyay, A. (2004). Inflammation: the link between insulin resistance, obesity and diabetes. Trends Immunol. *25*, 4–7.

Daneman, R., and Prat, A. (2015). The Blood–Brain Barrier. Cold Spring Harb. Perspect. Biol. *7*, a020412.

Dantzer, R., and Kelley, K.W. (2007). Twenty years of research on cytokine-induced sickness behavior. Brain. Behav. Immun. *21*, 153–160.

Das, U.N. (2001). Is obesity an inflammatory condition? Nutrition *17*, 953–966.

Davidson, T.L., Monnot, A., Neal, A.U., Martin, A.A., Horton, J.J., and Zheng, W. (2012). The effects of a high-energy diet on hippocampal-dependent discrimination performance and blood-brain barrier integrity differ for diet-induced obese and diet-resistant rats. Physiol. Behav. *107*, 26–33.

Davidson, T.L.L., Hargrave, S.L.L., Swithers, S.E.E., Sample, C.H.H., Fu, X., Kinzig, K.P.P., and Zheng, W. (2013). Inter-relationships among diet, obesity and hippocampal-dependent cognitive function. Neuroscience *253*, 110–122.

DeBruyne, J.P., Noton, E., Lambert, C.M., Maywood, E.S., Weaver, D.R., and Reppert, S.M. (2006). A Clock Shock: Mouse CLOCK Is Not Required for Circadian Oscillator Function. Neuron *50*, 465–477.

DeBruyne, J.P., Weaver, D.R., and Reppert, S.M. (2007). CLOCK and NPAS2 have overlapping roles in the suprachiasmatic circadian clock. Nat. Neurosci. *10*, 543–545.

DeFronzo, R.A., Jacot, E., Jequier, E., Maeder, E., Wahren, J., and Felber, J.P. (1981). The Effect of Insulin on the Disposal of Intravenous Glucose: Results from Indirect Calorimetry and Hepatic and Femoral Venous Catheterization. Diabetes *30*, 1000–1007.

Delezie, J., Dumont, S., Sandu, C., Reibel, S., Pevet, P., and Challet, E. (2016). Rev-erbα in the brain is essential for circadian food entrainment. Sci. Rep. *6*, 29386.

Després, J.-P., Lemieux, I., Bergeron, J., Pibarot, P., Mathieu, P., Larose, E., Rodés-Cabau, J., Bertrand, O.F., and Poirier, P. (2008). Abdominal Obesity and the Metabolic Syndrome: Contribution to Global Cardiometabolic Risk. Arterioscler. Thromb. Vasc. Biol. *28*, 1039–1049.

Devlin, P.F., and Kay, S.A. (1999). Cryptochromes – bringing the blues to circadian rhythms. Trends Cell Biol. *9*, 295–298.

Dibner, C., Schibler, U., and Albrecht, U. (2010). The Mammalian Circadian Timing System: Organization and Coordination of Central and Peripheral Clocks. Annu. Rev. Physiol. *72*, 517–549.

Dierickx, P., Vermunt, M.W., Muraro, M.J., Creyghton, M.P., Doevendans, P.A., van Oudenaarden, A., Geijsen, N., and Van Laake, L.W. (2017). Circadian networks in human embryonic stem cell-derived cardiomyocytes. EMBO Rep. *18*, 1199–1212.

Dierickx, P., Van Laake, L.W., and Geijsen, N. (2018). Circadian clocks: from stem cells to tissue homeostasis and regeneration. EMBO Rep. *19*, 18–28.

DiLeone, R.J., Taylor, J.R., and Picciotto, M.R. (2012). The drive to eat: comparisons and distinctions between mechanisms of food reward and drug addiction. Nat. Neurosci. *15*, 1330–1335.

Dudai, Y., Karni, A., and Born, J. (2015). The Consolidation and Transformation of Memory. Neuron *88*, 20–32.

Duffey, K.J., and Popkin, B.M. (2008). High-fructose corn syrup: is this what's for dinner? Am. J. Clin. Nutr. *88*, 1722S-1732S.

Duncan, M.J., Smith, J.T., Narbaiza, J., Mueez, F., Bustle, L.B., Qureshi, S., Fieseler, C., and Legan, S.J. (2016). Restricting feeding to the active phase in middle-aged mice attenuates adverse metabolic effects of a high-fat diet. Physiol. Behav. *167*, 1–9.

Eckel-Mahan, K.L. (2012). Circadian Oscillations within the Hippocampus Support Memory Formation and Persistence. Front. Mol. Neurosci. *5*, 46.

Eckel-Mahan, K.L., Phan, T., Han, S., Wang, H., Chan, G.C.K., Scheiner, Z.S., and Storm, D.R. (2008). Circadian oscillation of hippocampal MAPK activity and cAmp: implications for memory persistence. Nat. Neurosci. *11*, 1074–1082.

Eckel-Mahan, K.L., Patel, V.R., de Mateo, S., Orozco-Solis, R., Ceglia, N.J., Sahar, S., Dilag-Penilla, S.A., Dyar, K.A., Baldi, P., Sassone-Corsi, P., et al. (2013). Reprogramming of the Circadian Clock by Nutritional Challenge. Cell *155*, 1464–1478.

van Ee, R., Van de Cruys, S., Schlangen, L.J.M., and Vlaskamp, B.N.S. (2016). Circadian-Time Sickness: Time-of-Day Cue-Conflicts Directly Affect Health. Trends Neurosci. *39*, 738–749.

Eichenbaum, H. (2014). Time cells in the hippocampus: a new dimension for mapping memories. Nat. Rev. Neurosci. *15*, 732–744.

Eichenbaum, H. (2017). The role of the hippocampus in navigation is memory. J. Neurophysiol. *117*, 1785–1796.

Ekstrom, A.D., and Ranganath, C. (2018). Space, time, and episodic memory: The hippocampus is all over the cognitive map. Hippocampus *28*, 680–687.

El-Husseini, A.E., Schnell, E., Chetkovich, D.M., Nicoll, R.A., and Bredt, D.S. (2000). PSD-95 involvement in maturation of excitatory synapses. Science *290*, 1364–1368.

Ellacott, K.L.J., Morton, G.J., Woods, S.C., Tso, P., and Schwartz, M.W. (2010). Assessment of Feeding Behavior in Laboratory Mice. Cell Metab. *12*, 10–17.

Emery, P., So, W.V., Kaneko, M., Hall, J.C., and Rosbash, M. (1998). CRY, a Drosophila Clock and Light-Regulated Cryptochrome, Is a Major Contributor to Circadian Rhythm Resetting and Photosensitivity. Cell *95*, 669–679.

Emken, E.A. (1984). Nutrition and Biochemistry of Trans and Positional Fatty Acid Isomers in Hydrogenated Oils. Annu. Rev. Nutr. *4*, 339–376.

Essner, R.A., Smith, A.G., Jamnik, A.A., Ryba, A.R., Trutner, Z.D., and Carter, M.E. (2017). AgRP Neurons Can Increase Food Intake during Conditions of Appetite Suppression and Inhibit Anorexigenic Parabrachial Neurons. J. Neurosci. *37*, 8678–8687.

Even, P.C., and Nadkarni, N.A. (2012). Indirect calorimetry in laboratory mice and rats: principles, practical considerations, interpretation and perspectives. Am. J. Physiol. Integr. Comp. Physiol. *303*, R459–R476.

Fadel, J.R., and Reagan, L.P. (2016). Stop signs in hippocampal insulin signaling: the role of insulin resistance in structural, functional and behavioral deficits. Curr. Opin. Behav. Sci. *9*, 47–54.

Faria, J. de A., de Araújo, T.M.F., Razolli, D.S., Ignácio-Souza, L.M., Souza, D.N., Bordin, S., and Anhê, G.F. (2017). Metabolic Impact of Light Phase-Restricted Fructose Consumption Is Linked to Changes in Hypothalamic AMPK Phosphorylation and Melatonin Production in Rats. Nutrients *9*.

Farr, S.A., Yamada, K.A., Butterfield, D.A., Abdul, H.M., Xu, L., Miller, N.E., Banks, W.A., and Morley, J.E. (2008). Obesity and Hypertriglyceridemia Produce Cognitive Impairment. Endocrinology *149*, 2628–2636.

Felger, J.C., and Treadway, M.T. (2017). Inflammation Effects on Motivation and Motor Activity: Role of Dopamine. Neuropsychopharmacology *42*, 216–241.

Felger, J.C., Mun, J., Kimmel, H.L., Nye, J.A., Drake, D.F., Hernandez, C.R., Freeman, A.A., Rye, D.B., Goodman, M.M., Howell, L.L., et al. (2013). Chronic Interferon-α Decreases Dopamine 2 Receptor Binding and Striatal Dopamine Release in Association with Anhedonia-Like Behavior in Nonhuman Primates. Neuropsychopharmacology *38*, 2179–2187.

Fenselau, H., Campbell, J.N., Verstegen, A.M.J., Madara, J.C., Xu, J., Shah, B.P., Resch, J.M., Yang, Z., Mandelblat-Cerf, Y., Livneh, Y., et al. (2017). A rapidly acting glutamatergic ARC→PVH satiety circuit postsynaptically regulated by α-MSH. Nat. Neurosci. *20*, 42–51.

Finkelstein, E.A., Trogdon, J.G., Cohen, J.W., and Dietz, W. (2009). Annual Medical Spending Attributable To Obesity: Payer-And Service-Specific Estimates. Health Aff. *28*, w822–w831.

Flegal, K.M., Carroll, M.D., Ogden, C.L., and Curtin, L.R. (2010). Prevalence and Trends in Obesity Among US Adults, 1999-2008. JAMA *303*, 235.

la Fleur, S.E., Kalsbeek, A., Wortel, J., Fekkes, M.L., and Buijs, R.M. (2001). A Daily Rhythm in Glucose Tolerance. Diabetes *50*, 1237–1243.

Food and Drug Administration, HHS (2003). Food labeling: trans fatty acids in nutrition labeling, nutrient content claims, and health claims. Final rule. Fed. Regist. *68*, 41433–41506.

Food and Drug Administration (2015). Final Determination Regarding Partially Hydrogenated Oils. https://www.federalregister.gov/documents/2015/06/17/2015-14883/final-determination-regarding-partially-hydrogenated-oils.

Foster, R.G., and Wulff, K. (2005). The rhythm of rest and excess. Nat. Rev. Neurosci. *6*, 407–414.

Frank, M.G., and Cantera, R. (2014). Sleep, clocks, and synaptic plasticity. Trends Neurosci. *37*, 491–501.

Freeman, L.R., and Granholm, A.-C.E. (2012). Vascular Changes in Rat Hippocampus following a High Saturated Fat and Cholesterol Diet. J. Cereb. Blood Flow Metab. *32*, 643–653.

Furukawa, S., Fujita, T., Shimabukuro, M., Iwaki, M., Yamada, Y., Nakajima, Y., Nakayama, O., Makishima, M., Matsuda, M., and Shimomura, I. (2004). Increased oxidative stress in obesity and its impact on metabolic syndrome. J. Clin. Invest. *114*, 1752–1761.

Gabel, K., Hoddy, K.K., Haggerty, N., Song, J., Kroeger, C.M., Trepanowski, J.F., Panda, S., and Varady, K.A. (2018). Effects of 8-hour time restricted feeding on body weight and metabolic disease risk factors in obese adults: A pilot study. Nutr. Heal. Aging *4*, 345–353.

Gaby, A.R. (2005). Adverse effects of dietary fructose. Altern. Med. Rev. *10*, 294–306.

Garfield, A.S., Li, C., Madara, J.C., Shah, B.P., Webber, E., Steger, J.S., Campbell, J.N., Gavrilova, O., Lee, C.E., Olson, D.P., et al. (2015). A neural basis for melanocortin-4 receptor–regulated appetite. Nat. Neurosci. *18*, 863–871.

Gau, D., Lemberger, T., von Gall, C., Kretz, O., Le Minh, N., Gass, P., Schmid, W., Schibler, U., Korf, H.W., and Schütz, G. (2002). Phosphorylation of CREB Ser142 Regulates Light-Induced Phase Shifts of the Circadian Clock. Neuron *34*, 245–253.

Gaziano, T.A., Galea, G., and Reddy, K.S. (2007). Scaling up interventions for chronic disease prevention: the evidence. Lancet *370*, 1939–1946.

Gelbard-Sagiv, H., Mukamel, R., Harel, M., Malach, R., and Fried, I. (2008). Internally Generated Reactivation of Single Neurons in Human Hippocampus During Free Recall. Science (80-.). *322*, 96–101.

German, J.B., and Dillard, C.J. (2010). Saturated Fats: A Perspective from Lactation and

Milk Composition. Lipids *45*, 915–923.

Ghasemi, R., Haeri, A., Dargahi, L., Mohamed, Z., and Ahmadiani, A. (2013). Insulin in the Brain: Sources, Localization and Functions. Mol. Neurobiol. *47*, 145–171.

Giguère, V., McBroom, L.D., and Flock, G. (1995). Determinants of target gene specificity for ROR alpha 1: monomeric DNA binding by an orphan nuclear receptor. Mol. Cell. Biol. *15*, 2517–2526.

Gill, S., and Panda, S. (2015). A Smartphone App Reveals Erratic Diurnal Eating Patterns in Humans that Can Be Modulated for Health Benefits. Cell Metab. *22*, 789–798.

Gill, P.R., Mizumori, S.J.Y., and Smith, D.M. (2011). Hippocampal episode fields develop with learning. Hippocampus *21*, 1240–1249.

Ginty, D., Kornhauser, J., Thompson, M., Bading, H., Mayo, K., Takahashi, J., and Greenberg, M. (1993). Regulation of CREB phosphorylation in the suprachiasmatic nucleus by light and a circadian clock. Science. *260*, 238–241.

Glinsmann, W.H., and Bowman, B.A. (1993). The public health significance of dietary fructose. Am. J. Clin. Nutr. *58*, 820S-823S.

Goodwin, P.J., and Stambolic, V. (2015). Impact of the Obesity Epidemic on Cancer. Annu. Rev. Med. *66*, 281–296.

Greene, M.W., and Garofalo, R.S. (2002). Positive and Negative Regulatory Role of Insulin Receptor Substrate 1 and 2 (IRS-1 and IRS-2) Serine/Threonine Phosphorylation. Biochemistry *41*, 7082–7091.

Greene, M.W., Sakaue, H., Wang, L., Alessi, D.R., and Roth, R.A. (2003). Modulation of Insulin-stimulated Degradation of Human Insulin Receptor Substrate-1 by Serine 312 Phosphorylation. J. Biol. Chem. *278*, 8199–8211.

Greene, M.W., Burrington, C.M., Luo, Y., Ruhoff, M.S., Lynch, D.T., and Chaithongdi, N. (2014). PKCδ is activated in the liver of obese Zucker rats and mediates diet-induced whole body insulin resistance and hepatocyte cellular insulin resistance. J. Nutr. Biochem. *25*, 281–288.

Grief, S.N., and Miranda, R.L.F. (2010). Weight loss maintenance. Am. Fam. Physician *82*, 630–634.

Gropp, E., Shanabrough, M., Borok, E., Xu, A.W., Janoschek, R., Buch, T., Plum, L., Balthasar, N., Hampel, B., Waisman, A., et al. (2005). Agouti-related peptide–expressing neurons are mandatory for feeding. Nat. Neurosci. *8*, 1289–1291.

Gropper, S., and Smith, J. (2013). Advanced Nutrition and Human Metabolism (Belmont: Wadsworth).

Guenther, M.G., Lane, W.S., Fischle, W., Verdin, E., Lazar, M.A., and Shiekhattar, R. (2000). A core SMRT corepressor complex containing HDAC3 and TBL1, a WD40-repeat protein linked to deafness. Genes Dev. *14*, 1048–1057.

Guillaumond, F., Dardente, H., Giguère, V., and Cermakian, N. (2005). Differential Control of Bmal1 Circadian Transcription by REV-ERB and ROR Nuclear Receptors. J. Biol. Rhythms *20*, 391–403.

Guzowski, J.F., Setlow, B., Wagner, E.K., and McGaugh, J.L. (2001). Experience-Dependent Gene Expression in the Rat Hippocampus after Spatial Learning: A Comparison of the Immediate-Early GenesArc, c-fos, and zif268. J. Neurosci. *21*, 5089–5098.

Haber, S.N., and Knutson, B. (2010). The Reward Circuit: Linking Primate Anatomy and Human Imaging. Neuropsychopharmacology *35*, 4–26.

Hales, C.M., Carroll, M.D., Fryar, C.D., and Ogden, C.L. (2015). Prevalence of Obesity Among Adults and Youth: United States, 2015-2016 Key findings Data from the National Health and Nutrition Examination Survey.

Hales, C.M., Fryar, C.D., Carroll, M.D., Freedman, D.S., and Ogden, C.L. (2018). Trends in Obesity and Severe Obesity Prevalence in US Youth and Adults by Sex and Age, 2007-2008 to 2015-2016. JAMA *319*, 1723.

Hamby, M.E., Coppola, G., Ao, Y., Geschwind, D.H., Khakh, B.S., and Sofroniew, M. V. (2012). Inflammatory Mediators Alter the Astrocyte Transcriptome and Calcium Signaling Elicited by Multiple G-Protein-Coupled Receptors. J. Neurosci. *32*, 14489–14510.

Hamilton, J.A., and Brunaldi, K. (2007). A model for fatty acid transport into the brain. J. Mol. Neurosci. *33*, 12–17.

Hammond, R.A., and Levine, R. (2010). The economic impact of obesity in the United States. Diabetes. Metab. Syndr. Obes. *3*, 285–295.

Hanslmayr, S., Staudigl, T., and Fellner, M.-C. (2012). Oscillatory power decreases and long-term memory: the information via desynchronization hypothesis. Front. Hum. Neurosci. *6*, 74.

Haque, S.N., Booreddy, S.R., and Welsh, D.K. (2019). Effects of BMAL1 Manipulation on the Brain's Master Circadian Clock and Behavior. Yale J. Biol. Med. *92*, 251–258.

Hara, R., Wan, K., Wakamatsu, H., Aida, R., Moriya, T., Akiyama, M., and Shibata, S.

(2001). Restricted feeding entrains liver clock without participation of the suprachiasmatic nucleus. Genes to Cells *6*, 269–278.

Harding, H.P., and Lazar, M.A. (1995). The monomer-binding orphan receptor Rev-Erb represses transcription as a dimer on a novel direct repeat. Mol. Cell. Biol. *15*, 4791–4802.

Hargrave, S.L., Davidson, T.L., Zheng, W., and Kinzig, K.P. (2016). Western diets induce blood-brain barrier leakage and alter spatial strategies in rats. Behav. Neurosci. *130*, 123–135.

Hariri, N., and Thibault, L. (2010). High-fat diet-induced obesity in animal models. Nutr. Res. Rev. *23*, 270–299.

Harney, S.C., Jane, D.E., and Anwyl, R. (2008). Extrasynaptic NR2D-containing NMDARs are recruited to the synapse during LTP of NMDAR-EPSCs. J. Neurosci. *28*, 11685–11694.

Harrison, N.A., Voon, V., Cercignani, M., Cooper, E.A., Pessiglione, M., and Critchley, H.D. (2016). A Neurocomputational Account of How Inflammation Enhances Sensitivity to Punishments Versus Rewards. Biol. Psychiatry *80*, 73–81.

Harvard Health Publishing (2016). Weighing in on the value of the body mass index. https://www.health.harvard.edu/staying-healthy/weighing-in-on-the-value-of-the-body-mass-index.

Hatori, M., Vollmers, C., Zarrinpar, A., DiTacchio, L., Bushong, E.A., Gill, S., Leblanc, M., Chaix, A., Joens, M., Fitzpatrick, J.A.J., et al. (2012). Time-Restricted Feeding without Reducing Caloric Intake Prevents Metabolic Diseases in Mice Fed a High-Fat Diet. Cell Metab. *15*, 848–860.

Hauber, W., and Bareiß, A. (2001). Facilitative effects of an adenosine A1/A2 receptor blockade on spatial memory performance of rats: selective enhancement of reference memory retention during the light period. Behav. Brain Res. *118*, 43–52.

Hayden, M.S., and Ghosh, S. (2008). Shared Principles in NF-κB Signaling. Cell *132*, 344–362.

van Heesch, F., Prins, J., Korte-Bouws, G.A.H., Westphal, K.G.C., Lemstra, S., Olivier, B., Kraneveld, A.D., and Korte, S.M. (2013). Systemic tumor necrosis factor-alpha decreases brain stimulation reward and increases metabolites of serotonin and dopamine in the nucleus accumbens of mice. Behav. Brain Res. *253*, 191–195.

Heinz, F., Lamprecht, W., and Kirsch, J. (1968). Enzymes of fructose metabolism in human liver. J. Clin. Invest. *47*, 1826–1832.

Heisler, L.K., and Lam, D.D. (2017). An appetite for life: brain regulation of hunger and satiety. Curr. Opin. Pharmacol. *37*, 100–106.

Hernandez, E.M. (2016). Specialty Oils: Functional and Nutraceutical Properties. Funct. Diet. Lipids 69–101.

Ho, Y.-H., Lin, Y.-T., Wu, C.-W.J., Chao, Y.-M., Chang, A.Y.W., and Chan, J.Y.H. (2015). Peripheral inflammation increases seizure susceptibility via the induction of neuroinflammation and oxidative stress in the hippocampus. J. Biomed. Sci. *22*, 46.

Hoevenaars, F.P.M., Keijer, J., Swarts, H.J., Snaas-Alders, S., Bekkenkamp-Grovenstein, M., and van Schothorst, E.M. (2013). Effects of dietary history on energy metabolism and physiological parameters in C57BL/6J mice. Exp. Physiol. *98*, 1053–1062.

Hogenesch, J.B., Chan, W.K., Jackiw, V.H., Brown, R.C., Gu, Y.Z., Pray-Grant, M., Perdew, G.H., and Bradfield, C.A. (1997). Characterization of a subset of the basic-helix-loop-helix-PAS superfamily that interacts with components of the dioxin signaling pathway. J. Biol. Chem. *272*, 8581–8593.

Hogenesch, J.B., Gu, Y.Z., Jain, S., and Bradfield, C.A. (1998). The basic-helix-loop-helix-PAS orphan MOP3 forms transcriptionally active complexes with circadian and hypoxia factors. Proc. Natl. Acad. Sci. *95*, 5474–5479.

Holloway, F.A., and Wansley, R.A. (1973). Multiple retention deficits at periodic intervals after active and passive avoidance learning. Behav. Biol. *9*, 1–14.

Hooper, L., Martin, N., Abdelhamid, A., and Davey Smith, G. (2015). Reduction in saturated fat intake for cardiovascular disease. Cochrane Database Syst. Rev. *6*, 1-160.

Horst, G.T.J. van der, Muijtjens, M., Kobayashi, K., Takano, R., Kanno, S., Takao, M., Wit, J. de, Verkerk, A., Eker, A.P.M., Leenen, D. van, et al. (1999). Mammalian Cry1 and Cry2 are essential for maintenance of circadian rhythms. Nature *398*, 627–630.

Hotamisligil, G.S. (2003). Inflammatory pathways and insulin action. Int. J. Obes. *27*, S53–S55.

Hotamisligil, G. k. S., Peraldi, P., Budavari, A., Ellis, R., White, M.F., and Spiegelman, B.M. (1996). IRS-1-Mediated Inhibition of Insulin Receptor Tyrosine Kinase Activity in TNF-alpha- and Obesity-Induced Insulin Resistance. Science *271*, 665–670.

Hryhorczuk, C., Décarie-Spain, L., Sharma, S., Daneault, C., Rosiers, C. Des, Alquier, T., and Fulton, S. (2017). Saturated high-fat feeding independent of obesity alters hypothalamus-pituitary-adrenal axis function but not anxiety-like behaviour. Psychoneuroendocrinology *83*, 142–149.

Hsu, T.M., and Kanoski, S.E. (2014). Blood-brain barrier disruption: mechanistic links

between Western diet consumption and dementia. Front. Aging Neurosci. *6*, 88.

Hu, F.B., and Malik, V.S. (2010). Sugar-sweetened beverages and risk of obesity and type 2 diabetes: Epidemiologic evidence. Physiol. Behav. *100*, 47–54.

Institute for Health Metrics and Evaluation (2014). Obesity and overweight increasing worldwide. http://www.healthdata.org/infographic/obesity-and-overweight-increasing-worldwide.

Ishimoto, T., Lanaspa, M.A., Le, M.T., Garcia, G.E., Diggle, C.P., Maclean, P.S., Jackman, M.R., Asipu, A., Roncal-Jimenez, C.A., Kosugi, T., et al. Opposing effects of fructokinase C and A isoforms on fructose-induced metabolic syndrome in mice. Proc. Natl. Acad. Sci. *109*, 4320-4325.

Ishimoto, T., Lanaspa, M.A., Rivard, C.J., Roncal-Jimenez, C.A., Orlicky, D.J., Cicerchi, C., McMahan, R.H., Abdelmalek, M.F., Rosen, H.R., Jackman, M.R., et al. (2013). High-fat and high-sucrose (western) diet induces steatohepatitis that is dependent on fructokinase. Hepatology *58*, 1632–1643.

Ishizuka, T., and Lazar, M.A. (2003). The N-CoR/histone deacetylase 3 complex is required for repression by thyroid hormone receptor. Mol. Cell. Biol. *23*, 5122–5131.

Ishizuka, T., and Lazar, M.A. (2005). The Nuclear Receptor Corepressor Deacetylase Activating Domain Is Essential for Repression by Thyroid Hormone Receptor. Mol. Endocrinol. *19*, 1443–1451.

Ito, M. (1989). Long-Term Depression. Annu. Rev. Neurosci. *12*, 85–102.

Jakicic, J.M., Clark, K., Coleman, E., Donnelly, J.E., Foreyt, J., Melanson, E., Volek, J. and Volpe, S.L. (2001). Appropriate Intervention Strategies for Weight Loss and Prevention of Weight Regain for Adults. Med. Sci. Sport. Exerc. *33*, 2145–2156.

Jamshed, H., Beyl, R.A., Della Manna, D.L., Yang, E.S., Ravussin, E., and Peterson, C.M. (2019). Early Time-Restricted Feeding Improves 24-Hour Glucose Levels and Affects Markers of the Circadian Clock, Aging, and Autophagy in Humans. Nutrients *11*, 1234.

Jang, C., Hui, S., Lu, W., Cowan, A.J., Morscher, R.J., Lee, G., Liu, W., Tesz, G.J., Birnbaum, M.J., and Rabinowitz, J.D. (2018). The Small Intestine Converts Dietary Fructose into Glucose and Organic Acids. Cell Metab. *27*, 351-361.

Jegatheesan, P. and De Bandt, J. (2017). Fructose and NAFLD: The Multifaceted Aspe cts of Fructose Metabolism. Nutrients *9*, 230.

Jensen, T., Kiersgaard, M., Sørensen, D., and Mikkelsen, L. (2013). Fasting of mice: a review. Lab. Anim. *47*, 225–240.

Jeong, H.-K., Ji, K., Min, K., and Joe, E.-H. (2013). Brain Inflammation and Microglia: Facts and Misconceptions. Exp. Neurobiol. *22*, 59.

John, G.R., Lee, S.C., Song, X., Rivieccio, M., and Brosnan, C.F. (2005). IL-1-regulated responses in astrocytes: Relevance to injury and recovery. Glia *49*, 161–176.

Jones, J.R., Simon, T., Lones, L., and Herzog, E.D. (2018). SCN VIP Neurons Are Essential for Normal Light-Mediated Resetting of the Circadian System. J. Neurosci. *38*, 7986–7995.

Joo, J., Cox, C.C., Kindred, E.D., Lashinger, L.M., Young, M.E., and Bray, M.S. (2016). The acute effects of time-of-day-dependent high fat feeding on whole body metabolic flexibility in mice. Int. J. Obes. *40*, 1444–1451.

Jordan, S.D., Kriebs, A., Vaughan, M., Duglan, D., Fan, W., Henriksson, E., Huber, A.-L., Papp, S.J., Nguyen, M., Afetian, M., et al. (2017). CRY1/2 Selectively Repress PPARδ and Limit Exercise Capacity. Cell Metab. *26*, 243-255.

Jürgens, H., Haass, W., Castañeda, T.R., Schürmann, A., Koebnick, C., Dombrowski, F., Otto, B., Nawrocki, A.R., Scherer, P.E., Spranger, J., et al. (2005). Consuming Fructose-sweetened Beverages Increases Body Adiposity in Mice. Obes. Res. *13*, 1146–1156.

Kanoski, S.E., and Davidson, T.L. (2011). Western diet consumption and cognitive impairment: Links to hippocampal dysfunction and obesity. Physiol. Behav. *103*, 59–68.

Karatsoreos, I.N. (2014). Links between Circadian Rhythms and Psychiatric Disease. Front. Behav. Neurosci. *8*, 162.

Katan, M.B., Zock, P.L., and Mensink, R.P. Trans-Fatty acids and Their Effects on Likpoproteins in Humans. Annu. Rev. Nutr. 15, 473-493.

Kayman, S., Bruvold, W., and Stern, J.S. (1990). Maintenance and relapse after weight loss in women: behavioral aspects. Am. J. Clin. Nutr. *52*, 800–807.

Keesey, R.E., and Hirvonen, M.D. (1997). Body Weight Set-Points: Determination and Adjustment. J. Nutr. *127*, 1875S-1883S.

Kien, C.L., Bunn, J.Y., Stevens, R., Bain, J., Ikayeva, O., Crain, K., Koves, T.R., and Muoio, D.M. (2014). Dietary intake of palmitate and oleate has broad impact on systemic and tissue lipid profiles in humans. Am. J. Clin. Nutr. *99*, 436–445.

Kim, Y.S., and Joh, T.H. (2006). Microglia, major player in the brain inflammation: their roles in the pathogenesis of Parkinson's disease. Exp. Mol. Med. *38*, 333–347.

Kim, H., Zheng, Z., Walker, P.D., Kapatos, G., and Zhang, K. (2017). CREBH Maintains

Circadian Glucose Homeostasis by Regulating Hepatic Glycogenolysis and Gluconeogenesis. Mol. Cell. Biol. *37*.

Kim, P., Oster, H., Lehnert, H., Schmid, S.M., Salamat, N., Barclay, J.L., Maronde, E., Inder, W., and Rawashdeh, O. (2019). Coupling the Circadian Clock to Homeostasis: The Role of Period in Timing Physiology. Endocr. Rev. *40*, 66–95.

King, D.P., Zhao, Y., Sangoram, A.M., Wilsbacher, L.D., Tanaka, M., Antoch, M.P., Steeves, T.D.., Vitaterna, M.H., Kornhauser, J.M., Lowrey, P.L., et al. (1997). Positional Cloning of the Mouse Circadian Clock Gene. Cell *89*, 641–653.

Kitagami, T., Yamada, K., Miura, H., Hashimoto, R., Nabeshima, T., and Ohta, T. (2003). Mechanism of systemically injected interferon-alpha impeding monoamine biosynthesis in rats: role of nitric oxide as a signal crossing the blood–brain barrier. Brain Res. *978*, 104–114.

Klein, S., Sheard, N.F., Pi-Sunyer, X., Daly, A., Wylie-Rosett, J., Kulkarni, K., Clark, N.G., American Diabetes Association, North American Association for the Study of Obesity, and American Society for Clinical Nutrition (2004). Weight management through lifestyle modification for the prevention and management of type 2 diabetes: rationale and strategies. A statement from the American Diabetes Association, the North American Association for the Study of Obesity, and the American Society for Clinical Nutrition. Am. J. Clin. Nutr. *80*, 257–263.

Kliewer, K.L., Ke, J.-Y., Lee, H.-Y., Stout, M.B., Cole, R.M., Samuel, V.T., Shulman, G.I., and Belury, M.A. (2015). Short-term food restriction followed by controlled refeeding promotes gorging behavior, enhances fat deposition, and diminishes insulin sensitivity in mice. J. Nutr. Biochem. *26*, 721–728.

Klugmann, M., Leichtlein, C.B., Symes, C.W., Klaussner, B.C., Brooks, A.I., Young, D., and During, M.J. (2006). A novel role of circadian transcription factor DBP in hippocampal plasticity. Mol. Cell. Neurosci. *31*, 303–314.

Kohsaka, A., Laposky, A.D., Ramsey, K.M., Estrada, C., Joshu, C., Kobayashi, Y., Turek, F.W., and Bass, J. (2007). High-Fat Diet Disrupts Behavioral and Molecular Circadian Rhythms in Mice. Cell Metab. *6*, 414–421.

Kondratov, R. V, Kondratova, A.A., Gorbacheva, V.Y., Vykhovanets, O. V, and Antoch, M.P. (2006). Early aging and age-related pathologies in mice deficient in BMAL1, the core componentof the circadian clock. Genes Dev. *20*, 1868–1873.

Koronowski, K.B., Kinouchi, K., Welz, P.-S., Smith, J.G., Zinna, V.M., Shi, J., Samad, M., Chen, S., Magnan, C.N., Kinchen, J.M., et al. (2019). Defining the Independence of the Liver Circadian Clock. Cell *177*, 1448-1462.

Krashes, M.J., Koda, S., Ye, C., Rogan, S.C., Adams, A.C., Cusher, D.S., Maratos-Flier,

E., Roth, B.L., and Lowell, B.B. (2011). Rapid, reversible activation of AgRP neurons drives feeding behavior in mice. J. Clin. Invest. *121*, 1424–1428.

Kriebs, A., Jordan, S.D., Soto, E., Henriksson, E., Sandate, C.R., Vaughan, M.E., Chan, A.B., Duglan, D., Papp, S.J., Huber, A.-L., et al. (2017). Circadian repressors CRY1 and CRY2 broadly interact with nuclear receptors and modulate transcriptional activity. Proc. Natl. Acad. Sci. *114*, 8776–8781.

Kris-Etherton, P.M., Harris, W.S., and Appel, L.J. (2002). Fish Consumption, Fish Oil, Omega-3 Fatty Acids, and Cardiovascular Disease. Circulation *106*, 2747–2757.

Kume, K., Zylka, M.J., Sriram, S., Shearman, L.P., Weaver, D.R., Jin, X., Maywood, E.S., Hastings, M.H., and Reppert, S.M. (1999). mCRY1 and mCRY2 Are Essential Components of the Negative Limb of the Circadian Clock Feedback Loop. Cell *98*, 193–205.

Lamia, K.A., Sachdeva, U.M., DiTacchio, L., Williams, E.C., Alvarez, J.G., Egan, D.F., Vasquez, D.S., Juguilon, H., Panda, S., Shaw, R.J., et al. (2009). AMPK Regulates the Circadian Clock by Cryptochrome Phosphorylation and Degradation. Science *326*, 437–440.

Lamia, K.A., Papp, S.J., Yu, R.T., Barish, G.D., Uhlenhaut, N.H., Jonker, J.W., Downes, M., and Evans, R.M. (2011). Cryptochromes mediate rhythmic repression of the glucocorticoid receptor. Nature *480*, 552–556.

Lanaspa, M.A., Ishimoto, T., Li, N., Cicerchi, C., Orlicky, D.J., Ruzycki, P., Rivard, C., Inaba, S., Roncal-Jimenez, C.A., Bales, E.S., et al. (2013). Endogenous fructose production and metabolism in the liver contributes to the development of metabolic syndrome. Nat. Commun. *4*, 2434.

Latchoumane, C.-F. V., Ngo, H.-V. V., Born, J., Shin, H.-S., Tan, J., Gloss, B., Augustine, G.J., Deisseroth, K., Luo, M., Graybiel, A.M., et al. (2017). Thalamic Spindles Promote Memory Formation during Sleep through Triple Phase-Locking of Cortical, Thalamic, and Hippocampal Rhythms. Neuron *95,* 1-12.

Lazar, M.A., Hodin, R.A., Darling, D.S., and Chin, W.W. (1989). A novel member of the thyroid/steroid hormone receptor family is encoded by the opposite strand of the rat c-erbA alpha transcriptional unit. Mol. Cell. Biol. *9*, 1128–1136.

Lee, C., Etchegaray, J.-P., Cagampang, F.R.A., Loudon, A.S.I., and Reppert, S.M. (2001). Posttranslational Mechanisms Regulate the Mammalian Circadian Clock. Cell *107*, 855–867.

LeGates, T.A., Altimus, C.M., Wang, H., Lee, H.-K., Yang, S., Zhao, H., Kirkwood, A., Weber, E.T., and Hattar, S. (2012). Aberrant light directly impairs mood and learning through melanopsin-expressing neurons. Nature *491*, 594–598.

LeGates, T.A., Fernandez, D.C., and Hattar, S. (2014). Light as a central modulator of circadian rhythms, sleep and affect. Nat. Rev. Neurosci. *15*, 443–454.

Leibel, R.L., Rosenbaum, M., and Hirsch, J. (1995). Changes in Energy Expenditure Resulting from Altered Body Weight. N. Engl. J. Med. *332*, 621–628.

Li, A., Hindmarch, C.C.T., Nattie, E.E., and Paton, J.F.R. (2013). Antagonism of orexin receptors significantly lowers blood pressure in spontaneously hypertensive rats. J. Physiol. *591*, 4237–4248.

Li, M.-D., Vera, N.B., Yang, Y., Zhang, B., Ni, W., Ziso-Qejvanaj, E., Ding, S., Zhang, K., Yin, R., Wang, S., et al. (2018). Adipocyte OGT governs diet-induced hyperphagia and obesity. Nat. Commun. *9*, 5103.

Li, Y., Gao, X., Winkelman, J.W., Cespedes, E.M., Jackson, C.L., Walters, A.S., Schernhammer, E., Redline, S., and Hu, F.B. (2016). Association between sleeping difficulty and type 2 diabetes in women. Diabetologia *59*, 719–727.

Liang, W., Menke, A.L., Driessen, A., Koek, G.H., Lindeman, J.H., Stoop, R., Havekes, L.M., Kleemann, R., and van den Hoek, A.M. (2014). Establishment of a General NAFLD Scoring System for Rodent Models and Comparison to Human Liver Pathology. PLoS One *9*, e115922.

Liao, F., Yoon, H., and Kim, J. (2017). Apolipoprotein E metabolism and functions in brain and its role in Alzheimer's disease. Curr. Opin. Lipidol. *28*, 60–67.

Light, H.R., Tsanzi, E., Gigliotti, J., Morgan, K., and Tou, J.C. (2009). The Type of Caloric Sweetener Added to Water Influences Weight Gain, Fat Mass, and Reproduction in Growing Sprague-Dawley Female Rats. Exp. Biol. Med. *234*, 651–661.

Lin, J., Yang, R., Tarr, P.T., Wu, P.-H., Handschin, C., Li, S., Yang, W., Pei, L., Uldry, M., Tontonoz, P., et al. (2005). Hyperlipidemic Effects of Dietary Saturated Fats Mediated through PGC-1β Coactivation of SREBP. Cell *120*, 261–273.

Lisman, J., Buzsáki, G., Eichenbaum, H., Nadel, L., Ranganath, C., and Redish, A.D. (2017). Viewpoints: how the hippocampus contributes to memory, navigation and cognition. Nat. Neurosci. *20*, 1434–1447.

Liu, A.C., Welsh, D.K., Ko, C.H., Tran, H.G., Zhang, E.E., Priest, A.A., Buhr, E.D., Singer, O., Meeker, K., Verma, I.M., et al. (2007). Intercellular Coupling Confers Robustness against Mutations in the SCN Circadian Clock Network. Cell *129*, 605–616.

Liu, A.G., Ford, N.A., Hu, F.B., Zelman, K.M., Mozaffarian, D., and Kris-Etherton, P.M. (2017). A healthy approach to dietary fats: understanding the science and taking action to reduce consumer confusion. Nutr. J. *16*, 53.

Liu, X., Zwiebel, L.J., Hinton, D., Benzer, S., Hall, J.C., and Rosbash, M. (1992). The period gene encodes a predominantly nuclear protein in adult Drosophila. J. Neurosci. *12*, 2735–2744.

Logan, R.W., and McClung, C.A. (2019). Rhythms of life: circadian disruption and brain disorders across the lifespan. Nat. Rev. Neurosci. *20*, 49–65.

Loh, D.H., Jami, S.A., Flores, R.E., Truong, D., Ghiani, C.A., O'Dell, T.J., and Colwell, C.S. (2015). Misaligned feeding impairs memories. Elife *4*, e09460.

Lonardo, A., Ballestri, S., Targher, G., and Loria, P. (2015). Diagnosis and management of cardiovascular risk in nonalcoholic fatty liver disease. Expert Rev. Gastroenterol. Hepatol. *9*, 629–650.

Longato, L. (2013). Non-alcoholic fatty liver disease (NAFLD): a tale of fat and sugar? Fibrogenesis Tissue Repair *6*, 14.

Longo, V.D., and Panda, S. (2016). Cell Metabolism Perspective Fasting, Circadian Rhythms, and Time-Restricted Feeding in Healthy Lifespan.

Lopez, S., Bermudez, B., Pacheco, Y.M., Ortega, A., Varela, L.M., Abia, R., and Muriana, F.J.G. (2010). Oleic Acid: The Main Component of Olive Oil on Postprandial Metabolic Processes. Olives Olive Oil Heal. Dis. Prev. 1385–1393.

Lowrey, P.L., and Takahashi, J.S. (2004). MAMMALIAN CIRCADIAN BIOLOGY: Elucidating Genome-Wide Levels of Temporal Organization. Annu. Rev. Genomics Hum. Genet. *5*, 407–441.

Ludwig, D.S., Peterson, K.E., and Gortmaker, S.L. (2001). Relation between consumption of sugar-sweetened drinks and childhood obesity: a prospective, observational analysis. Lancet *357*, 505–508.

Luo, Y., Burrington, C.M., Graff, E.C., Zhang, J., Judd, R.L., Suksaranjit, P., Kaewpoowat, Q., Davenport, S.K., O'Neill, A.M., and Greene, M.W. (2016). Metabolic phenotype and adipose and liver features in a high-fat Western diet-induced mouse model of obesity-linked NAFLD. Am. J. Physiol. Metab. *310*, E418–E439.

Luppino, F.S., de Wit, L.M., Bouvy, P.F., Stijnen, T., Cuijpers, P., Penninx, B.W.J.H., and Zitman, F.G. (2010). Overweight, Obesity, and Depression. Arch. Gen. Psychiatry *67*, 220.

Ma, Z., Jiang, W., and Zhang, E.E. (2016). Orexin signaling regulates both the hippocampal clock and the circadian oscillation of Alzheimer's disease-risk genes. Sci. Rep. *6*, 36035.

Macdonald, I.A. (2016). A review of recent evidence relating to sugars, insulin resistance and diabetes. Eur. J. Nutr. *55*, 17–23.

MacDonald, C.J., Lepage, K.Q., Eden, U.T., and Eichenbaum, H. (2011). Hippocampal "Time Cells" Bridge the Gap in Memory for Discontiguous Events. Neuron *71*, 737–749.

MacDonald, C.J., Carrow, S., Place, R., and Eichenbaum, H. (2013). Distinct hippocampal time cell sequences represent odor memories in immobilized rats. J. Neurosci. *33*, 14607–14616.

MacLean, P.S., Wing, R.R., Davidson, T., Epstein, L., Goodpaster, B., Hall, K.D., Levin, B.E., Perri, M.G., Rolls, B.J., Rosenbaum, M., et al. (2015). NIH working group report: Innovative research to improve maintenance of weight loss. Obesity *23*, 7–15.

Malik, V.S., Schulze, M.B., and Hu, F.B. (2006). Intake of sugar-sweetened beverages and weight gain: a systematic review1–3. Am. J. Clin. Nutr. *84*, 274–288.

Malik, V.S., Popkin, B.M., Bray, G.A., Despres, J.-P., Willett, W.C., and Hu, F.B. (2010a). Sugar-Sweetened Beverages and Risk of Metabolic Syndrome and Type 2 Diabetes: A meta-analysis. Diabetes Care *33*, 2477–2483.

Malik, V.S., Popkin, B.M., Bray, G.A., Després, J.-P., and Hu, F.B. (2010b). Sugar-sweetened beverages, obesity, type 2 diabetes mellitus, and cardiovascular disease risk. Circulation *121*, 1356–1364.

Malik, V.S., Willett, W.C., and Hu, F.B. (2013). Global obesity: trends, risk factors and policy implications. Nat. Rev. Endocrinol. *9*, 13–27.

Manns, J.R., Howard, M.W., and Eichenbaum, H. (2007). Gradual Changes in Hippocampal Activity Support Remembering the Order of Events. Neuron *56*, 530–540.

Maren, S., Phan, K.L., and Liberzon, I. (2013). The contextual brain: implications for fear conditioning, extinction and psychopathology. Nat. Rev. Neurosci. *14*, 417–428.

Marwitz, S.E., Woodie, L.N., and Blythe, S.N. (2015). Western-style diet induces insulin insensitivity and hyperactivity in adolescent male rats. Physiol. Behav. *151*, 147–154.

Mason, C., Foster-Schubert, K.E., Imayama, I., Kong, A., Xiao, L., Bain, C., Campbell, K.L., Wang, C.-Y., Duggan, C.R., Ulrich, C.M., et al. (2011). Dietary Weight Loss and Exercise Effects on Insulin Resistance in Postmenopausal Women. Am. J. Prev. Med. *41*, 366–375.

Mayer, C.M., and Belsham, D.D. (2010). Palmitate Attenuates Insulin Signaling and Induces Endoplasmic Reticulum Stress and Apoptosis in Hypothalamic Neurons: Rescue of Resistance and Apoptosis through Adenosine 5′ Monophosphate-Activated Protein Kinase Activation. Endocrinology *151*, 576–585.

Maywood, E.S., O'Brien, J.A., and Hastings, M.H. (2003). Expression of mCLOCK and Other Circadian Clock-Relevant Proteins in the Mouse Suprachiasmatic Nuclei. J. Neuroendocrinol. *15*, 329–334.

Maywood, E.S., Reddy, A.B., Wong, G.K.Y., O'Neill, J.S., O'Brien, J.A., McMahon, D.G., Harmar, A.J., Okamura, H., and Hastings, M.H. (2006). Synchronization and Maintenance of Timekeeping in Suprachiasmatic Circadian Clock Cells by Neuropeptidergic Signaling. Curr. Biol. *16*, 599–605.

McDowell, J. (2002). Obesity examined. http://pubsapp.acs.org/subscribe/archive/tcaw/11/i02/html/02health.html?.

McHill, A.W., and Wright, K.P. (2019). Cognitive Impairments during the Transition to Working at Night and on Subsequent Night Shifts. J. Biol. Rhythms *34*, 432–446.

Menet, J.S., Pescatore, S., and Rosbash, M. (2014). CLOCK:BMAL1 is a pioneer-like transcription factor. Genes Dev. *28*, 8–13.

Mensink, R.P., and Katan, M.B. (1992). Effect of dietary fatty acids on serum lipids and lipoproteins. A meta-analysis of 27 trials. Arterioscler. Thromb. A J. Vasc. Biol. *12*, 911–919.

Michel, S., Itri, J., Han, J., Gniotczynski, K., and Colwell, C. (2006). Regulation of glutamatergic signalling by PACAP in the mammalian suprachiasmatic nucleus. BMC Neurosci. *7*, 15.

Milanski, M., Degasperi, G., Coope, A., Morari, J., Denis, R., Cintra, D.E., Tsukumo, D.M.L., Anhe, G., Amaral, M.E., Takahashi, H.K., et al. (2009). Cellular/Molecular Saturated Fatty Acids Produce an Inflammatory Response Predominantly through the Activation of TLR4 Signaling in Hypothalamus: Implications for the Pathogenesis of Obesity. J. Neurosci. *29*, 359-370.

Mimee, A., Smith, P.M., and Ferguson, A. V. (2013). Circumventricular organs: Targets for integration of circulating fluid and energy balance signals? Physiol. Behav. *121*, 96–102.

Miyajima, N., Horiuchi, R., Shibuya, Y., Fukushige, S., Matsubara, K., Toyoshima, K., and Yamamoto, T. (1989). Two erbA homologs encoding proteins with different T3 binding capacities are transcribed from opposite DNA strands of the same genetic locus. Cell *57*, 31–39.

Miyamoto, Y., and Sancar, A. (1998). Vitamin B2-based blue-light photoreceptors in the retinohypothalamic tract as the photoactive pigments for setting the circadian clock in mammals. Proc. Natl. Acad. Sci. *95*, 6097–6102.

Mock, K., Lateef, S., Benedito, V.A., and Tou, J.C. (2017). High-fructose corn syrup-55 consumption alters hepatic lipid metabolism and promotes triglyceride accumulation. J. Nutr. Biochem. *39*, 32–39.

Mohawk, J.A., Green, C.B., and Takahashi, J.S. (2012). Central and Peripheral Circadian Clocks in Mammals. Annu. Rev. Neurosci. *35*, 445–462.

Molteni, R., Barnard, R.J., Ying, Z., Roberts, C.K., and Gómez-Pinilla, F. (2002). A high-fat, refined sugar diet reduces hippocampal brain-derived neurotrophic factor, neuronal plasticity, and learning. Neuroscience *112*, 803–814.

de la Monte, S.M., and Wands, J.R. (2008). Alzheimer's Disease is Type 3 Diabetes—Evidence Reviewed. J. Diabetes Sci. Technol. *2*, 1101–1113.

Moore, R.Y., and Speh, J.C. (1993). GABA is the principal neurotransmitter of the circadian system. Neurosci. Lett. *150*, 112–116.

Moraes, J.C., Coope, A., Morari, J., Cintra, D.E., Roman, E.A., Pauli, J.R., Romanatto, T., Carvalheira, J.B., Oliveira, A.L.R., Saad, M.J., et al. (2009). High-Fat Diet Induces Apoptosis of Hypothalamic Neurons. PLoS One *4*.

Moriya, T., Takahashi, S., Ikeda, M., Suzuki-Yamashita, K., Asai, M., Kadotani, H., Okamura, H., Yoshioka, T., and Shibata, S. (2000). N-methyl-D-aspartate receptor subtype 2C is not involved in circadian oscillation or photoic entrainment of the biological clock in mice. J. Neurosci. Res. *61*, 663–673.

Moro, T., Tinsley, G., Bianco, A., Marcolin, G., Pacelli, Q.F., Battaglia, G., Palma, A., Gentil, P., Neri, M., and Paoli, A. (2016). Effects of eight weeks of time-restricted feeding (16/8) on basal metabolism, maximal strength, body composition, inflammation, and cardiovascular risk factors in resistance-trained males. J. Transl. Med. *14*, 290.

Morris, M., Araujo, I.C., Pohlman, R.L., Marques, M.C., Rodwan, N.S., and Farah, V.M. (2012). Timing of fructose intake: An important regulator of adiposity. Clin. Exp. Pharmacol. Physiol. *39*, 57–62.

Mozaffarian, D., Micha, R., and Wallace, S. (2010). Effects on Coronary Heart Disease of Increasing Polyunsaturated Fat in Place of Saturated Fat: A Systematic Review and Meta-Analysis of Randomized Controlled Trials. PLoS Med. *7*.

Mulder, C.K., Gerkema, M.P., and Van der Zee, E.A. (2013). Circadian clocks and memory: time-place learning. Front. Mol. Neurosci. *6*, 8.

Musiek, E.S. (2015). Circadian clock disruption in neurodegenerative diseases: cause and effect? Front. Pharmacol. *6*, 29.

Musiek, E.S., Xiong, D.D., and Holtzman, D.M. (2015). Sleep, circadian rhythms, and

the pathogenesis of Alzheimer Disease. Exp. Mol. Med. *47*.

Myers, J.L., and Allen, J.C. (2012). Nutrition and Inflammation. Am. J. Lifestyle Med. *6*, 14–17.

Nakahata, Y., Sahar, S., Astarita, G., Kaluzova, M., and Sassone-Corsi, P. (2009). Circadian Control of the NAD+ Salvage Pathway by CLOCK-SIRT1. Science *324*, 654–657.

Nakamura, A., and Terauchi, Y. (2013). Lessons from Mouse Models of High-Fat Diet-Induced NAFLD. Int. J. Mol. Sci. *14*, 21240–21257.

Nakanishi, S. (1992). Molecular diversity of glutamate receptors and implications for brain function. Science *258*, 597–603.

National Institutes of Health (2000). The Practical Guide Identification, Evaluation, and Treatment of Overweight and Obesity in Adults NHLBI Obesity Education Initiative. https://www.nhlbi.nih.gov/files/docs/guidelines/prctgd_c.pdf.

Nduhirabandi, F., Du Toit, E.F., Blackhurst, D., Marais, D., and Lochner, A. (2010). Chronic melatonin consumption prevents obesity-related metabolic abnormalities and protects the heart against myocardial ischemia and reperfusion injury in a prediabetic model of diet-induced obesity. J. Pineal Res. *50*.

Nedeltcheva, A. V., Kessler, L., Imperial, J., and Penev, P.D. (2009). Exposure to Recurrent Sleep Restriction in the Setting of High Caloric Intake and Physical Inactivity Results in Increased Insulin Resistance and Reduced Glucose Tolerance. J. Clin. Endocrinol. Metab. *94*, 3242–3250.

Neel, J. V. (2013). The Genetics of Diabetes Mellitus. In Early Diabetes: Advances in Metabolic Disorders, Volume 1, R. Levine, and R. Luft, eds. (New York, NY: Academic Press), pp. 3–10.

Nelson, G.J., Schmidt, P.C., and Kelley, D.S. (1995). Low-fat diets do not lower plasma cholesterol levels in healthy men compared to high-fat diets with similar fatty acid composition at constant caloric intake. Lipids *30*, 969–976.

Ngo, H.-V.V., Martinetz, T., Born, J., and Mölle, M. (2013). Auditory Closed-Loop Stimulation of the Sleep Slow Oscillation Enhances Memory. Neuron *78*, 545–553.

Nilsson, L.H., and Hultman, E. (1974). Liver and Muscle Glycogen in Man after Glucose and Fructose Infusion. Scand. J. Clin. Lab. Invest. *33*, 5–10.

Nunes, E.J., Randall, P.A., Estrada, A., Epling, B., Hart, E.E., Lee, C.A., Baqi, Y., Müller, C.E., Correa, M., and Salamone, J.D. (2014). Effort-related motivational effects of the pro-inflammatory cytokine interleukin 1-beta: studies with the concurrent fixed

ratio 5/ chow feeding choice task. Psychopharmacology. *231*, 727–736.

Nuttall, F.Q. Body Mass Index Obesity, BMI, and Health: A Critical Review. Nutr. Today *50*, 117-128.

O'Rahilly, S., and Farooqi, I.S. (2006). Genetics of obesity. Philos. Trans. R. Soc. B Biol. Sci. *361*, 1095–1105.

de Oliveira, D.L., Loss, C.M., Córdova, S.D., and Callegari-Jacques, S.M. (2014). Time-of-day influence on exploratory behaviour of rats exposed to an unfamiliar environment. Behaviour *151*, 1943–1966.

Oosterman, J.E., Foppen, E., van der Spek, R., Fliers, E., Kalsbeek, A., and la Fleur, S.E. (2015). Timing of fat and liquid sugar intake alters substrate oxidation and food efficiency in male Wistar rats. Chronobiol. Int. *32*, 289–298.

Oudiette, D., and Paller, K.A. (2013). Upgrading the sleeping brain with targeted memory reactivation. Trends Cogn. Sci. *17*, 142–149.

Ouyang, X., Cirillo, P., Sautin, Y., McCall, S., Bruchette, J.L., Diehl, A.M., Johnson, R.J., and Abdelmalek, M.F. (2008). Fructose consumption as a risk factor for non-alcoholic fatty liver disease. J. Hepatol. *48*, 993–999.

Oyarzún, J.P., Morís, J., Luque, D., de Diego-Balaguer, R., and Fuentemilla, L. (2017). Targeted Memory Reactivation during Sleep Adaptively Promotes the Strengthening or Weakening of Overlapping Memories. *37*, 7748–7758.

Panda, S. (2016). Circadian physiology of metabolism. Science *354*, 1008–1015.

Paoletti, P., Bellone, C., and Zhou, Q. (2013). NMDA receptor subunit diversity: impact on receptor properties, synaptic plasticity and disease. Nat. Rev. Neurosci. *14*, 383–400.

Papouin, T., Ladépêche, L., Ruel, J., Sacchi, S., Labasque, M., Hanini, M., Groc, L., Pollegioni, L., Mothet, J.-P., and Oliet, S.H.R. (2012). Synaptic and Extrasynaptic NMDA Receptors Are Gated by Different Endogenous Coagonists. Cell *150*, 633–646.

Parker, K., Salas, M., and Nwosu, V.C. (2010). High fructose corn syrup: Production, uses and public health concerns. Biotechnol. Mol. Biol. Rev. *5*, 71–78.

Pelley, J.W. (2007). Elsevier's Tissue Biochemistry (Philadelphia: Mosby Elsevier).

Pendergast, J.S., Branecky, K.L., Yang, W., Ellacott, K.L.J., Niswender, K.D., and Yamazaki, S. (2013). High-fat diet acutely affects circadian organisation and eating behavior. Eur. J. Neurosci. *37*, 1350–1356.

Pennartz, C.M.A., Hamstra, R., and Geurtsen, A.M.S. (2001). Enhanced NMDA receptor

activity in retinal inputs to the rat suprachiasmatic nucleus during the subjective night. J. Physiol. *532*, 181–194.

Peschke, E., Frese, T., Chankiewitz, E., Peschke, D., Preiss, U., Schneyer, U., Spessert, R., and Muhlbauer, E. (2006). Diabetic Goto Kakizaki rats as well as type 2 diabetic patients show a decreased diurnal serum melatonin level and an increased pancreatic melatonin-receptor status. J. Pineal Res. *40*, 135–143.

Pessin, J.E., and Saltiel, A.R. (2000). Signaling pathways in insulin action: molecular targets of insulin resistance. J. Clin. Invest. *106*, 165–169.

Phan, T.H., Chan, G.C.-K., Sindreu, C.B., Eckel-Mahan, K.L., Storm, D.R., and Storm, D.R. (2011). The Diurnal Oscillation of MAP (Mitogen-Activated Protein) Kinase and Adenylyl Cyclase Activities in the Hippocampus Depends on the Suprachiasmatic Nucleus. J. Neurosci. *31*, 10640–10647.

Pi-Sunyer, F.X. (2002). The Obesity Epidemic: Pathophysiology and Consequences of Obesity. Obes. Res. *10*, 97S-104S.

Plum, L., Schubert, M., and Brüning, J.C. (2005). The role of insulin receptor signaling in the brain. Trends Endocrinol. Metab. *16*, 59–65.

Popkin, B.M., and Gordon-Larsen, P. (2004). The nutrition transition: worldwide obesity dynamics and their determinants. Int. J. Obes. *28*, S2–S9.

Popkin, B.M., Adair, L.S., and Ng, S.W. (2012). Global nutrition transition and the pandemic of obesity in developing countries. Nutr. Rev. *70*, 3–21.

Posey, K.A., Clegg, D.J., Printz, R.L., Byun, J., Morton, G.J., Vivekanandan-Giri, A., Pennathur, S., Baskin, D.G., Heinecke, J.W., Woods, S.C., et al. (2009). Hypothalamic proinflammatory lipid accumulation, inflammation, and insulin resistance in rats fed a high-fat diet. Am. J. Physiol. Metab. *296*, E1003–E1012.

Preitner, N., Damiola, F., Luis-Lopez-Molina, Zakany, J., Duboule, D., Albrecht, U., and Schibler, U. (2002). The Orphan Nuclear Receptor REV-ERBα Controls Circadian Transcription within the Positive Limb of the Mammalian Circadian Oscillator. Cell *110*, 251–260.

Price, J.L., Blau, J., Rothenfluh, A., Abodeely, M., Kloss, B., and Young, M.W. (1998). double-time Is a Novel Drosophila Clock Gene that Regulates PERIOD Protein Accumulation. Cell *94*, 83–95.

Primeau, V., Coderre, L., Karelis, A.D., Brochu, M., Lavoie, M.-E., Messier, V., Sladek, R., and Rabasa-Lhoret, R. (2011). Characterizing the profile of obese patients who are metabolically healthy. Int. J. Obes. *35*, 971–981.

Raghuram, S., Stayrook, K.R., Huang, P., Rogers, P.M., Nosie, A.K., McClure, D.B., Burris, L.L., Khorasanizadeh, S., Burris, T.P., and Rastinejad, F. (2007). Identification of heme as the ligand for the orphan nuclear receptors REV-ERBα and REV-ERBβ. Nat. Struct. Mol. Biol. *14*, 1207–1213.

Rakai, B.D., Chrusch, M.J., Spanswick, S.C., Dyck, R.H., and Antle, M.C. (2014). Survival of Adult Generated Hippocampal Neurons Is Altered in Circadian Arrhythmic Mice. PLoS One *9*, e99527.

Ralph, M.R., Foster, R.G., Davis, F.C., and Menaker, M. (1990). Transplanted suprachiasmatic nucleus determines circadian period. Science *247*, 975– 978.

Ramsey, K.M., Yoshino, J., Brace, C.S., Abrassart, D., Kobayashi, Y., Marcheva, B., Hong, H.-K., Chong, J.L., Buhr, E.D., Lee, C., et al. (2009). Circadian Clock Feedback Cycle Through NAMPT-Mediated NAD+ Biosynthesis. Science *324*, 651–654.

Rankinen, T., Bray, M.S., Hagberg, J.M., Prusse, L., Roth, S.M., Wolfarth, B. and Bouchard, C. (2006). The Human Gene Map for Performance and Health-Related Fitness Phenotypes. Med. Sci. Sport. Exerc. *38*, 1863–1888.

Raspé, E., Duez, H., Mansén, A., Fontaine, C., Fiévet, C., Fruchart, J.-C., Vennström, B., and Staels, B. (2002). Identification of Rev-erbalpha as a physiological repressor of apoC-III gene transcription. J. Lipid Res. *43*, 2172–2179.

Reddon, H., Patel, Y., Turcotte, M., Pigeyre, M., and Meyre, D. (2018). Revisiting the evolutionary origins of obesity: lazy versus peppy-thrifty genotype hypothesis. Obes. Rev. *19*, 1525–1543.

Reick, M., Garcia, J.A., Dudley, C., and McKnight, S.L. (2001). NPAS2: An Analog of Clock Operative in the Mammalian Forebrain. Science *293*, 506–509.

Ríos-Lugo, M.J., Cano, P., Jiménez-Ortega, V., Fernández-Mateos, M.P., Scacchi, P.A., Cardinali, D.P., and Esquifino, A.I. (2010). Melatonin effect on plasma adiponectin, leptin, insulin, glucose, triglycerides and cholesterol in normal and high fat-fed rats. J. Pineal Res. *49*, 342–348.

Rippe, J.M., and Angelopoulos, T.J. (2013). Sucrose, High-Fructose Corn Syrup, and Fructose, Their Metabolism and Potential Health Effects: What Do We Really Know? Adv. Nutr. *4*, 236–245.

Ross, A.P., Bartness, T.J., Mielke, J.G., and Parent, M.B. (2009). A high fructose diet impairs spatial memory in male rats. Neurobiol. Learn. Mem. *92*, 410–416.

Rothschild, J., Hoddy, K.K., Jambazian, P., and Varady, K.A. (2014). Time-restricted feeding and risk of metabolic disease: a review of human and animal studies. Nutr. Rev. *72*, 308–318.

Ruxton, C.H.S., Gardner, E.J., and McNulty, H.M. (2009). Is Sugar Consumption Detrimental to Health? A Review of the Evidence 1995—2006. Crit. Rev. Food Sci. Nutr. *50*, 1–19.

Sacks, F.M., Bray, G.A., Carey, V.J., Smith, S.R., Ryan, D.H., Anton, S.D., McManus, K., Champagne, C.M., Bishop, L.M., Laranjo, N., et al. (2009). Comparison of Weight-Loss Diets with Different Compositions of Fat, Protein, and Carbohydrates. N. Engl. J. Med. *360*, 859–873.

Sakon, J.J., Naya, Y., Wirth, S., and Suzuki, W.A. (2014). Context-dependent incremental timing cells in the primate hippocampus. Proc. Natl. Acad. Sci. *111,* 18351–18356.

Salgado-Delgado, R., Angeles-Castellanos, M., Saderi, N., Buijs, R.M., and Escobar, C. (2010). Food Intake during the Normal Activity Phase Prevents Obesity and Circadian Desynchrony in a Rat Model of Night Work. Endocrinology *151*, 1019–1029.

Saltiel, A.R., and Kahn, C.R. (2001). Insulin signalling and the regulation of glucose and lipid metabolism. Nature *414*, 799–806.

Salz, D.M., Tiganj, Z., Khasnabish, S., Kohley, A., Sheehan, D., Howard, M.W., and Eichenbaum, H. (2016). Behavioral/Cognitive Time Cells in Hippocampal Area CA3. J. Neurosci. *36*, 7476-7484.

Samuel, V.T. (2011). Fructose induced lipogenesis: from sugar to fat to insulin resistance. Trends Endocrinol. Metab. *22*, 60–65.

Samuel, V.T., and Shulman, G.I. (2012). Mechanisms for Insulin Resistance: Common Threads and Missing Links. Cell *148*, 852–871.

Samuel, V.T., Petersen, K.F., and Shulman, G.I. (2010). Lipid-induced insulin resistance: unravelling the mechanism. Lancet *375*, 2267–2277.

Sarfert, K.S., Knabe, M.L., Gunawansa, N.S., and Blythe, S.N. (2019). Western-style diet induces object recognition deficits and alters complexity of dendritic arborization in the hippocampus and entorhinal cortex of male rats. Nutr. Neurosci. *22*, 344–353.

Sarjeant, K., and Stephens, J.M. (2012). Adipogenesis. Cold Spring Harb. Perspect. Biol. *4*, a008417–a008417.

Savage, D.B., Petersen, K.F., and Shulman, G.I. (2007). Disordered Lipid Metabolism and the Pathogenesis of Insulin Resistance. Physiol. Rev. *87*, 507–520.

Schmutz, I., Ripperger, J.A., Baeriswyl-Aebischer, S., and Albrecht, U. (2010). The mammalian clock component PERIOD2 coordinates circadian output by interaction with

nuclear receptors. Genes Dev. *24*, 345–357.

Schulze, M.B., Manson, J.E., Ludwig, D.S., Colditz, G.A., Stampfer, M.J., Willett, W.C., and Hu, F.B. (2004). Sugar-Sweetened Beverages, Weight Gain, and Incidence of Type 2 Diabetes in Young and Middle-Aged Women. JAMA *292*, 927.

Schwartz, G.J. (2000). The role of gastrointestinal vagal afferents in the control of food intake: current prospects. Nutrition *16*, 866–873.

Schwarz, J.-M., Noworolski, S.M., Wen, M.J., Dyachenko, A., Prior, J.L., Weinberg, M.E., Herraiz, L.A., Tai, V.W., Bergeron, N., Bersot, T.P., et al. (2015). Effect of a High-Fructose Weight-Maintaining Diet on Lipogenesis and Liver Fat. J. Clin. Endocrinol. Metab. *100*, 2434–2442.

Schwarz, J.-M., Noworolski, S.M., Erkin-Cakmak, A., Korn, N.J., Wen, M.J., Tai, V.W., Jones, G.M., Palii, S.P., Velasco-Alin, M., Pan, K., et al. (2017). Effects of Dietary Fructose Restriction on Liver Fat, De Novo Lipogenesis, and Insulin Kinetics in Children With Obesity. Gastroenterology *153*, 743–752.

Seibt, J., and Frank, M.G. (2012). Translation regulation in sleep. Commun. Integr. Biol. *5*, 491–495.

Seibt, J., Dumoulin, M.C., Aton, S.J., Coleman, T., Watson, A., Naidoo, N., and Frank, M.G. (2012). Protein Synthesis during Sleep Consolidates Cortical Plasticity In Vivo. Curr. Biol. *22*, 676–682.

Sellmann, C., Priebs, J., Landmann, M., Degen, C., Engstler, A.J., Jin, C.J., Gärttner, S., Spruss, A., Huber, O., and Bergheim, I. (2015). Diets rich in fructose, fat or fructose and fat alter intestinal barrier function and lead to the development of nonalcoholic fatty liver disease over time. J. Nutr. Biochem. *26*, 1183–1192.

Senador, D., Shewale, S., Irigoyen, M.C., Elased, K.M., and Morris, M. (2012). Effects of Restricted Fructose Access on Body Weight and Blood Pressure Circadian Rhythms. Exp. Diabetes Res. *2012*, 1–7.

Sherman, H., Genzer, Y., Cohen, R., Chapnik, N., Madar, Z., and Froy, O. (2012). Timed high-fat diet resets circadian metabolism and prevents obesity. FASEB *26*, 3493–3502.

Shigeyoshi, Y., Taguchi, K., Yamamoto, S., Takekida, S., Yan, L., Tei, H., Moriya, T., Shibata, S., Loros, J.J., Dunlap, J.C., et al. (1997). Light-Induced Resetting of a Mammalian Circadian Clock Is Associated with Rapid Induction of the mPer1 Transcript. Cell *91*, 1043–1053.

Shulman, G.I. (2014). Ectopic Fat in Insulin Resistance, Dyslipidemia, and Cardiometabolic Disease. N. Engl. J. Med. *371*, 1131–1141.

Siapas, A.G., and Wilson, M.A. (1998). Coordinated interactions between hippocampal ripples and cortical spindles during slow-wave sleep. Neuron *21*, 1123–1128.

Simonen, R.L., Rankinen, T., Perusse, L., Rice, T., Rao, D.C., Chagnon, Y., Bouchard, C., and Quebec Family Study (2003). Genome-wide linkage scan for physical activity levels in the Quebec Family study. Med. Sci. Sports Exerc. *35*, 1355–1359.

Simopoulos, A.P. (2002). Omega-3 Fatty Acids in Inflammation and Autoimmune Diseases. J. Am. Coll. Nutr. *21*, 495–505.

Sims-Robinson, C., Bakeman, A., Bruno, E., Jackson, S., Glasser, R., Murphy, G.G., and Feldman, E.L. (2016). Dietary Reversal Ameliorates Short- and Long-Term Memory Deficits Induced by High-fat Diet Early in Life. PLoS One *11*, e0163883.

Sinasac, D.S., Riordan, J.D., Spiezio, S.H., Yandell, B.S., Croniger, C.M., and Nadeau, J.H. (2016). Genetic control of obesity, glucose homeostasis, dyslipidemia and fatty liver in a mouse model of diet-induced metabolic syndrome. Int. J. Obes. *40*, 346–355.

Siri-Tarino, P.W., Sun, Q., Hu, F.B., and Krauss, R.M. (2010). Saturated Fatty Acids and Risk of Coronary Heart Disease: Modulation by Replacement Nutrients. Curr. Atheroscler. Rep. *12*, 384–390.

Sirota, A., Csicsvari, J., Buhl, D., and Buzsaki, G. (2003). Communication between neocortex and hippocampus during sleep in rodents. Proc. Natl. Acad. Sci. *100*, 2065–2069.

Slawik, H., Stoffel, M., Riedl, L., Veselý, Z., Behr, M., Lehmberg, J., Pohl, C., Meyer, B., Wiegand, M., and Krieg, S.M. (2016). Prospective Study on Salivary Evening Melatonin and Sleep before and after Pinealectomy in Humans. J. Biol. Rhythms *31*, 82–93.

Sobesky, J.L., Barrientos, R.M., De May, H.S., Thompson, B.M., Weber, M.D., Watkins, L.R., and Maier, S.F. (2014). High-fat diet consumption disrupts memory and primes elevations in hippocampal IL-1β, an effect that can be prevented with dietary reversal or IL-1 receptor antagonism. Brain. Behav. Immun. *42*, 22–32.

Sofer, S., Stark, A.H., and Madar, Z. (2015). Nutrition Targeting by Food Timing: Time-Related Dietary Approaches to Combat Obesity and Metabolic Syndrome. Adv. Nutr. *6*, 214–223.

Sofroniew, M. V. (2015). Astrocyte barriers to neurotoxic inflammation. Nat. Rev. Neurosci. *16*, 249–263.

Solt, L.A., Kojetin, D.J., and Burris, T.P. (2011). The REV-ERBs and RORs: molecular links between circadian rhythms and lipid homeostasis. Future Med. Chem. *3*, 623–638.

Sommer, J.B., Bach, A., Malá, H., Gynther, M., Bjerre, A.-S., Gram, M.G., Marschner, L., Strømgaard, K., Mogensen, J., and Pickering, D.S. (2017). Effects of Dimeric PSD-95 Inhibition on Excitotoxic Cell Death and Outcome After Controlled Cortical Impact in Rats. Neurochem. Res. *42*, 3401–3413.

de Souza, R.J., Mente, A., Maroleanu, A., Cozma, A.I., Ha, V., Kishibe, T., Uleryk, E., Budylowski, P., Schünemann, H., Beyene, J., et al. (2015). Intake of saturated and trans unsaturated fatty acids and risk of all cause mortality, cardiovascular disease, and type 2 diabetes: systematic review and meta-analysis of observational studies. BMJ *351*, h3978.

De Souza, C.T., Araujo, E.P., Bordin, S., Ashimine, R., Zollner, R.L., Boschero, A.C., Saad, M.J.A., and Velloso, L.A. (2005). Consumption of a Fat-Rich Diet Activates a Proinflammatory Response and Induces Insulin Resistance in the Hypothalamus. Endocrinology *146*, 4192–4199.

De Souza, C.T., Araújo, E.P., Stoppiglia, L.F., Pauli, J.R., Ropelle, E., Rocco, S.A., Marin, R.M., Franchini, K.G., Carvalheira, J.B., Saad, M.J., et al. (2007). Inhibition of UCP2 expression reverses diet-induced diabetes mellitus by effects on both insulin secretion and action. FASEB *21*, 1153–1163.

St-Onge, M.-P., Ard, J., Baskin, M.L., Chiuve, S.E., Johnson, H.M., Kris-Etherton, P., Varady, K., and American Heart Association Obesity Committee of the Council on Lifestyle and Cardiometabolic Health; Council on Cardiovascular Disease in the Young; Council on Clinical Cardiology; and Stroke Council (2017). Meal Timing and Frequency: Implications for Cardiovascular Disease Prevention: A Scientific Statement From the American Heart Association. Circulation *135*, e96–e121.

Stanewsky, R., Kaneko, M., Emery, P., Beretta, B., Wager-Smith, K., Kay, S.A., Rosbash, M., and Hall, J.C. (1998). The cryb Mutation Identifies Cryptochrome as a Circadian Photoreceptor in Drosophila. Cell *95*, 681–692.

Stanhope, K.L., and Havel, P.J. (2008). Endocrine and metabolic effects of consuming beverages sweetened with fructose, glucose, sucrose, or high-fructose corn syrup. Am. J. Clin. Nutr. *88*, 1733S-1737S.

Stanhope, K.L., Schwarz, J.M., Keim, N.L., Griffen, S.C., Bremer, A.A., Graham, J.L., Hatcher, B., Cox, C.L., Dyachenko, A., Zhang, W., et al. (2009). Consuming fructose-sweetened, not glucose-sweetened, beverages increases visceral adiposity and lipids and decreases insulin sensitivity in overweight/obese humans. J. Clin. Invest. *119*, 1322–1334.

Staresina, B.P., Bergmann, T.O., Bonnefond, M., van der Meij, R., Jensen, O., Deuker, L., Elger, C.E., Axmacher, N., and Fell, J. (2015). Hierarchical nesting of slow oscillations, spindles and ripples in the human hippocampus during sleep. Nat. Neurosci. *18*, 1679–1686.

Stice, E., Spoor, S., Bohon, C., and Small, D.M. (2008a). Relation between obesity and blunted striatal response to food is moderated by TaqIA A1 allele. Science *322*, 449–452.

Stice, E., Spoor, S., Bohon, C., Veldhuizen, M.G., and Small, D.M. (2008b). Relation of reward from food intake and anticipated food intake to obesity: A functional magnetic resonance imaging study. J. Abnorm. Psychol. *117*, 924–935.

Stote, K.S., Baer, D.J., Spears, K., Paul, D.R., Harris, G.K., Rumpler, W. V, Strycula, P., Najjar, S.S., Ferrucci, L., Ingram, D.K., et al. (2007). A controlled trial of reduced meal frequency without caloric restriction in healthy, normal-weight, middle-aged adults. Am. J. Clin. Nutr. *85*, 981–988.

Stratmann, M., and Schibler, U. (2012). REV-ERBs: More Than the Sum of the Individual Parts. Cell Metab. *15*, 791–793.

Strecker, G.J., Wuarin, J.-P., and Dudek, F.E. (1997). GABA $_{A}$ -Mediated Local Synaptic Pathways Connect Neurons in the Rat Suprachiasmatic Nucleus. J. Neurophysiol. *78*, 2217–2220.

Sujino, M., Masumoto, K., Yamaguchi, S., van der Horst, G.T.J., Okamura, H., and Inouye, S.-I.T. (2003). Suprachiasmatic Nucleus Grafts Restore Circadian Behavioral Rhythms of Genetically Arrhythmic Mice. Curr. Biol. *13*, 664–668.

Sun, K., Kusminski, C.M., and Scherer, P.E. (2011). Adipose tissue remodeling and obesity. J. Clin. Invest. *121*, 2094–2101.

Sun, Y., Yang, Z., Niu, Z., Wang, W., Peng, J., Li, Q., Ma, M.Y., and Zhao, Y. (2006). The mortality of MOP3 deficient mice with a systemic functional failure. J. Biomed. Sci. *13*, 845–851.

Sundaram, S., and Yan, L. (2016). Time-restricted feeding reduces adiposity in mice fed a high-fat diet. Nutr. Res. *36*, 603–611.

Sutton, E.F., Beyl, R., Early, K.S., Cefalu, W.T., Ravussin, E., and Peterson, C.M. (2018). Early Time-Restricted Feeding Improves Insulin Sensitivity, Blood Pressure, and Oxidative Stress Even without Weight Loss in Men with Prediabetes. Cell Metab. *27*, 1212-1221.

Swithers, S.E., and Davidson, T.L. (2008). A role for sweet taste: Calorie predictive relations in energy regulation by rats. Behav. Neurosci. *122*, 161–173.

Takahashi, J.S. (2017). Transcriptional architecture of the mammalian circadian clock. Nat. Rev. Genet. *18*, 164–179.

Takahashi, J.S., Hong, H.-K., Ko, C.H., and McDearmon, E.L. (2008). The genetics of mammalian circadian order and disorder: implications for physiology and disease. Nat.

Rev. Genet. *9*, 764–775.

Tamaru, T., Isojima, Y., Yamada, T., Okada, M., Nagai, K., and Takamatsu, K. (2000). Light and glutamate-induced degradation of the circadian oscillating protein BMAL1 during the mammalian clock resetting. J. Neurosci. *20*, 7525–7530.

Tan, D.-X., Manchester, L.C., and Reiter, R.J. (2016). CSF generation by pineal gland results in a robust melatonin circadian rhythm in the third ventricle as an unique light/dark signal. Med. Hypotheses *86*, 3–9.

Tan, D., Xu, B., Zhou, X., and Reiter, R. (2018). Pineal Calcification, Melatonin Production, Aging, Associated Health Consequences and Rejuvenation of the Pineal Gland. Molecules *23*, 301.

Tanti, J.-F., and Jager, J. (2009). Cellular mechanisms of insulin resistance: role of stress-regulated serine kinases and insulin receptor substrates (IRS) serine phosphorylation. Curr. Opin. Pharmacol. *9*, 753–762.

Tappy, L., Egli, L., and Tran, C. (2014). Metabolism of Nutritive Sweeteners in Humans. In Fructose, High Fructose Corn Syrup, Sucrose and Health, (New York, NY: Springer New York), pp. 35–50.

Teff, K.L., Elliott, S.S., Tschöp, M., Kieffer, T.J., Rader, D., Heiman, M., Townsend, R.R., Keim, N.L., D'Alessio, D., and Havel, P.J. (2004). Dietary Fructose Reduces Circulating Insulin and Leptin, Attenuates Postprandial Suppression of Ghrelin, and Increases Triglycerides in Women. J. Clin. Endocrinol. Metab. *89*, 2963–2972.

Thaler, J.P., Yi, C.-X., Schur, E.A., Guyenet, S.J., Hwang, B.H., Dietrich, M.O., Zhao, X., Sarruf, D.A., Izgur, V., Maravilla, K.R., et al. (2012). Obesity is associated with hypothalamic injury in rodents and humans. J. Clin. Invest. *122*, 153–162.

Than, N.N., and Newsome, P.N. (2015). A concise review of non-alcoholic fatty liver disease. Atherosclerosis *239*, 192–202.

The State of Obesity (2018a). Hypertension in the United States. https://stateofchildhoodobesity.org/hypertension/.

The State of Obesity (2018b). Diabetes in the United States. https://stateofchildhoodobesity.org/diabetes/.

Thornley, S., Tayler, R., and Sikaris, K. (2012). Sugar restriction: the evidence for a drug-free intervention to reduce cardiovascular disease risk. Intern. Med. J. *42*, 46–58.

Tiedemann, L.J., Schmid, S.M., Hettel, J., Giesen, K., Francke, P., Büchel, C., and Brassen, S. (2017). Central insulin modulates food valuation via mesolimbic pathways. Nat. Commun. *8*, 16052.

Tinsley, G.M., Forsse, J.S., Butler, N.K., Paoli, A., Bane, A.A., La Bounty, P.M., Morgan, G.B., and Grandjean, P.W. (2017). Time-restricted feeding in young men performing resistance training: A randomized controlled trial. Eur. J. Sport Sci. *17*, 200–207.

Tischkau, S.A., Mitchell, J.W., Tyan, S.-H., Buchanan, G.F., and Gillette, M.U. (2003). Ca2+/cAMP Response Element-binding Protein (CREB)-dependent Activation of Per1 Is Required for Light-induced Signaling in the Suprachiasmatic Nucleus Circadian Clock. J. Biol. Chem. *278*, 718–723.

Tremmel, M., Gerdtham, U.-G., Nilsson, P.M., and Saha, S. (2017). Economic Burden of Obesity: A Systematic Literature Review. Int. J. Environ. Res. Public Health *14*.

Trogdon, J.G., Finkelstein, E.A., Hylands, T., Dellea, P.S., and Kamal-Bahl, S.J. (2008). Indirect costs of obesity: a review of the current literature. Obes. Rev. *9*, 489–500.

Tsuneki, H., Sasaoka, T., and Sakurai, T. (2016). Sleep Control, GPCRs, and Glucose Metabolism. Trends Endocrinol. Metab. *27*, 633–642.

Turek, F.W., Joshu, C., Kohsaka, A., Lin, E., Ivanova, G., McDearmon, E., Laposky, A., Losee-Olson, S., Easton, A., Jensen, D.R., et al. (2005). Obesity and Metabolic Syndrome in Circadian Clock Mutant Mice. Science *308*, 1043–1045.

Tzeng, T.-T., Tsay, H.-J., Chang, L., Hsu, C.-L., Lai, T.-H., Huang, F.-L., and Shiao, Y.-J. (2013). Caspase 3 involves in neuroplasticity, microglial activation and neurogenesis in the mice hippocampus after intracerebral injection of kainic acid. J. Biomed. Sci. *20*, 90.

United States Departmen tof Agriculture (2019). Food Availability (Per Capita) Data System. https://www.ers.usda.gov/data-products/food-availability-per-capita-data-system/.

US Department of Health and Human Services (2015). 2015-2020 Dietary Guidelines. https://health.gov/dietaryguidelines/2015/.

Valdearcos, M., Robblee, M.M., Benjamin, D.I., Nomura, D.K., Xu, A.W., and Koliwad, S.K. (2014). Microglia Dictate the Impact of Saturated Fat Consumption on Hypothalamic Inflammation and Neuronal Function. Cell Rep. *9*, 2124–2138.

Vartanian, L.R., Schwartz, M.B., and Brownell, K.D. (2007). Effects of Soft Drink Consumption on Nutrition and Health: A Systematic Review and Meta-Analysis. Am. J. Public Health *97*, 667–675.

Vecsey, C.G., Peixoto, L., Choi, J.H.K., Wimmer, M., Jaganath, D., Hernandez, P.J., Blackwell, J., Meda, K., Park, A.J., Hannenhalli, S., et al. (2012). Genomic analysis of sleep deprivation reveals translational regulation in the hippocampus. Physiol. Genomics

44, 981–991.

Vicario-Abejón, C., Owens, D., McKay, R., and Segal, M. (2002). Role of neurotrophins in central synapse formation and stabilization. Nat. Rev. Neurosci. *3*, 965–974.

Vilar-Gomez, E., Martinez-Perez, Y., Calzadilla-Bertot, L., Torres-Gonzalez, A., Gra-Oramas, B., Gonzalez-Fabian, L., Friedman, S.L., Diago, M., and Romero-Gomez, M. (2015). Weight Loss Through Lifestyle Modification Significantly Reduces Features of Nonalcoholic Steatohepatitis. Gastroenterology *149*, 367-378.

Volkow, N.D., Wang, G.-J., and Baler, R.D. (2011). Reward, dopamine and the control of food intake: implications for obesity. Trends Cogn. Sci. *15*, 37–46.

Vollmers, C., Gill, S., Ditacchio, L., Pulivarthy, S.R., Le, H.D., and Panda, S. (2009). Time of feeding and the intrinsic circadian clock drive rhythms in hepatic gene expression. Proc. Natl. Acad. Sci. *106*, 21453-21458.

Vosshall, L., Price, J., Sehgal, A., Saez, L., and Young, M. (1994). Block in nuclear localization of period protein by a second clock mutation, timeless. Science *263*, 1606–1609.

Wadden, T.A. (1993). Treatment of obesity by moderate and severe caloric restriction. Results of clinical research trials. Ann. Intern. Med. *119*, 688–693.

Waise, T.M.Z., Toshinai, K., Naznin, F., NamKoong, C., Md Moin, A.S., Sakoda, H., and Nakazato, M. (2015). One-day high-fat diet induces inflammation in the nodose ganglion and hypothalamus of mice. Biochem. Biophys. Res. Commun. *464*, 1157–1162.

Wakamatsu, H., Yoshinobu, Y., Aida, R., Moriya, T., Akiyama, M., and Shibata, S. (2001). Restricted-feeding-induced anticipatory activity rhythm is associated with a phase-shift of the expression of mPer1 and mPer2 mRNA in the cerebral cortex and hippocampus but not in the suprachiasmatic nucleus of mice. Eur. J. Neurosci. *13*, 1190–1196.

Walker, P.D., and Carlock, L.R. (1993). Immediate early gene activation during the initial phases of the excitotoxic cascade. J. Neurosci. Res. *36*, 588–595.

Walker, R.W., Dumke, K.A., and Goran, M.I. (2014). Fructose content in popular beverages made with and without high-fructose corn syrup. Nutrition *30*, 928–935.

Wang, L.M., Schroeder, A., Loh, D., Smith, D., Lin, K., Han, J.H., Michel, S., Hummer, D.L., Ehlen, J.C., Albers, H.E., et al. (2008). Role for the NR2B subunit of the N-methyl-d-aspartate receptor in mediating light input to the circadian system. Eur. J. Neurosci. *27*, 1771–1779.

Wang, Q.A., Tao, C., Gupta, R.K., and Scherer, P.E. (2013). Tracking adipogenesis

during white adipose tissue development, expansion and regeneration. Nat. Med. *19*, 1338–1344.

Wehrens, S.M.T., Christou, S., Isherwood, C., Middleton, B., Gibbs, M.A., Archer, S.N., Skene, D.J., Johnston, J.D., Wright, K.P., Wright, J., et al. (2017). Meal Timing Regulates the Human Circadian System. Curr. Biol. *27*, 1768-1775.

Welsh, D.K., Takahashi, J.S., and Kay, S.A. (2010). Suprachiasmatic Nucleus: Cell Autonomy and Network Properties. Annu. Rev. Physiol. *72*, 551–577.

West, D.B., Goudey-Lefevre, J., York, B., and Truett, G.E. (1994). Dietary obesity linked to genetic loci on chromosomes 9 and 15 in a polygenic mouse model. J. Clin. Invest. *94*, 1410–1416.

White, J.S. (2008). Straight talk about high-fructose corn syrup: what it is and what it ain't. Am. J. Clin. Nutr. *88*, 1716S-1721S.

Wiebe, N., Padwal, R., Field, C., Marks, S., Jacobs, R., and Tonelli, M. (2011). A systematic review on the effect of sweeteners on glycemic response and clinically relevant outcomes. BMC Med. *9*, 123.

Wolf, A.M. (1998). What is the economic case for treating obesity? Obes. Res. *6 Suppl 1*, 2S-7S.

Won, J.C., Jang, P.-G., Namkoong, C., Koh, E.H., Kim, S.K., Park, J.-Y., Lee, K.-U., and Kim, M.-S. (2009). Central Administration of an Endoplasmic Reticulum Stress Inducer Inhibits the Anorexigenic Effects of Leptin and Insulin. Obesity *17*, 1861–1865.

Woodie, L., and Blythe, S. (2017). The differential effects of high-fat and high-fructose diets on physiology and behavior in male rats. Nutr. Neurosci. *21*, 328-336.

Woodie, L.N., Luo, Y., Wayne, M.J., Graff, E.C., Ahmed, B., O'Neill, A.M., and Greene, M.W. (2018). Restricted feeding for 9 h in the active period partially abrogates the detrimental metabolic effects of a Western diet with liquid sugar consumption in mice. Metabolism. *82*, 1-13.

Woodie, L.N., Altonji, O.M., Huggins, K.W., and Greene, M.W. (2019). The high-fat diet and the effects of its consumption on the hypothalamus and hippocampus. CAB Revs. *14*, 1-9.

World Health Organization (2009). Global Health Risks: Mortality and burden of disease attributable to selected major risks (Geneva: WHO Press).

World Health Organization (2018). Obesity and overweight. https://www.who.int/news-room/fact-sheets/detail/obesity-and-overweight.

Wu, T., Gao, X., Chen, M., and van Dam, R.M. (2009). Long-term effectiveness of diet-plus-exercise interventions vs. diet-only interventions for weight loss: a meta-analysis. Obes. Rev. *10*, 313–323.

Xu, B., and Xie, X. (2016). Neurotrophic factor control of satiety and body weight. Nat. Rev. Neurosci. *17*, 282–292.

Yamaguchi, S., Isejima, H., Matsuo, T., Okura, R., Yagita, K., Kobayashi, M., and Okamura, H. (2003). Synchronization of Cellular Clocks in the Suprachiasmatic Nucleus. Science (80-.). *302*, 1408–1412.

Yan, J., Wang, H., Liu, Y., and Shao, C. (2008). Analysis of Gene Regulatory Networks in the Mammalian Circadian Rhythm. PLoS Comput. Biol. *4*, e1000193.

Yan, L., Karatsoreos, I., LeSauter, J., Welsh, D.K., Kay, S., Foley, D., and Silver, R. (2007). Exploring Spatiotemporal Organization of SCN Circuits. Cold Spring Harb. Symp. Quant. Biol. *72*, 527–541.

Yasumoto, Y., Hashimoto, C., Nakao, R., Yamazaki, H., Hiroyama, H., Nemoto, T., Yamamoto, S., Sakurai, M., Oike, H., Wada, N., et al. (2016). Short-term feeding at the wrong time is sufficient to desynchronize peripheral clocks and induce obesity with hyperphagia, physical inactivity and metabolic disorders in mice. Metabolism *65*, 714–727.

Yin, L., and Lazar, M.A. (2005). The Orphan Nuclear Receptor Rev-erbα Recruits the N-CoR/Histone Deacetylase 3 Corepressor to Regulate the Circadian *Bmal1* Gene. Mol. Endocrinol. *19*, 1452–1459.

Yin, L., Wu, N., Curtin, J.C., Qatanani, M., Szwergold, N.R., Reid, R.A., Waitt, G.M., Parks, D.J., Pearce, K.H., Wisely, G.B., et al. (2007). Rev-erb , a Heme Sensor That Coordinates Metabolic and Circadian Pathways. Science *318*, 1786–1789.

Yin, L., Wu, N., and Lazar, M.A. (2010). Nuclear receptor Rev-erbalpha: a heme receptor that coordinates circadian rhythm and metabolism. Nucl. Recept. Signal. *8*, e001.

Young, M., and McGinnis, G. (2016). Circadian regulation of metabolic homeostasis: causes and consequences. Nat. Sci. Sleep *8*, 163.

Zamanian, J.L., Xu, L., Foo, L.C., Nouri, N., Zhou, L., Giffard, R.G., and Barres, B.A. (2012). Genomic analysis of reactive astrogliosis. J. Neurosci. *32*, 6391–6410.

Zamir, I., Harding, H.P., Atkins, G.B., Hörlein, A., Glass, C.K., Rosenfeld, M.G., and Lazar, M.A. (1996). A nuclear hormone receptor corepressor mediates transcriptional silencing by receptors with distinct repression domains. Mol. Cell. Biol. *16*, 5458–5465.

Zamir, I., Zhang, J., and Lazar, M.A. (1997). Stoichiometric and steric principles governing repression by nuclear hormone receptors. Genes Dev. *11*, 835–846.

Van der Zee, E.A., Havekes, R., Barf, R.P., Hut, R.A., Nijholt, I.M., Jacobs, E.H., and Gerkema, M.P. (2008). Circadian Time-Place Learning in Mice Depends on Cry Genes. Curr. Biol. *18*, 844–848.

Zehring, W.A., Wheeler, D.A., Reddy, P., Konopka, R.J., Kyriacou, C.P., Rosbash, M., and Hall, J.C. (1984). P-element transformation with period locus DNA restores rhythmicity to mutant, arrhythmic drosophila melanogaster. Cell *39*, 369–376.

Zhang, J., Kalkum, M., Chait, B.T., and Roeder, R.G. (2002). The N-CoR-HDAC3 nuclear receptor corepressor complex inhibits the JNK pathway through the integral subunit GPS2. Mol. Cell *9*, 611–623.

Zhang, X., Zhang, G., Zhang, H., Karin, M., Bai, H., and Cai, D. (2008). Hypothalamic IKKβ/NF-κB and ER Stress Link Overnutrition to Energy Imbalance and Obesity. Cell *135*, 61–73.

Zhang, Y., Fang, B., Emmett, M.J., Damle, M., Sun, Z., Feng, D., Armour, S.M., Remsberg, J.R., Jager, J., Soccio, R.E., et al. (2015). GENE REGULATION. Discrete functions of nuclear receptor Rev-erbα couple metabolism to the clock. Science *348*, 1488–1492.

Zheng, H., and Berthoud, H.-R. (2008). Neural Systems Controlling the Drive to Eat: Mind Versus Metabolism. Physiology *23*, 75–83.

Zhou, Y.D., Barnard, M., Tian, H., Li, X., Ring, H.Z., Francke, U., Shelton, J., Richardson, J., Russell, D.W., and McKnight, S.L. (1997). Molecular characterization of two mammalian bHLH-PAS domain proteins selectively expressed in the central nervous system. Proc. Natl. Acad. Sci. U. S. A. *94*, 713–718.

Ziegler, E. (1967). Secular changes in the stature of adults and the secular trend of the modern sugar consumption. Zeitschrift F□r Kinderheilkd. *99*, 146–166.

Zmuda, N. (2011). Bottom's Up! A Look at America's Drinking Habits | AdAge.

Zomer, E., Gurusamy, K., Leach, R., Trimmer, C., Lobstein, T., Morris, S., James, W.P.T., and Finer, N. (2016). Interventions that cause weight loss and the impact on cardiovascular risk factors: a systematic review and meta-analysis. Obes. Rev. *17*, 1001–1011.

Zuurbier, L.A., Luik, A.I., Hofman, A., Franco, O.H., Van Someren, E.J.W., and Tiemeier, H. (2015). Fragmentation and Stability of Circadian Activity Rhythms Predict Mortality. Am. J. Epidemiol. *181*, 54–63.

Zylka, M.J., Shearman, L.P., Weaver, D.R., and Reppert, S.M. (1998). Three period Homologs in Mammals: Differential Light Responses in the Suprachiasmatic Circadian Clock and Oscillating Transcripts Outside of Brain. Neuron *20*, 1103–1110.

Appendix 1

Supplemental Figure 1. Y Maze apparatus

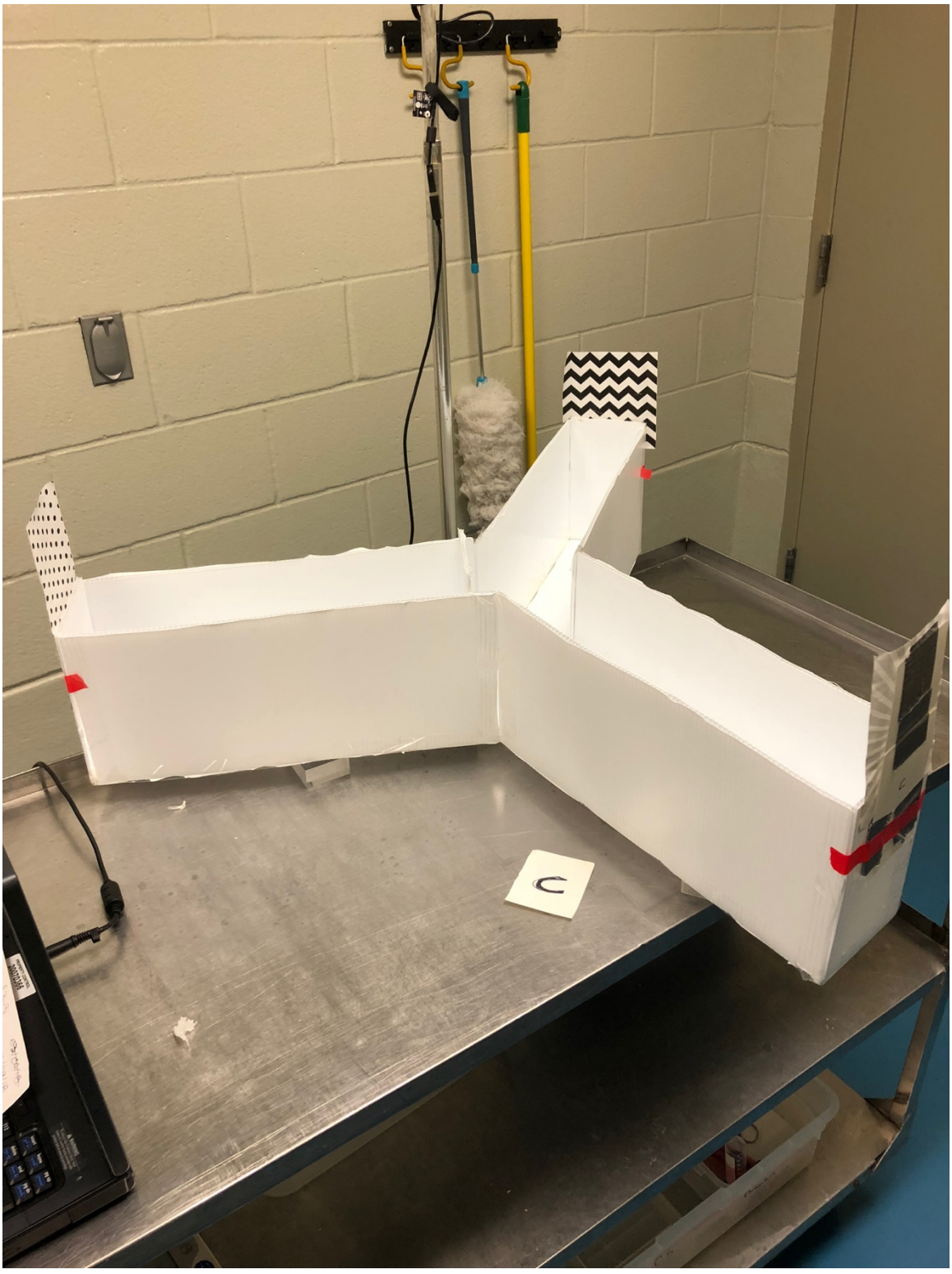

Supplemental Figure 2. Novel Object Recognition apparatus

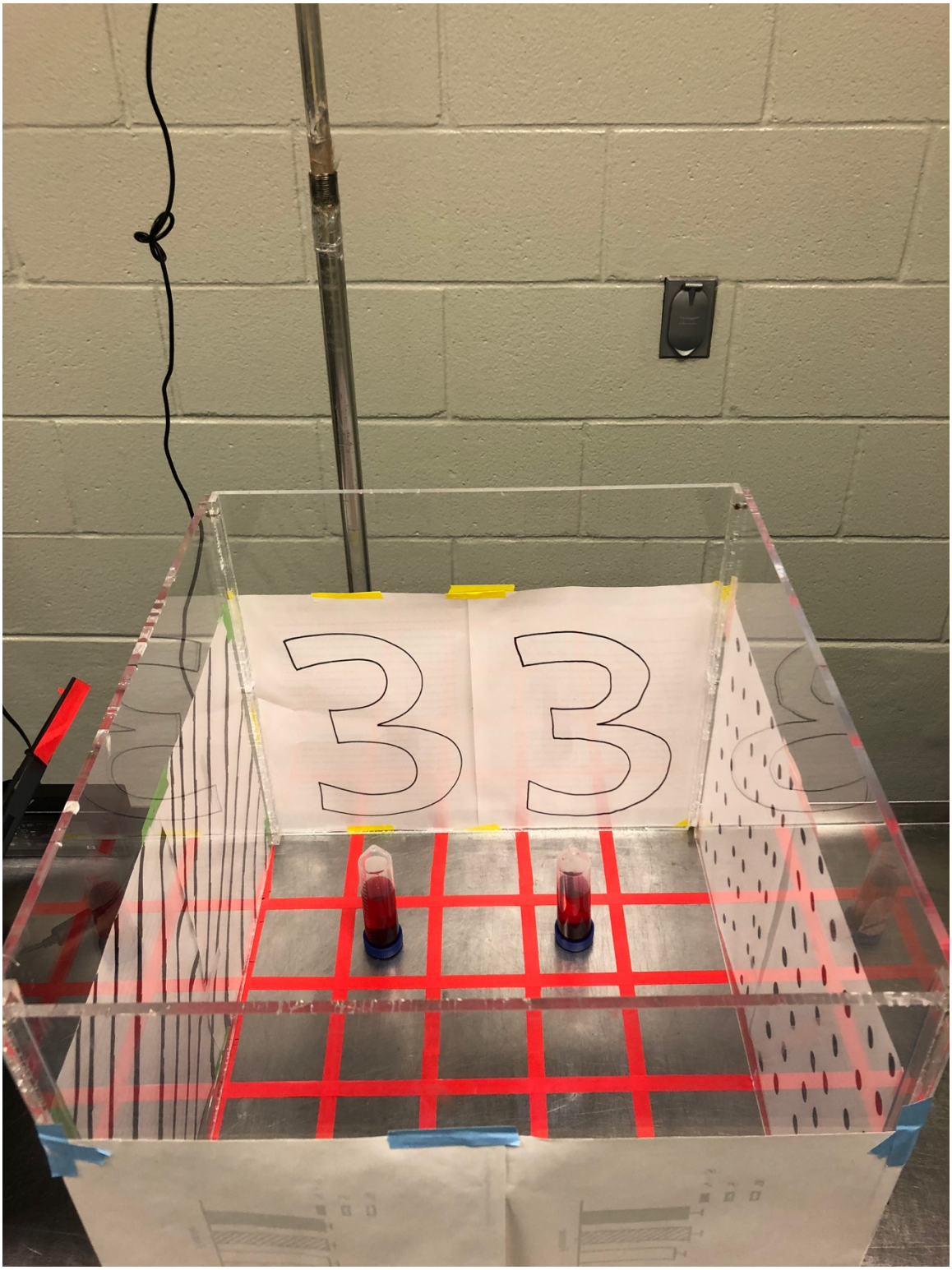

Supplemental Figure 3. Novel Object Recognition Familiar Objects (50 mL conical

tubes filled to 30 mL red-dyed tap water).

Supplemental Figure 4. Novel Object Recognition Familiar Object (50 mL conical tube filled with 30 mL red-dyed tap water) and Novel Object (bottle caps).

Supplementary Text 1. Example of R code and output used to determine rhythmic gene expression in diurnal RT-qPCR results via cosinor-based rhythmometry.

```
#Code for cosine rhythmometry of RT-qPCR data from AAES 2017-2019 hippo
campus.

#Package from William Revelle.
library(psych)
setwd("/Users/lnw0013/Desktop/RFiles/cosinor/Hipp")
Time=read.csv("time.csv", header=TRUE, sep=",")
Diet = c("CD", "CD", "CD", "CD", "CD", "CD", "CD", "CD", "CD", "CD", "C
D", "CD","WD", "WD", "WD", "WD", "WD", "WD", "WD", "WD", "WD", "WD", "W
D", "WD")


#Cryptochrome 1
  #CD
    CDCry1=read.csv("CDCry1.csv", header=TRUE, sep=",")
    cosinor(Time,CDCry1)

##           phase       fit amplitude        sd     mean intercept
## RelExp 12.16565 0.8360994 0.8360994 0.2803279 1.133495 0.8993331

  #WD
    WDCry1 = read.csv("WDCry1.csv", header=TRUE, sep=",")
    cosinor(Time,WDCry1)

##           phase       fit amplitude        sd      mean intercept
## RelExp 13.14667 0.9041191 0.9041191 0.3192775 0.6533666 0.3776114

  #graph
    CDandWDCry1=rbind(CDCry1, WDCry1)
    Cry1plot=data.frame(Time, Diet, CDandWDCry1)
    cosinor.plot(1, 3, data=Cry1plot, IDloc=2, ID="CD", ylim=c(0,3), yl
ab= "Relative Expression", xlab = "ZT", pch=15, lty=1)
    cosinor.plot(1, 3, data=Cry1plot, IDloc=2, ID="WD", add=TRUE, lty=2
, pch= 16)
    legend("bottomright", inset=0.01, title="Diet", c("CD", "WD"), pch=
c(15,16))
```

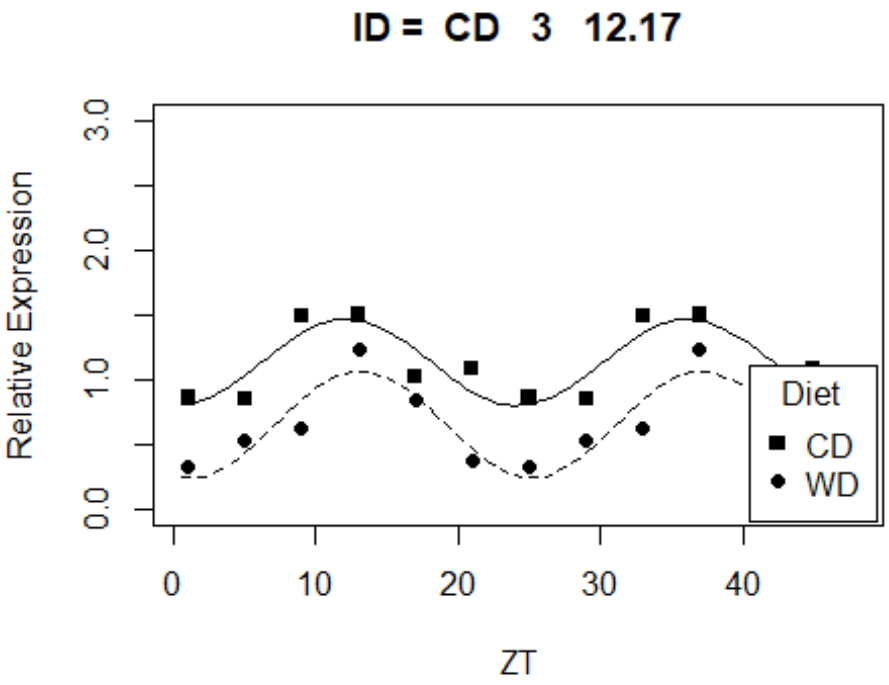
ID = CD 3 12.17
Relative Expression
0.0
1.0
2.0
3.0
0
10
20
30
40
ZT
Diet
CD
WD

Supplementary Text 2. Example of R code and output used to determine rhythmic gene expression in diurnal RT-qPCR results via JTK_CYCLE.

```
setwd("~/Dropbox/AAES_2017-19/Cohort2/RFiles/JTK_CYCLE/Hipp")

source("JTK_CYCLEv3.1.R")

project <- "HIPP_AAESrtqpcr"

options(stringsAsFactors=FALSE)
annot <- read.delim("Hipp_annot.txt")
data <- read.delim("Hipp_data.txt")

rownames(data) <- data[,1]
data <- data[,-1]
jtkdist(12,1)

periods <- 4:6
jtk.init(periods,4)

cat("JTK analysis started on",date(),"\n")

## JTK analysis started on Tue Oct  1 17:52:48 2019

flush.console()

st <- system.time({
  res <- apply(data,1,function(z) {
    jtkx(z)
    c(JTK.ADJP,JTK.PERIOD,JTK.LAG,JTK.AMP)
  })
  res <- as.data.frame(t(res))
  bhq <- p.adjust(unlist(res[,1]),"BH")
  res <- cbind(bhq,res)
  colnames(res) <- c("BH.Q","ADJ.P","PER","LAG","AMP")
  results <- cbind(annot,res,data)
  results <- results[order(res$ADJ.P,-res$AMP),]
})
print(st)

##    user  system elapsed
##   0.090   0.002   0.094

save(results,file=paste("JTK",project,"rda",sep="."))
write.table(results,file=paste("JTK",project,"txt",sep="."),row.names=F
,col.names=T,quote=F,sep="\t")
```

```
Diet Probe BH.Q             ADJ.P              PER LAG AMP
CD   Cry1  0.61015096015096 0.247873827561328 24  12  0.292626981532809
```